Charge and Proton Transport of Electrocatalysis by Polymer Encapsulated Cobalt Phthalocyanine

by

Taylor L. Soucy

A dissertation submitted in partial fulfillment
of the requirements for the degree of
Doctor of Philosophy
(Chemistry)
in the University of Michigan
2022

Doctoral Committee:

Assistant Professor Charles C. L. McCrory, Chair
Professor Nicolai Lehnert
Professor Suljo Linic
Professor Anne J. McNeil

Taylor L. Soucy

tsoucy@umich.edu

ORCID: 0000-0002-0090-6721

Dedication

In loving memory of Louise, Nancy, and Harry.

Acknowledgements

First and foremost, thank you to Professor Charles C. L. McCrory, who has been both a research advisor and an incredible mentor to me for the last five years. Thank you so much for teaching me everything I know about electrochemistry and for the endless encouragement, most importantly when I didn't believe in myself. I learned so much about leadership watching Charles navigate his research group through a global pandemic. I have been so grateful to learn about becoming an electrochemist, a scientist, a researcher, and a leader by being a part of this group.

The other members of my thesis committee, Professor Nicolai Lehnert, Professor Suljo Linic, and Professor Anne McNeil, have each made important critiques and suggestions on the improvements of my research and my development as a scientist, and I'm extremely grateful for their time serving on my committee. I am grateful to Professor Banaszak Holl who gave me the opportunity to rotate in his research lab. I am grateful that I was able to learn and develop as a communicator, writer, organizer, and leader by participating in the professional development opportunities, particularly the department's writing program led by Professor Anne McNeil and Dr. Ryan McCarty, and CSIE|UM/CALC|UM/Alum|NUM led by Professor Brian Coppola.

I am grateful to our collaborators, Professor Adam Matzger and Dr. Leila Foroughi for their expertise in the synthesis and characterization of the copolymers used for Chapter 4. Thank you to members of the chemistry instruments staff, especially James Windak and Russ Bornshein. Roy Wentz constructed all of my electrochemical cells and fixed my favorite graduated cylinder when I was tired and knocked it over. A very big thank you to the members of the student support staff, particularly Katie Foster, Heather Hanosh, Emma Houle, Brendan Locke, and Liz Oxford,

among other staff members in safety, maintenance, and waste management who have done so much work to allow this department to run. Importantly – the custodial staff with whom I interacted are some of the kindest people. A very special thank you to Denise, who never let me get through a morning without smiling.

Additionally, I acknowledge the members (past and present) of Charles' research group who helped me in developing my scientific skills and knowledge. I was fortunate enough to work with Dr. Yingshuo Liu on one of the chapters presented here. I spent most mornings of my first four years talking to Dr. Samuel Michaud and Dr. Weixuan Nie in the lab, and I will always be grateful to them for their time spent mentoring and teaching me. I also worked directly with Dr. Kwan Leung. I had the joy of working with Kevin E. Rivera Cruz, who is also one of my favorite people to be around. William Dean was my most frequent collaborator on successful and unsuccessful projects (and was a one-year housemate). I am so grateful for their insights and collaboration. I'm also grateful I got the chance to work other members of the lab: Dr. Jeremy D. Kallick, Robert E. Bonsall, Jukai Zhou, Maiko J. Askari, Lirong Shi, Drew Tarnopol, Mike Rhies, and Michaela Barber. To Jonah B. Eisenberg, who joined us as an undergraduate and who spent hours painstakingly collecting crucial pieces of electrochemistry data to complete some of the stories herein: Thank you for your work (and for being the only lab mate to sing *In the Heights* with me).

While the last 5 years have produced the work for this PhD, the mentorship I received throughout the first 22 years of my life set me up to arrive here. Every teacher I have ever had was crucial to me for developing such a strong love of learning and foundation for math and science, but importantly, I decided to become a chemist due to the influence of Ms. Robin Rimback at MPHS. I'll never stop being grateful that I learned to love research as an undergraduate in the

lab of Professor Ray Schaak. Thank you to Dr. Julie Fenton. Thank you to the Millennium Scholars Program at Penn State - Professor Nate Brown, Georjanne Williams, Tina Thomas, and Elaine Barsness, along with other administrative staff who worked behind the scenes to create and sustain the MSP.

Out of everyone I met through the MSP, I am most wildly grateful to Star Sharp, who is one of the most brilliant and wonderful people I have ever met in my entire life. I likely would not have made it through my undergraduate degree without her support and guidance (and willingness to take me to the hospital in the middle of the night– also thank you to Gabby Richards, who met us in the ER at 2 am and kept me distracted from a spinal tap by educating me about reality TV). I am also grateful for the other members of the Millennium Scholars Program, especially in cohorts 1 and 2. This PhD is a product of "focus, focus, focus", but also a testament to the building of a family and "beginning with the end in mind". Each member of my cohort played a crucial part in my life at Penn State, but I'd like to especially thank Becca and Nico, who continued to support me throughout graduate school. The biggest thank you to Luke, who has unconditionally supported me with so much intentionality during the last 9 years of our friendship – thank you for sending me coffee from California and having my back since day 6.

A very big thank you to my wide network of friends from Ann Arbor, Penn State, and Delaware. I am in awe of my luck when I think about how my friends and extended family are so kind, brilliant, and generous. I'd like to especially acknowledge the people who supported me during graduate school: Olivia and her Jean Grey, Gloria Diaz, Nevo, Becca, Gloria de la Garza, Kate, Hope & Dan, Elissa, Alissa, Jessi, Jessica, Ciara, Ted, Alyah, Janna, Justin, Emily, Eli, Diane, Emma, Alice, Victoria, and Matt, my countless bible studies, my official and unofficial roommates over the last five years (especially the people who let me crash on their couches when

my apartment flooded four times in six weeks); and my friends and family from the East Coast - Sage, MAC, Becca and the Kling family, Morgan and the Gott family, Gabby and the Richards family, and Ms. Kathy. Thank you so much to the church communities I have found over the years. I hope that the work presented here provides evidence that in my life, science and faith are not mutually exclusive; verily, I find that each highlights the beauty and complexity of the other.

A million thanks to Sam, my very best friend who has pushed me to be the strongest and most hard-working version of myself in and out of the lab. Thank you for always asking me questions about my experiments, poking holes in my arguments, letting me clean your kitchen, and telling me what I needed to hear even (especially) if I didn't want to hear it.

My family has always been my rock and support system: my sister-in-law has been the sweetest addition to our family for the last three years; my siblings have been my best friends since they were born; my parents are my heroes. A gigantic thank you to my sister and brother, who have spent the entirety of their lives trying to get me to laugh and to not take myself too seriously. My parents have taught me the true meaning of determination, grit, and sacrifice in service to others. I am grateful that they spent 15 years driving me all over the state of Delaware to make sure I was being challenged in my education and teaching me to set challenging goals and then chase them.

The work discussed herein was funded by a National Science Foundation CAREER award (CHE-1751791). During my graduate education, I was funded by a National Science Foundation Graduate Research Fellowship (NSF GRFP, DGE 1256260) and by a University of Michigan Rackham Merit Fellowship.

Table of Contents

List of Tables

List of Figures

Abstract

The electrocatalytic CO_2 reduction reaction (CO_2RR) is one proposed method to convert industrial waste CO_2 into value-added products using renewable electricity. There are many (photo)electrocatalysts that can decrease the costly kinetic barrier to overcome for this process, but one method involves the use of molecular catalysts. Cobalt phthalocyanine (CoPc) is one catalyst that can perform CO_2RR with CO and methanol as possible products and when CoPc is encapsulated in a poly(4-vinylpyridine) (P4VP) polymer, it exhibits enhanced activity and selectivity metrics for the CO_2RR compared to its non-encapsulated parent complex. Specifically, the reaction activity is quadrupled, and the selectivity for CO_2RR over the hydrogen evolution reaction (HER) is enhanced due to three effects of the encapsulation: a primary coordination sphere effect, a secondary coordination sphere effect, and an outer-coordination proton transport effect. Previous members of the McCrory lab have studied the primary sphere effect of pyridyl residues interacting with CoPc by using multiple tools: electrochemistry, spectroscopy, and computations. Unfortunately, the secondary coordination sphere involves the stabilization of the reactive intermediate COO^- as it undergoes the reductive process at the CoPc site and has been challenging to study. Previous members of the McCrory lab also studied outer coordination sphere effects by using the electrochemical proton inventory technique to show that there was a proton relay through the polymer, controlling proton delivery from the electrolyte to CoPc active sites.

With the knowledge that transport of protons is important, I focused my sties on modulating the transport of electrons and protons within the CoPc-P4VP system. First, I conducted a comprehensive study to incorporate graphite powder (GP) into the catalyst-polymer system and

studied how this increased activity. Specifically, I found that the CoPc:GP ratio was important for achieving maximum activity. I also explored the best practice for preparing the CoPc-P4VP/GP slurries by showing that not including centrifugation in the preparation method of the deposition inks showed lower activity at all CoPc loadings.

I also studied the impact of pH on the activity and selectivity of the CO_2RR by CoPc-P4VP. The rate of transport from the electrolyte to catalytic active sites within the polymer is proportional to the bulk concentration of protons in solution. I saw that fractional protonation of the polymer changed as a function of electrolyte pH, and that increased pH resulted in an increase in CO_2RR selectivity and activity. I also found that the concentration of electrolyte impacts the fractional protonation of the polymer, and these results had implications for the HER as catalyzed by CoPc-P4VP. The increase in fractional protonation of the polymer resulted in an observed kinetic isotope effect, indicating that a protonation event was likely the rate-limiting step for the HER but may not be observed unless there was sufficient protonation of the polymer.

Finally, I studied the impact of incorporating styrene moieties into a polymer using copolymers with varying styrene:4-vinylpyridine molar concentrations. The study was performed with the express intent to shut down proton relays. I found that the activity decreased with small amounts of styrene within the copolymer, but kinetic isotope effect studies indicated that a possible loss of axial coordination from the pyridyl residues may have caused this diminished activity. The insights from this work may be applied to CO_2 electrolyzer devices as polymer-bound molecular catalysts with carbon supports are used in flow cell reactor systems.

Chapter 1 Introduction

1.1 Preface

This chapter introduces cobalt phthalocyanine-catalyzed electroreduction of CO_2 to value-added products and discusses methods that have been developed to perform and understand this reaction. A specific focus on the reasons for the enhancement of carbon dioxide reduction reaction by cobalt phthalocyanine when the molecular catalyst is encapsulated in poly-4-vinylpyridine and adsorbed onto a graphitic electrode. This chapter of my dissertation is partially derived from a manuscript as originally published in *Accounts of Chemical Research*.[1] I was the first author upon which this chapter is based and wrote most of the manuscript and edited all of the manuscript. A small portion of this chapter is derived with permission from a manuscript as originally published in *Comments on Inorganic Chemistry*,[2] where I was a coauthor and contributed the portion of writing enclosed herein.

(1) Soucy, T. L.; Dean, W. S.; Zhou, J.; Rivera Cruz, K. E.; McCrory, C. C. L. "Considering the Influence of Polymer–Catalyst Interactions on the Chemical Microenvironment of Electrocatalysts for the CO2 Reduction Reaction," *Accounts of Chemical Research* **2022**. http://dx.doi.org/10.1021/acs.accounts.1c00633

(2) Liu, Y.; Leung, K. Y.; Michaud, S. E.; Soucy, T. L.; McCrory, C. C. L. "Controlled Substrate Transport to Electrocatalyst Active Sites for Enhanced Selectivity in the Carbon Dioxide Reduction Reaction," *Comments on Inorganic Chemistry* **2019**, *39*, 242-269. http://dx.doi.org/10.1080/02603594.2019.1628025

1.2 Abstract

The electrochemical CO_2 reduction reaction (CO_2RR) is an attractive method for capturing intermittent renewable energy sources and converting waste CO_2 into value-added products with a goal of carbon neutrality. Of the many options for CO_2RR (photo)electrocatalysis, our group has made recent progress in the development of polymer-encapsulated cobalt phthalocyanine (CoPc). When CoPc is adsorbed onto a carbon electrode and encapsulated in poly(4-vinylpyridine) (P4VP), the activity and reaction selectivity over the competitive hydrogen evolution reaction, HER, are enhanced by three synergistic effects: a primary axial coordination effect, a secondary reaction intermediate stabilization effect, and an outer-coordination proton transport effect. We have studied multiple aspects of this system using electrochemical, spectroscopic, and computational tools. Specifically, we confirmed that the pyridyl residues from the polymer were indeed axially coordinating to the CoPc metal center via X-ray spectroscopy measurements and showed via electrochemical activity studies that increased donating ability of a nitrogen-containing axial ligand would result in increased activity. We proved via electrochemical proton-inventory studies that a proton relay through the polymer matrix was responsible for controlled proton delivery to an electrocatalytic CoPc center. Additionally, we performed a comprehensive study using graphite powder as a carbon support in order to increase activity while determining best practices for incorporating carbon supports into a catalyst-polymer composite. In this Chapter, I describe these studies in detail, organizing our discussion by three types of microenvironmental interactions that affect the catalyst performance: ligand effects of the primary and secondary sphere, substrate transport of protons and CO_2, and charge transport from the electrode surface to the catalyst sites. I explain the types of experiments we are able to perform to understand how all three factors affect the overall activity and selectivity of the electrocatalyst.

The work presented and discussed here shows that careful electroanalytical study and interpretation can be valuable in developing a robust and comprehensive understanding of the reasons for catalyst performance. In addition to our work with polymer encapsulated CoPc, we provide examples of similar surface-adsorbed molecular and solid-state systems that benefit from interactions between active catalytic sites and a polymer system. We also compare the activity results from our systems to other results in the CoPc literature, and other examples of molecular CO_2RR catalysts on modified electrode surfaces. Finally, I speculate how the insights gained from studying CoPc could guide the field in designing other polymer-electrocatalyst systems. As CO_2RR technologies become commercially viable and expand into the space of flow cells and gas-diffusion electrodes, I propose that overall device efficiency may benefit from understanding and promoting synergistic polymer-encapsulation effects in the microenvironment of these catalyst systems.

1.3 General Background of CoPc-catalyzed CO_2RR

The electrocatalytic carbon dioxide reduction reaction (CO_2RR) is an important strategy to both convert industrial waste CO_2 into value-added products and store renewable energy from intermittent sources in the form of chemical precursors or fuels.[3-9] A major challenge is that the CO_2RR can produce numerous products, including H_2, from the competing hydrogen evolution reaction (HER), leading to downstream separations issues.[10-13] One method to improve selectivity for specific CO_2RR products while maintaining high activity is to use membrane-coated electrocatalysts (MCECs). Our group and others have reviewed the impacts of MCECs on the CO_2RR, which include preventing catalyst poisoning, improving substrate concentration near the electrode, and promoting selective transport of substrate and/or products.[14-16] Another strategy for developing highly active and selective electrocatalysts is the heterogenization of traditionally homogeneous molecular catalysts.[17,18] A specific case is that of heterogenized molecular catalysts incorporated *within* a MCEC film via 3D and extended structures, such as a metal organic framework (MOF) or porous polymer, where the formation of chemically linked, rigid networks also has the benefit of reducing catalyst aggregation.[19,20]

One molecular catalyst that has been heterogenized frequently for the CO_2RR is cobalt phthalocyanine (CoPc). CoPc was first reported for the CO_2RR in the 1970s,[21] and has been shown to operate with moderate activity and reaction selectivity with a Faradaic efficiency of approximately 35-60% for CO production (FE_{CO}) over the competing HER in aqueous phosphate buffer when coated onto a planar carbon electrode.[22,23] More recently, it has been reported that CoPc can catalyze the reduction of CO_2 to formic acid and methanol under specific conditions,[24-26] making CoPc one of the only molecular catalysts capable of reducing CO_2 to highly-reduced products. In addition, the activity and stability of CoPc-based system can be tuned by modulating

the electronic structure of the system through axial coordination[27] and/or synthetic modification of the Pc ring.[26,28] For these reasons, CoPc one of the most promising and well-studied CoN_4 porphyrinoid catalyst for the CO_2RR.

Polymer encapsulation has been considered a method for CoPc heterogenization since the first report of CO_2RR by CoPc, where the authors demonstrated that using polystyrene as a binding agent decreased activity compared to that of the parent CoPc complex.[21] Kaneko and coworkers used polymer encapsulation within putative hydrophobic polymers to improve the selectivity of molecular CO_2RR electrocatalysts in aqueous electrolytes,[29,30] and showed that encapsulating CoPc within poly(4-vinylpyridine) (P4VP) enhanced the selectivity for CO_2 reduction to CO over the competitive HER.[31-34] In Table 1.1 is summarized a few recent studies of the turnover frequency for the CO_2RR to CO by heterogenized CoPc prepared and related Co porphyrinoid materials prepared with different binders and supports and measured in various electrolyte conditions.

Table 1.1. A few recent studies of CoPc and related Co-porphynrinoid materials for the CO_2RR, along with their corresponding turnover frequency (TOF) for CO production.

Catalyst	Electrode	Polymer or Binder	Electrolyte (pH)	Potential / V vs. RHE	TOF_{CO} / s^{-1}	Ref
CoPc	Edge-Plane Graphite (EPG)	N/A	0.1 M NaH_2PO_4 (4.7)	−0.73	1.1	[35]
CoPc-P4VP	Edge-Plane Graphite (EPG)	P4VP	0.1 M NaH_2PO_4 (4.7)	−0.73	4.2	[35]
CoPc-P4VP/Graphite Powder	Glassy Carbon (GCE)	P4VP	0.1 M NaH_2PO_4 (4.7)	−0.73	3.1	[36]
CoPc/CNTs	Carbon Paper	Nafion	0.5 M $NaHCO_3$ (7.3)	−0.67	4.1	[37]
CoPc/CNTs	Carbon Paper	Nafion	0.1 M $NaHCO_3$ (6.8)	−0.63	4.1	[38]
Cobalt Protoporphyrin/CNT (CoPP)	Carbon Paper	Nafion	0.5 M $NaHCO_3$ (7.3)	−0.65	2.1	[39]
Cobalt Tetraphenyl Porphyrin/CNT (CoTPP)	Glassy Carbon (GCE)	None	0.5 M $NaHCO_3$ (7.2)	−0.68	2.7	[40]
Covalent Organic Framework COF-36-Co(1%)	Carbon Fabric	None	0.5 M $NaHCO_3$ (7.3)	−0.67	2.6	[41]

Although many researchers use polymers as binding agents for adhering catalysts to surfaces, relatively few studies have investigated the effects of polymer encapsulation on CO_2RR photocatalysts[17,42-47] and electrocatalysts.[43-45,48-51] The few studies that have considered these interactions include work by Koper and coworkers examining the impact of different encapsulating polymers on the CO_2RR performance of indium protoporphyrin (InPP);[48] studies by Grubbs, Gray, and coworkers examining the effect of brush polymer ion gels on the activity of Re-based CO_2RR molecular electrocatalysts;[49,50] and Reisner and coworkers tuning the CO:H_2 product ratio in a series of polymer-catalyst materials by tuning the hydrophobicity of the polymer moieties.[51]

Our research interests have focused on understanding the specific influence of P4VP polymers on the activity of CoPc in CoPc-P4VP composite polymer-catalyst systems. We have shown that CoPc-P4VP operates with a ~4-fold enhancement in CO_2RR activity compared to the parent CoPc, and with nearly quantitative Faradaic Efficiency for CO production ($FE_{CO} \approx 100\%$) compared to the parent CoPc which operates with $FE_{CO} \approx 60\%$. Our work has focused on understanding the reason for this increased activity and selectivity of CoPc upon encapsulation by P4VP by testing three core hypotheses regarding polymer-catalyst interactions (Figure 1.1 CoPc encapsulated by P4VP, showing the axial coordination of pyridyl residues of the polymer (primary coordination sphere effect), the H-bond stabilizing the reactive intermediate (secondary coordination sphere effect), and the proton relay by the pyridyl residues of the polymer (outer coordination sphere effect). Figure reproduced with permission from Ref. [53]. Copyright 2020 Royal Society of Chemistry.): (1) pyridyl moieties from the polymer axially coordinate to the cobalt center, increasing affinity for CO_2 coordination and reduction; (2) partially protonated pyridyl moieties from P4VP provide secondary coordination sphere effects via hydrogen bonding;

and (3) proton delivery in P4VP is controlled by a multisite proton relay involving the polymer pyridyl moieties.[52]

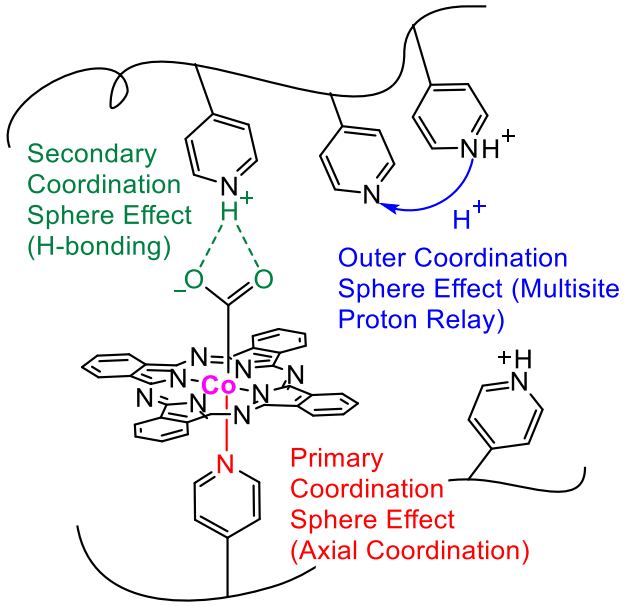

Figure 1.1 CoPc encapsulated by P4VP, showing the axial coordination of pyridyl residues of the polymer (primary coordination sphere effect), the H-bond stabilizing the reactive intermediate (secondary coordination sphere effect), and the proton relay by the pyridyl residues of the polymer (outer coordination sphere effect). Figure reproduced with permission from Ref. [53]. Copyright 2020 Royal Society of Chemistry.

Here, we highlight our studies of CoPc-P4VP and related systems that provide evidence supporting our three core hypotheses. In particular, we focus on how ligand-sphere effect and substrate transport impact the activity and selectivity of CoPc-P4VP compared to the parent CoPc system. In addition, we explore how charge transport and the incorporation of a carbon support influences the catalytic activity and mechanism for CoPc-P4VP and other systems. We conclude by discussing these results in the context of the broader research areas of polymer effects on molecular and solid-state electrocatalysis. We also briefly consider how these insights may be applied to solving challenges in implementing industrial CO_2RR via gas-fed electrolyzers.

1.4 Ligand Sphere Effects: Primary and Secondary Coordination Sphere

In our first studies of polymer-encapsulated CoPc, we concluded that axial coordination of pyridyl residues from the P4VP polymer in the CoPc-P4VP composite film was crucial to the increased activity and selectivity of CoPc-P4VP for the CO_2RR compared to the CoPc parent system.[35,52] This conclusion was based on experiments that explored how systematic modifications to the catalyst-polymer system influenced catalytic activity as determined by the turnover frequency for CO production per CoPc catalyst (TOF_{CO}) and selectivity as determined by the Faradaic Efficiency for CO production (FE_{CO}) (Figure 1.2). The 5-coordinate CoPc(py) complex with no polymer and an axially coordinated pyridine reduces CO_2 with a modest increase in activity and selectivity compared to the parent CoPc complex. In contrast, encapsulating CoPc with the non-coordinating P2VP polymer results in no increase in CO_2RR activity and a modest increase in selectivity compared to CoPc. Combining these effects in the CoPc(py)-P2VP system results in a large increase in CO_2RR activity and selectivity, as observed with CoPc-P4VP. We interpreted these results to suggest that 1) axial coordination in the primary coordination sphere is crucial for the observed enhanced activity and 2) this influence of the axial coordination works synergistically with other effects imbued by the polymer to achieve the enhanced activity and selectivity observed in CoPc(py)-P2VP and CoPc-P4VP.[52]

To confirm that the pyridyl residue of the P4VP was indeed axially coordinating to the CoPc molecule, we performed *in situ* X-ray Absorbance Near-Edge Structure (XANES) measurements (Figure 1.3).[53] CoPc exhibits a strong 1s-4p pre-edge peak at ~7716 eV (Figure 3a), characteristic of macrocyclic square planar Co complexes.[54,55] Conversion of the metal center into a square pyramidal geometry leads to a dramatic decrease in peak intensity,[55] as observed for CoPc(py) and CoPc-P4VP (Figure 1.3b-c). This loss of the 1s-4p pre-edge peak intensity is not

observed for CoPc-P2VP in the non-coordinating P2VP polymer,[53] so we interpret these results to mean that the pyridyl residues in P4VP axially-coordinate to the Co center in CoPc-P4VP, as hypothesized in Figure 1.1. Notably, applying reducing or oxidizing potentials does not appreciably change the intensity of the 1s-4p pre-edge peak, suggesting the polymer remains coordinated even under CO_2RR conditions. The *in situ* XANES measurements also provided insight regarding the site of reduction (ligand-centered vs. metal-centered), interpreted from shifts in the Co K-edge as a function of applied potential. In particular, for CoPc(py) and CoPc-P4VP, there is a shift in the Co K-edge upon reduction at -1.25 V vs SCE that is not observed for CoPc. This suggests that the first reduction of the 5-coordinate CoPc(py) and CoPc-P4VP systems have a significant metal character, different from the 4-coordinate parent compound, which undergoes ligand-based reductions.

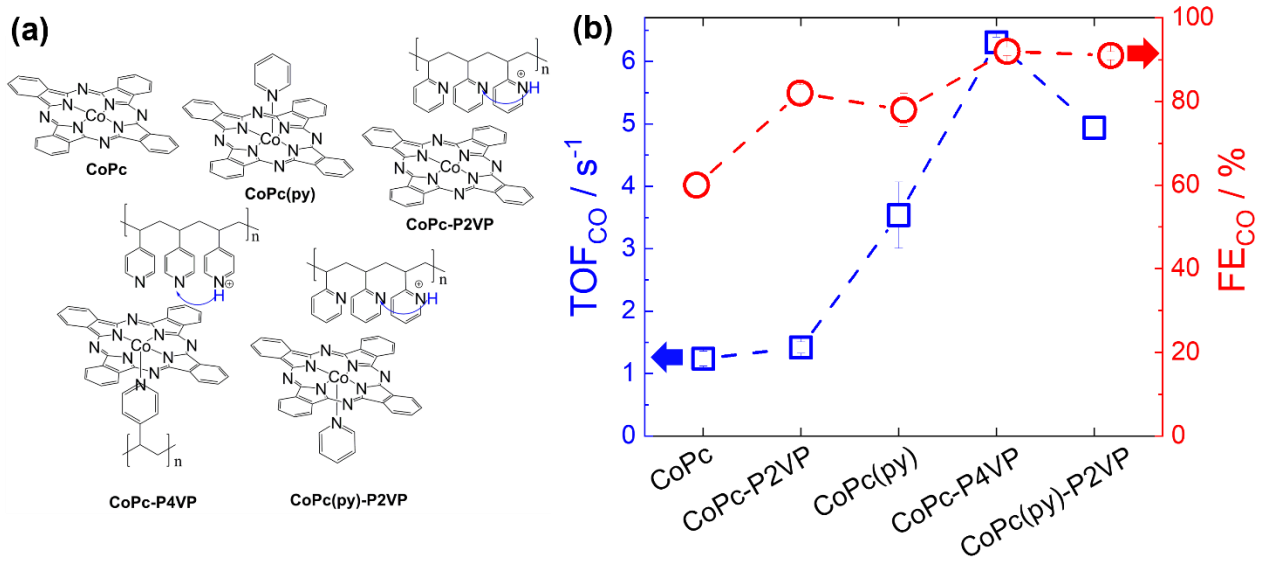

Figure 1.2**.** (a) Different combinations of the parent complex CoPc with polymers and ligands discussed herein, along with the proposed coordination environment and proton transport mechanism. Adapted with permission from Ref. [35]. Copyright 2019 Liu, Y. and McCrory, C.C.L. Published by Springer Nature under a Creative Commons CC BY 4.0 license http://creativecommons.org/licenses/by/4.0. (b) The turnover frequency (TOF_{CO}) and Faradaic Efficiency (FE_{CO}) for CO production of each catalyst-polymer composites. Data from Ref. [35].

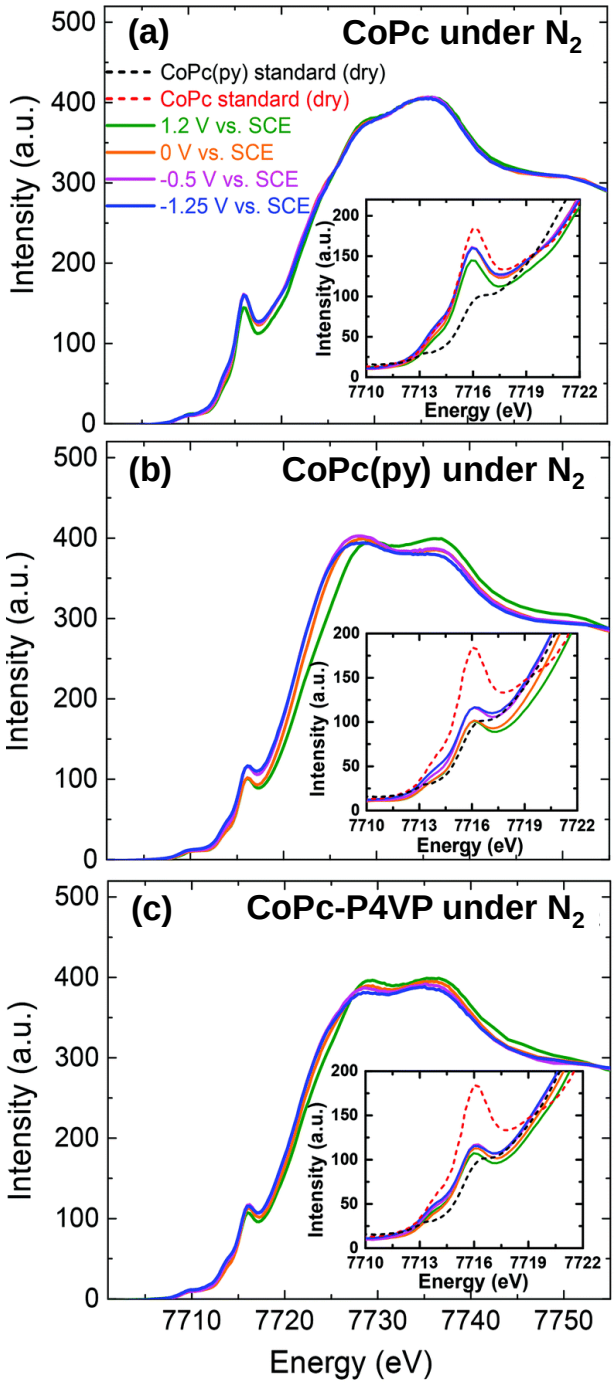

Figure 1.3 X-ray absorbance near edge structure (XANES) measurements at different applied potentials under N_2 of (a) CoPc, (b) CoPc(py), and (c) CoPc-P4VP. The insets show the 1s-4p pre-edge peak used to determine whether the system is primarily 4-coordinate or 5-coordinate. Figure reproduced with permission from Ref. [53]. Copyright 2020 Royal Society of Chemistry.

We hypothesized that coordination of an axial ligand to the CoPc increases the electron density on the metal center, thereby increasing the metal site nucleophilicity and its ability to coordinate and activate CO_2. Thus, the increased electron density on the Co site ultimately results in increased activity for the CO_2RR. Axial coordination also increases the selectivity for the CO_2RR over competitive HER—CoPc(py) operates with FE_{CO} ~ 75% compared to CoPc with FE_{CO} ~ 60% (Figure 1.2).[35,52] This increased reaction selectivity for CoPc(py) suggests that the postulated increased binding affinity for CO_2 by 5-coordinate CoPc(py) compared to CoPc causes a change in the rate-determining step (RDS) of the mechanism. Two proposed mechanisms for CO_2 reduction by CoPc are shown in Figure 1.4a. In both mechanisms, the CO_2 binding step (i) is the selectivity-determining step between the CO_2RR and competitive HER pathways. A change in the RDS from CO_2 binding (i) to a subsequent proton-transfer step (ii) upon axial coordination leads to a decreased retention of the reduced CoPc intermediate, thus decreasing the likelihood of the system to continue down the HER pathway and resulting in the observed increase in FE_{CO} for CoPc(py) compared to CoPc. This change in RDS was further confirmed through kinetic isotope effect (KIE) studies in which the aqueous buffer and water were replaced with their deuterated analogues.[35] For 5-coordinate CoPc(py), CoPc-P4VP, and CoPc(py)-P2VP, a KIE ≈ 3 is observed, which is consistent with a proton transfer event in the RDS. In contrast, for 4-coordinate CoPc and CoPc-P2VP, a KIE = 1 is observed, which suggests the RDS of the 4-coordinate species does not include a proton-transfer event. These KIE results support our hypothesis that axial coordination to the CoPc center changes the RDS from CO_2 binding to a subsequent protonation event, which in turn is responsible for the increased reaction selectivity of CoPc(py) for the CO_2RR over the HER. Note that the smaller KIE ≈ 2 for CoPc-P4VP and CoPc(py)-P2VP compared to KIE ≈ 3

for CoPc(py) is a consequence of the proton transfer mechanism within the encapsulating polymer and is discussed in detail in Section 1.5.

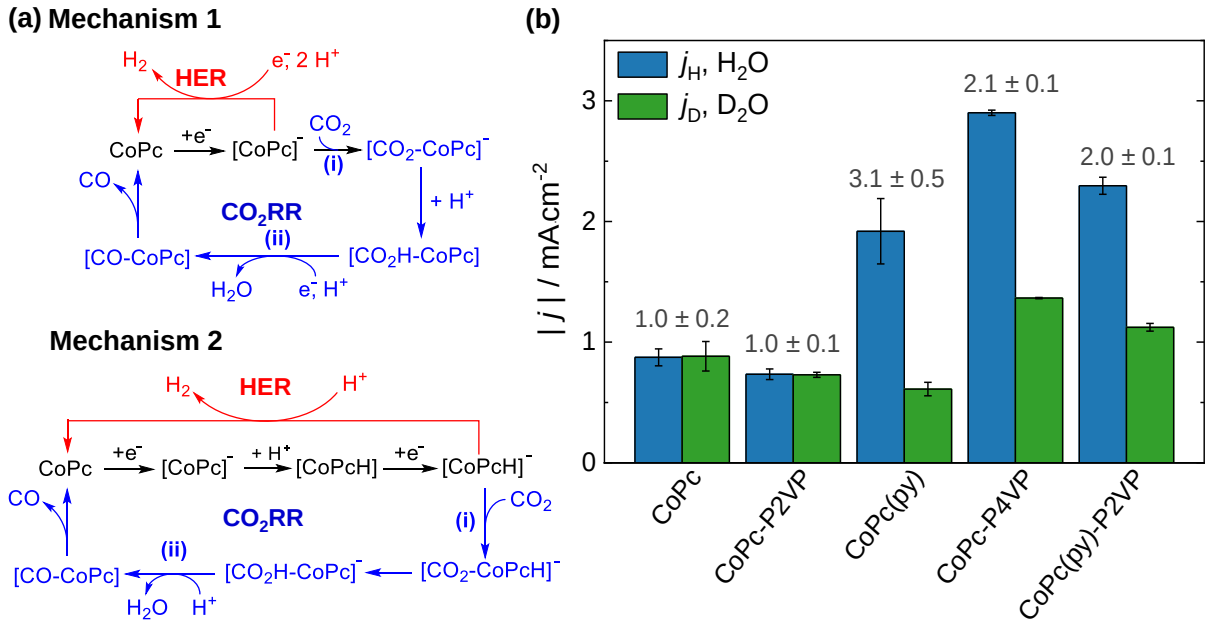

Figure 1.4 (a) Two proposed mechanisms of CoPc-catalyzed CO_2 reduction. In both mechanisms, CO_2 binding (i) is the selectivity-determining step between the HER and CO_2RR pathways and is a possible rate-determining step (RDS). The subsequent proton-transfer step (ii) is also a possible RDS. Adapted with permission from Ref. 4. Copyright 2021 American Chemical Society. (b) Measured current densities for CO_2 reduction by CoPc-polymer composites exposed to protonated and deuterated electrolytes at pH/pD = 4.7 under 1 atm of CO_2. The KIE is listed above each bar graph. Adapted with permission from Ref. [35]. Copyright 2019 Liu, Y. and McCrory, C.C.L. Published by Springer Nature under a Creative Commons CC BY 4.0 license http://creativecommons.org/licenses/by/4.0.

In our initial study of CoPc-P4VP, we postulated that the increased electron density on the Co center from the axial coordination of the pyridyl moieties resulted in an increase in the energy of the dz^2 orbital of the Co center. Because the Co dz^2 orbital is geometrically most likely to interact with CO_2, we postulated that the increased energy of this orbital drive the increased ability of the 5-coordinate complex to bind and reduce CO_2.[52] The corollary to this hypothesis is that increasing the σ-donor ability of the axial ligand will further increase the energy of the dz^2 orbital, and further increase the activity for the CO_2RR. In a combined experimental and computational study, we showed that increasing the σ-donor ability of the axial ligand (L) results in an increase in the CO_2RR activity by CoPc(L) (Figure 5).[27] Computational studies confirmed that the strength of the σ-donor ability was correlated with the relative energy of the dz^2 orbitals, that the HOMO of the pertinent reduced $[CoPc(L)\text{-}CO_2]^-$ involves an interaction between the dz^2 orbital and the CO_2 adduct, and that Mechanism 1 in Figure 1.4a is likely the operative mechanism under our CO_2RR conditions.[27]

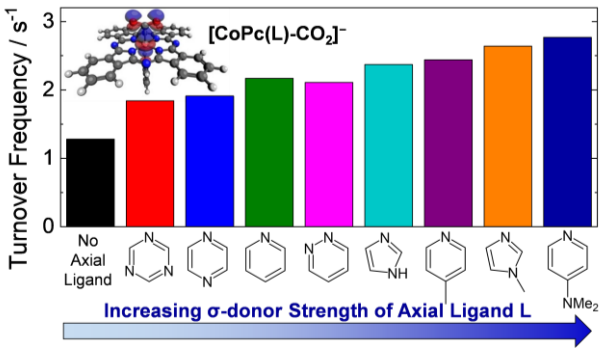

Figure 1.5 Turnover frequency for CO production for CoPc(L) with various axial ligands L. Activity increases as a function of σ-donor strength of the axially coordinating ligand. The calculated HOMO of the reduced CO_2 adduct from Mechanism 1 for CoPc(L8) is shown in the inset, highlighting the interaction between CO_2 and the Co dz^2 orbital. Adapted with permission from Ref. [27]. Copyright 2021 American Chemical Society.

In our studies of the polymer-encapsulated CoPc systems, we have been unable to isolate the secondary coordination sphere effects from other polymer effects. However, the increased activity of CoPc-P4VP and CoPc(py)-P2VP compared to CoPc(py) provide circumstantial support for the role of secondary-coordination sphere effects in enhancing catalytic activity. Moreover, it is well established that secondary coordination sphere effects play an important role in enzymatic systems—for example, interactions from proximal histidine and lysine residues near the active site of carbon monoxide dehydrogenase stabilize catalytic intermediates and facilitate reversible conversion between CO and CO_2.[56-61] These same effects have been observed in numerous molecular electrocatalysts for the CO_2RR and have been reviewed elsewhere.[62-68] In one representative example, Jiang and coworkers showed that iron(tetraphenylporpyrin) (FeTPP) catalysts with appended polymeric poly(ethylene glycol) (PEG) chains show enhanced activity for the CO_2RR by establishing an H-bonding network that stabilizes reduced CO_2 intermediates at the Fe site.[69,70] In another example, Shafaat and coworkers demonstrated that cationic buffers facilitate enhanced CO_2 reduction activity at Ni(cyclam) catalysts, and this increased activity is attributed to the ability of cationic buffers to form pseudo-secondary coordination spheres near the catalyst that functionally mimic the secondary coordination sphere effects of native enzymes.[71] Solid-state systems also experience these types of secondary-coordination sphere effects, where CO_2 activation is facilitated through stabilization of reactive intermediates by functional groups from polymers coating the catalyst surface.[14,72-77] For example, Kenis, Zimmerman, Gewirth and coworkers showed that polyamine-encapsulated Cu nanoparticles enhances electrocatalytic activity for CO_2 reduction to ethylene due to the stabilization of reduced CO_2 intermediates through H-bonding and electrostatic stabilization.[72] Thus, although we were not able to distinguish unambiguously secondary coordination sphere effects in the case of CoPc-P4VP, it is likely that

these effects play an essential role in polymer-catalyst composite systems based on literature precedent.

Importantly, these polymer ligand-sphere effects are not universally applicable to every polymer-catalyst composite system, and consideration must be taken to optimize the interactions between the polymer, catalyst, and catalytic intermediates. The need for correct polymer-catalyst synergy was demonstrated convincingly by Koper and coworkers, who systematically studied the activity and selectivity of indium protoporphyrin (InPP) encapsulated by a series of different polymers (Figure 1.6).[48] Electrodes with adsorbed InPP encapsulated in coordinating polymers such as P4VP and poly-(3,4-ethylenedioxythiophene) polystyrenesulfonate (PEDOT:PSS) operated with higher CO_2RR activity, selectivity, and stability compared to systems with adsorbed InPP encapsulated within non-coordinating polymers such as didodecyldimethylammonium bromide (DDAB) and Nafion, or InPP adsorbed on the surface with no polymer (Figure 1.6b). The coordination of the polymer to InPP is thought to help adhere the catalyst to the surface in the case of P4VP and PEDOT:PSS, and the secondary and outer coordination sphere environments are thought to help drive the activity and selectivity for the CO_2RR. This study suggests that the interactions between the polymer and catalysts must be carefully considered when designing catalyst-polymer composite materials.

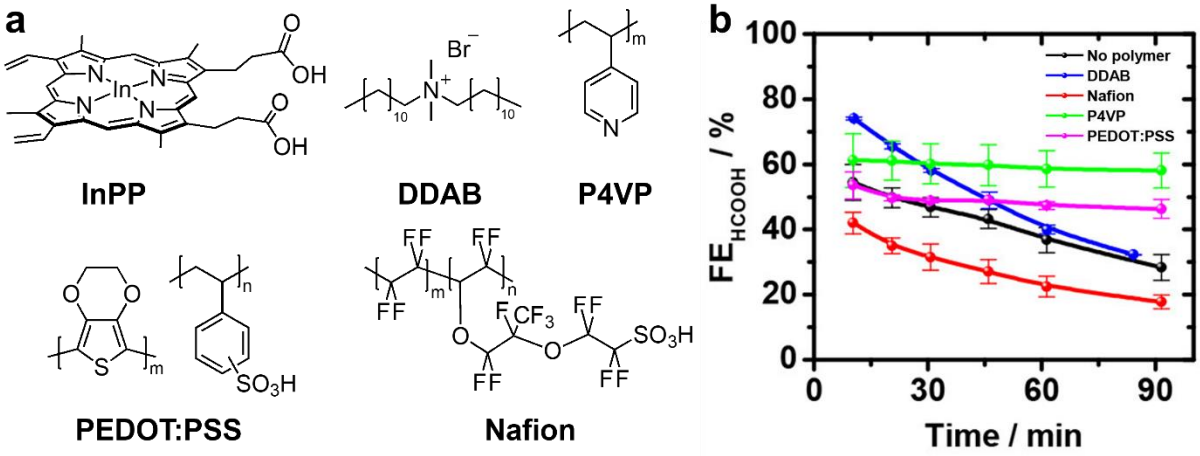

Figure 1.6 (a) Koper and coworkers explored the activity, selectivity, and stability of the CO_2RR electrocatalyst indium protoporphyrin (InPP) encapsulated in the polymers shown here. (b) InPP encapsulated in P4VP and PEDOT:PSS operated with higher Faradaic efficiency for HCOOH production compared to the non-coordinating DDAB polymer and Nafion. Adapted with permission from Ref. [48]. Copyright 2018 American Chemical Society.

1.5 Proton Transport within Polymer-Catalyst Systems

Encapsulating polymers are often used to increase the hydrophobicity surrounding the catalyst, thereby enhancing CO_2RR selectivity by suppressing competitive HER.[51,72] For example, Kaneko and coworkers showed that incorporating various Re- and Co-based molecular catalysts within Nafion enhanced their activity for the CO_2RR over competitive HER due to the relative hydrophobicity of Nafion exposed to pH 7 electrolyte under their catalytic conditions.[29,30] Notably, Kaneko and coworkers also suggest that controlled proton transport plays an important role in the enhanced CO_2RR selectivity of CoPc-P4VP compared to the parent CoPc complex.[31-34] In a more recent study, Reisner and coworkers showed that appending Co(terpyridine)-based molecular catalysts to hydrophobic polymers results in enhanced CO_2RR selectivity due to suppression of proton transport and reduction.[51]

After our initial study of CoPc-P4VP for the CO_2RR,[52] we became interested in understanding better the mechanism of proton transport in the polymer-catalyst system. In particular, we hypothesized that proton transport might occur via a multisite proton relay, similar to those frequently proposed in enzymatic and bioinspired systems.[78-82] To test this hypothesis, we conducted a series of proton inventory studies, a technique in which the attenuation in activity is measured as a function of the fractional deuteration of the system.[82-87] Specifically, we measured the relative current densities of various CoPc-polymer systems in the partially-deuterated electrolyte (j_n) compared to the current densities in a fully protonated electrolyte (j_0), and then plotted this ratio as a function of the fractional deuteration of the electrolyte (n_{D2O}) where n_{D2O} = 1 is fully deuterated and n_{D2O} = 0 is fully protonated (Figure 7).[35] For systems in which the rate-determining step (RDS) does not involve a proton transfer event such as CoPc and CoPc-P2VP,

KIE = 1 and so there is no attenuation of activity at any level of deuteration, and we cannot use this technique to describe proton transport.

For systems where the RDS involves a proton transfer event such as CoPc(py), CoPc(py)-P2VP, and CoPc-P4VP, the shape of the curve in Figure 7a provides information about the proton relay mechanism. For CoPc(py), the linear curve is consistent with a normal kinetic isotope effect involving a single hydrogenic site in the RDS.[88,89] However, for CoPc(py)-P2VP and CoPc-P4VP, the non-linear dome-shaped response of the relative activity as a function of fractional electrolyte deuteration is consistent with a normal isotope effect at a single hydrogenic site in the RDS preceded by an aggregate inverse isotope effect involving multiple hydrogenic sites on the polymer.[84,90] This aggregate inverse isotope effect is also responsible for the decrease in the KIE from KIE ~ 3 for CoPc(py) to KIE ~ 2.1 for CoPc-P4VP and CoPc(py)-P2VP. We interpret these results as evidence that proton delivery in the P2VP- and P4VP-encapsulated systems occur via a multisite proton relay involving the pyridyl residues on the polymer.[35] Importantly, the proton relay effect in the polymer-encapsulated systems is only observed in polymers with a protonatable moiety. For example, immobilizing CoPc(py) in polystyrene (CoPc(py)-PS) results in a linear curve and KIE ~ 3 similar to that of CoPc(py) in the absence of polymer (Figure 1.7b). To our knowledge, this study was the first example using proton inventory measurements to provide evidence for the existence of a multisite proton-relay effect in a synthetic electrocatalytic system.

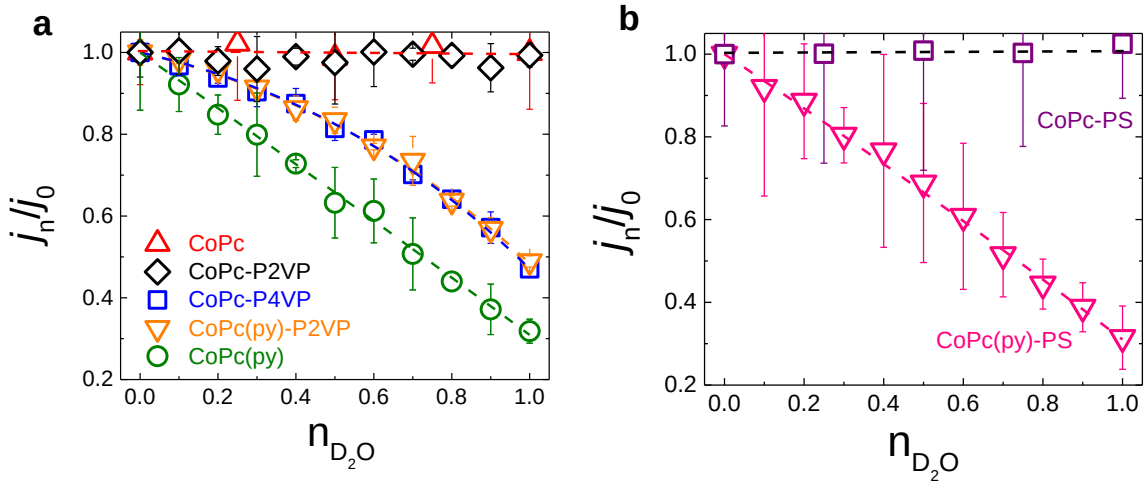

Figure 1.7 (a) Proton-inventory studies for CoPc, CoPc-P2VP, CoPc-P4VP, CoPc(py)-P2VP, and CoPc(py) and (b) CoPc-Ps and CoPc(py)-PS. Adapted with permission from Ref. [35]. Copyright 2019 Liu, Y. and McCrory, C.C.L. Published by Springer Nature under a Creative Commons CC BY 4.0 license http://creativecommons.org/licenses/by/4.0.

Somewhat related to the transport of protons through the polymer film via a proton relay is developing a comprehensive understanding of the mechanism and rate of substrate and electron transport to electrocatalyst sites. In electrochemistry, where electrochemical transformations must occur near the surface of the electrode, understanding the transport of these species is crucial for rationally designing new polymer-catalyst composite films. Transport and activity in polymer-catalyst composite films can be described by a combination of five interdependent rates, expressed as currents, since the net measured current is directly proportional to a rate of reaction:[91-96] *(1)* i_A, the rate of transport of substrate through the electrolyte solution to the film, (2) i_S, the rate of transport of substrate within the polymer film to the catalyst, (3) i_p, the rate of substrate transport across the polymer/electrolyte interface, (4) i_E, the rate of electron transport through the film to the randomly-distributed catalysts, and (5) i_K, is the rate of the catalytic transformation and is not dependent on transport. Although exact relationship between these five rates and measured catalytic activity is complicated,[91-96] better understanding how each of these rates contributes to overall activity of polymer-composite electrocatalysts will inform the design of new, more active materials for the CO_2RR.

1.6 Charge Transport and Carbon Supports

As one considers integrating polymer-catalyst composites into electrochemical reactors, it is crucial to consider not only controlling substrate transport, but also maintaining efficient charge transport.[20,49] The incorporation of carbon supports into the polymer-catalyst system is a common strategy for increasing charge transport in CoPc-based catalyst-polymer composites for the CO_2RR.[25,26,38,97,98] In some cases, incorporation of specific carbons supports have resulted in new product formation—both Wang and coworkers and Robert and coworkers demonstrated that CoPc immobilized ofnto multiwalled carbon nanotubes (MWCNTs) with a Nafion film reduce CO_2 to CH_3OH via a cascade catalysis mechanism,[25,26] but that this product selectivity is not seen when CoPc is immobilized onto other supports.[26] The unique product selectivity of CoPc on MWCNTs may arise from perturbations of the electronic structure of CoPc that arises from π-stacking interactions between the phthalocyanine ring and the carbon nanotubes.[98]

Chapter 2 will discuss our work in this area has focused on studying how incorporating graphite powder (GP) within CoPc-P4VP systems influences the performance of these systems for the CO_2RR .[36] Importantly, it is not enough simply to mix the CoPc-P4VP and GP together—doing so results in no enhancement of activity upon the addition of GP. Instead, it is crucial to develop deposition procedures that facilitate interaction between the CoPc and GP supports. When no GP is present, we observe no appreciable change in activity for CoPc-P4VP as a function of catalyst film loading, suggesting that only a small constant amount of CoPc near the electrode surface is active for CO_2RR due to inefficient charge transport within the film.

When moderate loadings of GP (0.26 mg cm^{-2}) are incorporated into the CoPc-P4VP film using our optimized deposition procedure, we observe significantly higher activity for the CO_2RR, suggesting that incorporation of GP increases the effective distance of charge transport within the film and, thus, increases the number of CoPc sites that are active. However, as we increase the film loading while holding the GP loading constant, we observe a corresponding decrease in activity. We interpret this result to suggest that the GP particles are spaced further apart in the thicker catalyst films, thus decreasing the effective charge transport. CoPc sites near the exterior of the polymer film have reduced activity due to this inefficient charge transport in the thicker polymer films with only moderate GP loadings.

At sufficiently high loadings of GP (0.51 mg cm^{-2}), the activity increases and then plateaus as a function of increasing catalyst film loading. This suggests that charge transport is not limiting at these high GP loadings, and instead, catalytic activity is limited by another parameter—possibly inefficient substrate transport to interior sites or CoPc aggregation at high catalyst loadings. Note that aggregation is particularly problematic for CO_2RR systems based on CoPc due to the molecule's high propensity to aggregate because of the strong π-π interactions between CoPc molecules. CoPc aggregation has been specifically linked to decreased activity in polymer-catalyst systems at high loadings.[19] In nanoparticulate systems, deleterious aggregation can be mitigated through polymer encapsulation in some studies.[99,100] We are currently exploring whether polymer encapsulation can be similarly used to control the extent of aggregation in CoPc-P4VP and related systems.

1.7 Outlook

The McCrory lab members have focused on understanding how encapsulating catalysts within coordinating polymers influences the chemical microenvironment surrounding the catalyst active site and influences the activity and reaction selectivity for the CO_2 reduction reaction (CO_2RR). In particular, we have extensively studied the influence of primary, secondary, and outer-coordination spheres of encapsulating poly-(4-vinylpyridine) (P4VP) polymers on the CO_2RR activity of cobalt phthalocyanine (CoPc) and shown that these ligand fields and proton transport effects work synergistically to increase the activity and selectivity of CoPc-P4VP and related systems for the CO_2RR. We have also begun to explore the extent to which the incorporation of carbon supports influences the chemical microenvironment around the CoPc site and overall CO_2RR activity and selectivity.

The insights gained from using CoPc as a model catalytic system have ultimately led to interesting considerations for future catalyst development for the CO_2RR and other relevant electrocatalytic small-molecule transformations. Specifically, the use of coordinating polymers to modulate the chemical microenvironment in every coordination sphere—axial coordination to the metal centers, secondary coordination sphere effects, and controlled proton delivery to catalyst active sites—has been shown effective in promoting reaction selectivity, and this strategy can be adapted to other catalytic systems. We note that the identity the polymers used in catalyst-polymer composite systems should be carefully considered for optimal effectiveness, as shown in examples where encapsulating catalyst within polymers such as P2VP and Nafion does not result in optimal activity or selectivity.

Most of the studies discussed in this introduction (and certainly all studies performed within this dissertation) were conducted using an electrolysis cell in which CO_2 is delivered to the

electrode from a CO_2-saturated aqueous solution via convection of a stirbar or via diffusion with rotation with the use of rotating disk electrode setups. However, practical gas-fed CO_2 electrolyzers typically incorporate gas diffusion electrodes (GDEs) that dramatically enhance the maximum CO_2RR rate by delivering gaseous CO_2 directly to the catalyst, but many GDEs use a polymer to maintain a triple-phase boundary where the gaseous CO_2, protons from aqueous electrolyte, and the electron come together to perform the CO_2RR.[101-103] In future studies, we propose that applying the lessons learned from polymer-catalyst composite designs on the small scale may be useful when optimizing catalyst-polymer composites that may be used for these reactor systems, including looking to rethink and expand the role of binding polymers.[8,101-106] Next-generation polymer architectures that incorporate multiple synergistic functionalities could be an effective strategy for optimizing device performance. Polymer blends, copolymers with different functional blocks, electropolymerized catalysts, and multilayered structures all merit further investigation. Together, these advances could radically improve the performance of CO_2RR electrolyzers and push them into the realm of commercial viability.

The contents of this dissertation delve into the transport of protons and electrons in a polymer-encapsulated cobalt phthalocyanine system for electrocatalytic transformations – specifically the CO_2RR and the HER. In Chapter 2, I discuss the method development for the addition of graphite powder into the CoPc-polymer complex, which showed enhanced charge transport and therefore activity. In Chapter 3, I discuss the modulation of the electrolyte pH and its impacts on CO_2RR activity, selectivity, and rate-determining step as measured by the kinetic isotope effect. Additionally, I discuss the impact of electrolyte concentration on the fractional protonation of the polymer layer, which has consequences for the measured kinetic isotope effect, especially with regards to the hydrogen evolution reaction (HER). In Chapter 4, I show that

incorporating styrene moieties into the copolymer shut down activity by impacting proton transport and the possible loss of axial coordination from the pyridyl residues in the polymer, and how other polymers could also provide the positive effects of encapsulation that are seen with the encapsulation of CoPc by P4VP.

The insights from this work have consequences for similar membrane coated electrode systems where small molecule electrochemical conversions take place. Additionally, the understanding of charge and proton transport of these systems could be translated to lab-scale CO_2 electrolyzers where conductive carbon supports and polymer binders are used in the gas diffusion electrodes of those devices.

1.8 References

(1) Soucy, T. L.; Dean, W. S.; Zhou, J.; Rivera Cruz, K. E.; McCrory, C. C. L. "Considering the Influence of Polymer–Catalyst Interactions on the Chemical Microenvironment of Electrocatalysts for the CO2 Reduction Reaction," *Accounts of Chemical Research* **2022**. http://dx.doi.org/10.1021/acs.accounts.1c00633

(2) Liu, Y.; Leung, K. Y.; Michaud, S. E.; Soucy, T. L.; McCrory, C. C. L. "Controlled Substrate Transport to Electrocatalyst Active Sites for Enhanced Selectivity in the Carbon Dioxide Reduction Reaction," *Comments on Inorganic Chemistry* **2019**, *39*, 242-269. http://dx.doi.org/10.1080/02603594.2019.1628025

(3) Verma, S.; Kim, B.; Jhong, H.-R. M.; Ma, S.; Kenis, P. J. A. "A Gross-Margin Model for Defining Technoeconomic Benchmarks in the Electroreduction of CO2," *ChemSusChem* **2016**, *9*, 1972-1979. http://dx.doi.org/https://doi.org/10.1002/cssc.201600394

(4) Nocera, D. G. "Solar Fuels and Solar Chemicals Industry," *Accounts of Chemical Research* **2017**, *50*, 616-619. http://dx.doi.org/10.1021/acs.accounts.6b00615

(5) Spurgeon, J. M.; Kumar, B. "A comparative technoeconomic analysis of pathways for commercial electrochemical CO2 reduction to liquid products," *Energy & Environmental Science* **2018**, *11*, 1536-1551. http://dx.doi.org/10.1039/C8EE00097B

(6) De Luna, P.; Hahn, C.; Higgins, D.; Jaffer, S. A.; Jaramillo, T. F.; Sargent, E. H. "What would it take for renewably powered electrosynthesis to displace petrochemical processes?," *Science* **2019**, *364*, eaav3506. http://dx.doi.org/10.1126/science.aav3506

(7) Crabtree, R. H. "Alternate Strategies for Solar Fuels from Carbon Dioxide," *ACS Energy Letters* **2020**, *5*, 2505-2507. http://dx.doi.org/10.1021/acsenergylett.0c01359

(8) Jin, S.; Hao, Z.; Zhang, K.; Yan, Z.; Chen, J. "Advances and Challenges for the Electrochemical Reduction of CO2 to CO: From Fundamentals to Industrialization," *Angewandte Chemie International Edition* **2021**, *60*, 20627-20648. http://dx.doi.org/https://doi.org/10.1002/anie.202101818

(9) Senftle, T. P.; Carter, E. A. "The Holy Grail: Chemistry Enabling an Economically Viable CO2 Capture, Utilization, and Storage Strategy," *Accounts of Chemical Research* **2017**, *50*, 472-475. http://dx.doi.org/10.1021/acs.accounts.6b00479

(10) Whipple, D. T.; Kenis, P. J. A. "Prospects of CO2 Utilization via Direct Heterogeneous Electrochemical Reduction," *The Journal of Physical Chemistry Letters* **2010**, *1*, 3451-3458. http://dx.doi.org/10.1021/jz1012627

(11) Nitopi, S.; Bertheussen, E.; Scott, S. B.; Liu, X.; Engstfeld, A. K.; Horch, S.; Seger, B.; Stephens, I. E. L.; Chan, K.; Hahn, C.; Nørskov, J. K.; Jaramillo, T. F.; Chorkendorff, I. "Progress and Perspectives of Electrochemical CO2 Reduction on Copper in Aqueous Electrolyte," *Chemical Reviews* **2019**, *119*, 7610-7672. http://dx.doi.org/10.1021/acs.chemrev.8b00705

(12) Hori, Y.; Wakebe, H.; Tsukamoto, T.; Koga, O. "Electrocatalytic process of CO selectivity in electrochemical reduction of CO2 at metal electrodes in aqueous media," *Electrochimica Acta* **1994**, *39*, 1833-1839. http://dx.doi.org/https://doi.org/10.1016/0013-4686(94)85172-7

(13) Gattrell, M.; Gupta, N.; Co, A. "A review of the aqueous electrochemical reduction of CO2 to hydrocarbons at copper," *Journal of Electroanalytical Chemistry* **2006**, *594*, 1-19. http://dx.doi.org/https://doi.org/10.1016/j.jelechem.2006.05.013

(14) Liu, Y.; Leung, K. Y.; Michaud, S. E.; Soucy, T. L.; McCrory, C. C. L. "Controlled Substrate Transport To Electrocatalyst Active Sites For Enhanced Selectivity In The Carbon Dioxide

Reduction Reaction," *Comments Inorg. Chem.* **2019**, 1-28. http://dx.doi.org/10.1080/02603594.2019.1628025
(15) Esposito, D. V. "Membrane-Coated Electrocatalysts—An Alternative Approach To Achieving Stable and Tunable Electrocatalysis," *ACS Catalysis* **2018**, *8*, 457-465. http://dx.doi.org/10.1021/acscatal.7b03374
(16) Casado-Coterillo, C.; Marcos-Madrazo, A.; Garea, A.; Irabien, Á. "An Analysis of Research on Membrane-Coated Electrodes in the 2001–2019 Period: Potential Application to CO2 Capture and Utilization," *Catalysts* **2020**, *10*. http://dx.doi.org/10.3390/catal10111226
(17) Mak, C. H.; Han, X.; Du, M.; Kai, J.-J.; Tsang, K. F.; Jia, G.; Cheng, K.-C.; Shen, H.-H.; Hsu, H.-Y. "Heterogenization of homogeneous photocatalysts utilizing synthetic and natural support materials," *Journal of Materials Chemistry A* **2021**, *9*, 4454-4504. http://dx.doi.org/10.1039/D0TA08334H
(18) Costentin, C.; Robert, M.; Savéant, J.-M. "Molecular catalysis of electrochemical reactions," *Current Opinion in Electrochemistry* **2017**, *2*, 26-31. http://dx.doi.org/https://doi.org/10.1016/j.coelec.2017.02.006
(19) Corbin, N.; Zeng, J.; Williams, K.; Manthiram, K. "Heterogeneous molecular catalysts for electrocatalytic CO2 reduction," *Nano Research* **2019**, *12*, 2093-2125. http://dx.doi.org/10.1007/s12274-019-2403-y
(20) Costentin, C.; Savéant, J.-M. "Molecular approach to catalysis of electrochemical reaction in porous films," *Current Opinion in Electrochemistry* **2019**, *15*, 58-65. http://dx.doi.org/https://doi.org/10.1016/j.coelec.2019.03.014
(21) Meshitsuka, S.; Ichikawa, M.; Tamaru, K. "Electrocatalysis by metal phthalocyanines in the reduction of carbon dioxide," *Journal of the Chemical Society, Chemical Communications* **1974**, 158-159. http://dx.doi.org/10.1039/C39740000158
(22) Lieber, C. M.; Lewis, N. S. "Catalytic reduction of carbon dioxide at carbon electrodes modified with cobalt phthalocyanine," *Journal of the American Chemical Society* **1984**, *106*, 5033-5034. http://dx.doi.org/10.1021/ja00329a082
(23) Furuya, N.; Matsui, K. "Electroreduction of carbon dioxide on gas-diffusion electrodes modified by metal phthalocyanines," *Journal of electroanalytical chemistry and interfacial electrochemistry* **1989**, *271*, 181-191.
(24) Kapusta, S.; Hackerman, N. "Carbon Dioxide Reduction at a Metal Phthalocyanine Catalyzed Carbon Electrode," *J. Electrochem. Soc.* **1984**, *131*, 1511-1514. http://dx.doi.org/10.1149/1.2115882
(25) Boutin, E.; Wang, M.; Lin, J. C.; Mesnage, M.; Mendoza, D.; Lassalle-Kaiser, B.; Hahn, C.; Jaramillo, T. F.; Robert, M. "Aqueous Electrochemical Reduction of Carbon Dioxide and Carbon Monoxide into Methanol with Cobalt Phthalocyanine," *Angewandte Chemie International Edition* **2019**, *58*, 16172-16176. http://dx.doi.org/https://doi.org/10.1002/anie.201909257
(26) Wu, Y.; Jiang, Z.; Lu, X.; Liang, Y.; Wang, H. "Domino electroreduction of CO2 to methanol on a molecular catalyst," *Nature* **2019**, *575*, 639-642. http://dx.doi.org/10.1038/s41586-019-1760-8
(27) Rivera Cruz, K. E.; Liu, Y.; Soucy, T. L.; Zimmerman, P. M.; McCrory, C. C. L. "Increasing the CO2 Reduction Activity of Cobalt Phthalocyanine by Modulating the σ-Donor Strength of Axially Coordinating Ligands," *ACS Catal.* **2021**, *11*, 13203-13216. http://dx.doi.org/10.1021/acscatal.1c02379

(28) Wu, Y.; Hu, G.; Rooney, C. L.; Brudvig, G. W.; Wang, H. "Heterogeneous Nature of Electrocatalytic CO/CO2 Reduction by Cobalt Phthalocyanines," *ChemSusChem* **2020**, *n/a*. http://dx.doi.org/10.1002/cssc.202001396
(29) Yoshida, T.; Iida, T.; Shirasagi, T.; Lin, R.-J.; Kaneko, M. "Electrocatalytic reduction of carbon dioxide in aqueous medium by bis(2,2′: 6′,2″-terpyridine)cobalt(II) complex incorporated into a coated polymer membrane," *Journal of Electroanalytical Chemistry* **1993**, *344*, 355-362. http://dx.doi.org/https://doi.org/10.1016/0022-0728(93)80066-Q
(30) Yoshida, T.; Tsutsumida, K.; Teratani, S.; Yasufuku, K.; Kaneko, M. "Electrocatalytic reduction of CO2 in water by [Re(bpy)(CO)3Br] and [Re(terpy)(CO)3Br] complexes incorporated into coated nafion membrane (bpy = 2,2′-bipyridine; terpy = 2,2′;6′,2″-terpyridine)," *Journal of the Chemical Society, Chemical Communications* **1993**, 631-633. http://dx.doi.org/10.1039/C39930000631
(31) Zhao, F.; Zhang, J.; Abe, T.; Wöhrle, D.; Kaneko, M. "Electrocatalytic proton reduction by phthalocyanine cobalt derivatives incorporated in poly(4-vinylpyridine-co-styrene) film," *Journal of Molecular Catalysis A: Chemical* **1999**, *145*, 245-256. http://dx.doi.org/https://doi.org/10.1016/S1381-1169(99)00013-8
(32) Abe, T.; Imaya, H.; Yoshida, T.; Tokita, S.; Schlettwein, D.; Wöhrle, D.; Kaneko, M. "Electrochemical CO2 Reduction Catalysed by Cobalt Octacyanophthalocyanine and its Mechanism," *J. Porphyrins Phthalocyanines* **1997**, *01*, 315-321. http://dx.doi.org/10.1002/(sici)1099-1409(199710)1:4<315::Aid-jpp35>3.0.Co;2-v
(33) Abe, T.; Yoshida, T.; Tokita, S.; Taguchi, F.; Imaya, H.; Kaneko, M. "Factors affecting selective electrocatalytic co2 reduction with cobalt phthalocyanine incorporated in a polyvinylpyridine membrane coated on a graphite electrode," *Journal of Electroanalytical Chemistry* **1996**, *412*, 125-132. http://dx.doi.org/https://doi.org/10.1016/0022-0728(96)04631-1
(34) Yoshida, T.; Kamato, K.; Tsukamoto, M.; Iida, T.; Schlettwein, D.; Wöhrle, D.; Kaneko, M. "Selective electroacatalysis for CO2 reduction in the aqueous phase using cobalt phthalocyanine/poly-4-vinylpyridine modified electrodes," *Journal of Electroanalytical Chemistry* **1995**, *385*, 209-225. http://dx.doi.org/https://doi.org/10.1016/0022-0728(94)03762-R
(35) Liu, Y.; McCrory, C. C. L. "Modulating the mechanism of electrocatalytic CO2 reduction by cobalt phthalocyanine through polymer coordination and encapsulation," *Nature Communications* **2019**, *10*, 1683. http://dx.doi.org/10.1038/s41467-019-09626-8
(36) Soucy, T. L.; Liu, Y.; Eisenberg, J. B.; McCrory, C. C. L. "Enhancing the Electrochemical CO2 Reduction Activity of Polymer-Encapsulated Cobalt Phthalocyanine Films by Modulating the Loading of Catalysts, Polymers, and Carbon Supports. ," *ACS Appl. Energy Mater.* **2021**, *ASAP*. http://dx.doi.org/10.1021/acsaem.1c02689
(37) Wang, M.; Torbensen, K.; Salvatore, D.; Ren, S.; Joulie, D.; Dumoulin, F.; Mendoza, D.; Lassalle-Kaiser, B.; Isci, U.; Berlinguette, C. P.; Robert, M. "CO2 electrochemical catalytic reduction with a highly active cobalt phthalocyanine," *Nat Commun* **2019**, *10*, 3602. http://dx.doi.org/10.1038/s41467-019-11542-w
(38) Zhang, X.; Wu, Z.; Zhang, X.; Li, L.; Li, Y.; Xu, H.; Li, X.; Yu, X.; Zhang, Z.; Liang, Y.; Wang, H. "Highly selective and active CO2 reduction electrocatalysts based on cobalt phthalocyanine/carbon nanotube hybrid structures," *Nature Communications* **2017**, *8*, 14675. http://dx.doi.org/10.1038/ncomms14675
(39) Zhu, M.; Chen, J.; Huang, L.; Ye, R.; Xu, J.; Han, Y.-F. "Covalently Grafting Cobalt Porphyrin onto Carbon Nanotubes for Efficient CO2 Electroreduction," *Angewandte Chemie*

International Edition **2019**, *58*, 6595-6599. http://dx.doi.org/https://doi.org/10.1002/anie.201900499
(40) Hu, X.-M.; Rønne, M. H.; Pedersen, S. U.; Skrydstrup, T.; Daasbjerg, K. "Enhanced Catalytic Activity of Cobalt Porphyrin in CO2 Electroreduction upon Immobilization on Carbon Materials," *Angewandte Chemie International Edition* **2017**, *56*, 6468-6472. http://dx.doi.org/https://doi.org/10.1002/anie.201701104
(41) Lin, S.; Diercks, C. S.; Zhang, Y.-B.; Kornienko, N.; Nichols, E. M.; Zhao, Y.; Paris, A. R.; Kim, D.; Yang, P.; Yaghi, O. M.; Chang, C. J. "Covalent organic frameworks comprising cobalt porphyrins for catalytic CO_2 reduction in water," *Science* **2015**, *349*, 1208-1213. http://dx.doi.org/10.1126/science.aac8343
(42) Orchanian, N. M.; Hong, L. E.; Skrainka, J. A.; Esterhuizen, J. A.; Popov, D. A.; Marinescu, S. C. "Surface-Immobilized Conjugated Polymers Incorporating Rhenium Bipyridine Motifs for Electrocatalytic and Photocatalytic CO2 Reduction," *ACS Applied Energy Materials* **2019**, *2*, 110-123. http://dx.doi.org/10.1021/acsaem.8b01745
(43) Kamata, R.; Kumagai, H.; Yamazaki, Y.; Sahara, G.; Ishitani, O. "Photoelectrochemical CO2 Reduction Using a Ru(II)–Re(I) Supramolecular Photocatalyst Connected to a Vinyl Polymer on a NiO Electrode," *ACS Applied Materials & Interfaces* **2019**, *11*, 5632-5641. http://dx.doi.org/10.1021/acsami.8b05495
(44) Tsounis, C.; Kuriki, R.; Shibata, K.; Vequizo, J. J. M.; Lu, D.; Yamakata, A.; Ishitani, O.; Amal, R.; Maeda, K. "Copolymerization Approach to Improving Ru(II)-Complex/C3N4 Hybrid Photocatalysts for Visible-Light CO2 Reduction," *ACS Sustainable Chemistry & Engineering* **2018**, *6*, 15333-15340. http://dx.doi.org/10.1021/acssuschemeng.8b03782
(45) Roy, S.; Reisner, E. "Visible-Light-Driven CO2 Reduction by Mesoporous Carbon Nitride Modified with Polymeric Cobalt Phthalocyanine," *Angewandte Chemie International Edition* **2019**, *58*, 12180-12184. http://dx.doi.org/https://doi.org/10.1002/anie.201907082
(46) Dong, X.-Y.; Si, Y.-N.; Wang, Q.-Y.; Wang, S.; Zang, S.-Q. "Integrating Single Atoms with Different Microenvironments into One Porous Organic Polymer for Efficient Photocatalytic CO2 Reduction," *Advanced Materials* **2021**, *33*, 2101568. http://dx.doi.org/https://doi.org/10.1002/adma.202101568
(47) Wagner, A.; Sahm, C. D.; Reisner, E. "Towards molecular understanding of local chemical environment effects in electro- and photocatalytic CO2 reduction," *Nature Catalysis* **2020**, *3*, 775-786. http://dx.doi.org/10.1038/s41929-020-00512-x
(48) Birdja, Y. Y.; Vos, R. E.; Wezendonk, T. A.; Jiang, L.; Kapteijn, F.; Koper, M. T. M. "Effects of Substrate and Polymer Encapsulation on CO2 Electroreduction by Immobilized Indium(III) Protoporphyrin," *ACS Catalysis* **2018**, *8*, 4420-4428. http://dx.doi.org/10.1021/acscatal.7b03386
(49) Sato, S.; McNicholas, B. J.; Grubbs, R. H. "Aqueous electrocatalytic CO2 reduction using metal complexes dispersed in polymer ion gels," *Chem. Commun.* **2020**, *56*, 4440-4443. http://dx.doi.org/10.1039/D0CC00791A
(50) McNicholas, B. J.; Blakemore, J. D.; Chang, A. B.; Bates, C. M.; Kramer, W. W.; Grubbs, R. H.; Gray, H. B. "Electrocatalysis of CO2 Reduction in Brush Polymer Ion Gels," *J. Am. Chem. Soc.* **2016**, *138*, 11160-11163. http://dx.doi.org/10.1021/jacs.6b08795
(51) Leung, J. J.; Vigil, J. A.; Warnan, J.; Edwardes Moore, E.; Reisner, E. "Rational Design of Polymers for Selective CO2 Reduction Catalysis," *Angew Chem Int Ed Engl* **2019**, *58*, 7697-7701. http://dx.doi.org/10.1002/anie.201902218

(52) Kramer, W. W.; McCrory, C. C. L. "Polymer coordination promotes selective CO2 reduction by cobalt phthalocyanine," *Chemical Science* **2016**, *7*, 2506-2515. http://dx.doi.org/10.1039/C5SC04015A
(53) Liu, Y.; Deb, A.; Leung, K. Y.; Nie, W.; Dean, W. S.; Penner-Hahn, J. E.; McCrory, C. C. L. "Determining the coordination environment and electronic structure of polymer-encapsulated cobalt phthalocyanine under electrocatalytic CO_2 reduction conditions using in situ X-Ray absorption spectroscopy," *Dalton Trans.* **2020**, *49*, 16329-16339. http://dx.doi.org/10.1039/D0DT01288B
(54) Dodelet, J.-P. "Oxygen Reduction in PEM Fuel Cell Conditions: Heat-Treated Non-Precious Metal-N4 Macrocycles and Beyond," In *N4-Macrocyclic Metal Complexes*; Zagal, J. H., Bedioui, F., Dodelet, J.-P., Eds.; Springer New York: New York, NY, 2006, p 83-147.
(55) Kau, L. S.; Spira-Solomon, D. J.; Penner-Hahn, J. E.; Hodgson, K. O.; Solomon, E. I. "X-ray absorption edge determination of the oxidation state and coordination number of copper. Application to the type 3 site in Rhus vernicifera laccase and its reaction with oxygen," *J. Am. Chem. Soc.* **1987**, *109*, 6433-6442. http://dx.doi.org/10.1021/ja00255a032
(56) Smith, P. T.; Nichols, E. M.; Cao, Z.; Chang, C. J. "Hybrid Catalysts for Artificial Photosynthesis: Merging Approaches from Molecular, Materials, and Biological Catalysis," *Accounts of Chemical Research* **2020**, *53*, 575-587. http://dx.doi.org/10.1021/acs.accounts.9b00619
(57) Jeoung, J.-H.; Dobbek, H. "Carbon Dioxide Activation at the Ni,Fe-Cluster of Anaerobic Carbon Monoxide Dehydrogenase," *Science* **2007**, *318*, 1461-1464. http://dx.doi.org/doi:10.1126/science.1148481
(58) Drennan, C. L.; Heo, J.; Sintchak, M. D.; Schreiter, E.; Ludden, P. W. "Life on carbon monoxide: X-ray structure of Rhodospirillum rubrum Ni-Fe-S carbon monoxide dehydrogenase," *Proc. Natl. Acad. Sci. U.S.A.* **2001**, *98*, 11973-11978. http://dx.doi.org/10.1073/pnas.211429998
(59) Fesseler, J.; Jeoung, J.-H.; Dobbek, H. "How the [NiFe4S4] Cluster of CO Dehydrogenase Activates CO2 and NCO−," *Angew. Chem. Int. Ed.* **2015**, *54*, 8560-8564. http://dx.doi.org/https://doi.org/10.1002/anie.201501778
(60) Can, M.; Armstrong, F. A.; Ragsdale, S. W. "Structure, Function, and Mechanism of the Nickel Metalloenzymes, CO Dehydrogenase, and Acetyl-CoA Synthase," *Chem. Rev.* **2014**, *114*, 4149-4174. http://dx.doi.org/10.1021/cr400461p
(61) Mondal, B.; Song, J.; Neese, F.; Ye, S. "Bio-inspired mechanistic insights into CO2 reduction," *Curr. Opin. Chem. Biol.* **2015**, *25*, 103-109. http://dx.doi.org/https://doi.org/10.1016/j.cbpa.2014.12.022
(62) Costentin, C.; Robert, M.; Saveant, J. M. "Catalysis of the electrochemical reduction of carbon dioxide," *Chem Soc Rev* **2013**, *42*, 2423-2436. http://dx.doi.org/10.1039/c2cs35360a
(63) Costentin, C.; Robert, M.; Savéant, J.-M. "Current Issues in Molecular Catalysis Illustrated by Iron Porphyrins as Catalysts of the CO2-to-CO Electrochemical Conversion," *Acc. Chem. Res.* **2015**, *48*, 2996-3006. http://dx.doi.org/10.1021/acs.accounts.5b00262
(64) Chabolla, S. A.; Yang, J. Y. "For CO2 Reduction, Hydrogen-Bond Donors Do the Trick," *ACS Cent. Sci.* **2018**, *4*, 315-317. http://dx.doi.org/10.1021/acscentsci.8b00087
(65) Nichols, A. W.; Machan, C. W. "Secondary-Sphere Effects in Molecular Electrocatalytic CO2 Reduction," *Frontiers in Chemistry* **2019**, *7*. http://dx.doi.org/10.3389/fchem.2019.00397

(66) Takeda, H.; Cometto, C.; Ishitani, O.; Robert, M. "Electrons, Photons, Protons and Earth-Abundant Metal Complexes for Molecular Catalysis of CO2 Reduction," *ACS Catal.* **2017**, *7*, 70-88. http://dx.doi.org/10.1021/acscatal.6b02181
(67) Schneider, J.; Jia, H.; Muckerman, J. T.; Fujita, E. "Thermodynamics and kinetics of CO2, CO, and H+ binding to the metal centre of CO2reductioncatalysts," *Chem. Soc. Rev.* **2012**, *41*, 2036-2051. http://dx.doi.org/10.1039/C1CS15278E
(68) Elgrishi, N.; Chambers, M. B.; Wang, X.; Fontecave, M. "Molecular polypyridine-based metal complexes as catalysts for the reduction of CO2," *Chemical Society Reviews* **2017**, *46*, 761-796. http://dx.doi.org/10.1039/C5CS00391A
(69) Chaturvedi, A.; Williams, C. K.; Devi, N.; Jiang, J. J. "Effects of Appended Poly(ethylene glycol) on Electrochemical CO2 Reduction by an Iron Porphyrin Complex," *Inorg Chem* **2021**, *60*, 3843-3850. http://dx.doi.org/10.1021/acs.inorgchem.0c03612
(70) Devi, N.; Williams, C. K.; Chaturvedi, A.; Jiang, J. J. "Homogeneous Electrocatalytic CO2 Reduction Using a Porphyrin Complex with Flexible Triazole Units in the Second Coordination Sphere," *ACS Appl. Energy Mater.* **2021**, *4*, 3604-3611. http://dx.doi.org/10.1021/acsaem.1c00027
(71) Schneider, C. R.; Lewis, L. C.; Shafaat, H. S. "The good, the neutral, and the positive: buffer identity impacts CO2 reduction activity by nickel(ii) cyclam," *Dalton Transactions* **2019**, *48*, 15810-15821. http://dx.doi.org/10.1039/C9DT03114F
(72) Chen, X.; Chen, J.; Alghoraibi, N. M.; Henckel, D. A.; Zhang, R.; Nwabara, U. O.; Madsen, K. E.; Kenis, P. J. A.; Zimmerman, S. C.; Gewirth, A. A. "Electrochemical CO2-to-ethylene conversion on polyamine-incorporated Cu electrodes," *Nature Catalysis* **2020**, *4*, 20-27. http://dx.doi.org/10.1038/s41929-020-00547-0
(73) Kim, W.; Seok, T.; Choi, W. "Nafion layer-enhanced photosynthetic conversion of CO2 into hydrocarbons on TiO2 nanoparticles," *Energy & Environmental Science* **2012**, *5*. http://dx.doi.org/10.1039/c2ee03338k
(74) Kuwahara, Y.; Fujie, Y.; Mihogi, T.; Yamashita, H. "Hollow Mesoporous Organosilica Spheres Encapsulating PdAg Nanoparticles and Poly(Ethyleneimine) as Reusable Catalysts for CO2 Hydrogenation to Formate," *ACS Catalysis* **2020**, *10*, 6356-6366. http://dx.doi.org/10.1021/acscatal.0c01505
(75) Wei, X.; Yin, Z.; Lyu, K.; Li, Z.; Gong, J.; Wang, G.; Xiao, L.; Lu, J.; Zhuang, L. "Highly Selective Reduction of CO2 to C2+ Hydrocarbons at Copper/Polyaniline Interfaces," *ACS Catalysis* **2020**, *10*, 4103-4111. http://dx.doi.org/10.1021/acscatal.0c00049
(76) Li, F.; Zhao, S.-F.; Chen, L.; Khan, A.; MacFarlane, D. R.; Zhang, J. "Polyethylenimine promoted electrocatalytic reduction of CO2to CO in aqueous medium by graphene-supported amorphous molybdenum sulphide," *Energy & Environmental Science* **2016**, *9*, 216-223. http://dx.doi.org/10.1039/c5ee02879e
(77) Nam, D. H.; De Luna, P.; Rosas-Hernandez, A.; Thevenon, A.; Li, F.; Agapie, T.; Peters, J. C.; Shekhah, O.; Eddaoudi, M.; Sargent, E. H. "Molecular enhancement of heterogeneous CO2 reduction," *Nat Mater* **2020**, *19*, 266-276. http://dx.doi.org/10.1038/s41563-020-0610-2
(78) O'Hagan, M.; Shaw, W. J.; Raugei, S.; Chen, S.; Yang, J. Y.; Kilgore, U. J.; DuBois, D. L.; Bullock, R. M. "Moving Protons with Pendant Amines: Proton Mobility in a Nickel Catalyst for Oxidation of Hydrogen," *Journal of the American Chemical Society* **2011**, *133*, 14301-14312. http://dx.doi.org/10.1021/ja201838x
(79) Cornish, A. J.; Ginovska, B.; Thelen, A.; da Silva, J. C. S.; Soares, T. A.; Raugei, S.; Dupuis, M.; Shaw, W. J.; Hegg, E. L. "Single-Amino Acid Modifications Reveal Additional Controls on

the Proton Pathway of [FeFe]-Hydrogenase," *Biochemistry* **2016**, *55*, 3165-3173. http://dx.doi.org/10.1021/acs.biochem.5b01044
(80) Shaw, W. J. "The Outer-Coordination Sphere: Incorporating Amino Acids and Peptides as Ligands for Homogeneous Catalysts to Mimic Enzyme Function," *Catalysis Reviews* **2012**, *54*, 489-550. http://dx.doi.org/10.1080/01614940.2012.679453
(81) Laureanti, J. A.; Ginovska, B.; Buchko, G. W.; Schenter, G. K.; Hebert, M.; Zadvornyy, O. A.; Peters, J. W.; Shaw, W. J. "A Positive Charge in the Outer Coordination Sphere of an Artificial Enzyme Increases CO2 Hydrogenation," *Organometallics* **2020**, *39*, 1532-1544. http://dx.doi.org/10.1021/acs.organomet.9b00843
(82) Fan, G.; Wasuwanich, P.; Furst, A. L. "Biohybrid Systems for Improved Bioinspired, Energy-Relevant Catalysis," *ChemBioChem* **2021**, *22*, 2353-2367. http://dx.doi.org/https://doi.org/10.1002/cbic.202100037
(83) Schowen, K. B.; Schowen, R. L. "[29] Solvent isotope effects on enzyme systems," In *Methods Enzymol.*; Academic Press: 1982; Vol. 87, p 551-606.
(84) Schowen, R. L. "The use of solvent isotope effects in the pursuit of enzyme mechanisms," *Journal of Labelled Compounds and Radiopharmaceuticals* **2007**, *50*, 1052-1062. http://dx.doi.org/10.1002/jlcr.1436
(85) Efimov, I.; Badyal, S. K.; Metcalfe, C. L.; Macdonald, I.; Gumiero, A.; Raven, E. L.; Moody, P. C. E. "Proton Delivery to Ferryl Heme in a Heme Peroxidase: Enzymatic Use of the Grotthuss Mechanism," *Journal of the American Chemical Society* **2011**, *133*, 15376-15383. http://dx.doi.org/10.1021/ja2007017
(86) Pankhurst, K. L.; Mowat, C. G.; Rothery, E. L.; Hudson, J. M.; Jones, A. K.; Miles, C. S.; Walkinshaw, M. D.; Armstrong, F. A.; Reid, G. A.; Chapman, S. K. "A Proton Delivery Pathway in the Soluble Fumarate Reductase from Shewanella frigidimarina," *J. Biol. Chem.* **2006**, *281*, 20589-20597. http://dx.doi.org/10.1074/jbc.M603077200
(87) Barbara Schowen, K.; Schowen, R. L. "[29] Solvent isotope effects on enzyme systems," In *Methods Enzymol.*; Daniel, L. P., Ed.; Academic Press: 1982; Vol. Volume 87, p 551-606.
(88) Karsten, W. E.; Cook, P. F. "Substrate and pH dependence of isotope effects in enzyme catalyzed reactions," In *Isotope Effects in Chemistry and Biology* 2006, p 793-810.
(89) Northrop, D. B. "Steady-state analysis of kinetic isotope effects in enzymic reactions," *Biochemistry* **1975**, *14*, 2644-2651. http://dx.doi.org/10.1021/bi00683a013
(90) Kohen, A.; Limbach, H. H. *Isotope effects in chemistry and biology*; cRc Press: Boca Raton, 2005.
(91) Andrieux, C. P.; Dumas-Bouchiat, J. M.; Saveant, J. M. "Homogeneous redox catalysis of electrochemical reactions: Part II. Rate determining electron transfer, evaluation of rate and equilibrium parameters," *J. Electroanal. Chem.* **1978**, *87*, 55-65. http://dx.doi.org/10.1016/s0022-0728(78)80379-9
(92) Andrieux, C. P.; Dumas-Bouchiat, J. M.; Saveant, J. M. "Homogenous Redox Catalysis of Electrochemical Reactions. Part IV. Kinetic Controls in the Homogenous Process as Characterized by Stationary and Quasi-Stationary Electrochemical Techniques.," *J. Electroanal. Chem.* **1980**, *113*, 1-18. http://dx.doi.org/10.1016/S0022-0728(80)80507-9
(93) Andrieux, C. P.; Dumas-Bouchiat, J. M.; Savéant, J. M. "Catalysis of electrochemical reactions at redox polymer electrodes: Kinetic model for stationary voltammetric techniques," *J. Electroanal. Chem.* **1982**, *131*, 1-35. http://dx.doi.org/10.1016/0022-0728(82)87059-9

(94) Buttry, D. A.; Anson, F. C. "Effects of electron exchange and single-file diffusion on charge propagation in Nafion films containing redox couples," *J. Am. Chem. Soc.* **1983**, *105*, 685-689. http://dx.doi.org/10.1021/ja00342a001
(95) Leddy, J.; Bard, A. J.; Maloy, J. T.; Savéant, J. M. "Kinetics of film-coated electrodes: Effect of a finite mass transfer rate of substrate across the film—solution interface at steady state," *J. Electroanal. Chem.* **1985**, *187*, 205-227. http://dx.doi.org/10.1016/0368-1874(85)85779-8
(96) Amarasinghe, S.; Ta-Yung, C.; Moberg, P.; Paul, H. J.; Tinoco, F.; Zook, L. A.; Leddy, J. "Models for mediated reactions at film modified electrodes: controlled electrode potential," *Analytica Chimica Acta* **1995**, *307*, 227-244. http://dx.doi.org/https://doi.org/10.1016/0003-2670(95)00003-I
(97) Jiang, Z.; Wang, Y.; Zhang, X.; Zheng, H.; Wang, X.; Liang, Y. "Revealing the hidden performance of metal phthalocyanines for CO2 reduction electrocatalysis by hybridization with carbon nanotubes," *Nano Research* **2019**, *12*, 2330-2334. http://dx.doi.org/10.1007/s12274-019-2455-z
(98) Huai, M.; Yin, Z.; Wei, F.; Wang, G.; Xiao, L.; Lu, J.; Zhuang, L. "Electrochemical CO2 reduction on heterogeneous cobalt phthalocyanine catalysts with different carbon supports," *Chemical Physics Letters* **2020**, *754*, 137655. http://dx.doi.org/https://doi.org/10.1016/j.cplett.2020.137655
(99) Tang, J.-K.; Zhu, C.-Y.; Jiang, T.-W.; Wei, L.; Wang, H.; Yu, K.; Yang, C.-L.; Zhang, Y.-B.; Chen, C.; Li, Z.-T.; Zhang, D.-W.; Zhang, L.-M. "Anion exchange-induced single-molecule dispersion of cobalt porphyrins in a cationic porous organic polymer for enhanced electrochemical CO2 reduction via secondary-coordination sphere interactions," *Journal of Materials Chemistry A* **2020**, *8*, 18677-18686. http://dx.doi.org/10.1039/D0TA07068H
(100) Wang, Y.; Wang, D.; Dares, C. J.; Marquard, S. L.; Sheridan, M. V.; Meyer, T. J. "CO2 reduction to acetate in mixtures of ultrasmall (Cu) n ,(Ag) m bimetallic nanoparticles," *Proc Natl Acad Sci U S A* **2018**, *115*, 278-283. http://dx.doi.org/10.1073/pnas.1713962115
(101) Higgins, D.; Hahn, C.; Xiang, C.; Jaramillo, T. F.; Weber, A. Z. "Gas-Diffusion Electrodes for Carbon Dioxide Reduction: A New Paradigm," *ACS Energy Letters* **2019**, *4*, 317-324. http://dx.doi.org/10.1021/acsenergylett.8b02035
(102) Masel, R. I.; Liu, Z.; Yang, H.; Kaczur, J. J.; Carrillo, D.; Ren, S.; Salvatore, D.; Berlinguette, C. P. "An industrial perspective on catalysts for low-temperature CO2 electrolysis," *Nature Nanotechnology* **2021**, *16*, 118-128. http://dx.doi.org/10.1038/s41565-020-00823-x
(103) Rabiee, H.; Ge, L.; Zhang, X.; Hu, S.; Li, M.; Yuan, Z. "Gas diffusion electrodes (GDEs) for electrochemical reduction of carbon dioxide, carbon monoxide, and dinitrogen to value-added products: a review," *Energy & Environmental Science* **2021**, *14*, 1959-2008. http://dx.doi.org/10.1039/D0EE03756G
(104) Zheng, T.; Jiang, K.; Wang, H. "Recent Advances in Electrochemical CO2-to-CO Conversion on Heterogeneous Catalysts," *Advanced Materials* **2018**, *30*, 1802066. http://dx.doi.org/https://doi.org/10.1002/adma.201802066
(105) Weekes, D. M.; Salvatore, D. A.; Reyes, A.; Huang, A.; Berlinguette, C. P. "Electrolytic CO2 Reduction in a Flow Cell," *Accounts of Chemical Research* **2018**, *51*, 910-918. http://dx.doi.org/10.1021/acs.accounts.8b00010
(106) Torbensen, K.; Joulié, D.; Ren, S.; Wang, M.; Salvatore, D.; Berlinguette, C. P.; Robert, M. "Molecular Catalysts Boost the Rate of Electrolytic CO2 Reduction," *ACS Energy Letters* **2020**, *5*, 1512-1518. http://dx.doi.org/10.1021/acsenergylett.0c00536

Chapter 2 Enhancing Electrochemical CO_2 Reduction Activity of Polymer-Encapsulated Cobalt Phthalocyanine Films by Modulating the Loading of Catalysts, Polymers, and Carbon Supports

2.1 Preface

This chapter presents how the incorporation of graphite powder into a CoPc-P4VP system impacted the CO_2 reduction activity and selectivity of the electrocatalyst system. We developed a strategy and method for preparing the graphite powder deposition inks while providing insight into the best choice of procedure and polymer. Additionally, we found that the graphite: cobalt ratio was extremely important for maximizing activity. This chapter of my dissertation is derived from a manuscript originally published in *ACS Applied Energy Materials*.[1] I was the primary author on the manuscript and was responsible for electrochemical studies and sample preparation for the second half of the work, ICP-MS analysis of all samples, as well as data organization, manuscript writing, and preparation of the manuscript. Dr. Yingshuo Liu developed the original method for graphite powder deposition inks and collected electrochemical measurements for two figures. Jonah Eisenberg collected some of the electrochemical experiments for two figures and assisted in preparing some of the deposition inks. Dr. Charles McCrory provided significant insight and expertise in electroanalytical techniques and analysis, and reviewed, edited, and revised the manuscript.

2.2 Abstract

Cobalt phthalocyanine (CoPc) has been extensively studied as a catalyst for the electrochemical reduction of CO_2 to value-added products. Previous studies have shown that CoPc is a competent and efficient catalyst when immobilized onto carbon-based electrodes using a polymer binder, especially when immobilized with a graphitic carbon powder support to increase charge transport. In this study, we systematically explore the influence of incorporating graphite powder (GP) into a polymer-encapsulated CoPc on the system's activity for the electrochemical reduction of CO_2. We report a protocol for incorporating GP into CoPc/polymer/GP catalyst films that facilitates physisorption of CoPc to GP, leading to increased activity for CO_2 reduction. We show that the activity for CO_2 reduction increases with GP loading at low GP loadings, but at sufficiently high GP loadings the activity plateaus as charge transfer is sufficiently fast to no longer be rate limiting. We also demonstrate that axial coordination is still important even in the presence of GP, suggesting that CoPc does not fully coordinate to heteroatoms on the GP surface. We develop a set of optimized conditions under which the CoPc/polymer/GP catalyst systems reduce CO_2 with higher activity and similar selectivity to previously reported CoPc/polymer films on edge-plane graphite electrodes. The procedures outlined in this study will be used in future studies to optimize catalyst, polymer, and carbon support loadings for other polymer-catalyst composite systems for electrocatalytic transformations.

2.3 Introduction

There has been intense recent interest in cobalt phthalocyanine (CoPc) as an active and efficient electrocatalyst for the CO_2 reduction reaction (CO_2RR).[2-45] Recent studies have shown that CoPc is even capable of reducing CO_2 to methanol via a cascade (or domino) catalysis mechanism involving a CO intermediate when CoPc is adsorbed onto carbon nanotubes (CNTs) and studied under specific conditions.[20,30,34,46,47] Our interest in CoPc has focused on using the system as a model for understanding the parameters that influence the electrocatalytic activity of polymer-encapsulated molecular catalysts and related membrane-coated electrocatalyst systems.[48] In particular, our work and that of others has shown that incorporating CoPc within a poly-4-vinylpyridine (P4VP) polymer results in increased activity and reaction selectivity for the CO_2RR to CO over the competitive hydrogen evolution reaction (HER) in pH 5 phosphate electrolytes (Figure 2.1).[4,6,14] By using a combination of systematic modifications of the polymer-catalyst composite system,[14,25] kinetic isotope effect and proton inventory studies,[25] and *in situ* electrochemical X-ray absorbance spectroscopy measurements,[37] we have shown that both the coordination environment and chemical microenvironment surrounding the CoPc active sites play a crucial role in modulating the activity and selectivity of the CoPc-P4VP composite materials (Figure 2.1).

In our previous studies, we avoided the use of conductive carbon powder supports commonly used to enhance charge transport because these carbon powders can influence the nature of the polymer-catalyst interactions. For example, carbon powders with large concentrations of heteroatoms such as doped graphene and graphene oxide can facilitate interactions between the CoPc and the S, N, or O heteroatoms on the carbon surface, thus influencing the catalytic mechanism.[28,49,50] Moreover, planar metal phthalocyanines and related complexes strongly

physisorb to graphitic carbon surfaces due to π-π interactions between the conjugated graphitic surfaces and the aromatic Pc ring which affects the electronic structure of the system, as shown in several CoPc-CNT X-ray absorption studies.[9,15,51-55] Therefore, increasing the surface area of graphitic carbon through the incorporation of carbon powders may alter the electronic and chemical microenvironment surrounding the CoPc and complicate mechanistic understanding while increasing overall activity.[56] While our choice to avoid using conductive carbon-powder supports enabled us to better study the influence of polymer encapsulation on catalytic mechanisms, it likely limited the overall activity of our catalyst-polymer system due to inefficient charge transport.[48,57,58]

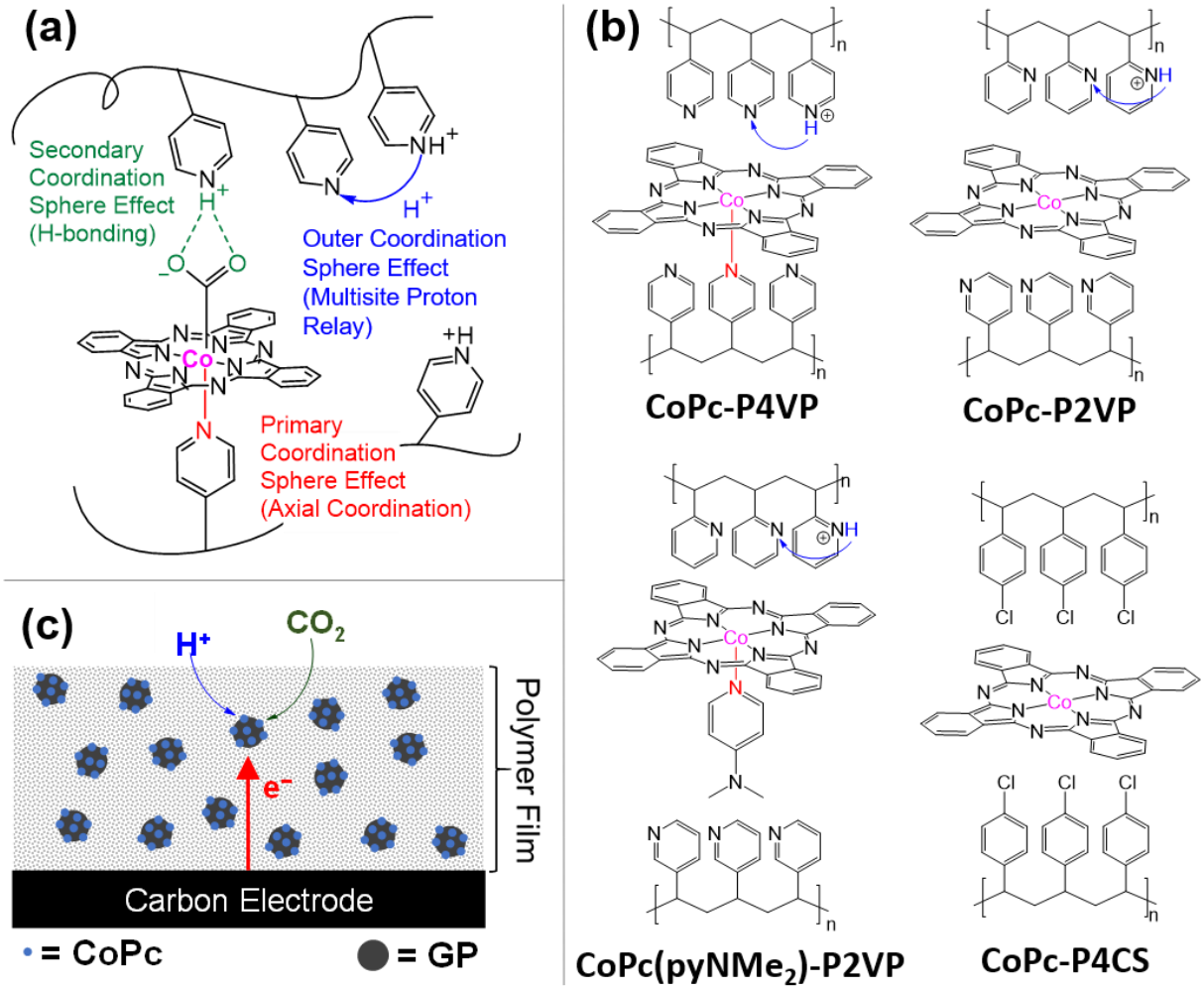

Figure 2.1 Encapsulating cobalt phthalocyanine (CoPc) within the coordinating polymer poly-4-vinylpyridine (P4VP) and other polymers. (a) Resultant composite CoPc-P4VP system that shows enhanced activity for the CO_2 reduction reaction compared to the parent CoPc system. The increased activity is attributed to primary, secondary, and outer-coordination sphere effects imbued by the P4VP polymer on the CoPc catalyst active site. Adapted from Ref. [37] with permission from The Royal Society of Chemistry. (b) Polymer-catalyst composite systems investigated in this work along with their postulated coordination environments and proton relays. (c) A schematic illustration of CoPc immobilized onto a graphite-powder support and encapsulated within a polymer film composed of the various polymers show in (b).

In a few studies, researchers have incorporated graphitic carbon into CoPc films with the purpose to improve charge transport (see Table 2.1). For example, in one study, a 10-fold increase in activity was observed when Vulcan XC-72 and CNTs were incorporated into a CoPc catalyst deposition solution.[34] In another study, major activity differences were observed in CoPc-based gas-fed electrolyzers that incorporated different carbon sources (carbon fibers, graphite, Vulcan XC-72, and activated carbon).[47] However, there are few studies with experiments to explicitly explore the impacts of charge and substrate transport on the CO_2RR by CoPc-polymer composite catalysts. Such studies are crucial because, as demonstrated in this report, activity metrics can vary significantly despite very similar preparation methods.

Based on these previous uses of carbon supports in CoPc systems for the CO_2RR, we believe there is significant space to improve the overall activity of the CoPc-P4VP system through the incorporation of carbon powder supports. However, care must be taken to understand how the impact of incorporating this graphitic support influences the selectivity and activity of the CO_2RR. Understanding of the effects of incorporating carbon supports us particularly important in developing gas-fed flow electrolyzer systems incorporating molecular catalyst such as CoPc.[26,59]

In this study, we directly add graphite powder (GP) as a carbon support to CoPc/polymer electrocatalyst to increase charge transport within the resulting polymer films (Figure 1b). We show that incorporating GP within the CoPc-P4VP system deposited onto a glassy carbon electrode leads to a CoPc-P4VP/GP/GCE composite material that operates with the similar reaction selectivity but significantly increased activity for the CO_2RR compared to CoPc-P4VP without incorporated GP deposited onto glassy carbon (CoPc-P4VP/GCE) and edge-plane graphite electrodes (CoPc-P4VP/EPG).

We postulate that observed increases to catalytic activity are because GP incorporation into the film facilitates electron transport to the exterior catalytic sites, which increases the total number of sites within the film that are active for the CO_2RR and decreases the average distance substrate must transport through the film to reach an electroactive CoPc catalyst molecule.[12] To test this postulate, we explored how different loadings and ratios of CoPc and GP influenced the catalytic activity of the system. For example, we show that at sufficiently high loading of CoPc in the CoPc-P4VP/GP/GCE system, further increasing the loading of CoPc has no appreciable effect on activity—there is a plateau in activity as CoPc loading is increased. We also show that increasing the CoPc-P4VP loading while keeping the GP loading constant leads to a decrease in overall activity, but that increasing the CoPc-P4VP loading *with* added GP (increasing GP loading along with CoPc and P4VP) results in an increase in overall activity at a smaller CoPc loading, before eventually reaching a plateau where increasing CoPc-P4VP and GP loading no longer influences activity. These observed activity plateaus suggest that at sufficiently high CoPc, P4VP, and GP loading, another effect limits the activity. This other effect may be inefficient CO_2 or H^+ transport, CoPc aggregation, or a combination of these effects.[19,22]

In addition, we show that axial coordination to the CoPc by the polymer in CoPc-P4VP/GP or an added ligand in CoPc(pyNMe_2)-P2VP/GP is necessary to achieve the highest maximum activity. This result suggests that although we cannot exclude the possibility that functional groups on the GP coordinate to CoPc in the composite system, axial coordination to a pyridyl or pyNMe_2 residue is still important for catalytic activity and outcompetes any coordination to functional groups on the carbon surface.

Through these systematic studies of the effect of catalyst, polymer, and graphite powder loading on catalyst activity for the CO_2RR by CoPc-P4VP/GP/GCE, we elucidate the relative

importance of charge and substrate transport on catalytic activity. We demonstrate that optimizing catalyst/polymer systems for activity and selectivity requires careful consideration of both the loading and preparation of the catalyst/polymer composite materials and carbon supports.

2.4 Experimental

2.4.1 Materials

All purchased chemicals were used as received unless otherwise specified. All water used in this study was ultrapure water (18.2MΩ cm resistivity), purified with a Thermo Scientific GenPure UV-TOC/UF x CAD-plus water purification system. Carbon dioxide (CO_2, 99.8%) was purchased from Cryogenic Gases and was used as received. Nitrogen (N_2) was boil-off gas from a liquid nitrogen source and was used without further purification. Cobalt phthalocyanine (CoPc, 97%), poly-4-vinylpyridine (P4VP, average Mw ~ 160,000), poly-2-vinylpyridine (P2VP, average Mw ~ 159,000), poly-4-chlorostyrene (P4CS, average Mw ~ 75,000), N,N-Dimethylformamide (DMF, ACS grade), ferrocene carboxylic acid (97%), sodium phosphate monobasic (BioXtra, >99.0%), 4-dimethylaminopyridine ($pyNMe_2$, $\geq$ 99%), graphite powder (GP, synthetic 20 μm) and Nafion-117 cation exchange membrane (Nafion) were purchased from Sigma Aldrich and used as received. Sodium hydroxide (NaOH, TraceMetal grade) was obtained from Fisher Scientific. Nitric acid (TraceMetal grade, 67-70%) was purchased from Fisher Scientific. Cobalt ICP standard (1000 ppm in 3% HNO_3) was purchased from Ricca Chemical Company.

2.4.2 Electrolyte Solution Preparation and pH Measurements

All electrolyte solutions were prepared using ultrapure water. All experiments were performed in phosphate solutions of 0.1 M NaH_2PO_4 adjusted to pH 5 by the addition of 1 M

NaOH. Prior to each experiment, the working chamber was sparged with the appropriate gas by using a section of Tygon tubing for at least 30 minutes. The pH after sparging with CO_2 was 4.7. The electrolyte pH before-and-after CO_2 sparging was confirmed using a Fisher Scientific Accumet AB200 pH meter with an Atlas Scientific pH probe electrode calibrated with a three-point calibration curve at pH = 4.01, 7.00, and 10.01.

2.4.3 Preparation of Catalyst Preparation Suspensions

The specified concentrations of the CoPc, polymer, and graphite powder in the preparation suspensions (along with the corresponding CoPc and polymer loading determined by ICP-MS and gravimetric analysis, respectively) are listed in Table 2.2-Table 2.19.

CoPc-polymer deposition inks without GP were prepared using the following procedure: a 0.2 mM solution of CoPc dispersed in DMF was prepared via sonication of 0.0058 g of CoPc in 50 mL of DMF for 1 hour in an aluminum foil-jacketed polypropylene conical centrifuge tube (Basix™). The 0.2 mM solution was then diluted to the desired concentration via the addition of the stock solution to DMF, and the corresponding polymer was added to the diluted CoPc solution.

CoPc-polymer/GP preparation suspensions were prepared via sonication of 0.0052 g of CoPc in 45 mL of DMF for 1 hour in an aluminum foil-jacketed polypropylene conical centrifuge tube (Basix™). The 0.2 mM CoPc/DMF solution was then diluted to 1 mL of the desired concentration via the addition of the stock solution to DMF in a 20 mL glass scintillation vial. A given mass of polymer was then added to the 20 mL scintillation vial that contained the 1 mL of CoPc/DMF in order to form the desired CoPc-polymer solution. The CoPc-polymer solution was sonicated for 30 minutes to ensure dispersion of the polymer. A given mass of graphite powder was then added

to the CoPc-polymer solution to form the CoPc-polymer/GP preparation suspension. Polymer and graphite powder concentrations are denoted w/v %, meaning 0.01 g GP in 1 mL of CoPc/DMF solution is denoted as 1% GP. Note: graphite powder particles with a diameter of < 20 μm was used in this study—films made with larger graphite powder particles (diameter ~100 μm) led to visible delamination during the electrochemical measurements.

CoPc(pyNMe$_2$)-P2VP/GP preparation suspensions were prepared via sonication of 0.00518 g of CoPc and 1.0995 g of 4-Dimethylaminopyridine in 45 mL of DMF for 1 hour in an aluminum foil-jacketed polypropylene conical centrifuge tube (Basix™) to form a 0.2 mM CoPc / 0.2 M pyNMe$_2$ / DMF solution, ensuring 5-coordinate character by using 1000:1 pyNMe$_2$:CoPc ratio, as we have done previously.[45] This solution was then diluted to 1 mL of the desired CoPc and pyNMe$_2$ concentration via the addition of the stock solution to DMF in a 20 mL scintillation vial. A given mass of P2VP was then added to the 20 mL scintillation vial that contained the 1 mL of CoPc/DMF in order to form the desired CoPc(pyNMe$_2$)-P2VP solution, which was then sonicated for 30 minutes to ensure the dispersion of P2VP. A mass of 0.01 g of graphite powder was then added to the CoPc(pyNMe$_2$)-P2VP solution and was sonicated for 30 minutes to ensure the dispersion of graphite powder.

2.4.4 Preparation of Deposition Inks

After the addition of GP, the CoPc-polymer/GP or CoPc(pyNMe$_2$)-P2VP/GP preparation suspensions were sonicated for 30 min to ensure dispersion of the GP. A Teflon stir bar was added to the scintillation vial, and the preparation suspension was stirred for 12 h at 500 rpm. The preparation suspension was then centrifuged at 14,000 rpm for 30 minutes at -11ºC in an Eppendorf

5430R refrigerated centrifuge. The DMF was decanted, and 1 mL of fresh DMF was added to the remaining pellet. The remaining graphitic pellet suspended in fresh DMF (denoted as the deposition ink) was vortexed for 30 sec at 3000 rpm, and sonicated for 30 sec.

The catalyst loading in the deposition inks were determined by digesting the graphitic pellet after the centrifugation step and measuring the metal content using inductively coupled plasma-mass spectrometry (ICP-MS, PerkinElmer Nexion 2000). A volume of 15 mL of 1 M TraceMetal Grade HNO_3 was added to the graphitic pellet, and the resulting graphite/nitric acid slurry was stirred overnight. The slurry was then filtered using a cellulose syringe (0.45 µm, Titan 3 regenerated cellulose, Fisher Scientific) to remove graphite powder and polymer. The cobalt concentration of the resulting solution was then measured using ICP-MS, calibrated using Co calibration standards in 1 M HNO_3 at 10, 50, 100, and 500 ppb, and standard at 0 ppb along with internal standard of Bismuth. The conversion between the calculated ppb to molar CoPc loading in the deposition ink is shown in Equations 2.1-2.3.

$$X \text{ ppb} \times \frac{\frac{1\ \mu g}{\text{L}}}{1 \text{ ppb}} \times 0.015 \text{ L} = \text{mass Co in } \mu\text{g}$$

Equation 2.1

$$\text{mass in } \mu\text{g x } \frac{1 \text{ mol Co}}{58.93 \text{ g Co}} \times \frac{10^{-6} \text{ g}}{1\ \mu\text{g}} = \text{ mol CoPc}$$

Equation 2.2

$$\frac{\text{mol CoPc}}{0.0010 \text{ L initial deposition ink}} = M \text{ CoPc in deposition ink}$$

Equation 2.3

The loading of CoPc for each deposition ink was determined via ICP-MS measurements in at least 3 independently prepared samples, and the average values are reported in Table 2.2-Table 2.19 along with standard deviations.

The polymer loading in each deposition ink was determined by estimating the mass of polymer removed from the preparation solution during the centrifugation step. After the supernatant is decanted from the graphite pellet left after centrifugation of the preparation solution, the solvent was evaporated from the supernatant and the mass of the resulting residue (m_{residue}) was measured. The mass loading of polymer in the catalyst deposition ink ($m_{\text{polymer in ink}}$) was estimated by subtracting the mass of catalyst left over in the supernatant ($m_{\text{CoPc in supernatant}}$) from the total mass of the residue (m_{residue}) as shown in Equations 2.4-2.7.

$$m_{CoPc\ in\ prep\ solution} - m_{CoPc\ in\ deposition\ ink} = m_{CoPc\ in\ supernatant}$$

Equation 2.4

$$m_{\text{residue}} - m_{\text{CoPc in supernatant}} = m_{\text{polymer in supernatant}}$$

Equation 2.5

$$m_{\text{polymer in preparation suspension}} - m_{\text{polymer in supernatant}} = m_{\text{polymer in deposition ink}}$$

Equation 2.6

$$\frac{m_{\text{polymer in deposition ink}}}{1.0\ \text{mL}} = \text{polymer loading}$$

Equation 2.7

2.4.5 Preparation of Modified Electrodes

5 mm diameter glassy carbon disk electrodes (GCEs) (4 mm thick, 0.196 cm^2 surface area, Sigradur G, HTW Hochtemperatur-Werkstoffe GmbH) or 5 mm edge plane graphite (EPG) disk electrodes (3.81 mm EPG disk encapsulated in epoxy, 0.114 cm^2 effective surface area, Pine Research Instrumentation) were used as working electrodes. The GC disk electrodes were polished using a Struers LaboPol-5 polisher with a LaboForce-1 specimen mover. The GC disks electrodes were loaded into a custom-designed brass electrode holder held by the specimen mover

with ~5 psi of applied pressure per disk. The GC disk electrodes were sequentially polished with diamond abrasive slurries (DiaDuo-2, Struers) in an order of 9 µm, 6 µm, 3 µm, and 1 µm diameter particle slurries for 1 minute each on synthetic nap polishing pads (MD Floc, Stuers). During polishing, the platen speed was held at 200 rpm, and the head speed at 8 rpm in the opposite rotation from the platen. Between each polishing step, the GC disks were rinsed with water. After the final polishing step, the GC disks were sonicated sequentially in isopropyl alcohol for 3 minutes, ultrapure water for 3 minutes, and 1 M HNO_3 for 30 minutes. The GC disk electrodes were then rinsed with ultrapure water and dried under an N_2 stream. EPG electrodes were polished manually on 600 grit silicon carbide polishing paper (Buehler, CarbiMet) followed by sonication in ultrapure water for ~1 minute and drying under an N_2 stream.

The addition of catalyst deposition ink to the GCE or EPG took place via the following procedure: CoPc-polymer solution was coated on the electrodes via dropcasting 5 µL of solution, allowing the surface to dry in an oven at 60ºC for 10 minutes, and then applying a second coating of 5 µL of the solution and drying at the same temperature. For the experiment where the CoPc:P4VP:GP loading was held constant, the CoPc loading was increased by preparing a preparation slurry with 0.0125 mM CoPc and 0.75% P4VP, along with 1%, 0.5%, or 0.1% GP. The resultant CoPc concentrations in deposition inks are reported in Table 2.8Table 2.10Table 2.12, respectively. To increase the concentration of CoPc, P4VP, and GP, the deposition ink was dropcasted in 10 µL layers, with each increase in Co and GP being proportional to the addition of another 10 µL deposition. The number of 10 µL layers and the resulting electrode CoPc and GP loadings for this study can be found in Table 2.9, Table 2.11, and Table 2.13.

All calculated CoPc, polymer, and GP electrode loadings are organized by figure, and can be found in Table 2.2-Table 2.19.

2.4.6 Electrochemical Measurements

Electrochemical measurements were conducted using a Bio-Logic SP200 potentiostat/galvanostat, and data were recorded using the Bio-Logic EC-Lab software package. Reference electrodes were commercial saturated calomel electrode (SCE), externally referenced to ferrocenecarboxylic acid in 0.2 M phosphate buffer at pH 7 (0.284 V vs. SCE), and auxiliary electrodes were carbon rods (99.999%, Strem Chemicals Inc.). Working electrodes were the CoPc-polymer/GP-, CoPc(L)-polymer/GP-, or CoPc-polymer-modified GCEs or the CoPc-polymer EPGs. In all cases, the working electrode was separated from the auxiliary electrode by a Nafion membrane. Unless otherwise noted, all electrochemical measurements were conducted at least three times with independently prepared electrodes, all values reported are the average of these repetitions, and all reported errors are standard deviations. Data were recorded using the Bio-Logic EC-Lab software package.

For rotating disk electrode chronoamperomentric step (RDE-CA) measurements, the modified GCE working compartment was assembled using a Pine Research Instrumentation E6-series change disk rotating disk electrode (RDE) assembly attached to an MSR rotator. RDE-CA measurements were conducted at 1600 rpm with 2-minute potential steps at every 0.05 V from -1.00 to -1.25 V vs. SCE. The 1600 rpm rotation rate was used to ensure steady-state substrate delivery to the electrode surface in a way that is not present in a longer controlled potential electrolysis (CPE) experiment. RDE-CA measurements were conducted in a custom two-compartment glass cell. In the first compartment, the working electrode with GCE assembly was suspended in 30 mL buffer solution with 3 gas inlets and one inlet for the reference electrode. The second compartment contained ~15 mL solution with the auxiliary electrode. The compartments

were separated by a Nafion membrane. Both compartments were sparged with N_2 or CO_2 for ~30 minutes prior to each set of measurements, and the headspace was blanketed with CO_2 during the measurements. The CO_2 used for these electrochemical experiments was first saturated with electrolyte solution by bubbling through a gas washing bottle filled with water, to minimize electrolyte evaporation in the cell throughout the course of the measurements. iR drop was measured prior to the experiment and was compensated at 85% via a positive feedback loop from the software. In general, our electrochemical cell for CA measurement had Ru ~150 Ω in all electrolyte solutions.

Controlled potential electrolysis (CPE) experiments were conducted at room temperature in custom, gas-tight, two-chamber U-cells as previously reported.[25] The modified working electrode was held in an RDE internal hardware kit (Pine Research Instrumentation) and mounted into a custom PEEK sleeve. For the electrolysis measurements, the main chamber held the working electrode and an SCE reference electrode in ~25 mL electrolyte, and the headspace was measured after each experiment by measuring the amount of water needed to refill the main chamber. The auxiliary chamber held the auxiliary carbon rod electrode in 15 mL electrolyte. The two chambers were separated by Nafion cation exchange membrane. Prior to each experiment, both chambers were sparged with CO_2 for ~30 min and then the main chamber was sealed under CO_2 atmosphere. The uncompensated resistance of the cell was measured with a single-point high-frequency impedance measurement. The CPE measurements were not compensated for iR drop, and the potential value reported is the real applied potential. In general, our electrochemical cell for CPE had Ru = ~300 Ω. Product distribution for controlled potential electrolysis results can be found in Table 2.31.

2.4.7 Product Detection and Quantification

After CPE, gaseous and liquid samples were collected and analyzed using gas chromatography (GC). For gaseous samples, analysis was conducted using a Thermo Scientific Trace 1310 GC system with two separate analyzer channels for the detection of H_2 and C1-C2 products. A Pressure-Lok gas-tight syringe (10 mL, Valco VICI Precision Sampling, Inc.) was used to collect 5 mL aliquots from the main chamber headspace of the cell, and each aliquot was injected directly into the 3 mL sample loop. Using a custom valve system, column configuration, and method provided by Thermo Scientific, gases were separated such that H_2 was detected on the first channel using an Ar carrier gas and thermal conductivity detector (TCD) and all other gases were detected on the second channel using a He carrier gas and a TCD. The GC system was calibrated using calibration gas mixtures (SCOTTY Specialty Gas) at H_2 = 0.01, 0.02, 0.05, 0.5, and 1% v/v and CO = 0.02, 0.05, 0.5, 1, and 7% v/v. Chromatographs were analyzed by using the Chromeleon Console WorkStation software.

Faradaic efficiencies of gaseous products were calculated via Equation 2.8:

$$\mathrm{FE} = \frac{\frac{V_{HS}}{V_g} \times G \times n \times F}{Q}$$

Equation 2.8

In this equation, the variables are defined as follows: V_{HS} is the headspace volume in mL of the working chamber, V_g is the molar volume of gas at 25ºC and 1.0 atm (24,500 mL/mol), G is the volume percent of gaseous product determined by GC (%), n is the number of electrons required for each product (n = 2 for H_2 and CO), F is the Faraday constant (C/mol) and Q is the charge passed in Coulombs.

2.5 Results and Discussion

In our prior work in this area, we immobilized CoPc-P4VP and related systems onto edge-plane graphite (EPG) electrodes to form CoPc-P4VP/EPG materials.[14,37,45,48] In these studies, we sought to understand the microenvironment surrounding the polymer-encapsulated CoPc site. EPGs were an optimal choice of electrode because the high surface area of the electrode surface and intercalation of the CoPc catalyst between the graphitic sheets facilitated charge transport to the CoPc active sites. In this study, to understand better the role of the graphite powder support (GP) on activity, we immobilized polymer/catalyst composite system onto planar glassy carbon electrodes (GCEs) and measured the activity of multiple samples with varying levels of CoPc loading (Figure 2.2a). Planar GCEs are smoother than EPG electrodes and do not have aligned graphite sheets that allow for intercalation; they are therefore an appropriate electrode material for studying the effect of graphite powder incorporation on charge transport. Activity is reported as the absolute value of the catalytic current density measured in CO_2-saturated phosphate solutions at pH 5.

CoPc-P4VP films incorporating graphite powder on the GCE electrodes (CoPc-P4VP/GP/GCE) have more than double the activity compared to CoPc-P4VP/GCE without graphite powder at any given catalyst and polymer loading (Figure 2.2a). CoPc-P4VP/GCE not only reduces CO_2 with less activity than CoPc-P4VP/GP/GCE, but also with significantly less activity than CoPc-P4VP films on edge-plane graphite (CoPc-P4VP/EPG). We postulate that the small magnitude current densities for CoPc-P4VP/GCE compared to CoPc-P4VP/EPG and CoPc-P4VP/GP/GCE is due to poor charge transport through the polymer film on the GCE surface. SEM images for CoPc-P4VP/GP/GCE (Figure 2.2b) show that GP incorporation into the film leads to high surface area features that enhance charge transport throughout the polymer film. SEM images

of CoPc-P4VP/EPG (Figure 2.2c) show similar high-surface area carbon features with slightly more rigid parallel packing due to the EPG electrode structure. CoPc-P4VP/GCE with no carbon support is relatively featureless aside from slight pitting due to polishing methods (Figure 2.2d). The lack of high-surface area carbon features in CoPc-P4VP/GCE make it more difficult for charge to transport from the smooth electrode surface to CoPc molecules at the exterior of the film compared to CoPc-P4VP/EPG and CoPc-P4VP/GP/GCE.

Note that the increased activity with added GP for the CoPc-P4VP/GP/GCE system only occurs when the films are prepared as described in the experimental section with centrifugation. Simply mixing the GP into a CoPc-P4VP ink with no centrifugation step results in films that have markedly lower activity for the CO_2RR (Figure 2.7). The centrifugation step concentrates the CoPc-P4VP system near the GP and likely facilitates physisorption to the particles, which in turn promotes efficient charge transport to the CoPc.[34,60,61] Note that most other reported methods for preparing CoPc films with carbon supports do not include this centrifugation step, which could be one reason for such large differences in the reported performance of these systems.

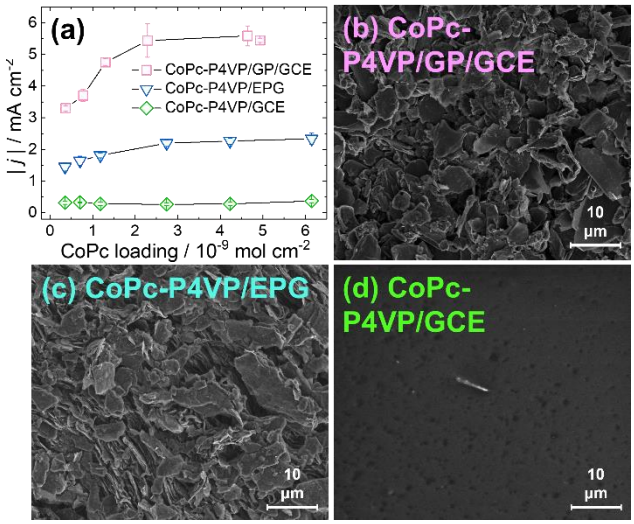

Figure 2.2 CoPc-P4VP/GP/GCE, CoPc-P4VP/EPG, and CoPc-P4VP activity and corresponding SEM images.(a) A plot of the absolute value of the average current density from RDE-CA measurements at −1.25 V vs SCE in CO_2-saturated 0.1 M phosphate solution at pH 5 reported as a function of CoPc loading for CoPc-P4VP/GP/GCE (10 mg/mL GP), CoPc-P4VP/EPG, and CoPc-P4VP/GCE. Each film has the approximately same CoPc:P4VP loading. All data points are reported as averages from at least three experiments on independently prepared samples, and the error bars represent standard deviations. The solid black lines connecting the points are guides to the eye, and not indicative of fits of the data. The loadings of CoPc, P4VP, and GP for each data point is summarized in Table 2.2, Table 2.3, and Table 2.4, representative RDE-CAs for selected CoPc loadings are shown in Figure 2.8, Figure 2.10, and Figure 2.11, and activity data is summarized in Table 2.20. (b)-(d) SEM images of the catalyst-modified electrodes (b) CoPc-P4VP/GP/GCE (c) CoPc-P4VP/EPG and (d) CoPc-P4VP/GCE.

To determine how modulating the CoPc and GP loading within the CoPc-P4VP/GP/GCE affects the CO_2RR activity, we systematically changed the amount of CoPc and GP in the catalyst deposition inks while maintaining constant CoPc:P4VP ratios. The specific concentrations of CoPc, P4VP, and GP in the deposition inks investigated and the measured loadings on the resulting CoPc-P4VP/GP/GCE electrodes are summarized in Table 2.2, Table 2.5, Table 2.6, and Table 2.7. A plot of catalytic activity as a function of CoPc loading at different GP loadings is shown in Figure 2.3a. Another way to visualize this data is by dividing the catalytic activity by the CoPc loading, resulting in a per-CoPc activity metric j_{CoPc}. A plot of j_{CoPc} as a function of CoPc loadings at different GP loadings is shown in Figure 2.3b.

When no GP is present in the film (0 mg cm^{-2} GP loading), the measured CO_2RR activity is relatively constant with increasing CoPc loading (Figure 2.3a) and there is a corresponding decrease in the normalized activity per CoPc with increasing CoPc loading (Figure 2.3b). We interpret this result to mean that only a small, constant amount of CoPc near the electrode surface is active as the film loading increases due to inefficient charge transfer to exterior CoPc sites far from the surface in the film.

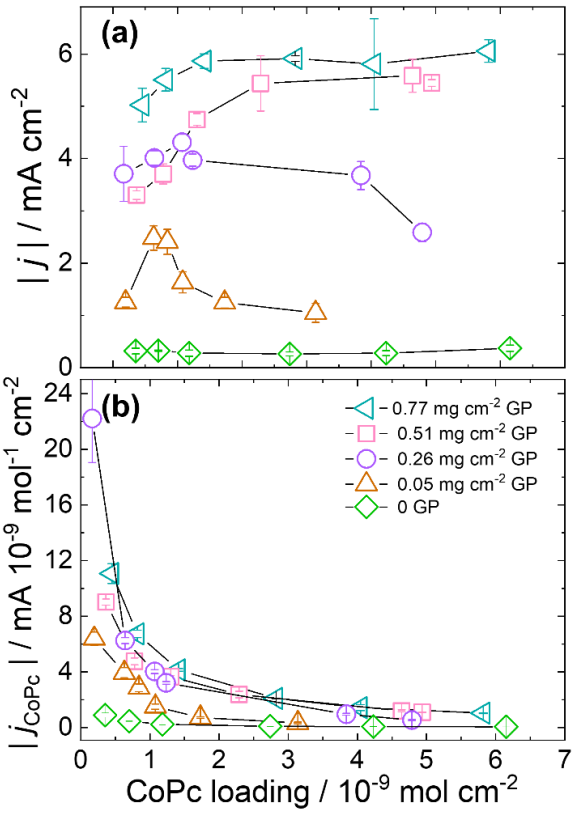

Figure 2.3 Activity measured as current density as shown by different CoPc loadings. (a) A plot of the absolute value of the average total current density from RDE-CA measurements at −1.25 V vs SCE in CO_2-saturated 0.1 M phosphate solution at pH 5 reported as a function of CoPc loading for CoPc-P4VP/GP/GCE at different GP loadings. For each set of measurements at a given GP loading, the CoPc:P4VP ratio stays constant as CoPc increases. (b) The same data as in (a), but normalized for CoPc loading. The resulting total charge density normalized for CoPc loading, j_{CoPc} decreases as CoPc loading increases. All data points are reported as averages from at least three experiments on independently prepared samples, and the error bars represent standard deviations. The solid black lines connecting the points are guides to the eye, and not indicative of fits of the data. For all measurements, the loading of CoPc, P4VP, and GP for each data point is summarized in Table 2.2, Table 2.3, Table 2.5, Table 2.6 ,and Table 2.7, representative RDE-CAs for selected CoPc loadings are shown in Figure 2.8, Figure 2.12, Figure 2.13, Figure 2.14, and activity data is summarized in Table 2.20, Table 2.21, Table 2.22, Table 2.23, and Table 2.24.

For CoPc-P4VP/GP/GCE films with low GP loadings of = 0.05 mg cm^{-2}, there is an initial increase in the overall activity as the CoPc loading increases, followed by a sharp decrease at higher CoPc loadings (Figure 2.3a). We interpret these results to suggest that the addition of moderate amounts of GP to the film increases the effective distance in which efficient charge transfer occurs and thus increases activity. However, as the film loading increases with higher CoPc loading at constant CoPc:P4VP ratios, the average film thickness of the resulting CoPc-P4VP/GP/GCE films also increases. The net result is that the individual GP particles are spaced further apart in these thicker films at higher film loadings, inhibiting efficient charge transport to the exterior CoPc. This leads to decreased activity at higher CoPc loadings for these films with relatively moderate or low GP loadings.

At sufficiently high GP loadings ≥ 0.51 mg cm^{-2}, the activity of the CoPc-P4VP/GP/GCE system increases as the CoPc loading increases until finally reaching a plateau of $j \approx 6$ mA cm^{-2} at CoPc loadings of ~4 x 10^{-9} mol cm^{-2}. The fact that these CoPc-P4VP/GP/GCE films with high GP loading plateau in activity, rather than decrease, at high CoPc loading and film thickness suggest that charge transport may not be the main limitation to activity. Instead, we suspect that either detrimental CoPc aggregation[19] due to high CoPc loading or poor CO_2 and H^+ transport to interior sites due to the increased film thickness may limit activity at high CoPc loadings in the high-GP films. Note that the same plateauing effect is seen for the CoPc-P4VP/EPG system in Figure 2.2a.

As previously discussed, for CoPc-P4VP/GP/GCE films with moderate GP loadings of ≤ 0.26 mg cm^{-2}, there is a decrease in measured activity with increasing CoPc loading (Figure 2.3a). We postulate that this decrease in activity at higher CoPc loading is due to further spacing between the GP particles in the film as the CoPc loading and film thickness increase, which in turn leads to inefficient charge transport and decreased activity compared to the thinner films at the same GP

loading and decreased CoPc loadings. To test this postulate, we designed a set of experiments keeping the GP:CoPc-P4VP ratios constant. Three catalyst preparation suspensions were prepared where the amounts of CoPc (0.0125 mM) and P4VP (0.75% w/v) were the same in each suspension, but the amount of GP differed (1 mg/mL, 5 mg/mL, 10 mg/mL). The suspensions were then centrifuged, the supernatant decanted, and the resultant deposition inks were deposited onto the GCEs according to the procedure in the Experimental section. Sequential layers of the deposition inks were then added to the surface to increase simultaneously the CoPc, P4VP, and GP loading while keeping the ratio of the three loadings constant. The resulting specific film compositions are reported in Table 2.8-Table 2.13. In each case, the activity increases with increasing CoPc loading to a plateau at CoPc loadings of ~1.25×10^{-9} mol cm^{-2} as shown in Figure 2.4 and reported in Table 2.25, Table 2.26, and Table 2.27.

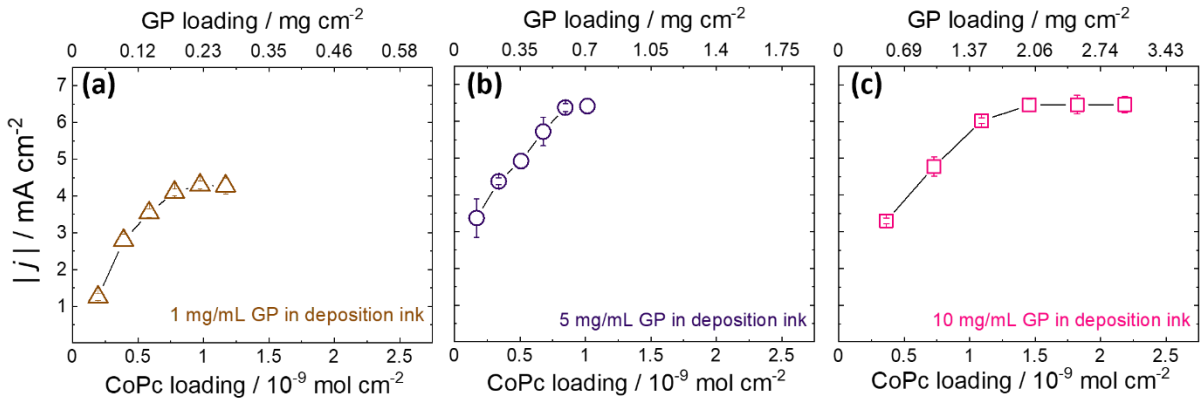

Figure 2.4 Activity measured as current density as a function of CoPc loadings with different CoPc:GP ratios held constant. A plot of the absolute value of the average total measured current density from RDE-CA measurements at −1.25 V vs SCE in CO_2-saturated 0.1 M phosphate solution at pH 5 reported as a function of CoPc loading for CoPc-P4VP/GP/GCE. The GP:CoPc-P4VP ratio is constant within each prepared set of catalyst preparation suspensions: 0.0125 mM CoPc with 0.75% P4VP and either (a) 1 mg/mL, (b) 5 mg/mL, or (c) 10 mg/mL of graphite powder. Note that even though the CoPc and P4VP loadings in the preparation suspensions were the same for each GP loading, the loadings are different in the deposition ink after the centrifugation step, and are summarized in Table 2.9, Table 2.11, and Table 2.13. The CoPc, P4VP, and GP loadings were increased by adding additional layers of the deposition ink in 10 µL increments, and so the CoPc:P4VP:GP ratio remained constant in each set of experiments. The film thickness increased along with the CoPc loading due to the stepwise deposition of P4VP and GP. All data points are reported as averages from at least three experiments on independently prepared samples, and the error bars represent standard deviations. The solid black lines connecting the points are guides to the eye, and not indicative of fits of the data. For all measurements, the loading of CoPc, P4VP, and GP for each data point is summarized in Table 2.8- Table 2.13, representative RDE-CAs for selected CoPc loadings are shown in Figure 2.15, Figure 2.16, Figure 2.17, and activity data is summarized in Table 2.25, Table 2.26, and Table 2.27.

The fact that the activity plateaus as the film loading increases when the GP:CoPc-P4VP ratio remains constant in Figure 2.4 suggests that charge transport is not limiting even at high film loadings. In contrast, for CoPc-P4VP/GP/GCE films with fixed moderate GP loadings of ≤ 0.26 mg cm^{-2} in Figure 2.3, the GP:CoPc-P4VP ratio decreases as the film loading increases, resulting in decreased activity. The different activity trends for these two systems supports our postulate that the decreased activity for CoPc-P4VP/GP/GCE films at high film loading and low GP loading is due to inefficient charge transport due to the increased spacing between the GP particles, and that this limitation can be overcome by keeping the CoPc:P4VP:GP ratios constant, thereby ensuring that GP loading increases at the same rate as CoPc and P4VP. The plateau in activity at sufficiently high GP and CoPc-P4VP loadings in Figure 2.4a, b, and c is qualitatively similar to the plateau in activity observed for the CoPc-P4VP/GP/GCE films at high fixed GP loadings $\geq$ 0.51 mg cm^{-2} in Figure 2.3a. In particular, the plateau in activity occurs at similar CoPc and P4VP loading in Figure 2.4b and Figure 2.4c, even though the GP loading is lower at this CoPc and P4VP concentration in Figure 2.4b compared to that in Figure 2.4c. These results suggest that as long as the GP:CoPc:P4VP ratio is sufficiently large and remains constant during film deposition, then charge transport is not rate limiting regardless of the film loading and thickness. Instead, the activity in systems with sufficiently large GP:CoPc:P4VP ratios may be limited by decreased H^+ or CO_2 transport to interior CoPc sites within the film, or by CoPc aggregation at higher loadings that may limit the number of active CoPc sites.

One component contributing to the high activity and selectivity of the CoPc-P4VP/EPG system is the axial coordination of the pyridyl moieties on the polymer to the CoPc center.[14,25,37] This axial coordination of σ-donating moieties to CoPc shifts the rate-determining step of the CO_2 reduction mechanism from an initial CO_2 binding step to a subsequent proton transfer event,

resulting in increases in selectivity and activity for the CO_2RR compared to four-coordinate CoPc systems.[25,45] An important question is whether such axial-coordination is still beneficial to the activity of CoPc-P4VP/GP/GCE systems. In our systems with added GP, strong interaction between the CoPc and the GP particles are likely necessary to facilitate efficient charge transport,[34,58,62,63] and these CoPc-GP interactions might be inhibited by axial coordination of the CoPc to the polymer or other pyridyl species. To help address this question, we measured the activity and selectivity of the CO_2RR as we modulated the extent of axial coordination through systematic modifications of the CoPc-polymer-GP system. In particular, we compared the CO_2RR performance of 1) CoPc-P4VP/GP/GCE, where CoPc is axially coordinated to the pyridyl moieties in P4VP;[25,37] 2) CoPc-P2VP/GP/GCE, where no axial coordination between CoPc and the poly-2-vinylpyridine (P2VP) polymer is expected;[25,37] 3) CoPc($pyNMe_2$)-P2VP/GP/GCE, where the CoPc is axially coordinated to the strong σ-donor 4-dimethylaminopyridine ($pyNMe_2$) and embedded in the non-coordinating (P2VP) polymer,[45] and 4) CoPc-P4CS/GP/GCE, where we expect sluggish activity due to both a lack of axial coordination to the poly-4-chloropolystyrene polymer (P4CS) and poor H^+ transport due to lack of multisite proton relays in the system.[25]

The results of the measured activity at different CoPc loadings with a fixed CoPc: polymer ratio and a fixed GP loading of 0.51 mg cm^{-2} are shown in Figure 2.5. In general, the systems with axial coordination to the pyridyl moieties on the P4VP polymer (CoPc-P4VP/GP/GCE) or prepared as the 5-coordinate CoPc($pyNMe_2$) species and encapsulated in the non-coordinating P2VP polymer (CoPc($pyNMe_2$)-P2VP/GP/GCE) showed similar high activity at most CoPc loadings. Both CoPc-P4VP/GP/GCE and CoPc($pyNMe_2$)-P2VP/GP/GCE showed slightly higher activity than CoPc-P2VP/GP/GCE with no axial coordination at most CoPc loadings > 1×10^{-9} mol cm^{-2}, but the difference was not as pronounced as when comparing similar systems deposited

on EPG. For instance, we had previously shown that CoPc-P4VP/EPG operates with > 4× the activity of CoPc-P2VP/EPG,[14,25] whereas CoPc-P4VP/GP/GCE operates with only ~1.5× the activity of CoPc-P2VP/GP/GCE at most CoPc loadings (Figure 2.5). These results suggest that axial coordination is still important to maximizing activity of the system with added GP, but it has a smaller effect on the overall activity compared to systems without added GP. One explanation may be that the CoPc partially coordinates to heteroatoms on the GP particles, meaning that some fraction of CoPc in the non-coordinating P2VP case is still 5-coordinate. Such partial axial coordination of CoPc to surface species carbon systems has been previously suggested,[28] and could result in the observed higher-than-expected activity for CoPc-P2VP/GP/GCE.

Note that in all systems in Figure 2.5, there is a decrease in activity at the highest CoPc loadings measured. In particular, in the case of CoPc(pyNMe$_2$)-P2VP/GP/GCE there is a measurable decrease in activity at the highest CoPc loading, to the point where the activity of CoPc(pyNMe$_2$)-P2VP/GP/GCE and CoPc-P2VP/GP/GCE have similar activities at the highest CoPc loading. We attribute this decreased activity at the highest CoPc loadings to the inefficient charge transport. In the systems reported in Figure 2.5, GP loading is held constant as the film loading increases. As we discussed above for films with intermediate GP loadings in Figure 3, as the film loading increases, the individual GP particles are spaced further apart, and charge transport is inhibited at higher film loadings. The important takeaway from these studies is that axial coordination increases activity for the CO_2RR by the CoPc system with added GP, but this axial coordination becomes less important under charge transport limitations. Even when we encapsulate CoPc(pyNMe$_2$) within the coordinating P4VP polymer, to ensure CoPc is axially coordinated, the activity at the highest CoPc loading is similar to that for CoPc-P2VP/GP/GCE

(see Table 2.18). CoPc aggregation and/or inefficient CO_2 or H^+ transport at higher CoPc and film loadings may also contribute to this observed decreased activity.

We also measured the activity in CoPc-P4CS/GP/GCE, where the polymer is unable to coordinate axially to the CoPc, and the polymer cannot participate in the proton transfer mechanism via multisite proton relays. In previous studies, we used PS as a non-coordinating, inert polymer.[25] Unfortunately, the large polymer loadings used in the preparation suspensions in this study resulted in aggregation and precipitation of the PS from the suspensions. P4CS was chosen as an alternate polymer that does not aggregate under these conditions due the added steric bulk of the Cl group, but also does not interact with the CoPc and does not have a proton-shuttling moiety. The electrochemical stability of P4CS has not been rigorously addressed in the literature, but it shows similar stability to thermal degradation compared to PS and P4VP,[64-66] and we observed no evidence of activity loss or polymer degradation during our electrochemical measurements. We expected that CoPc-P4CS should behave similarly to CoPc-PS with low activity for the CO_2RR. Indeed, CoPc-P4CS/GP/GCE showed little activity for the CO_2RR as expected. In previous studies, we used CoPc-polystyrene (CoPc-PS) to show that the pyridyl moieties within the polymer are vital to the effects that we see due to P4VP encapsulation of CoPc.

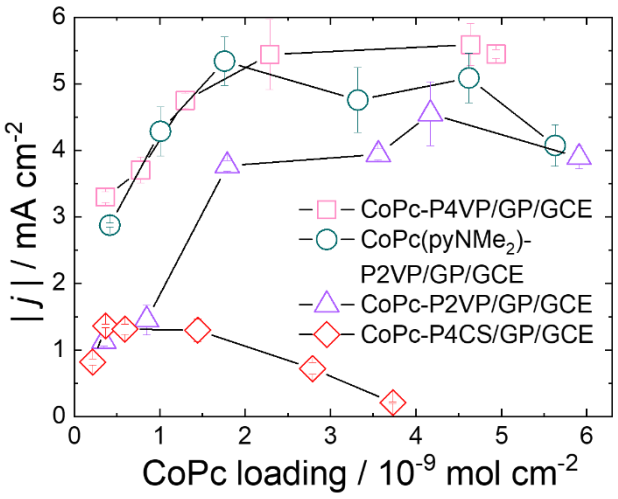

Figure 2.5 The effect of axial coordination on activity of catalyst-polymer composites with graphite powder (GP) on GCEs. The overall activity of the system is higher when the CoPc is coordinated to either the polymer (in the case of CoPc-P4VP/GP/GCE) or to a fifth ligand (in the case CoPc(pyNMe2)-P2VP/GP/GCE). Activity is reported as the absolute value of the average total measured current density from RDE-CA measurements at −1.25 V vs SCE in CO_2-saturated 0.1 M phosphate solution at pH 5 reported as a function of CoPc loading. For each set of measurements, the GP loading is 10 mg/mL or 0.51 mg/cm^2 and the CoPc:polymer ratio stays constant as the CoPc loading increases. All data points are reported as averages from at least three experiments on independently prepared samples, and the error bars represent standard deviations. The solid black lines connecting the points are guides to the eye, and not indicative of fits of the data. For all measurements, the loading of CoPc, polymer, and GP for each data point is summarized in Table 2.2, Table 2.14, Table 2.15, Table 2.16. A sample of representative RDE-CAs for selected CoPc loadings are shown in Figure 2.8 and Figure 2.18, Figure 2.19, Figure 2.20, and activity data is summarized in Table 2.21, Table 2.28, Table 2.29, Table 2.30.

Based on the measurements above, we chose an optimized loading for CoPc-P4VP/GP/GCE consisting of 0.05 mM CoPc – 3% P4VP – 1% GP in the preparation slurry, corresponding to 0.023 mM CoPc – 0.3% P4VP – 1% GP deposition ink and we conducted selectivity measurements for the CO_2RR at this optimized loading. We compared the selectivity measurements for CoPc-P4VP/GP/GCE to those for CoPc-P2VP/GP/GCE and CoPc(pyNMe_2)-P2VP/GP/GCE at similar CoPc, polymer, and CP loadings as shown in Figure 2.6. The trends in selectivity for the CoPc-polymer/GP/GCE systems are qualitatively similar to those observed on the CoPc-polymer/EPG systems without the added GP.[14,25] In particular, on both EPG and GP/GCE, CoPc-P4VP and CoPc(pyNMe_2)-P2VP show the highest selectivity for the CO_2RR due to the synergistic effects of axial coordination facilitating CO_2 binding and the polymer controlling H^+ transport and inhibiting the competitive HER. In comparison, on both EPG and GP/GCE, CoPc-P2VP shows slightly lower selectivity for the CO_2RR—it benefits from the controlled H^+ transport, but not the axial coordination effects. The systems on GP/GCE overall have slightly lower selectivity for the CO_2RR compared to the systems on EPG, and we attribute this to increased background HER on the GP itself. Control experiments conducted with CoPc-P4VP/GP prepared at the same polymer and CoPc loadings but without centrifugation showed similar Faradaic efficiency for CO production of 82% compared to the centrifuged CoPc-P4VP/GP/GCE case (Table 2.31), but substantially lower overall activity in the CPE measurements consistent with our RDE-CA measurements of the same system (Figure 2.7).

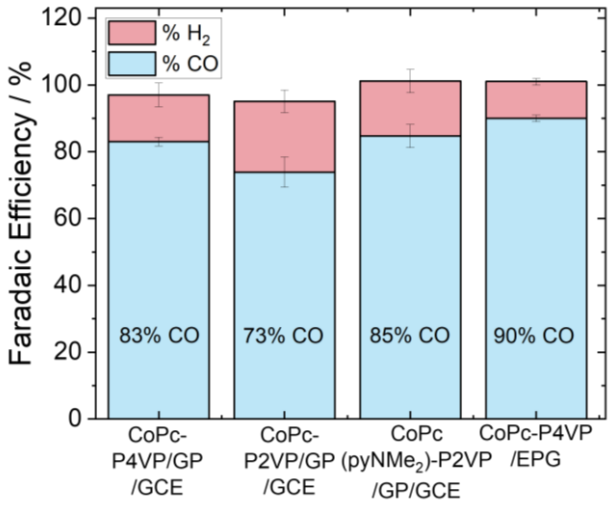

Figure 2.6 The measured Faradaic Efficiency for different CoPc-polymer systems on GP/GCE and EPG. CoPc-P4VP and CoPc(pyNMe$_2$)-P2VP operate with the highest Faradaic Efficiency, and thus the highest selectivity for the CO_2RR, on GP/GCE and EPG. CoPc-P2VP operates with comparatively lower CO_2RR selectivity. The CoPc-P4VP system on GP/GCE operates with similar but slightly lower Faradaic Efficiency than of that on EPG, and this is attributed to the higher background HER on the added GP in the GP/GCE system. All reported Faradaic Efficiencies are reported as averages from at least three CPE experiments on independently prepared samples, and the error bars represent standard deviations. The loading of CoPc, polymer, and GP for each data point is summarized in Table 2.19, representative current-potential traces for each CPE are shown in Figure 2.22, Figure 2.23, and Figure 2.24, and the metrics from the CPE measurements are summarized in Table 2.31.

2.6 Conclusions

Incorporating graphite powder into a catalyst-polymer composite system such as CoPc-P4VP increases charge transport and therefore increases activity—this is expected activity based on numerous previous studies. Importantly, we developed a specific multistep deposition procedure that maximizes the interactions between the CoPc and GP to facilitate efficient charge transport.

We show that there is a point of diminishing returns where further increasing the graphite powder loading, where sufficient loading of either 0.51 mg cm^{-2} or 0.76 mg cm^{-2} resulted in similar overall activity (Figure 2.3a). At low to moderate constant GP loadings, increasing the CoPc and P4VP polymer loadings results in losses in activity at sufficiently high film thicknesses, presumably due to inefficient charge transport (Figure 2.3a).

When GP loading remains constant in relation to CoPc and P4VP, increasing the CoPc and P4VP polymer loadings results in a plateau, not a loss, in activity at sufficiently high catalyst loading (Figure 2.4). This plateau in the catalytic activity at high CoPc, P4VP, and GP loadings is attributed to either inefficient H^+ and CO_2 transport to interior CoPc sites, or lower per-Co activity due to CoPc aggregation since the GP:CoPc:P4VP ratio remained constant, and was therefore sufficiently large to allow for charge transport as the film thickness increased. Axial coordination is still required for the highest activity in the polymer composite systems even in the presence of GP (Figure 2.5), suggesting that the CoPc does not fully coordinate to heteroatoms on the GP surface, although some extent of coordination between CoPc and the GP surface may be present.

Based on the various activity measurements as a function of CoPc, P4VP, and GP loading, we determined a set of optimized loading conditions that maximized the catalytic activity. Under

these optimized conditions, we showed that the selectivity for the CO_2RR over competitive HER was similar to those measured previously on EPG, but with much higher catalytic activity in the GP/GCE case (Figure 2.6). The detailed study presented here will be used in future studies to develop optimal loading conditions for other polymer-catalyst composite systems with various carbon supports. Future studies for this system may also include *in situ* XAS measurements to understand better the nature of the catalyst/polymer/GP interactions as a function of loading and applied potential.

2.7 Supplementary Information

2.7.1 Supplementary Tables

Table 2.1 Comparison of Reported Preparation Methods for CoPc-Carbon Support Catalysis of CO_2

Catalyst	Polymer	Centr-ifuged	Depo-sition Solve-nt	CoPc Loading / 10^{-9} mol cm^{-2}	Carbon Loading / mg mL^{-1}	Pote-ntial / V vs RHE	Electrolyte (pH)	FE_{CO} (FE_{MeOH}) / %	TOF_{CO} / s^{-1}	Ref.
CoPc/GP GCE	P4VP	Yes	DMF	1.3	10	-0.73	0.1 M NaH_2PO_4 (4.7)	85	3.1[a]	This Work
CoPc/GP GCE	P2VP	Yes	DMF	1.8	10	-0.73	0.1 M NaH_2PO_4 (4.7)	73	1.6[a]	This Work
CoPc/ EPG	P4VP	No	DMF	1.2	0	-0.73	0.1 M NaH_2PO_4 (4.7)	91	1.4[a]	This Work
CoPc/ Vulcan XC-72 GCE	Nafion	No	Pyridin e	70	2.5	-0.7	0.1 M $KHCO_3$ (6.8)	88	0.38[a]	[34]
CoPc/ CNTs GCE	Nafion	No	Pyridin e	70	2.5	-0.7	0.1 M $KHCO_3$ (6.8)	88	0.88[a]	[34]
CoPc/ MWCNT s Carbon Paper	Nafion	No	Ethylen e Glycol/ Ethanol	23.3	1.5	-0.67	0.5 M $NaHCO_3$ (7.3)	93	4.1[b]	[67]
CoPc/ MWCNT s Carbon Paper	Nafion	No	Ethylen e Glycol/ Ethanol	15.7	3	-0.88	0.5 M $KHCO_3$ (7.2)	33.6 (0.03)	1.28[a]	[20]
CoPc/CN T Carbon Fiber Paper (CFP)	Nafion	Yes	Ethanol	18	25	-0.63	0.1 M $KHCO_3$ (6.8)	92	2.7[a]	[16]
CoPc/CB CFP	Nafion	Yes	Ethanol	18	30	-0.63	0.1 M $KHCO_3$ (6.8)	92	0.56[a]	[16]
CoPc/RG O CFP	Nafion	Yes	Ethanol	18	20	-0.63	0.1 M $KHCO_3$ (6.8)	92	0.93[a]	[16]
CoPc/CN Ts CFP	Nafion	Yes	Ethanol	18	25	-0.94	0.1 M $KHCO_3$ (6.8)	26 (43)	0.5[a]	[30]
CoPc/Ch emically converted Graphene / CFP	None	Yes	THF/D MF	1.4	~ 0.6	-0.59	0.1 M $KHCO_3$ (6.8)	66	~ 2[b]	[22]

Catalyst	Polymer	Centr-ifuged	Depo-sition Solvent	CoPc Loading / 10^{-9} mol cm^{-2}	Carbon Loading / mg mL^{-1}	Pote-ntial / V vs RHE	Electrolyte (pH)	FE_{CO} (FE_{MeOH}) / %	TOF_{CO} / s^{-1}	Ref.
CoPc/CNT/ CFP	Nafion	No	DMF	21	1.5	-0.65	0.1 M $KHCO_3$ (6.8)	90	1.3 [a]	[68]
CoPc-CNT/Carbon Paper	Nafion	No	DMF	5	5	-0.67	0.2 M $NaHCO_3$ (7.0)	96	4.5 [a]	[31]
Co-PolyPc CNTs/ Ketjen Carbon/CFP	Nafion	Yes	Ethanol	64	~ 4	-0.61	0.5 M $NaHCO_2$ (7.4)	90	1.36 [b]	[15]

[a] CoPc loading is total amount of CoPc dropcasted onto working electrode

[b] Electroactive CoPc loading determined by CV

Table 2.2 Preparation conditions for CoPc-P4VP/GP/GCE as shown in Figure 2.2a, Figure 2.3, and Figure 2.5. Columns 1-3 detail the concentrations of cobalt phthalocyanine (CoPc), poly-(4-vinylpyridine) (P4VP), and graphite powder (GP) in the preparation suspension. Columns 4-6 detail the measured conditions of the preparation conditions of the CoPc loading, P4VP loading, and GP loading, with errors being the standard deviation of at least 3 individually prepared measurements. Columns 7-9 detail the catalyst, polymer, and GP loading on the 0.196 cm^2 glassy carbon electrodes (GCEs).

CoPc-P4VP/GP/GCE: 0.51 mg cm^{-2} GP								
Before Centrifugation			After Centrifugation			Electrode Loading		
Preparation Suspension			Deposition Ink			Deposition Ink Dropcasted		
CoPc loading / mM	P4VP loading / mg mL^{-1}	GP loading / mg mL^{-1}	CoPc loading / mM	P4VP loading / mg mL^{-1}	GP loading / mg mL^{-1}	CoPc loading / 10^{-9} mol cm^{-2}	P4VP loading / mg cm^{-2}	GP loading / mg cm^{-2}
0.2	120	10	0.096 ± 0.009	40 ± 13	10	4.9 ± 0.4	2.0 ± 0.7	0.513
0.15	90	10	0.091 ± 0.002	33 ± 3	10	4.6 ± 0.1	1.6 ± 0.1	0.513
0.1	60	10	0.044 ± 0.004	12 ± 3	10	2.3 ± 0.2	0.6 ± 0.2	0.513
0.05	30	10	0.025 ± 0.003	3 ± 1	10	1.3 ± 0.1	0.1 ± 0.04	0.513
0.025	15	10	0.015 ± 0.005	2 ± 0.4	10	0.8 ± 0.2	0.09 ± 0.02	0.513
0.0125	7.5	10	0.007 ± 0.001	0.9 ± 0.1	10	0.4 ± 0.04	0.05 ± 0.01	0.513

Table 2.3 Preparation Conditions for CoPc-P4VP/GCE in Figure 2.2 and Figure 2.3. There was no centrifugation in this system, so columns 4-6 detail the measured conditions of the preparation conditions of the CoPc loading and P4VP loading as directly prepared for the deposition ink. Columns 7-9 detail the CoPc, polymer, and GP loading on the 0.196 cm^2 GCEs.

CoPc-P4VP/GCE								
Before Centrifugation			After Centrifugation			Electrode Loading		
Preparation Suspension			Deposition Ink			Deposition Ink Dropcasted		
CoPc loading / mM	P4VP loading / mg mL^{-1}	GP loading / mg mL^{-1}	CoPc loading / mM	P4VP loading / mg mL^{-1}	GP loading / mg mL^{-1}	CoPc loading / 10^{-9} mol cm^{-2}	P4VP loading / mg cm^{-2}	GP loading / mg cm^{-2}
N/A (no centrifugation)		0	0.12	30	0	6.1	0.15	0.000
		0	0.0825	25	0	4.2	0.12	0.000
		0	0.0534	20	0	2.7	0.10	0.000
		0	0.023	10	0	1.2	0.051	0.000
		0	0.0137	5	0	0.7	0.026	0.000
		0	0.00687	3	0	0.4	0.015	0.000

Table 2.4 Preparation Conditions for CoPc-P4VP/EPG in Figure 2.2. There was no centrifugation in this system, so columns 4-6 detail the measured conditions of the preparation conditions of the CoPc loading and P4VP loading as directly prepared for the deposition ink. Columns 7-9 detail the CoPc, polymer, and GP loading on the total surface area of the electrode surface, 0.196 cm^2 (conductive surface area: 0.114 cm^2 due to encapsulating non-conductive polymer epoxy).

Before Centrifugation			After Centrifugation			Electrode Loading		
Preparation Suspension			Deposition Ink			Deposition Ink Dropcasted		
CoPc loading / mM	P4VP loading / mg mL^{-1}	GP loading / mg mL^{-1}	CoPc loading / mM	P4VP loading / mg mL^{-1}	GP loading / mg mL^{-1}	CoPc loading / 10^{-9} mol cm^{-2}	P4VP loading / mg cm^{-2}	GP loading / mg cm^{-2}
N/A (no centrifugation)		0	0.12	30	0	6.15	1.54	0.000
		0	0.082	25	0	4.23	1.28	0.000
		0	0.0534	20	0	2.73	1.03	0.000
		0	0.023	10	0	1.17	0.51	0.000
		0	0.0137	5	0	0.70	0.26	0.000
		0	0.00687	3	0	0.35	0.15	0.000

Table 2.5 Preparation conditions for CoPc-P4VP/GP/GCE as shown in Figure 2.3. Columns 1-3 detail the concentrations of CoPc, P4VP, and GP in the preparation suspension. Columns 4-6 detail the measured conditions of the preparation conditions of the CoPc loading, P4VP loading, and GP loading, with errors being the standard deviation of at least 3 individually prepared measurements. Columns 7-9 detail the CoPc, polymer, and GP loading on the 0.196 cm^2 GCEs.

0.77 mg cm^{-2} GP								
Before Centrifugation			After Centrifugation			Electrode Loading		
Preparation Suspension			Deposition Ink			Deposition Ink Dropcasted		
CoPc loading / mM	P4VP loading / mg mL^{-1}	GP loading / mg mL^{-1}	CoPc loading / mM	P4VP loading / mg mL^{-1}	GP loading / mg mL^{-1}	CoPc loading / 10^{-9} mol cm^{-2}	P4VP loading / mg cm^{-2}	GP loading / mg cm^{-2}
0.2	120	15	0.114 ± 0.003	53.1 ± 13.0	15	5.81 ± 0.19	2.72 ± 0.67	0.769
0.15	90	15	0.079 ± 0.007	29.4 ± 1.2	15	4.04 ± 0.37	1.51 ± 0.06	0.769
0.1	60	15	0.055 ± 0.007	14.6 ± 5.6	15	2.82 ± 0.36	0.75 ± 0.28	0.769
0.05	30	15	0.027 ± 0.005	6.6 ± 2.8	15	1.41 ± 0.25	0.34 ± 0.14	0.769
0.025	15	15	0.016 ± 0.001	0.51 ± 0.88	15	0.81 ± 0.08	0.026 ± 0.04558	0.769
0.0125	7.5	15	0.009 ± 0.001	-0.62 ± 0.72	15	0.45 ± 0.06	-0.032 ± 0.037	0.769

Table 2.6 Preparation conditions for CoPc-P4VP/GP/GCE as shown in Figure 2.3. Columns 1-3 detail the concentrations of CoPc, P4VP, and GP in the preparation suspension. Columns 4-6 detail the measured conditions of the preparation conditions of the CoPc loading, P4VP loading, and GP loading, with errors being the standard deviation of at least 3 individually prepared measurements. Columns 7-9 detail the CoPc, polymer, and GP loading on the 0.196 cm^2 GCEs.

0.26 mg cm^{-2} GP								
Before Centrifugation			After Centrifugation			Electrode Loading		
Preparation Suspension			Deposition Ink			Deposition Ink Dropcasted		
CoPc loading / mM	P4VP loading / mg mL^{-1}	GP loading / mg mL^{-1}	CoPc loading / mM	P4VP loading / mg mL^{-1}	GP loading / mg mL^{-1}	CoPc loading / 10^{-9} mol cm^{-2}	P4VP loading / mg cm^{-2}	GP loading / mg cm^{-2}
0.2	120	5	0.093 ± 0.020	38.09 ± 16.11	5	4.88 ± 1.0	1.95 ± 0.82	0.256
0.15	90	5	0.075 ± 0.003	14.61 ± 10.66	5	3.5 ± 0.2	0.74 ± 0.54	0.256
0.1	60	5	0.024 ± 0.001	11.12 ± 1.27	5	1.23 ± 0.04	0.57 ± 0.06	0.256
0.05	30	5	0.020 ± 0.003	1.12 ± 0.52	5	1.07 ± 0.14	0.058 ± 0.027	0.256
0.025	15	5	0.013 ± 0.001	1.24 ± 0.15	5	0.64 ± 0.07	0.064 ± 0.008	0.256
0.0125	7.5	5	0.003 ± 0.0004	0.31 ± 0.60	5	0.16 ± 0.02	0.016 ± 0.031	0.256

Table 2.7 Preparation conditions for CoPc-P4VP/GP/GCE as shown in Figure 2.3. Columns 1-3 detail the concentrations of CoPc, P4VP, and GP in the preparation suspension. Columns 4-6 detail the measured conditions of the preparation conditions of the CoPc loading, P4VP loading, and GP loading, with errors being the standard deviation of at least 3 individually prepared measurements. Columns 7-9 detail the CoPc, polymer, and GP loading on the 0.196 cm^2 GCEs.

0.051 mg cm^{-2} GP								
Before Centrifugation			After Centrifugation			Electrode Loading		
Preparation Suspension			Deposition Ink			Deposition Ink Dropcasted		
CoPc loading / mM	P4VP loading / mg mL^{-1}	GP loading / mg mL^{-1}	CoPc loading / mM	P4VP loading / mg mL^{-1}	GP loading / mg mL^{-1}	CoPc loading / 10^{-9} mol cm^{-2}	P4VP loading / mg cm^{-2}	GP loading / mg cm^{-2}
0.2	120	1	0.062 ± 0.013	41.8 ± 6.0	1	3.14 ± 0.66	2.14 ± 0.31	0.051
0.15	90	1	0.034 ± 0.004	34.7 ± 4.5	1	1.73 ± 0.20	1.78 ± 0.23	0.051
0.1	60	1	0.021 ± 0.001	11.9 ± 1.6	1	1.08 ± 0.06	0.61 ± 0.08	0.051
0.05	30	1	0.016 ± 0.002	1.0 ± 1.9	1	0.84 ± 0.10	0.051 ± 0.09	0.051
0.025	15	1	0.012 ± 0.002	-0.56 ± 1.0	1	0.63 ± 0.19	-0.029 0.52	0.051
0.0125	7.5	1	0.004 ± 0.0005	0.33 ± 0.38	1	0.19 ± 0.02	0.017 ± 0.019	0.051

Table 2.8 Preparation conditions for deposition ink for the CoPc-P4VP/GP/GCE as shown in Figure 2.4. Columns 1-3 detail the concentrations of CoPc, P4VP, and GP in the preparation suspension. Columns 4-6 detail the measured conditions of the preparation conditions of the CoPc loading, P4VP loading, and GP loading, with errors being the standard deviation of at least 3 individually prepared measurements. Columns 7-9 detail the CoPc, polymer, and GP loading on the 0.196 cm2 GCEs.

Before Centrifugation			After Centrifugation			Electrode Loading		
Preparation Suspension			Deposition Ink			Deposition Ink Dropcasted		
CoPc loading / mM	P4VP loading / mg mL^{-1}	GP loading / mg mL^{-1}	CoPc loading / mM	P4VP loading / mg mL^{-1}	GP loading / mg mL^{-1}	CoPc loading / 10^{-9} mol cm^{-2}	P4VP loading / mg cm^{-2}	GP loading / mg cm^{-2}
0.0125	7.5	10	0.0071 ± 0.0009	0.94 ± 0.15	10	0.37 ± 0.05	0.048 ± 0.008	0.513

Table 2.9 Number of 10 μL depositions of the CoPc-P4VP/GP deposition ink described in Table 2.8., resulting in the CoPc, P4VP, and GP loadings detailed in columns 2-4.

# of 10 μL layers	CoPc loading / 10^{-9} mol cm^{-2}	P4VP loading / mg cm^{-2}	GP loading / mg cm^{-2}
1	0.364	0.048	0.513
2	0.728	0.096	1.026
3	1.092	0.144	1.538
4	1.456	0.192	2.051
5	1.821	0.240	2.564
6	2.185	0.288	3.077

Table 2.10 Preparation conditions for deposition ink for the CoPc-P4VP/GP/GCE as shown in Figure 2.4. Columns 1-3 detail the concentrations of CoPc, P4VP, and GP in the preparation suspension. Columns 4-6 detail the measured conditions of the preparation conditions of the CoPc loading, P4VP loading, and GP loading, with errors being the standard deviation of at least 3 individually prepared measurements. Columns 7-9 detail the CoPc, polymer, and GP loading on the 0.196 cm^2 GCEs.

Before Centrifugation			After Centrifugation			Electrode Loading		
Preparation Suspension			Deposition Ink			Deposition Ink Dropcasted		
CoPc loading / mM	P4VP loading / mg mL^{-1}	GP loading / mg mL^{-1}	CoPc loading / mM	P4VP loading / mg mL^{-1}	GP loading / mg mL^{-1}	CoPc loading / 10^{-9} mol cm^{-2}	P4VP loading / mg cm^{-2}	GP loading / mg cm^{-2}
0.0125	7.5	5	0.003 ± 0.0004	0.31 ± 0.60	5	0.16 ± 0.02	0.016 ± 0.031	0.256

Table 2.11 Number of 10 μL depositions of the CoPc-P4VP/GP deposition ink described in Table 2.10, resulting in the CoPc, P4VP, and GP loadings detailed in columns 2-4.

# of 10 μL layers	CoPc loading / 10^{-9} mol cm^{-2}	P4VP loading / mg cm^{-2}	GP loading / mg cm^{-2}
1	0.169	0.016	0.256
2	0.338	0.031	0.513
3	0.508	0.047	0.769
4	0.677	0.063	1.026
5	0.846	0.079	1.282
6	1.015	0.094	1.538

Table 2.12 Preparation conditions for deposition ink for the CoPc-P4VP/GP/GCE as shown in Figure 2.4. Columns 1-3 detail the concentrations of CoPc, P4VP, and GP in the preparation suspension. Columns 4-6 detail the measured conditions of the preparation conditions of the CoPc loading, P4VP loading, and GP loading, with errors being the standard deviation of at least 3 individually prepared measurements. Columns 7-9 detail the CoPc, polymer, and GP loading on the 0.196 cm^2 GCEs.

Before Centrifugation			After Centrifugation			Electrode Loading		
Preparation Suspension			Deposition Ink			Deposition Ink Dropcasted		
CoPc loading / mM	P4VP loading / mg mL^{-1}	GP loading / mg mL^{-1}	CoPc loading / mM	P4VP loading / mg mL^{-1}	GP loading / mg mL^{-1}	CoPc loading / 10^{-9} mol cm^{-2}	P4VP loading / mg cm^{-2}	GP loading / mg cm^{-2}
0.0125	7.5	1	0.004 ± 0.0005	0.33 ± 0.38	1	0.19 ± 0.02	0.017 ± 0.019	0.051

Table 2.13. Number of 10 μL depositions of the CoPc-P4VP/GP deposition ink described in Table 2.12 resulting in the CoPc, P4VP, and GP loadings detailed in columns 2-4.

# of 10 μL layers	CoPc loading / 10^{-9} mol cm^{-2}	P4VP loading / mg cm^{-2}	GP loading / mg cm^{-2}
1	0.195	0.017	0.051
2	0.390	0.034	0.103
3	0.585	0.052	0.154
4	0.779	0.069	0.205
5	0.974	0.086	0.256
6	1.169	0.103	0.308

Table 2.14 Preparation conditions for deposition ink for the CoPc-P2VP/GP/GCE as shown in Figure 2.5. Columns 1-3 detail the concentrations of CoPc, P2VP, and GP in the preparation suspension. Columns 4-6 detail the measured conditions of the preparation conditions of the CoPc loading, P2VP loading, and GP loading, with errors being the standard deviation of at least 3 individually prepared measurements. Columns 7-9 detail the CoPc, polymer, and GP loading on the 0.196 cm^2 GCEs.

CoPc-P2VP/GP/GCE								
Before Centrifugation			After Centrifugation			Electrode Loading		
Preparation Suspension			Deposition Ink			Deposition Ink Dropcasted		
CoPc loading / mM	P2VP loading / mg mL^{-1}	GP loading / mg mL^{-1}	CoPc loading / mM	P2VP loading / mg mL^{-1}	GP loading/ mg mL^{-1}	CoPc loading / 10^{-9} mol cm^{-2}	P2VP loading / mg cm^{-2}	GP loading / mg cm^{-2}
0.2	120	10	0.115 ± 0.019	31.6 ± 12.3	10	5.91 ± 0.95	1.62 ± 0.63	0.513
0.15	90	10	0.082 ± 0.007	20.7 ± 8.0	10	4.17 ± 0.35	1.06 ± 0.41	0.513
0.1	60	10	0.070 ± 0.006	15.0 ± 3.7	10	3.56 ± 0.32	0.77 ± 0.19	0.513
0.05	30	10	0.035 ± 0.003	9.0 ± 2.5	10	1.79 ± 0.17	0.46 ± 0.13	0.513
0.025	15	10	0.017 ± 0.002	6.8 ± 1.4	10	0.84 ± 0.10	0.35 ± 0.07	0.513
0.0125	7.5	10	0.007 ± 0.001	3.5 ± 1.1	10	0.34 ± 0.07	0.18 ± 0.06	0.513

Table 2.15 Preparation conditions for deposition ink for the CoPc(pyNMe$_2$)-P2VP/GP/GCE as shown in Figure 2.5. Columns 1-3 detail the concentrations of CoPc, P2VP, and GP in the preparation suspension. Columns 4-6 detail the measured conditions of the preparation conditions of the CoPc loading, P2VP loading, and GP loading, with errors being the standard deviation of at least 3 individually prepared measurements. Columns 7-9 detail the CoPc, polymer, and GP loading on the 0.196 cm^2 GCEs.

CoPc(pyNMe$_2$)P2VP/GP/GCE								
Before Centrifugation			After Centrifugation			Electrode Loading		
Preparation Suspension			Deposition Ink			Deposition Ink Dropcasted		
CoPc loading / mM	P2VP loading / mg mL^{-1}	GP loading / mg mL^{-1}	CoPc loading / mM	P2VP loading / mg mL^{-1}	GP loading/ mg mL^{-1}	CoPc loading / 10^{-9} mol cm^{-2}	P2VP loading / mg cm^{-2}	GP loading / mg cm^{-2}
0.2	120	10	0.111 ± 0.021	Not Measured	10	5.66 ± 1.10	Not Measured	0.513
0.15	90	10	0.090 ± 0.008	Not Measured	10	4.59 ± 0.40	Not Measured	0.513
0.1	60	10	0.075 ± 0.024	Not Measured	10	3.81 ± 1.24	Not Measured	0.513
0.05	30	10	0.034 ± 0.006	Not Measured	10	1.75 ± 0.31	Not Measured	0.513
0.025	15	10	0.019 ± 0.004	Not Measured	10	1.01 ± 0.23	Not Measured	0.513
0.0125	7.5	10	0.008 ± 0.007	Not Measured	10	0.41 ± 0.38	Not Measured	0.513

Table 2.16 Preparation conditions for deposition ink for the CoPc-P4CS/GP/GCE as shown in Figure 2.5. Columns 1-3 detail the concentrations of CoPc, P4CS, and GP in the preparation suspension. Columns 4-6 detail the measured conditions of the preparation conditions of the CoPc loading, P4CS loading, and GP loading, with errors being the standard deviation of at least 3 individually prepared measurements. Columns 7-9 detail the CoPc, polymer, and GP loading on the 0.196 cm^2 GCEs.

CoPc-P4CS/GP/GCE								
Before Centrifugation			After Centrifugation			Electrode Loading		
Preparation Suspension			Deposition Ink			Deposition Ink Dropcasted		
CoPc loading / mM	P4CS loading / mg mL^{-1}	GP loading / mg mL^{-1}	CoPc loading / mM	P4CS loading / mg mL^{-1}	GP loading / mg mL^{-1}	CoPc loading / 10^{-9} mol cm^{-2}	P4CS loading / mg cm^{-2}	GP loading / mg cm^{-2}
0.2	12	10	0.069 ± 0.004	43.4 ± 11.6	10	3.59 ± 0.18	2.23 ± 0.59	0.513
0.15	9	10	0.045 ± 0.008	20.2 ± 3.1	10	2.31 ± 0.40	1.04 ± 0.16	0.513
0.1	6	10	0.023 ± 0.005	13.2 ± 3.1	10	1.15 ± 0.25	0.67 ± 0.16	0.513
0.05	3	10	0.008 ± 0.003	10.5 ± 2.2	10	0.43 ± 0.13	0.54 ± 0.11	0.513
0.025	1.5	10	0.0041 ± 0.0027	5.1 ± 2.2	10	0.21 ± 0.14	0.26 ± 0.11	0.513
0.0125	0.75	10	0.0024 ± 0.0016	2.0 ± 1.1	10	0.12 ± 0.08	0.10 ± 0.06	0.513

Table 2.17 Preparation conditions for deposition ink for the CoPc(pyNMe$_2$)-P4VP/GP/GCE as shown in Figure 2.5. Columns 1-3 detail the concentrations of CoPc, P4VP, and GP in the preparation suspension. Columns 4-6 detail the measured conditions of the preparation conditions of the CoPc loading, P4VP loading, and GP loading, with errors being the standard deviation of at least 3 individually prepared measurements. Columns 7-9 detail the CoPc, polymer, and GP loading on the 0.196 cm^2 GCEs.

CoPc(pyNMe$_2$)P4VP/GP/GCE								
Before Centrifugation			After Centrifugation			Electrode Loading		
Preparation Suspension			Deposition Ink			Deposition Ink Dropcasted		
CoPc loading / mM	P4VP loading / mg mL^{-1}	GP loading / mg mL^{-1}	CoPc loading / mM	P4VP loading / mg mL^{-1}	GP loading/ mg mL^{-1}	CoPc loading / 10^{-9} mol cm^{-2}	P4VP loading / mg cm^{-2}	GP loading / mg cm^{-2}
0.2	120	10	0.127 ± 0.003	Not Measured	10	6.45 ± 0.18	Not Measured	0.513

Table 2.18 CoPc($pyNMe_2$) P4VP/GP/GCE, GP loading: 0.51 mg cm^{-2} Activity results of rotating disk chronoamperometry (RDE-CA) experiment at -1.25 V vs. SCE, conducted under 1 atm CO_2 in 0.1 M NaH_2PO_4 at ~pH 4.7 under 1600 rpm rotation rate for CoPc($pyNMe_2$)-P4VP/GP/GCE with 10 mg/mL graphite powder in the catalyst ink solution, corresponding to a loading of 0.51 mg cm^{-2}.

Co loading / 10^{-9} mol cm^{-2}	$\lvert j \rvert$ @ -1.25 V vs SCE / mA cm^{-2}	Standard Deviation ± $\lvert j \rvert$ @ -1.25 V vs SCE / mA cm^{-2}
6.45	4.10	0.43

Table 2.19 Preparation conditions for deposition ink for CoPc-P4VP/GP/GCE, CoPc-P2VP/GP/GCE, CoPc($pyNMe_2$)-P2VP/GP/GCE, CoPc-P4VP/EPG controlled potential electrolysis experiments. Columns 1-3 detail the concentrations of CoPc, polymer, and GP in the preparation suspension. Columns 4-6 detail the measured conditions of the preparation conditions of the CoPc loading, polymer loading, and GP loading, with errors being the standard deviation of at least 3 individually prepared measurements. Columns 7-9 detail the CoPc, polymer, and GP loading on the 0.196 cm^2 electrodes. Row 7 shows preparation conditions for CoPc-P4VP/EPG. There was no centrifugation in this system, so columns 4-6 detail the measured conditions of the preparation conditions of the CoPc loading and P4VP loading as directly prepared for the deposition ink. Columns 7-9 detail the CoPc, polymer, and GP loading on the total surface area of the electrode surface, 0.196 cm^2 (conductive surface area: 0.114 cm^2 due to encapsulating non-conductive polymer epoxy). Row 5 (P4VP/GP) is a control CPE, run without any CoPc in the preparation suspension.

	Before Centrifugation			After Centrifugation			Electrode Loading		
	Preparation Suspension			Deposition Ink			Deposition Ink Dropcasted		
	CoPc loading / mM	Polymer loading / mg mL^{-1}	GP loading / mg mL^{-1}	CoPc loading / mM	Polymer loading / mg mL^{-1}	GP loading / mg mL^{-1}	CoPc loading / 10^{-9} mol cm^{-2}	Polymer loading / mg cm^{-2}	GP loading / mg cm^{-2}
CoPc-P4VP/ GP/GCE	0.05	30	10	0.026 ± 0.003	3.01 ± 0.97	10	1.30 ± 0.16	0.117 ± 0.049	0.513
CoPc-P2VP/ GP/GCE	0.05	30	10	0.035 ± 0.003	9.03 ± 2.54	10	1.79 ± 0.17	0.463 ± 0.1306	0.513
CoPc-$pyNMe_2$-P2VP/ GP/GCE	0.05	30	10	0.034 ± 0.006	Not Measured	10	1.75 ± 0.31	Not Measured	0.513
CoPc-P4VP/EPG	N/A (no centrifugation)		0	0.023	1	0	1.17	0.051	0.000
P4VP/GP	0	30	10	0	Not Measured	10	0	Not Measured	0.513

Table 2.20 Activity results for CoPc-P4VP on EPG and GCE. Activity results of rotating disc electrode chronoamperometry (RDE-CA) step experiment at a potential of -1.25 V vs. SCE, conducted under 1 atm CO_2 in 0.1 M NaH_2PO_4 at ~pH 4.7 under 1600 rpm rotation rate for CoPc-P4VP on an edge-plane graphite (EPG) electrode and CoPc-P4VP with no graphite powder on a glassy carbon electrode (GCE).

		CoPc-P4VP EPG		**CoPc-P4VP GCE**	
Co loading/ 10^{-9} mol cm^{-2}	P4VP loading %, w/v	$\|j\|$ @ -1.25 V vs SCE (mA cm^{-2})	Standard Deviation ± $\|j\|$ @ -1.25 V vs SCE / mA cm^{-2}	$\|j\|$ @ -1.25 V vs SCE (mA cm^{-2})	Standard Deviation ± $\|j\|$ @ -1.25 V vs SCE / mA cm^{-2}
0.352	0.3	1.44	0.13	0.317	0.054
0.702	0.5	1.63	0.14	0.324	0.010
1.18	1.0	1.81	0.08	0.278	0.059
2.74	2.0	2.19	0.10	0.263	0.039
4.23	2.5	2.26	0.10	0.278	0.046
6.15	3.0	2.33	0.19	0.370	0.059

Table 2.21 GP loading in catalyst deposition ink: 10 mg mL^{-1}. Activity results of rotating disk chronoamperometry (RDE-CA) step experiment at -1.25 V vs. SCE, conducted under 1 atm CO_2 in 0.1 M NaH_2PO_4 at ~pH 4.7 under 1600 rpm rotation rate for CoPc-P4VP/GP/GCE with 10 mg/mL graphite powder in the catalyst ink solution, corresponding to a loading of 0.51 mg cm^{-2}.

Co loading/ 10^{-9} mol cm^{-2}	$\|j\|$ @ -1.25 V vs SCE / mA cm^{-2}	Standard Deviation ± $\|j\|$ @ -1.25 V vs SCE / mA cm^{-2}
0.366	3.29	0.08
0.778	3.70	0.19
1.30	4.74	0.11
2.29	5.44	0.53
4.64	5.59	0.31
4.93	5.45	0.06

Table 2.22 GP loading in catalyst deposition ink: 15 mg mL^{-1} Activity Results for CoPc-P4VP/GP/GCE 0.77 mg cm^{-2} in Figure 2.3. Activity results of rotating disk chronoamperometry (RDE-CA) step experiment at -1.25 V vs. SCE, conducted under 1 atm CO_2 in 0.1 M NaH_2PO_4 at ~pH 4.7 under 1600 rpm rotation rate for CoPc-P4VP/GP/GCE with 15 mg/mL graphite powder in the catalyst ink solution, corresponding to a loading of 0.77 mg cm^{-2}.

Co loading/ 10^{-9} mol cm^{-2}	$\|j\|$ @ -1.25 V vs SCE / mA cm^{-2}	Standard Deviation $\pm \|j\|$ @ -1.25 V vs SCE / mA cm^{-2}
0.454	5.02	0.33
0.818	5.50	0.22
1.41	5.86	0.14
2.82	5.91	0.05
4.04	5.81	0.86
5.81	6.06	0.21

Table 2.23 GP loading in catalyst deposition ink: 5 mg mL^{-1}. Activity Results CoPc-P4VP/GP/GCE 0.26 mg cm^{-2} in Figure 2.3. Activity results of rotating disk chronoamperometry (RDE-CA) step experiment at -1.25 V vs. SCE, conducted under 1 atm CO_2 in 0.1 M NaH_2PO_4 at ~pH 4.7 under 1600 rpm rotation rate for CoPc-P4VP/GP/GCE with 5 mg/mL graphite powder in the catalyst ink solution, corresponding to a loading of 0.26 mg cm^{-2}.

Co loading/ 10^{-9} mol cm^{-2}	$\|j\|$ @ -1.25 V vs SCE / mA cm^{-2}	Standard Deviation $\pm \|j\|$ @ -1.25 V vs SCE / mA cm^{-2}
0.16	3.70	0.52
0.64	4.01	0.13
1.07	4.31	0.15
1.23	3.96	0.11
3.84	3.67	0.26
4.79	2.58	0.17

Table 2.24 GP loading in catalyst deposition ink: 1 mg mL^{-1} Activity Results CoPc-P4VP/GP/GCE 0.051 mg cm^{-2} in Figure 2.3. Activity results of rotating disk chronoamperometry (RDE-CA) step experiment at -1.25 V vs. SCE, conducted under 1 atm CO_2 in 0.1 M NaH_2PO_4 at ~pH 4.7 under 1600 rpm rotation rate for CoPc-P4VP/GP/GCE with 1 mg/mL graphite powder in the catalyst ink solution, corresponding to a loading of 0.051 mg cm^{-2}.

Co loading / 10^{-9} mol cm^{-2}	$\lvert j \rvert$ @ -1.25 V vs SCE / mA cm^{-2}	Standard Deviation $\pm \lvert j \rvert$ @ -1.25 V vs SCE / mA cm^{-2}
0.196	1.25	0.09
0.630	2.48	0.23
0.843	2.40	0.23
1.08	1.62	0.20
1.73	1.24	0.10
3.14	1.05	0.18

Table 2.25 10 mg/mL in catalyst deposition ink Activity Results CoPc-P4VP/GP/GCE in Figure 2.4. Activity results of rotating disk chronoamperometry (RDE-CA) step experiment at -1.25 V vs. SCE, conducted under 1 atm CO_2 in 0.1 M NaH_2PO_4 at ~pH 4.7 under 1600 rpm rotation rate for CoPc-P4VP/GP/GCE with 10 mg/mL graphite powder in the original catalyst ink solution. The increase in Co, polymer, and GP were all directly proportional as increasing Co loading was due to the addition of layers of ink on the electrode in 10 µL increments.

Co loading / 10^{-9} mol cm^{-2}	GP loading / mg cm^{-2}	$\lvert j \rvert$ @ -1.25 V vs SCE / mA cm^{-2}	Standard Deviation ± $\lvert j \rvert$ @ -1.25 V vs SCE / mA cm^{-2}
0.364	0.51	3.29	0.08
0.728	1.02	4.77	0.26
1.09	1.53	6.02	0.07
1.45	2.05	6.44	0.15
1.82	2.56	6.45	0.25
2.18	3.07	6.46	0.22

Table 2.26 Activity Results CoPc-P4VP/GP/GCE in Figure 2.4. 5 mg/mL in catalyst deposition ink. Activity results of rotating disk chronoamperometry (RDE-CA) step experiment at -1.25 V vs. SCE, conducted under 1 atm CO_2 in 0.1 M NaH_2PO_4 at ~pH 4.7 under 1600 rpm rotation rate for CoPc-P4VP/GP/GCE with 5 mg/mL graphite powder in the original catalyst ink solution. The increase in Co, polymer, and GP were all directly proportional as increasing Co loading was due to the addition of layers of ink on the electrode in 10 µL increments.

Co loading / 10^{-9} mol cm^{-2}	GP loading / mg cm^{-2}	$\lvert j \rvert$ @ -1.25 V vs SCE / mA cm^{-2}	Standard Deviation ± $\lvert j \rvert$ @ -1.25 V vs SCE / mA cm^{-2}
0.169	0.26	3.37	0.52
0.338	0.51	4.37	0.09
0.508	0.76	4.91	0.21
0.677	1.03	5.72	0.38
0.846	1.28	6.37	0.10
1.015	1.54	6.41	0.20

Table 2.27 Activity Results CoPc-P4VP/GP/GCE in Figure 2.4. 1 mg/mL in catalyst deposition ink. Activity results of rotating disk chronoamperometry (RDE-CA) step experiment at -1.25 V vs. SCE, conducted under 1 atm CO_2 in 0.1 M NaH_2PO_4 at ~pH 4.7 under 1600 rpm rotation rate for CoPc-P4VP/GP/GCE with 1 mg/mL graphite powder in the original catalyst ink solution. The increase in Co, polymer, and GP were all directly proportional as increasing Co loading was due to the addition of layers of ink on the electrode in 10 µL increments.

Co loading / 10^{-9} mol cm^{-2}	GP loading / mg cm^{-2}	$\lvert j \rvert$ @ -1.25 V vs SCE / mA cm^{-2}	Standard Deviation $\pm \lvert j \rvert$ @ -1.25 V vs SCE / mA cm^{-2}
0.227	0.051	1.25	0.09
0.453	0.102	2.79	0.17
0.680	0.153	3.54	0.11
0.907	0.205	4.10	0.09
1.13	0.256	4.29	0.10
1.36	0.307	4.27	0.21

Table 2.28 Activity Results for CoPc-P2VP/GP/GCE in Figure 2.5. CoPc-P2VP/GP/GCE, GP loading: 0.51 mg cm^{-2}. Activity results of rotating disk chronoamperometry (RDE-CA) experiment at -1.25 V vs. SCE, conducted under 1 atm CO_2 in 0.1 M NaH_2PO_4 at ~pH 4.7 under 1600 rpm rotation rate for CoPc-P2VP/GP/GCE with 10 mg/mL graphite powder in the catalyst ink solution, corresponding to a loading of 0.51 mg cm^{-2}.

Co loading / 10^{-9} mol cm^{-2}	$\|j\|$ @ -1.25 V vs SCE / mA cm^{-2}	Standard Deviation $\pm \|j\|$ @ -1.25 V vs SCE / mA cm^{-2}
0.347	1.13	0.06
0.848	1.45	0.21
1.79	3.76	0.08
3.56	3.93	0.08
4.17	4.55	0.47
5.91	3.89	0.16

Table 2.29 Activity Results for CoPc(pyNMe$_2$)-P2VP/GP/GCE in Figure 2.5. CoPc(pyNMe$_2$) P2VP/GP/GCE, GP loading: 0.51 mg cm^{-2}. Activity results of rotating disk chronoamperometry (RDE-CA) experiment at -1.25 V vs. SCE, conducted under 1 atm CO_2 in 0.1 M NaH_2PO_4 at ~pH 4.7 under 1600 rpm rotation rate for CoPc(pyNMe$_2$)-P2VP/GP/GCE with 10 mg/mL graphite powder in the catalyst ink solution, corresponding to a loading of 0.51 mg cm^{-2}.

Co loading / 10^{-9} mol cm^{-2}	$\lvert j \rvert$ @ -1.25 V vs SCE / mA cm^{-2}	Standard Deviation $\pm \lvert j \rvert$ @ -1.25 V vs SCE / mA cm^{-2}
0.417	2.87	0.03
1.01	4.28	0.37
1.76	5.34	0.36
3.32	4.75	0.49
4.62	5.08	0.37
5.63	4.07	0.31

Table 2.30 Activity Results CoPc-P4CS/GP/GCE in Figure 2.5. CoPc-P4CS/GP/GCE, GP loading: 0.51 mg cm^{-2}. Activity results of rotating disk chronoamperometry (RDE-CA) experiment at -1.25 V vs. SCE, conducted under 1 atm CO_2 in 0.1 M NaH_2PO_4 at ~pH 4.7 under 1600 rpm rotation rate for CoPc-P4CS/GP/GCE with 10 mg/mL graphite powder in the catalyst ink solution, corresponding to a loading of 0.51 mg cm^{-2}.

Co loading / 10^{-9} mol cm^{-2}	$\|j\|$ @ -1.25 V vs SCE / mA cm^{-2}	Standard Deviation $\pm \|j\|$ @ -1.25 V vs SCE / mA cm^{-2}
0.12	0.82	0.04
0.21	1.36	0.02
0.44	1.31	0.07
1.15	1.29	0.17
2.31	0.72	0.09
3.49	0.21	0.01

Table 2.31 Controlled Potential Electrolysis Results. Product distribution of CO and H_2 for 2 h controlled potential electrolysis (CPE) measurements in a CO_2 atmosphere at -1.25 V vs. SCE for CoPc-P4VP/GP on glassy carbon electrode (GCE); CoPc(pyNMe$_2$)-P2VP/GP/GCE; CoPc-P4VP on edge-plane graphite (EPG) electrode without graphite powder, preparation conditions found in Table 2.19 and prepared according to the experimental section.

	Charge / C	FE_{CO} / %	FE_{H2} / %	FE_{Total} / %
CoPc-P4VP/GP/GCE	2.8 ± 0.8	83.0 ± 1.3	14.0 ± 3.6	97.0 ± 2.7
CoPc(pyNMe$_2$)-P2VP/GP GCE	4.8 ± 0.7	84.7 ± 3.5	16.4 ± 3.4	101.1 ± 6.9
CoPc-P2VP/GP/GCE	2.6 ± 0.2	73.9 ± 4.5	21.2 ± 3.4	95.0 ± 3.2
CoPc-P4VP/EPG	1.2 ± 0.1	90.4 ± 0.9	11.8 ± 0.7	102.0 ± 0.4
CoPc-P4VP/GP/GCE not centrifuged	1.2 ± 0.08	81.8 ± 0.9	15.7 ± 09	97.5 ± 1.5
P4VP/GP/GCE (no CoPc)	0.07 ± 0.02	None Detected	104.5 ± 13.6	104.5 ± 13.6

Table 2.32 CoPc-P4VP/GP/GCE Loading for Non-Centrifuged Samples. Preparation conditions for deposition ink for the CoPc-P4VP/GP/GCE without centrifugation as shown in Figure 2.7. Columns 1-3 detail the concentrations of CoPc, P4VP, and GP in the preparation suspension. Columns 4-6 detail the measured conditions of the preparation conditions of the CoPc loading, P4VP loading, and GP loading. Columns 7-9 detail the CoPc, P4VP, and GP loading on the 0.196 cm^2 GCEs.

CoPc-P4VP/GP/GCE								
Before Centrifugation			After Centrifugation			Electrode Loading		
Preparation Suspension			Deposition Ink			Deposition Ink Dropcasted		
CoPc loading / mM	P4VP loading mg mL^{-1}	GP loading mg mL^{-1}	CoPc loading / mM	P4VP loading / mg mL^{-1}	GP loading / mg mL^{-1}	CoPc loading / 10^{-9} mol cm^{-2}	P4VP loading / mg cm^{-2}	GP loading / mg cm^{-2}
0.2	12	10	0.122	3	10	6.256	0.154	0.513
0.15	9	10	0.0833	2.5	10	4.272	0.128	0.513
0.1	6	10	0.0534	2	10	2.738	0.103	0.513
0.05	3	10	0.0228	1	10	1.169	0.051	0.513
0.025	1.5	10	0.0138	0.5	10	0.708	0.026	0.513
0.0125	0.75	10	0.00727	0.3	10	0.373	0.015	0.513

Table 2.33 Preparation of P4VP/GP Deposition Ink without CoPc. Preparation of P4VP/GP Deposition ink without CoPc as a control to show that little activity occurs without CoPc. Columns 1-3 detail the concentrations of CoPc, P4VP, and GP in the preparation suspension. Columns 4-6 detail the measured conditions of the preparation conditions of the CoPc loading, P4VP loading, and GP loading. Columns 7-9 detail the CoPc, P4VP, and GP loading on the 0.196 cm^2 GCEs.

Before Centrifugation			After Centrifugation			Electrode Loading		
Preparation Suspension			Deposition Ink			Deposition Ink Dropcasted		
CoPc loading / mM	P4VP loading / mg mL^{-1}	GP loading / mg mL^{-1}	CoPc loading / mM	P4VP loading / mg mL^{-1}	GP loading / mg mL^{-1}	CoPc loading / 10^{-9} mol cm^{-2}	P4VP loading / mg cm^{-2}	GP loading / mg cm^{-2}
0	30	10	0	Not Measured	10	0	Not Measured	0.513

2.7.2 Supplementary Figures

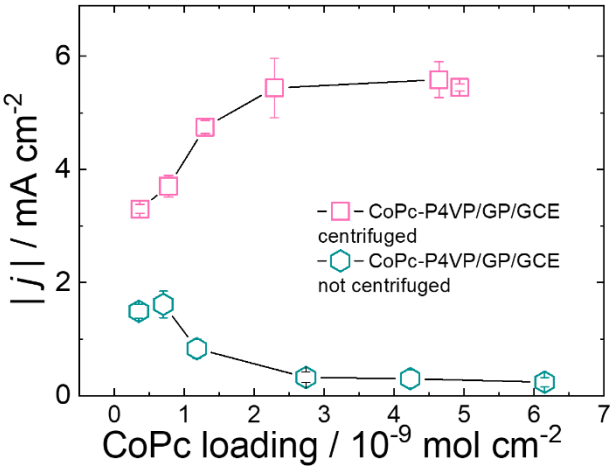

Figure 2.7 Comparing activity of. CoPc-P4VP/GP/GCE with and without centrifugation. Loading is tabulated in Table 2.2 and CoPc-P4VP/GP/GCE not centrifuged prepared with CoPc, P4VP, and GP loadings as tabulated in Table 2.32 and experimental conditions outlined in the Experimental Section.

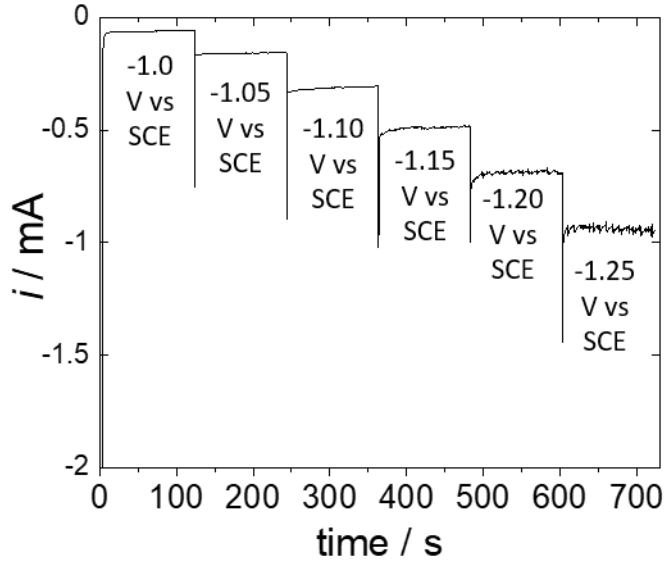

Figure 2.8 Representative RDE-CA: CoPc-P4VP/GP/GCE in Figure 2.2, Figure 2.3, and Figure 2.5. Representative rotating disk chronoamperometric step measurements conducted at 1600 rpm with 2-minute potential steps from 1.00 V to -1.25 V vs. SCE at 0.05 V increments of CoPc-P4VP/GP/GCE (0.05 mM CoPc-3%P4VP-1%GP in preparation suspension – loading found in Table 2.2, row 4).

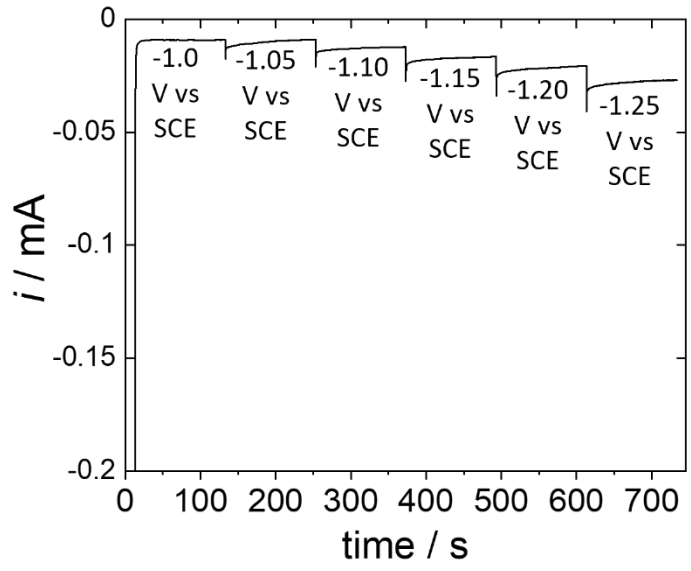

Figure 2.9 Representative CA: P4VP/GP/GCE without CoPc. Representative rotating disk chronoamperometric step measurements conducted at 1600 rpm with 2-minute potential steps from 1.00 V to -1.25 V vs. SCE at 0.05 V increments of P4VP/GP/GCE (no CoPc-3%P4VP-1%GP in preparation suspension – loading found in Table 2.33).

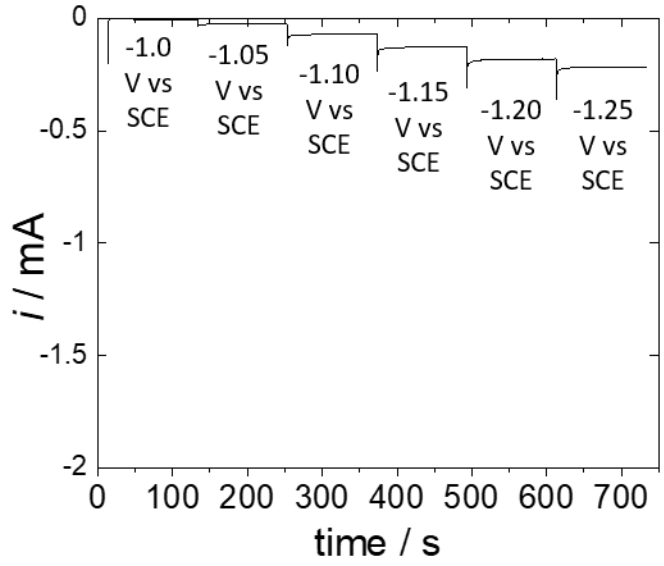

Figure 2.10 Representative RDE-CA: CoPc-P4VP/EPG (no graphite powder). Representative rotating disk chronoamperometric step measurements conducted at 1600 rpm with 2-minute potential steps from 1.00 V to -1.25 V vs. SCE at 0.05 V increments of CoPc-P4VP/EPG (0.023 mM CoPc – 1%P4VP – 1% GP in deposition ink) – loading found in Table 2.4, Row 4.

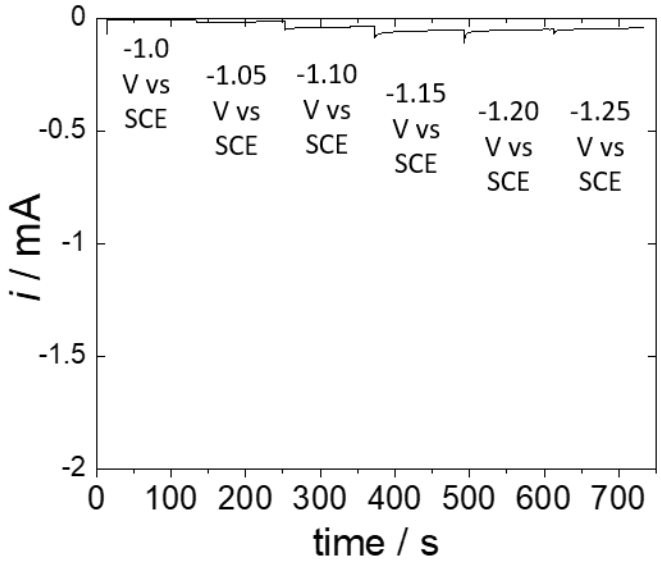

Figure 2.11 Representative RDE-CA: CoPc-P4VP/GCE (no graphite powder). Representative rotating disk chronoamperometric step measurements conducted at 1600 rpm with 2-minute potential steps from 1.00 V to -1.25 V vs. SCE at 0.05 V increments of CoPc-P4VP/GCE (0.023 mM CoPc – 1%P4VP – 0% GP in deposition ink) – loading found in Table 2.3, Row 4.

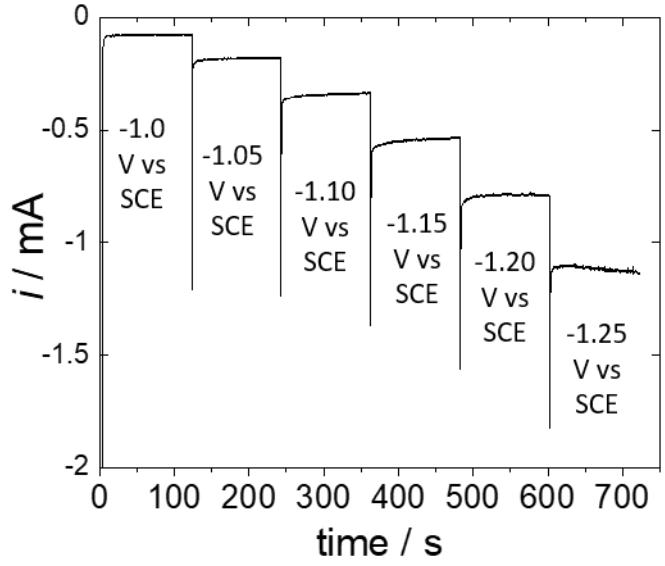

Figure 2.12 Representative RDE-CA: CoPc-P4VP/GP/GCE 15 mg/mL GP from Figure 2.3a. Representative rotating disk chronoamperometric step measurements conducted at 1600 rpm with 2-minute potential steps from 1.00 V to -1.25 V vs. SCE at 0.05 V increments of CoPc-P4VP/GP/GCE (0.05 mM CoPc – 3%P4VP – 1.5% GP in preparation suspension) – loading found in Table 2.5, Row 4.

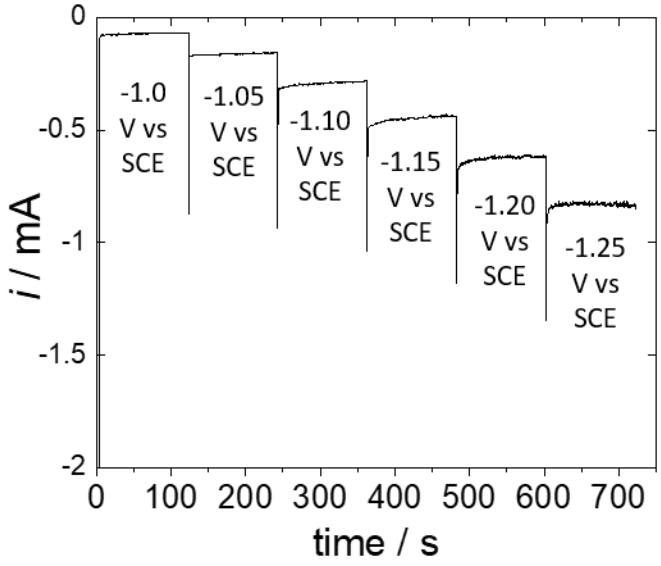

Figure 2.13 Representative RDE-CA: CoPc-P4VP/GP/GCE 5 mg/mL GP from Figure 2.3a. Representative rotating disk chronoamperometric step measurements conducted at 1600 rpm with 2-minute potential steps from 1.00 V to -1.25 V vs. SCE at 0.05 V increments of CoPc-P4VP/GP/GCE (0.05 mM CoPc – 3%P4VP – 0.5% GP in preparation suspension) – loading found in Table 2.6, Row 4.

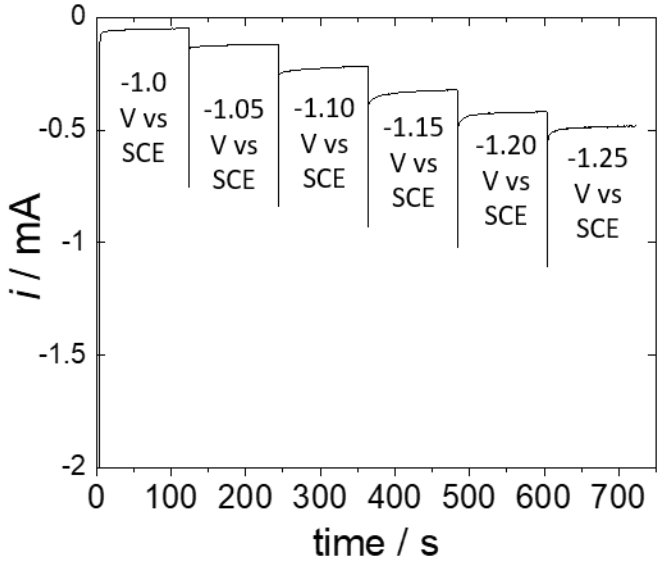

Figure 2.14 Representative RDE-CA: CoPc-P4VP/GP/GCE 1 mg/mL GP from Figure 2.3a. Representative rotating disk chronoamperometric step measurements conducted at 1600 rpm with 2-minute potential steps from 1.00 V to -1.25 V vs. SCE at 0.05 V increments of CoPc-P4VP/GP/GCE (0.05 mM CoPc – 3%P4VP – 0.1% GP in preparation suspension) – loading found in Table 2.7, Row 4.

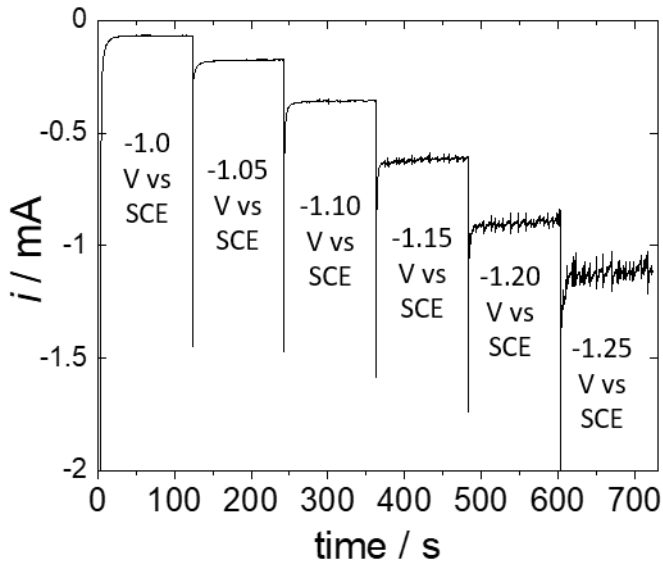

Figure 2.15 Representative RDE-CA: CoPc-P4VP/GP/GCE 10 mg/mL GP in Figure 2.4c. Representative rotating disk chronoamperometric step measurements conducted at 1600 rpm with 2-minute potential steps from 1.00 V to -1.25 V vs. SCE at 0.05 V increments of CoPc-P4VP/GP/GCE (0.0125 mM CoPc – 0.75% P4VP – 1% GP in preparation suspension). Resulting CoPc deposition ink loading found in Table 2.8 with 60 μL deposited resulting in the electrode loading found in Table 2.9, Row 6.

.

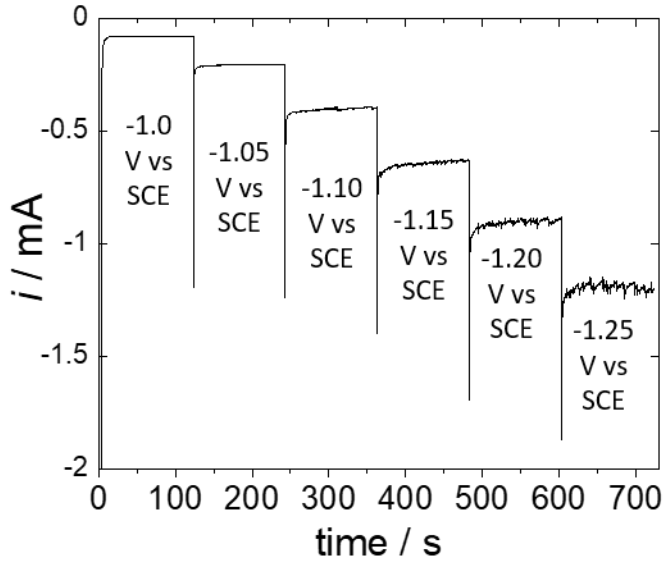

Figure 2.16 Representative RDE-CA: CoPc-P4VP/GP/GCE 5 mg/mL GP in Figure 2.4b. Representative rotating disk chronoamperometric step measurements conducted at 1600 rpm with 2-minute potential steps from 1.00 V to -1.25 V vs. SCE at 0.05 V increments of CoPc-P4VP/GP/GCE (0.0125 mM CoPc – 0.75%P4VP – 0.5% GP in preparation suspension). Resulting CoPc deposition ink loading found in Table 2.10 with 60 μL deposited resulting in the electrode loading found in Table 2.11, Row 6.

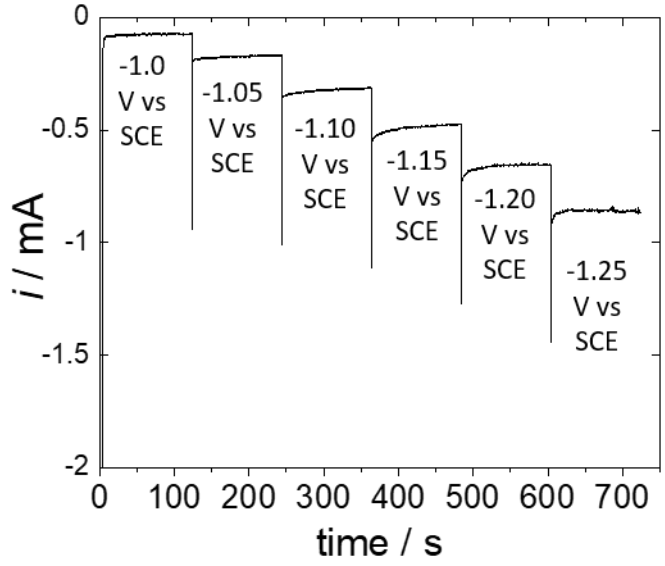

Figure 2.17 Representative rotating disk chronoamperometric step measurements shown in Figure 2.4a conducted at 1600 rpm with 2-minute potential steps from 1.00 V to -1.25 V vs. SCE at 0.05 V increments of CoPc-P4VP/GP/GCE (0.0125 mM CoPc – 0.75%P4VP – 0.1% GP in preparation suspension). Resulting CoPc deposition ink loading found in Table 2.12 with 60 μL deposited resulting in the electrode loading found in Table 2.13, Row 6.

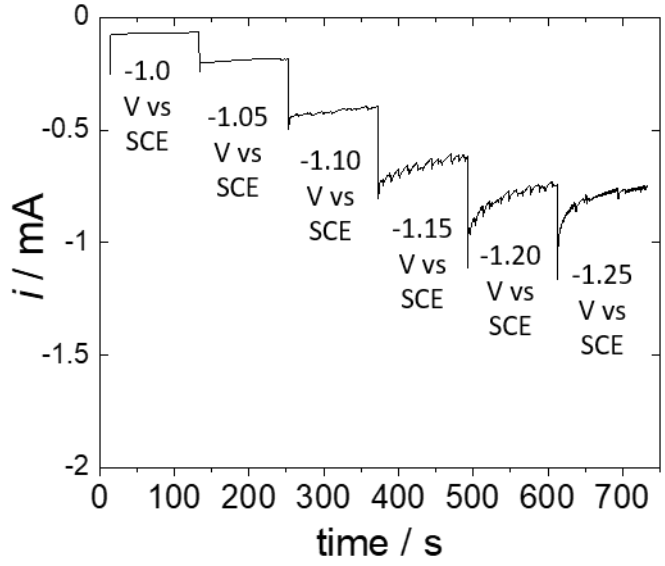

Figure 2.18. Representative rotating disk chronoamperometric step measurements of data shown in Figure 2.5 conducted at 1600 rpm with 2-minute potential steps from 1.00 V to -1.25 V vs. SCE at 0.05 V increments of CoPc-P2VP/GP/GCE (0.05 mM CoPc – 3%P2VP – 1% GP in preparation suspension) – loading found in Table 2.14, Row 4.

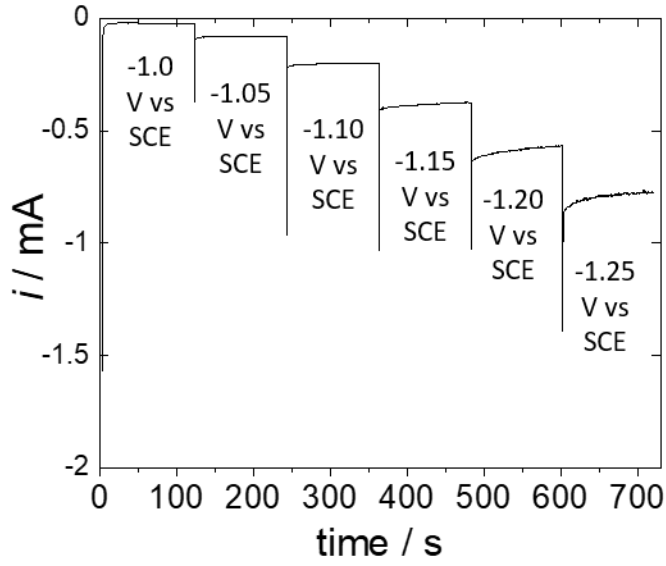

Figure 2.19 Representative rotating disk chronoamperometric step measurements of data shown in Figure 2.5 conducted at 1600 rpm with 2-minute potential steps from 1.00 V to -1.25 V vs. SCE at 0.05 V increments of CoPc(pyNMe$_2$)-P2VP/GP/GCE (0.05 mM CoPc – 0.05 M pyNMe$_2$ - 3%P2VP – 1% GP in preparation suspension) – loading found in Table 2.15, Row 4.

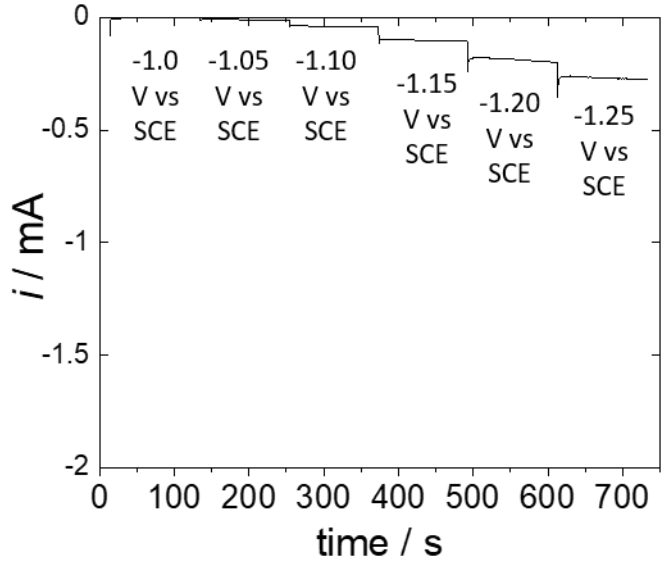

Figure 2.20. Representative rotating disk chronoamperometric step measurements for data shown in Figure 2.5 conducted at 1600 rpm with 2-minute potential steps from 1.00 V to -1.25 V vs. SCE at 0.05 V increments of CoPc-P4CS/GP/GCE (0.05 mM CoPc – 3%P4CS – 1% GP in preparation suspension) – loading found in Table 2.16, Row 4.

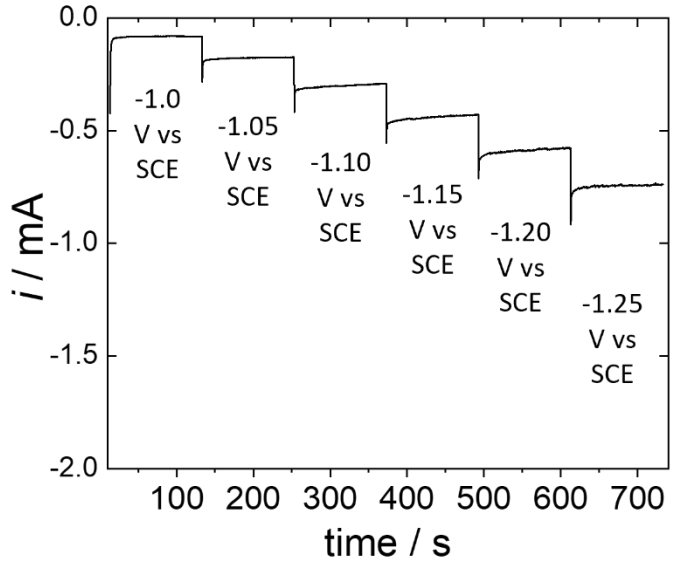

Figure 2.21 Representative rotating disk chronoamperometric step measurements conducted at 1600 rpm with 2-minute potential steps from 1.00 V to -1.25 V vs. SCE at 0.05 V increments of CoPc(pyNMe$_2$)-P4VP/GP/GCE (0.2 mM CoPc – 0.2 M pyNMe$_2$ - 12%P4VP – 1% GP in preparation suspension) – loading found in Table 2.18.

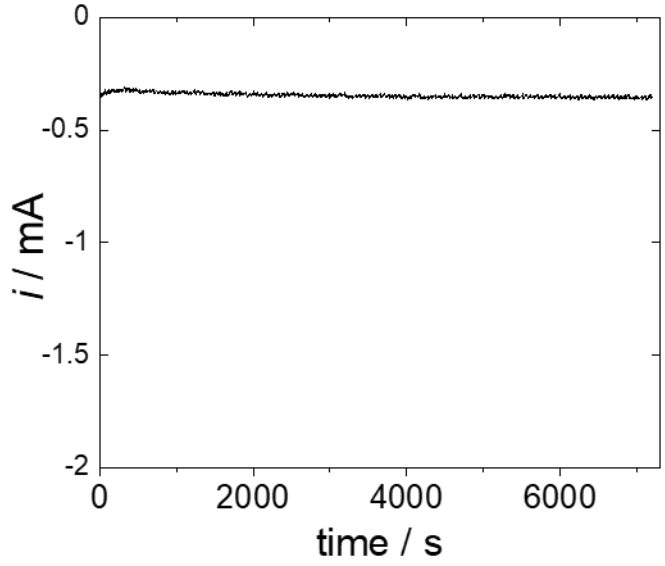

Figure 2.22 Representative chronoamperometric trace of CoPc-P4VP/GP/GCE for a 2-hour controlled potential electrolysis experiment at -1.25 V vs SCE. Loading found in Table 2.19.

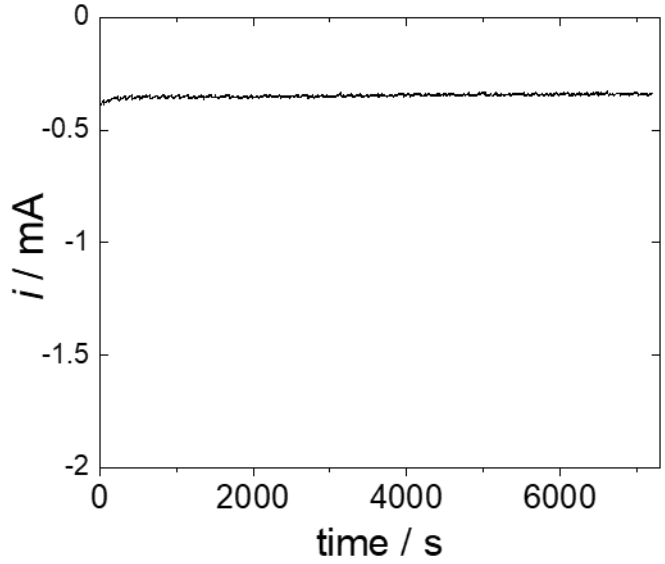

Figure 2.23 Representative chronoamperometric trace of CoPc-P2VP/GP/GCE for a 2-hour controlled potential electrolysis experiment at -1.25 V vs SCE. Loading found in Table 2.19.

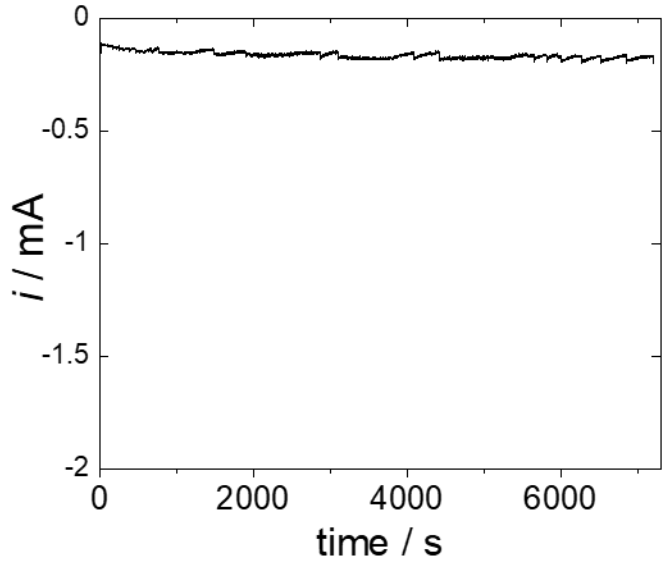

Figure 2.24 Representative chronoamperometric trace of CoPc-P4VP/EPG for a 2 hour controlled potential electrolysis experiment at -1.25 V vs SCE. Loading found in Table 2.19.

2.8 References

(1) Soucy, T. L.; Liu, Y.; Eisenberg, J. B.; McCrory, C. C. L. "Enhancing the Electrochemical CO2 Reduction Activity of Polymer-Encapsulated Cobalt Phthalocyanine Films by Modulating the Loading of Catalysts, Polymers, and Carbon Supports," *ACS Applied Energy Materials* **2021**. http://dx.doi.org/10.1021/acsaem.1c02689

(2) Meshitsuka, S.; Ichikawa, M.; Tamaru, K. "Electrocatalysis by metal phthalocyanines in the reduction of carbon dioxide," *Journal of the Chemical Society, Chemical Communications* **1974**, 158-159. http://dx.doi.org/10.1039/C39740000158

(3) Lieber, C. M.; Lewis, N. S. "Catalytic reduction of carbon dioxide at carbon electrodes modified with cobalt phthalocyanine," *Journal of the American Chemical Society* **1984**, *106*, 5033-5034. http://dx.doi.org/10.1021/ja00329a082

(4) Yoshida, T.; Kamato, K.; Tsukamoto, M.; Iida, T.; Schlettwein, D.; Wöhrle, D.; Kaneko, M. "Selective electroacatalysis for CO2 reduction in the aqueous phase using cobalt phthalocyanine/poly-4-vinylpyridine modified electrodes," *Journal of Electroanalytical Chemistry* **1995**, *385*, 209-225. http://dx.doi.org/https://doi.org/10.1016/0022-0728(94)03762-R

(5) Nyokong, T. "Equilibrium and kinetic studies of the reaction between pyridine and cobalt(II) phthalocyanine in DMSO," *Polyhedron* **1995**, *14*, 2325-2329. http://dx.doi.org/https://doi.org/10.1016/0277-5387(95)00090-F

(6) Abe, T.; Yoshida, T.; Tokita, S.; Taguchi, F.; Imaya, H.; Kaneko, M. "Factors affecting selective electrocatalytic co2 reduction with cobalt phthalocyanine incorporated in a polyvinylpyridine membrane coated on a graphite electrode," *Journal of Electroanalytical Chemistry* **1996**, *412*, 125-132. http://dx.doi.org/https://doi.org/10.1016/0022-0728(96)04631-1

(7) Abe, T.; Imaya, H.; Yoshida, T.; Tokita, S.; Schlettwein, D.; Wöhrle, D.; Kaneko, M. "Electrochemical CO2 Reduction Catalysed by Cobalt Octacyanophthalocyanine and its Mechanism," *J. Porphyrins Phthalocyanines* **1997**, *01*, 315-321. http://dx.doi.org/10.1002/(sici)1099-1409(199710)1:4<315::Aid-jpp35>3.0.Co;2-v

(8) Schulte, K.; Swarbrick, J. C.; Smith, N. A.; Bondino, F.; Magnano, E.; Khlobystov, A. N. "Assembly of Cobalt Phthalocyanine Stacks inside Carbon Nanotubes," *Advanced Materials* **2007**, *19*, 3312-3316. http://dx.doi.org/https://doi.org/10.1002/adma.200700188

(9) Wang, Y.; Hu, N.; Zhou, Z.; Xu, D.; Wang, Z.; Yang, Z.; Wei, H.; Kong, E. S.-W.; Zhang, Y. "Single-walled carbon nanotube/cobalt phthalocyanine derivative hybrid material: preparation, characterization and its gas sensing properties," *Journal of Materials Chemistry* **2011**, *21*, 3779-3787. http://dx.doi.org/10.1039/C0JM03567J

(10) Zhao, H.; Zhang, Y.; Zhao, B.; Chang, Y.; Li, Z. "Electrochemical Reduction of Carbon Dioxide in an MFC–MEC System with a Layer-by-Layer Self-Assembly Carbon Nanotube/Cobalt Phthalocyanine Modified Electrode," *Environmental Science & Technology* **2012**, *46*, 5198-5204. http://dx.doi.org/10.1021/es300186f

(11) Hosu, I. S.; Wang, Q.; Vasilescu, A.; Peteu, S. F.; Raditoiu, V.; Railian, S.; Zaitsev, V.; Turcheniuk, K.; Wang, Q.; Li, M.; Boukherroub, R.; Szunerits, S. "Cobalt phthalocyanine tetracarboxylic acid modified reduced graphene oxide: a sensitive matrix for the electrocatalytic detection of peroxynitrite and hydrogen peroxide," *RSC Advances* **2015**, *5*, 1474-1484. http://dx.doi.org/10.1039/C4RA09781E

(12) Li, N.; Lu, W.; Pei, K.; Chen, W. "Interfacial peroxidase-like catalytic activity of surface-immobilized cobalt phthalocyanine on multiwall carbon nanotubes," *RSC Advances* **2015**, *5*, 9374-9380. http://dx.doi.org/10.1039/C4RA15306E

(13) Manbeck, G. F.; Fujita, E. "A review of iron and cobalt porphyrins, phthalocyanines and related complexes for electrochemical and photochemical reduction of carbon dioxide," *J. Porphyrins Phthalocyanines* **2015**, *19*, 45-64. http://dx.doi.org/10.1142/S1088424615300013
(14) Kramer, W. W.; McCrory, C. C. L. "Polymer coordination promotes selective CO2 reduction by cobalt phthalocyanine," *Chemical Science* **2016**, *7*, 2506-2515. http://dx.doi.org/10.1039/C5SC04015A
(15) Han, N.; Wang, Y.; Ma, L.; Wen, J.; Li, J.; Zheng, H.; Nie, K.; Wang, X.; Zhao, F.; Li, Y.; Fan, J.; Zhong, J.; Wu, T.; Miller, D. J.; Lu, J.; Lee, S.-T.; Li, Y. "Supported Cobalt Polyphthalocyanine for High-Performance Electrocatalytic CO2 Reduction," *Chem* **2017**, *3*, 652-664. http://dx.doi.org/https://doi.org/10.1016/j.chempr.2017.08.002
(16) Zhang, X.; Wu, Z.; Zhang, X.; Li, L.; Li, Y.; Xu, H.; Li, X.; Yu, X.; Zhang, Z.; Liang, Y.; Wang, H. "Highly selective and active CO2 reduction electrocatalysts based on cobalt phthalocyanine/carbon nanotube hybrid structures," *Nature Communications* **2017**, *8*, 14675. http://dx.doi.org/10.1038/ncomms14675
(17) Li, N.; Wang, Y.; Wu, C.; Lu, W.; Pei, K.; Chen, W. "Bioinspired catalytic generation of high-valent cobalt-oxo species by the axially coordinated CoPc on pyridine-functionalized MWCNTs for the elimination of organic contaminants," *Applied Surface Science* **2018**, *434*, 1112-1121. http://dx.doi.org/https://doi.org/10.1016/j.apsusc.2017.11.048
(18) Wu, H.; Zeng, M.; Zhu, X.; Tian, C.; Mei, B.; Song, Y.; Du, X.-L.; Jiang, Z.; He, L.; Xia, C.; Dai, S. "Defect Engineering in Polymeric Cobalt Phthalocyanine Networks for Enhanced Electrochemical CO2 Reduction," *ChemElectroChem* **2018**, *5*, 2717-2721. http://dx.doi.org/https://doi.org/10.1002/celc.201800806
(19) Zhu, M.; Ye, R.; Jin, K.; Lazouski, N.; Manthiram, K. "Elucidating the Reactivity and Mechanism of CO2 Electroreduction at Highly Dispersed Cobalt Phthalocyanine," *ACS Energy Letters* **2018**, *3*, 1381-1386. http://dx.doi.org/10.1021/acsenergylett.8b00519
(20) Boutin, E.; Wang, M.; Lin, J. C.; Mesnage, M.; Mendoza, D.; Lassalle-Kaiser, B.; Hahn, C.; Jaramillo, T. F.; Robert, M. "Aqueous Electrochemical Reduction of Carbon Dioxide and Carbon Monoxide into Methanol with Cobalt Phthalocyanine," *Angewandte Chemie International Edition* **2019**, *58*, 16172-16176. http://dx.doi.org/https://doi.org/10.1002/anie.201909257
(21) Chen, J.; Li, J.; Liu, W.; Ma, X.; Xu, J.; Zhu, M.; Han, Y.-F. "Facile synthesis of polymerized cobalt phthalocyanines for highly efficient CO2 reduction," *Green Chemistry* **2019**, *21*, 6056-6061. http://dx.doi.org/10.1039/C9GC02705J
(22) Choi, J.; Wagner, P.; Gambhir, S.; Jalili, R.; MacFarlane, D. R.; Wallace, G. G.; Officer, D. L. "Steric Modification of a Cobalt Phthalocyanine/Graphene Catalyst To Give Enhanced and Stable Electrochemical CO2 Reduction to CO," *ACS Energy Letters* **2019**, *4*, 666-672. http://dx.doi.org/10.1021/acsenergylett.8b02355
(23) Corbin, N.; Zeng, J.; Williams, K.; Manthiram, K. "Heterogeneous molecular catalysts for electrocatalytic CO2 reduction," *Nano Research* **2019**, *12*, 2093-2125. http://dx.doi.org/10.1007/s12274-019-2403-y
(24) Lin, L.; Li, H.; Yan, C.; Li, H.; Si, R.; Li, M.; Xiao, J.; Wang, G.; Bao, X. "Synergistic Catalysis over Iron-Nitrogen Sites Anchored with Cobalt Phthalocyanine for Efficient CO2 Electroreduction," *Advanced Materials* **2019**, *31*, 1903470. http://dx.doi.org/https://doi.org/10.1002/adma.201903470
(25) Liu, Y.; McCrory, C. C. L. "Modulating the mechanism of electrocatalytic CO2 reduction by cobalt phthalocyanine through polymer coordination and encapsulation," *Nature Communications* **2019**, *10*, 1683. http://dx.doi.org/10.1038/s41467-019-09626-8

(26) Ren, S.; Joulié, D.; Salvatore, D.; Torbensen, K.; Wang, M.; Robert, M.; Berlinguette, C. P. "Molecular electrocatalysts can mediate fast, selective CO2 reduction in a flow cell," *Science* **2019**, *365*, 367-369. http://dx.doi.org/10.1126/science.aax4608
(27) Roy, S.; Reisner, E. "Visible-Light-Driven CO2 Reduction by Mesoporous Carbon Nitride Modified with Polymeric Cobalt Phthalocyanine," *Angewandte Chemie International Edition* **2019**, *58*, 12180-12184. http://dx.doi.org/https://doi.org/10.1002/anie.201907082
(28) Wang, J.; Huang, X.; Xi, S.; Lee, J.-M.; Wang, C.; Du, Y.; Wang, X. "Linkage Effect in the Heterogenization of Cobalt Complexes by Doped Graphene for Electrocatalytic CO2 Reduction," *Angewandte Chemie International Edition* **2019**, *58*, 13532-13539. http://dx.doi.org/https://doi.org/10.1002/anie.201906475
(29) Wang, M.; Torbensen, K.; Salvatore, D.; Ren, S.; Joulié, D.; Dumoulin, F.; Mendoza, D.; Lassalle-Kaiser, B.; Işci, U.; Berlinguette, C. P.; Robert, M. "CO_2 electrochemical catalytic reduction with a highly active cobalt phthalocyanine," *Nat. Commun.* **2019**, *10*, 3602. http://dx.doi.org/10.1038/s41467-019-11542-w
(30) Wu, Y.; Jiang, Z.; Lu, X.; Liang, Y.; Wang, H. "Domino electroreduction of CO2 to methanol on a molecular catalyst," *Nature* **2019**, *575*, 639-642. http://dx.doi.org/10.1038/s41586-019-1760-8
(31) Zhu, M.; Chen, J.; Guo, R.; Xu, J.; Fang, X.; Han, Y.-F. "Cobalt phthalocyanine coordinated to pyridine-functionalized carbon nanotubes with enhanced CO2 electroreduction," *Applied Catalysis B: Environmental* **2019**, *251*, 112-118. http://dx.doi.org/https://doi.org/10.1016/j.apcatb.2019.03.047
(32) Chen, J.; Zhu, M.; Li, J.; Xu, J.; Han, Y.-F. "Structure–Activity Relationship of the Polymerized Cobalt Phthalocyanines for Electrocatalytic Carbon Dioxide Reduction," *The Journal of Physical Chemistry C* **2020**, *124*, 16501-16507. http://dx.doi.org/10.1021/acs.jpcc.0c04741
(33) De Riccardis, A.; Lee, M.; Kazantsev, R. V.; Garza, A. J.; Zeng, G.; Larson, D. M.; Clark, E. L.; Lobaccaro, P.; Burroughs, P. W. W.; Bloise, E.; Ager, J. W.; Bell, A. T.; Head-Gordon, M.; Mele, G.; Toma, F. M. "Heterogenized Pyridine-Substituted Cobalt(II) Phthalocyanine Yields Reduction of CO2 by Tuning the Electron Affinity of the Co Center," *ACS Applied Materials & Interfaces* **2020**, *12*, 5251-5258. http://dx.doi.org/10.1021/acsami.9b18924
(34) Huai, M.; Yin, Z.; Wei, F.; Wang, G.; Xiao, L.; Lu, J.; Zhuang, L. "Electrochemical CO2 reduction on heterogeneous cobalt phthalocyanine catalysts with different carbon supports," *Chemical Physics Letters* **2020**, *754*, 137655. http://dx.doi.org/https://doi.org/10.1016/j.cplett.2020.137655
(35) Li, T.-T.; Mei, Y.; Li, H.; Qian, J.; Wu, M.; Zheng, Y.-Q. "Highly Selective and Active Electrochemical Reduction of CO2 to CO on a Polymeric Co(II) Phthalocyanine@Graphitic Carbon Nitride Nanosheet–Carbon Nanotube Composite," *Inorg. Chem.* **2020**. http://dx.doi.org/10.1021/acs.inorgchem.0c01977
(36) Lin, L.; Liu, T.; Xiao, J.; Li, H.; Wei, P.; Gao, D.; Nan, B.; Si, R.; Wang, G.; Bao, X. "Enhancing CO2 Electroreduction to Methane with a Cobalt Phthalocyanine and Zinc–Nitrogen–Carbon Tandem Catalyst," *Angewandte Chemie International Edition* **2020**, *59*, 22408-22413. http://dx.doi.org/https://doi.org/10.1002/anie.202009191
(37) Liu, Y.; Deb, A.; Leung, K. Y.; Nie, W.; Dean, W. S.; Penner-Hahn, J. E.; McCrory, C. C. L. "Determining the coordination environment and electronic structure of polymer-encapsulated cobalt phthalocyanine under electrocatalytic CO_2 reduction conditions using in situ X-Ray absorption spectroscopy," *Dalton Trans.* **2020**, *49*, 16329-16339. http://dx.doi.org/10.1039/D0DT01288B

(38) Xia, Y.; Kashtanov, S.; Yu, P.; Chang, L.-Y.; Feng, K.; Zhong, J.; Guo, J.; Sun, X. "Identification of dual-active sites in cobalt phthalocyanine for electrochemical carbon dioxide reduction," *Nano Energy* **2020**, *67*, 104163. http://dx.doi.org/https://doi.org/10.1016/j.nanoen.2019.104163
(39) Wang, X.; Cai, Z.-F.; Wang, Y.-Q.; Feng, Y.-C.; Yan, H.-J.; Wang, D.; Wan, L.-J. "In Situ Scanning Tunneling Microscopy of Cobalt-Phthalocyanine-Catalyzed CO2 Reduction Reaction," *Angewandte Chemie International Edition* **2020**, *59*, 16098-16103. http://dx.doi.org/https://doi.org/10.1002/anie.202005242
(40) Wu, Y.; Hu, G.; Rooney, C. L.; Brudvig, G. W.; Wang, H. "Heterogeneous Nature of Electrocatalytic CO/CO2 Reduction by Cobalt Phthalocyanines," *ChemSusChem* **2020**, *n/a*. http://dx.doi.org/10.1002/cssc.202001396
(41) Yang, Z.; Zhang, X.; Long, C.; Yan, S.; Shi, Y.; Han, J.; Zhang, J.; An, P.; Chang, L.; Tang, Z. "Covalently anchoring cobalt phthalocyanine on zeolitic imidazolate frameworks for efficient carbon dioxide electroreduction," *CrystEngComm* **2020**, *22*, 1619-1624. http://dx.doi.org/10.1039/C9CE01517E
(42) Zeng, J. S.; Corbin, N.; Williams, K.; Manthiram, K. "Kinetic Analysis on the Role of Bicarbonate in Carbon Dioxide Electroreduction at Immobilized Cobalt Phthalocyanine," *ACS Catalysis* **2020**, *10*, 4326-4336. http://dx.doi.org/10.1021/acscatal.9b05272
(43) Zhang, H.; Min, S.; Wang, F.; Zhang, Z. "Immobilizing cobalt phthalocyanine into a porous carbonized wood membrane as a self-supported heterogenous electrode for selective and stable CO2 electroreduction in water," *Dalton Transactions* **2020**, *49*, 15607-15611. http://dx.doi.org/10.1039/D0DT03304A
(44) Gu, S.; Marianov, A. N.; Zhu, Y.; Jiang, Y. "Cobalt porphyrin immobilized on the TiO2 nanotube electrode for CO2 electroreduction in aqueous solution," *Journal of Energy Chemistry* **2021**, *55*, 219-227. http://dx.doi.org/https://doi.org/10.1016/j.jechem.2020.06.067
(45) Rivera Cruz, K. E.; Liu, Y.; Soucy, T. L.; Zimmerman, P. M.; McCrory, C. C. L. "Increasing the CO2 Reduction Activity of Cobalt Phthalocyanine by Modulating the σ-Donor Strength of Axially Coordinating Ligands," *ACS Catalysis* **2021**, 13203-13216. http://dx.doi.org/10.1021/acscatal.1c02379
(46) Sun, L.; Reddu, V.; Fisher, A. C.; Wang, X. "Electrocatalytic reduction of carbon dioxide: opportunities with heterogeneous molecular catalysts," *Energy & Environmental Science* **2020**, *13*, 374-403. http://dx.doi.org/10.1039/C9EE03660A
(47) Yamanaka, I.; Tabata, K.; Mino, W.; Furusawa, T. "Electroreduction of carbon dioxide to carbon monoxide by Co-pthalocyanine electrocatalyst under ambient conditions," *ISIJ International* **2015**, *55*, 399-403.
(48) Liu, Y.; Leung, K. Y.; Michaud, S. E.; Soucy, T. L.; McCrory, C. C. L. "Controlled Substrate Transport To Electrocatalyst Active Sites For Enhanced Selectivity In The Carbon Dioxide Reduction Reaction," *Comments Inorg. Chem.* **2019**, 1-28. http://dx.doi.org/10.1080/02603594.2019.1628025
(49) Zhu, M.; Chen, J.; Huang, L.; Ye, R.; Xu, J.; Han, Y.-F. "Covalently Grafting Cobalt Porphyrin onto Carbon Nanotubes for Efficient CO2 Electroreduction," *Angewandte Chemie International Edition* **2019**, *58*, 6595-6599. http://dx.doi.org/https://doi.org/10.1002/anie.201900499
(50) Zhu, M.; Cao, C.; Chen, J.; Sun, Y.; Ye, R.; Xu, J.; Han, Y.-F. "Electronic Tuning of Cobalt Porphyrins Immobilized on Nitrogen-Doped Graphene for CO2 Reduction," *ACS Applied Energy Materials* **2019**, *2*, 2435-2440. http://dx.doi.org/10.1021/acsaem.9b00368

(51) Bottari, G.; de la Torre, G.; Guldi, D. M.; Torres, T. "Covalent and Noncovalent Phthalocyanine−Carbon Nanostructure Systems: Synthesis, Photoinduced Electron Transfer, and Application to Molecular Photovoltaics," *Chemical Reviews* **2010**, *110*, 6768-6816. http://dx.doi.org/10.1021/cr900254z
(52) Zhang, X.; Feng, Y.; Tang, S.; Feng, W. "Preparation of a graphene oxide–phthalocyanine hybrid through strong π–π interactions," *Carbon* **2010**, *48*, 211-216. http://dx.doi.org/https://doi.org/10.1016/j.carbon.2009.09.007
(53) Wang, X.; Liu, Y.; Qiu, W.; Zhu, D. "Immobilization of tetra-tert-butylphthalocyanines on carbon nanotubes: a first step towards the development of new nanomaterials," *Journal of Materials Chemistry* **2002**, *12*, 1636-1639. http://dx.doi.org/10.1039/B201447E
(54) Murakami, H.; Nakamura, G.; Nomura, T.; Miyamoto, T.; Nakashima, N. "Noncovalent porphyrin-functionalized single-walled carbon nanotubes: solubilization and spectral behaviors," *J. Porphyrins Phthalocyanines* **2007**, *11*, 418-427. http://dx.doi.org/10.1142/s1088424607000473
(55) Tasis, D.; Tagmatarchis, N.; Bianco, A.; Prato, M. "Chemistry of Carbon Nanotubes," *Chemical Reviews* **2006**, *106*, 1105-1136. http://dx.doi.org/10.1021/cr050569o
(56) Chen, K.; Downes, C. A.; Schneider, E.; Goodpaster, J. D.; Marinescu, S. C. "Improving and Understanding the Hydrogen Evolving Activity of a Cobalt Dithiolene Metal–Organic Framework," *ACS Applied Materials & Interfaces* **2021**, *13*, 16384-16395. http://dx.doi.org/10.1021/acsami.1c01727
(57) Bott, A. W. "Electrochemical techniques for the characterization of redox polymers," *Curr. Sep.* **2001**, *19*, 71-75.
(58) Costentin, C.; Savéant, J.-M. "Molecular approach to catalysis of electrochemical reaction in porous films," *Current Opinion in Electrochemistry* **2019**, *15*, 58-65. http://dx.doi.org/https://doi.org/10.1016/j.coelec.2019.03.014
(59) Torbensen, K.; Joulié, D.; Ren, S.; Wang, M.; Salvatore, D.; Berlinguette, C. P.; Robert, M. "Molecular Catalysts Boost the Rate of Electrolytic CO2 Reduction," *ACS Energy Letters* **2020**, *5*, 1512-1518. http://dx.doi.org/10.1021/acsenergylett.0c00536
(60) Tan, D. C. L.; Sato, H. "Enhancing Catalytic Activity of Bioanode for Glucose Biofuel Cell by Compressing Enzyme, Mediator and Carbon Support through Centrifugation," *Chem. Eur. J.* **2017**, *23*, 11485-11488. http://dx.doi.org/https://doi.org/10.1002/chem.201702100
(61) Blanch, A. J.; Lenehan, C. E.; Quinton, J. S. "Parametric analysis of sonication and centrifugation variables for dispersion of single walled carbon nanotubes in aqueous solutions of sodium dodecylbenzene sulfonate," *Carbon* **2011**, *49*, 5213-5228. http://dx.doi.org/https://doi.org/10.1016/j.carbon.2011.07.039
(62) Mak, C. H.; Han, X.; Du, M.; Kai, J.-J.; Tsang, K. F.; Jia, G.; Cheng, K.-C.; Shen, H.-H.; Hsu, H.-Y. "Heterogenization of homogeneous photocatalysts utilizing synthetic and natural support materials," *Journal of Materials Chemistry A* **2021**, *9*, 4454-4504. http://dx.doi.org/10.1039/D0TA08334H
(63) Costentin, C.; Robert, M.; Savéant, J.-M. "Molecular catalysis of electrochemical reactions," *Current Opinion in Electrochemistry* **2017**, *2*, 26-31. http://dx.doi.org/https://doi.org/10.1016/j.coelec.2017.02.006
(64) Khairou, K. S.; Diab, M. A. "Stability and degradation of poly(4-vinylpyridine) and copolymers of 4-vinylpyridine with methyl methacrylate," *Polymer Degradation and Stability* **1994**, *44*, 17-20. http://dx.doi.org/https://doi.org/10.1016/0141-3910(94)90026-4

(65) Sikorski, R. T.; Mirkiewicz, G.; Varga, J.; Biró, O. "Influence of substituents in chloropolystyrenes and styrene copolymers on their thermal stability," *Journal of thermal analysis* **1990**, *36*, 1795-1802. http://dx.doi.org/10.1007/BF01913426
(66) Camps, M.; Jebri, A.; Drouet, J.-C. "Comparative study of thermal stabilities and limiting oxygen indexes of chlorinated, brominated, and iodinated polystyrenes," *Journal of fire sciences* **1996**, *14*, 251-262.
(67) Wang, M.; Torbensen, K.; Salvatore, D.; Ren, S.; Joulie, D.; Dumoulin, F.; Mendoza, D.; Lassalle-Kaiser, B.; Isci, U.; Berlinguette, C. P.; Robert, M. "CO2 electrochemical catalytic reduction with a highly active cobalt phthalocyanine," *Nat Commun* **2019**, *10*, 3602. http://dx.doi.org/10.1038/s41467-019-11542-w
(68) Jiang, Z.; Wang, Y.; Zhang, X.; Zheng, H.; Wang, X.; Liang, Y. "Revealing the hidden performance of metal phthalocyanines for CO2 reduction electrocatalysis by hybridization with carbon nanotubes," *Nano Research* **2019**, *12*, 2330-2334. http://dx.doi.org/10.1007/s12274-019-2455-z

Chapter 3 The Selectivity, Activity, and Mechanistic Impacts of Bulk Electrolyte pH on CO_2 and Proton Reduction by Polymer-Encapsulated Cobalt Phthalocyanine

3.1 Preface

This chapter discusses the effects of bulk electrolyte pH and concentration impact the activity, selectivity, and mechanism for the CO_2 reduction reaction and hydrogen evolution reaction when catalyzed by the CoPc-P4VP system. This chapter of my dissertation is derived from a manuscript in preparation for submission. I was the primary author on the manuscript and was responsible for all electrochemical studies, sample preparation, ICP-MS analysis of the samples, as well as data organization, manuscript writing, figure creation, and preparation of the manuscript. William S. Dean conceived of the idea to use IR spectroscopy to determine fractional protonation of the polymer and performed sample preparation and IR spectroscopy. Jonah B. Eisenberg collected some of the electrochemical experiments for one figure and assisted in sample preparation as well as some data organization and interpretation. Dr. Charles C. L. McCrory provided significant direction for the project and useful insight and expertise for electroanalytical techniques and experimental interpretation. All authors provided edits and reviewed the manuscript.

3.2 Abstract

Polymer-encapsulated cobalt phthalocyanine (CoPc) is an attractive model polymer-electrocatalyst system for the electrocatalytic transformation of CO_2 and protons in aqueous electrolyte and can also be used as a model to understand polymer-encapsulated catalysis and membrane-coated electrode systems. A complete understanding of electrolyte and proton concentrations within the polymer is crucial for not only this catalyst system but for other polymer-catalyst or polymer-coated electrode systems. In this work, we show that electrolyte concentration impacts the fractional protonation of a polymer film, providing both electrochemical and spectroscopic evidence that anion concentration in the aqueous electrolyte is directly related to the proton concentration within a polymer film, and that the wicking of a counterion, and therefore proton transport, could be the rate-limiting step for electrocatalytic HER by polymer-encapsulated CoPc. We confirm these results by performing electrolyte concentration dependent kinetic isotope effect studies and further show that the KIE for the HER decreases as we increase the pH, thereby confirming in another way that a decrease in available protons results in a decrease in the measured electrochemical KIE – likely moving away from the rate-determining step being a proton-transfer event in the mechanism and toward a transport-related issue being the rate limiter. A pH-dependent study for the activity and selectivity of the CO_2RR show that as pH increases, reaction selectivity of the CO_2RR over the HER increases, and while total activity peaks near pH 5, the activity for CO_2RR plateaus near that same pH. These insights reveal that so-called "spectator ions" may play a role in polymer-coated electrocatalyst systems with regards to mechanism and transport and should be thoroughly considered when performing small molecule transformations and other electrochemical processes.

3.3 Introduction

The increase in CO_2 concentration in the atmosphere due to emissions has warranted a serious discussion regarding the burning of fossil fuels, and the conversion of industrial waste CO_2 into value-added products using renewable energy is one proposed way to harness intermittent energy sources.[1-11] The electrocatalytic CO_2 reduction reaction (CO_2RR) has been studied as one way to accomplish this. In order to decrease the activation barrier required for this kinetically demanding reaction, the method can use molecular[12-17] and solid-state catalysts,[18-24] each which pose issues with regards to activity and selectivity. Regarding the solid-state catalyst, a major barrier is product selectivity, as solid-state materials electrocatalytically convert CO_2 into 16 different products highly reduced products with little selectivity, and the competing hydrogen evolution reaction also poses a separation issue which is particularly prevalent in aqueous electrolyte due to the ubiquitous nature of protons present in water.[25] One proposed method to decrease separations issues is to use a molecular catalyst, and many catalysts have been studied to perform the CO_2RR, and one class of molecular catalyst is metal porphyrin and phthalocyanines.

Porphyrins and phthalocyanines have been studied as molecular electrocatalysts for the CO_2RR, with cobalt phthalocyanine (CoPc) being a particularly well-studied catalyst due to its unique electron configuration and favorable binding energy to CO_2.[26-39] CoPc was also shown to be adsorbed to the electrode surface in order to perform CO_2RR in in particular was shown to be a catalyst for the CO_2RR in the late 20th century and has been important in studying the CO_2RR as a model system.[38,39] Additionally, CoPc is a particularly interesting electrocatalyst as one of the first molecular catalysts to reduce CO_2 to the more highly reduced product of methanol in appreciable amounts.[26,36] Our particular interest has focused on improving the selectivity of CoPc-catalyzed CO_2RR over the competing HER was to encapsulate the parent complex in a polymer

and coat that catalyst-polymer system onto a graphitic electrode. Our group[40] and others[41,42] showed that this encapsulation in poly(4-vinylpyridine) (P4VP) resulted in increased reaction activity and selectivity over the HER - specifically, the CoPc-P4VP faradaic efficiency for CO production improved to > 90% compared to the parent complex's 60%, and turnover frequency was four times faster than without P4VP, and proposed three hypotheses for the reasons behind the increase in activity and selectivity for the CO_2RR upon polymer encapsulation.[40]

Previous members of the McCrory group determined that the primary, secondary, and outer coordination spheres all played a role in this change in selectivity and activity between the parent complex and the polymer-encapsulated system. In previous studies, we were able to systematically study the effect to which the primary and outer coordination sphere influence the activity and selectivity of this system. First, we confirmed that the axial coordination indeed was occurring by the polymer residues by performing X-ray spectroscopy, showing a decrease in the absorbance associated with the 4-coordinate character of the CoPc when either encapsulated by a P4VP or axially coordinated by a free pyridine ligand (we also confirmed that poly-2-vinylpyridine, P2VP, does not show this decrease in absorbance and therefore likely does not axially coordinate to the CoPc center due to the steric backbone of the polymer). While we have thus been unable to confirm the secondary coordination sphere effects, we know from picket-fence porphyrin and biological systems that there could be secondary coordination sphere effects by the protonated pyridyl residues, which can help to stabilize the reactive intermediate by hydrogen bonding.[43-46] Finally, we confirmed the outer coordination sphere effects of the proton relay, a controlled proton delivery mechanism from the aqueous electrolyte through the polymer matrix to the catalytic active sites, which assists in preventing HER, but also allows for controlled proton delivery which is necessary for the CO_2RR. These electrochemical kinetic isotope effect and proton inventory

studies were unique and gave us incredible insight into the microenvironment of the polymer matrix using the macroscale technique of electrochemical current measurements.

We hypothesized that the pyridyl residue from the polymer backbone allowed for controlled proton delivery to the catalytic active site using a proton relay.[35] This proton-hopping mechanism via the pyridyl residues in the polymer allowed for swift proton delivery, which is required for the CO_2RR. In addition, the controlled delivery of protons to the catalytic active site resulted in high selectivity for the CO_2RR over the HER. A complicating factor for this polymer-encapsulated catalytic system is the estimated pKa of the protonated pyridyl residue of the polymer, which may provide artificial buffering and likely has an impact on the microenvironment of the reactive intermediate of CO_2 as it undergoes catalytic reduction. As determined by potentiometric titration, the pKa of the protonated pyridyl residue is 3.5, slightly lower than the analogous monomer, which is likely due to the hydrophobic backbone of the polymer.[47] Our studies on this specific catalytic system have been performed at pH 5 (after CO_2 purge and blanketing, the pH decreases to ~ 4.7 due to the presence of carbonic acid in the electrolyte). While trying to understand the transport of protons and apply those insights to other similar polymer-encapsulated catalyst systems, one research question involved understanding how bulk pH impacted CO_2RR and HER by CoPc-P4VP. This project involved manipulating the bulk concentration of protons in the electrolyte and analyze changes in product distribution, activity, and mechanism as a function of change in pH, which should change the partial protonation of the polymer. Additionally, due to the inherent issues with CO_2 reduction, specifically, the selectivity and CO_2 solubility issues in aqueous electrolyte, we believe that insights from a comprehensive, systematic study of how bulk pH affects the outcomes of this model system would prove useful for the community as these systems are implemented into industrially relevant technologies. For

example, studies have discussed how the selectivity of CO_2 electroreduction of copper and gold can cause changes in product distribution and activity.[48,49] Numerous studies have discussed that pH is important in practical applications for the reduction of CO_2 in an electrochemical fuel cell system, especially when considering the impact of electrolyte identity and concentration and how these experimental parameters can impact the local pH.[50-52]

This project began with the hypothesis that the proton relay should operate under intermediate pH conditions and therefore intermediate fractional protonation within the polymer. We postulated (Figure 3.2) that under mostly protonated (pH 3) conditions, we expect proton transport to operate under diffusion, with each proton consumed being immediately replaced on a pyridyl moiety. Additionally, at pH 7, the polymer remains completely unprotonated and the proton delivery mechanism operates via diffusion. Under intermediate conditions, we expect the proton delivery mechanism to be proton hopping, allowing for facile and controlled proton delivery for the selective CO_2RR.

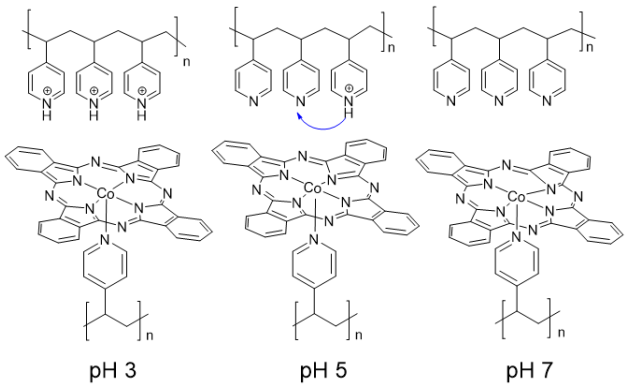

Figure 3.1 Proposed protonation of the polymer as a function of bulk pH. We hypothesize that at pH 3, the polymer is fully protonated. We hypothesize that a proton relay can operate at pH 5, where the polymer is partially protonated, and at pH 7, the polymer is fully deprotonated.

As MCECs have become ubiquitous throughout the literature, the role of counterions and the electrolyte identity has been an outstanding question with regards to the intercalation of ions within the polymer or other membrane overlayer. This is particularly difficult to study within a polymer where the moieties have a pKa and therefore an artificial buffering system that likely changes as a function of distance from the electrolyte. Similar work by Koper and coworkers showed the importance of performing systematic studies to determine the interconnected role of cation concentration and pH by performing alkaline HER on a gold electrode, and showed that activity increased with increasing alkali metal concentration, but at higher concentration, the dependence on metal cations diminished and activity decreased.[53]

As discussed previously, the pH of the electrochemical system is important for practical reasons and to fundamentally understand the impacts of this system on the metrics of activity, selectivity, and proton transport mechanism. The effect of concentration of protons and electrolyte on the faradaic efficiency of the CO_2RR on electrodes such as gold and copper.[48,54-56] However, such studies are sparse for molecular catalysts, and especially for MCEC systems where the overlayer or polymer can further impact the electrochemical results from the system. an important result from this work was that we saw that the proton transport mechanism may also be dependent on a counterion to transport through the polymer matrix along with the proton.

Herein, we report that the selectivity of the catalyzed reaction for CO_2RR will improve as pH increases, that activity peaks at a slightly higher pH than the pKa of the protonated polymer, and that the measurement of a kinetic isotope effect (to determine whether the rate-determining step contains a proton transfer event) decreases as a function of pH. However, we were able to isolate the impact of the ion by performing an electrolyte and pH study for the production of H_2 (HER), which would not have multiple reaction mechanisms competing for electrons. In this

system, we found that activity increased with increasing electrolyte concentration. We also found that the HER activity decreased with increasing pH. Finally, when measuring the KIE of HER by system, we found that the KIE decreasing proton availability, which was counterintuitive to our previous assumptions, which centered around a KIE being dependent on the protonation event in a catalytic mechanism. This showed us that the KIE only reflects that protonation event if there are enough available protons, and when there are a shortage of protons (due either to the lack of a counterion or due to the high pH) the transport mechanism could be the limiting factor of this reaction, and the KIE would not be apparent for the HER.

3.4 Experimental

3.4.1 Materials

All purchased chemicals were used as received, unless otherwise specified. All water used in this study was ultrapure water (18.2 MΩ cm resistivity), prepared via purification by a Thermo Scientific GenPure UV-TOC/UF x CAD-plus water purification system. Carbon dioxide (CO_2, 99.8%) was purchased from Cryogenic Gases and was used as received, and nitrogen (N_2) was boil-off gas from a liquid nitrogen source and was used without further purification. The following chemicals were purchased from Sigma Aldrich and used as received: graphite powder (GP, synthetic < 20 μm), cobalt phthalocyanine (CoPc, 97%), poly-4-vinylpyridine (P4VP, average Mw ~ 160,000), N, N-Dimethylformamide (DMF, ACS grade), poly-2-vinylpyridine (P2VP, average Mw ~159,000), sodium phosphate monobasic (BioXtra, >99.0%), phosphoric acid-D3 solution (85 wt% in D_2O), phosphoric acid (85 wt% in H_2O), Nafion-117 cation exchange membrane (Nafion), ferrocene carboxylic acid (97%), and sodium hydroxide (NaOH, TraceMetal grade). Sodium deuteroxide (NaOD, 40 wt.% in D_2O) and sodium perchlorate anhydrous were purchased from Oakwood Chemical. Sodium perchlorate monohydrate ($NaClO_4$, 97%) was obtained from Alfa Aesar. Nitric acid (TraceMetal grade, 67-70%) was purchased from Fisher Scientific. Cobalt ICP standard (1000 ppm in 3% HNO_3) was purchased from Ricca Chemical Company. Deuterium oxide (D_2O, 99.9%) was purchased from Cambridge Isotope Labs, Inc. Glassy carbon disk electrodes (GCEs, 4 mm thick, 5 mm in diameter, effective electrode area 0.196 cm^2) were purchased from HTW Hochtemperatur-Werkstoff GmbH. Edge-plane graphite electrodes (EPGs, total area of 5 mm with 3.8 mm EPG disk encapsulated in epoxy, effective electrode area 0.114 cm^2) were purchased from Pine Research Instrumentation.

3.4.2 Electrolyte Solution Preparation and pH measurements

Unless otherwise stated, all experiments were performed in phosphate/perchlorate electrolyte solutions with concentrations explicitly stated in the main text. Experiments performed to determine the pH dependence of the electrochemical system were performed in electrolyte solutions of 0.4 M NaH_2PO_4 added to 0.5 M $NaClO_4$ in order to minimize any ionic strength differences across a variety of pH levels. Experiments used to study the activity dependence of buffer concentration were performed in varying concentrations of phosphate/perchlorate buffer systems as specified in the main text. To measure the kinetic isotope effects of these systems, electrochemical studies were performed in completely deuterated electrolyte, with 100% D_2O constituting the solvent and phosphoric acid-d3 (D_3PO_4), sodium deuteroxide (NaOD), and sodium perchlorate anhydrous being combined in oven-dried glassware to Importantly, all electrochemical glassware were vigorously washed, and prior to their use, the cells and Nafion membrane separators to be used in the electrochemical studies were soaked in water for at least 12 hours prior to the experiments to ensure that all salt was removed from the cell.

Prior to each experiment, the working chamber was sparged with the appropriate gas by using a section of Tygon tubing for at least 30 minutes. The pH after sparging varied from between 4.1 to 4.5 and was adjusted to the desired pH level for the experiment by titrating 1 M NaOH or 10% H_3PO_4 into the electrolyte while it was blanketed by CO_2 or N_2 and sealed under 1 atm of the appropriate gas. All pH measurements were conducted with a Fisher Scientific Accumet AB200 pH meter with an Atlas Scientific pH probe calibrated at three points with pH = 4.01, 7.00, and 10.01 calibration standards (Fisher Scientific). The pD of the electrolyte solutions was measured using the same pH meter using a simple correction.[57] The correction for measurement of pD using a pH meter is shown in Equation 3.1:

$$pD = pH_{meter\ reading} + 0.4$$

Equation 3.1

3.4.3 Preparation of Catalyst

CoPc-polymer/GP deposition inks were prepared as previously described.[58] The preparation conditions and resultant loadings of catalyst, polymer, and graphite powder can be found in Table 3.1.

CoPc-P4VP deposition inks (no graphite powder)

A solution of 0.05 mM CoPc in DMF was prepared by the addition of 0.0029 g of CoPc to 100 mL of DMF in a duct tape-jacketed 100 mL glass media jar (Fisher Scientific ®). The mixture was sonicated for 1 hour and then vortexed for 1 minute at 3000 rpm. Following the preparation of the 0.05 mM CoPc/DMF solution, 0.015 g P4VP was added to 5 mL of the CoPc/DMF mixture in a duct tape-jacketed 20 mL scintillation vial to create a 0.05 mM CoPc – 0.3% w/v P4VP in DMF. The P4VP was allowed to disperse by sonication for 30 minutes.

CoPc-polymer deposition inks with graphite powder

A solution of 0.05 mM CoPc in DMF was prepared by the addition of 0.0029 g of CoPc to 100 mL of DMF in a duct tape-jacketed 100 mL glass jar (Fisher Scientific ®). The mixture was sonicated for 1 hour and then vortexed for 1 minute at 3000 rpm. Following the preparation of the 0.05 mM CoPc/DMF solution, 0.03 g polymer was added to 1 mL of the CoPc/DMF mixture in a 20 mL duct tape-jacketed scintillation vial to create a 0.05 mM CoPc – 3% w/v polymer in DMF. The P4VP was allowed to disperse by sonication for 30 minutes. A mass of 0.01 g of graphite powder was then added to the CoPc-polymer mixture to create a 0.05 mM CoPc – 3% P4VP – 1% w/v GP preparation suspension. The suspension was allowed to disperse via sonication for 30 minutes. A Teflon stirbar was then added to the scintillation vial and the CoPc-polymer/GP

mixture was magnetically stirred by stirplate at 500 rpm for 12 h. After stirring, the preparation suspension was centrifuged in a 2 mL centrifuge tube (Fisherbrand™ Premium Microcentrifuge tube) at 14,000 rpm for 30 minutes at -4 ºC in an Eppendorf 5430R refrigerated centrifuge. The supernatant was decanted, and 1 mL of fresh DMF was added. The suspension was then vortexed for 30 sec at 3000 rpm, and sonicated for 30 sec.

3.4.4 Preparation of Modified Electrodes

Prior to modification, glassy carbon electrodes (GCEs) were polished on a Struers Labo Pol-5 polishing instrument with a LaboForce-1 specimen mover. The GCE disks were loaded into a custom-made brass electrode holder held by the specimen mover with polishing side on a MDFloc (Struers) synthetic nap polishing pad and were sequentially polished with diamond abrasive slurries (DiaDuo-2, Struers) in an order of 9 µm, 6 µm, 3 µm, and 1 µm diameter particle slurries for 1 minute. The speed of the was held at 200 rpm and, in the opposite rotation direction from the platen, the specimen mover was held at a speed of 8 rpm. Between each polish of the sequential diamond size, the electrodes were rinsed with water. After the final polishing step, the GCE disks were sonicated in isopropyl alcohol for 3 minutes, followed by water for 3 minutes, and in 1 M HNO_3 for 30 minutes. The electrodes were then rinsed with water and dried under an N_2 stream. In order to decrease any likelihood of water being present and skewing results due to the use of deuterated electrolyte, all electrodes were dried in an oven at 60ºC for 10 minutes prior to the dropcasting of deposition ink. The electrodes were coated by dropcasting 5 µL of the CoPc-P4VP/GP deposition ink, allowing the surface to dry in an oven at 60ºC for 10 minutes, and then was followed by a second coating of 5 µL of the deposition ink and drying at the same temperature.

Edge-plane graphite electrodes (EPGs) were polished by manually hand-polishing on a 600-git silicon carbide polishing paper (Buehler, CarbiMet) with water for 10 seconds. The electrodes

were rinsed with water then sonicated in isopropyl alcohol for 1 minute, rinsed with water, sonicated in water for 1 minute, and then dried under an N_2 stream. Prior to dropcasting, the electrodes were allowed to dry in an oven for 10 minutes at 60ºC. A volume of 5 µL of the CoPc-P4VP deposition ink was dropcasted onto the polished EPG and was allowed to dry in an oven for 10 minutes at 60 ºC.

3.4.5 Cobalt Loading Determination

Catalyst loading was determined as previously described.[28] After centrifugation, the graphitic pellet was digested by the addition of 15 mL TraceMetal Grade 1 M HNO_3. The solution was stirred overnight, and then was filtered using a cellulose syringe (Pore Size 0.45 µm, Titan 3 regenerated cellulose, Fisher Scientific) to remove the polymer and graphite powder. The metal content was then measured using inductively coupled plasma-mass spectrometry (ICP-MS, PerkinElmer Nexion2000). The ICP-MS was calibrated using internal standards at 10, 50, 100, and 500 ppb and standard nitric acid blank at 0 ppb. The conversion from ppb to molar CoPc loading in the deposition ink is shown Equation 3.2- Equation 3.4.

$$X \text{ ppb} \times \frac{\frac{1\ \mu g}{\text{L}}}{1 \text{ ppb}} \times 0.015 \text{ L} = \text{mass Co in } \mu\text{g}$$

Equation 3.2

$$\text{mass in } \mu\text{g x } \frac{1 \text{ mol Co}}{58.93 \text{ g Co}} \times \frac{10^{-6} \text{ g}}{1\ \mu\text{g}} = \text{ mol CoPc}$$

Equation 3.3

$$\frac{\text{mol CoPc}}{0.0010 \text{ L initial deposition ink}} = M \text{ CoPc in deposition ink}$$

Equation 3.4

3.4.6 Electrochemical Measurements

Electrochemical measurements were conducted using a Bio-Logic SP200 potentiostat/galvanostat, and data were recorded using the Bio-Logic EC-Lab software package. Reference electrodes were commercial saturated calomel electrode (SCE), externally referenced to ferrocenecarboxylic acid in pH 7, 0.2 M phosphate buffer (0.284 V vs. SCE), and auxiliary electrodes were carbon rods (99.999%, Strem Chemicals Inc.). Working electrodes were the modified GCEs or EPGs described in the previous section. In all cases, the working electrode was separated from the auxiliary electrode by a Nafion membrane. Unless otherwise noted, all electrochemical measurements were conducted at least three times with independently prepared electrodes, all values reported are the average of these repetitions, and all reported errors are standard deviations. The errors of interpretations that required mathematical operators were the standard errors of two standard deviations (for example, kinetic isotope measurements that required division of two average measurements).

For rotating disk electrode (RDE) chronoamperomentric (CA) step measurements, the modified GCE working compartment was assembled using a Pine Research Instrumentation E6-series change disk RDE assembly attached to an MSR rotator. CA measurements were conducted at 1600 rotations per minute (rpm) with a single 6-minute potential step held at -0.647 V vs. RHE (V vs. SCE varied depending on the electrolyte pH), to ensure equivalent thermodynamic potential against the concentration of protons. The 1600 rpm rotation rate was used to ensure steady-state CO_2 and/or proton delivery to the electrode surface in a way that is not present in a longer controlled potential electrolysis (CPE) experiment where substrate delivery is dependent on diffusion or convection by magnetic stirring.

RDE-CA measurements were conducted in a custom two-compartment glass cell. In the first compartment, the working electrode with GCE assembly was suspended in 30 mL buffer solution

with 3 gas inlets and one inlet for the reference electrode. The second compartment contained ~15 mL solution with the auxiliary electrode. The compartments were separated by a Nafion membrane. Both compartments were sparged with the gas (CO_2 or N_2) for ~30 minutes prior to each set of measurements, and the headspace was blanketed with the corresponding gas during the measurements. The gas used for all electrochemical experiments was first saturated with electrolyte solvent by bubbling the gas through a gas washing bottle filled with the same electrolyte solvent (water or deuterium oxide) used in the cell to minimize electrolyte evaporation in the cell during the course of the measurements. Solution resistance of the cell was measured prior to the experiment and was compensated via software at a rate of 85% via a positive feedback loop software correction. Solution resistance varied across electrolyte concentrations but were generally between 50 and 300 Ω.

CPE experiments were conducted at room temperature in custom, gas-tight, two-chamber U-cells. The modified working electrode was held in a RDE internal hardware kit (Pine Research Instrumentation) and mounted into a custom PEEK sleeve. For the electrolysis measurements, the main chamber held the working electrode and an SCE reference electrode in ~ 25 mL electrolyte, and the headspace was measured after each experiment by measuring the amount of water needed to refill the main chamber. The auxiliary chamber held the auxiliary carbon rod electrode in 15 mL electrolyte. The two chambers were separated by Nafion cation exchange membrane. Prior to each experiment, both chambers were sparged with CO_2 for ~20 min, the pH or pD was adjusted, the cell was sparged with CO_2 for ~20 min, and then the main chamber was sealed under CO_2 atmosphere. The pH of the electrolyte was measured immediately prior to the sealing of the cell after CO_2 purge. The resistance of the cell was measured with a single-point high-frequency

impedance measurement but was not compensated over the course of the experiment. In general, our electrochemical cell for CPE had Ru ~ 150 Ω in all pH or pD solutions.

3.4.7 Product detection and quantification

After CPE, gaseous and liquid samples were collected and analyzed using gas chromatography (GC) and high-performance liquid chromatography (HPLC), respectively. For gaseous samples, analysis was conducted using a Thermo Scientific Trace 1310 GC system with two separate analyzer channels for the detection of H_2 and C1-C2 products. A Pressure-Lok gas-tight syringe (10 mL, Valco VICI Precision Sampling, Inc.) was used to collect 5 mL aliquots from the main chamber headspace of the cell, and each aliquot was injected directly into the 3 mL sample loop. Using a custom valve system, column configuration, and method provided by Thermo Scientific, gases were separated such that H_2 was detected on the first channel using an Ar carrier gas and thermal conductivity detector (TCD) and all other gases were detected on the second channel using a He carrier gas and a TCD. The GC system was calibrated using calibration gas mixtures (SCOTTY Specialty Gas) at H_2 = 0.02, 0.05, 0.5, and 1% v/v and CO = 0.02, 0.05, 0.5, 1, and 7% v/v. Chromatographs were analyzed by using the Chromeleon Console.

Faradaic efficiencies of gaseous products were calculated via eq 1:

$$\mathrm{FE} = \frac{\frac{V_{HS}}{V_g} \times G \times n \times F}{Q}$$

where V_{HS} is the headspace volume in mL of the working chamber, V_g is the molar volume of gas at 25ºC and 1.0 atm (24500 mL/mol), G is the volume percent of gaseous product determined by GC (%), n is the number of electrons required for each product (n = 2 for H_2 and CO), F is the Faraday constant (C/mol) and Q is the charge passed in Coulombs.

3.4.8 Ex Situ Infrared Spectroscopy

To spectroscopically evaluate protonation of P4VP layers by different buffer solutions, *ex situ* transmission infrared experiments were performed using a Nicolet iS50 FTIR with an MCT detector. Each P4VP layer was prepared by drop casting 38.1 µL of a 1% P4VP/DMF solution onto a clean 0.5" diameter uncoated CaF_2 window (Thorlabs) and dried in an oven at 60°C overnight to drive off all DMF. Buffer solutions were prepared and brought to the desired pH as described above. Onto each P4VP-coated window, a 150 µL buffer droplet was deposited and allowed to soak for 45 minutes. The buffer droplet was then removed via pipette, and remaining buffer was wicked away using a Kimwipe. The window was dried in an oven at 60°C for 1 hour. To collect spectra (before and after buffer exposure), the windows were mounted inside the FTIR transmission chamber, and backgrounded against a clean CaF_2 window with a dry N_2 purge. Each spectrum was collected with 128 scans at 2 cm^{-1} resolution (data spacing of 0.241 cm^{-1}).

3.5 Results & Discussion

3.5.1 Dependence of pH on Fractional Protonation and CO_2RR Activity, Selectivity, and KIE

We proposed that the fractional protonation of the pyridyl moieties can be modeled as a function of pKa (Figure 3.2). This proposed fractional protonation of the polymer is crucial for the other characteristics of the system (the mechanism, the activity, and the product selectivity). Figure 3.2b outlines the proposed pH-dependent mechanistic changes based on the kinetic isotope effect (KIE). KIE involves the measurement of steady-state current at a catalytic potential in both protonated and deuterated electrolyte to determine whether the rate-determining step (RDS) of the catalytic cycle involves a proton transfer event. In previous studies, we showed that when encapsulated in P4VP, the RDS does involve a proton transfer event, but the KIE is artificially deflated (from KIE ~ 3 without polymer to KIE ~ 2 with a polymer) at a pH where the proton relay was most prevalent, slightly above the pKa of the polymer at pH 5. We hypothesized that activity for CO production as a function of pH would be highest near the pKa of the polymer, as proton availability at low pH would result in HER, while decreased proton availability at high pH would decrease the overall activity. Finally, we hypothesized that as pH increases, a corresponding increase will follow for the reaction selectivity of CO_2RR over the competing HER.

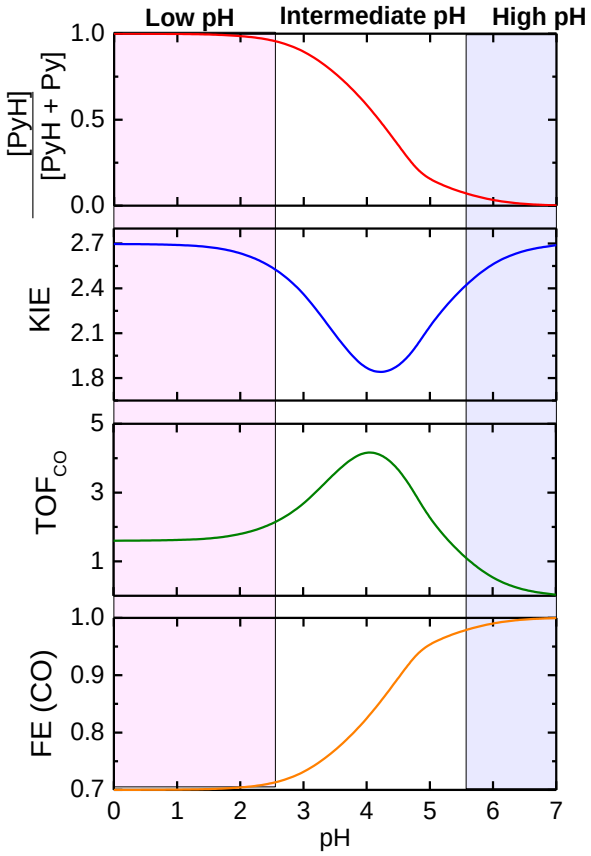

Figure 3.2 Initial hypotheses of the pH dependence of (a) the partial protonation of the polymer, (b) the expected mechanistic changes as measured by the observed KIE which indicates the mechanism's RDS, (c) activity for CO production, and (d) the product selectivity as a function of pH, and which are each an extrapolation based on the pKa of the protonated pyridyl residues. These curves were drawn based on intuitive understanding of the pKa of protonated pyridyl moieties within the polymer and were not modeled.

In order to measure the fractional protonation as a function of electrolyte pH, we turned to spectroscopic methods. Specifically, we measured the absorbance of a ring breathing mode of pyridinium at ~1640 cm^{-1} using IR spectroscopy after the polymer had been exposed to electrolyte pH levels. This mode is associated with the breathing of a protonated pyridyl residue that is not present in a deprotonated prydiyl residue. The results of this study are shown in **Error! Reference source not found.**, where the fractional protonation as measured by IR spectroscopy shown to increase with increasing proton concentration (decreasing pH) at a constant 0.1 M phosphate concentration. This provides spectroscopic confirmation that decreasing pH leads to increased fractional protonation within the polymer.

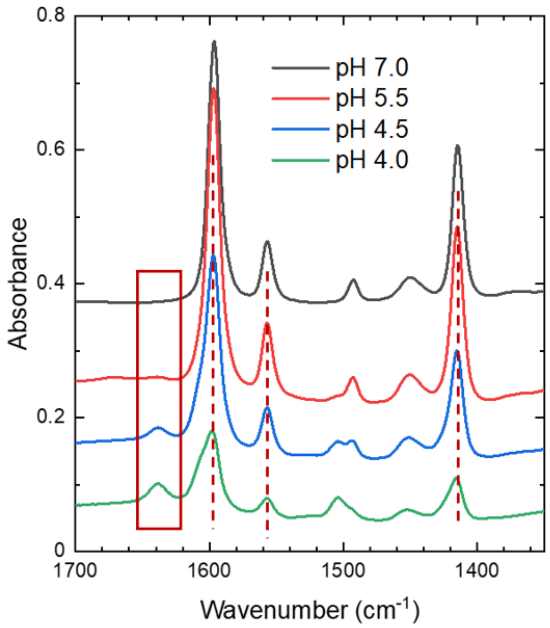

Figure 3.3 Infrared spectra showing P4VP under different pH levels. Highlighted: stretching frequency at ~1640 cm^{-1}, which shows an increase in absorbance that corresponds to a ring breathing mode of a protonated pyridyl functional group.

We postulated that an increase in pH of the electrolyte would result in a corresponding increase in reaction selectivity for the CO_2RR over the competing HER. We hypothesized that the availability of protons within the polymer as seen by fractional protonation would increase the

likelihood that CoPc-catalyzed HER would proceed, while higher pH and lower fractional protonation would provide the dual result of an increase of hydrophobicity of the polymer layer (increasing the CO_2 concentration within the polymer film) and a decrease in available protons, which decreases the likelihood of HER.

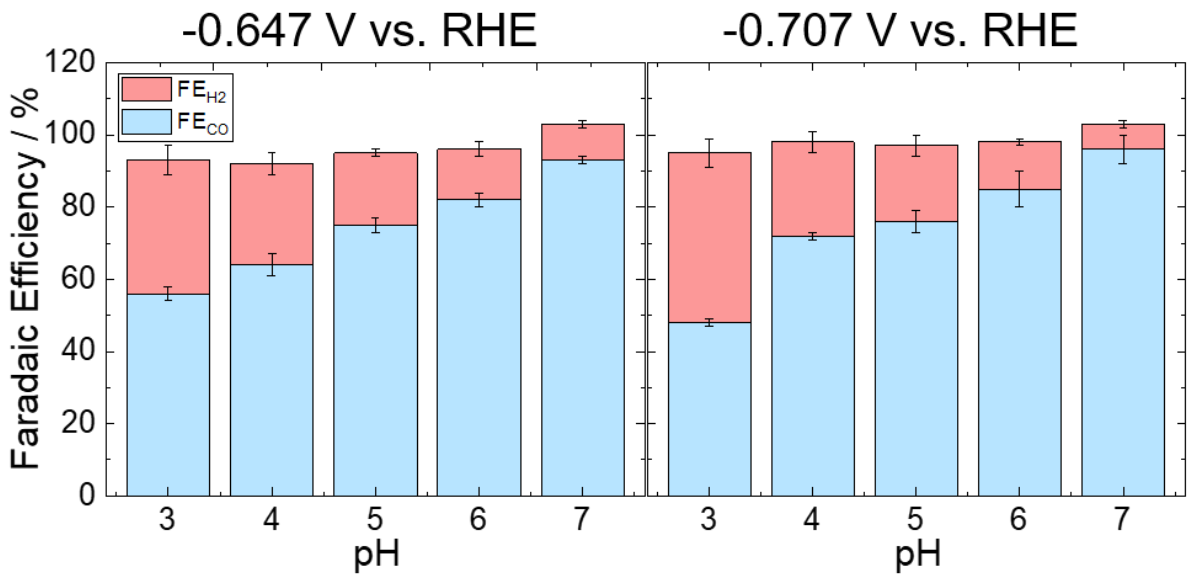

Figure 3.4 Reaction selectivity as a function of pH, measured by faradaic efficiency of the CO_2RR product, CO, and the HER product, H_2. As the pH increases, the reaction selectivity for CO_2RR also increases. This trend holds at -0.647 V vs. RHE (where a majority of experiments in this paper were studied) and a more negative potential of -0.707 V vs RHE, with a considerably higher H_2 production at pH 3. Controlled potential electrolysis experiments were performed in a sealed H-cell in 0.4 M phosphate/0.5 M perchlorate electrolyte as described in the Experimental Section.

An important parameter for determining the optimal pH for performance of this reaction is activity. We had hypothesized that the pKa of the polymer would be important for optimal activity, as the delivery of protons is a key component of the CO_2RR, but with high proton availability, HER would dominate most of the current passed in the system. It was important to consider the total activity and the total activity toward CO production, as determined by the CPE selectivity measurements. The results of this activity study are presented in Figure 3.5.

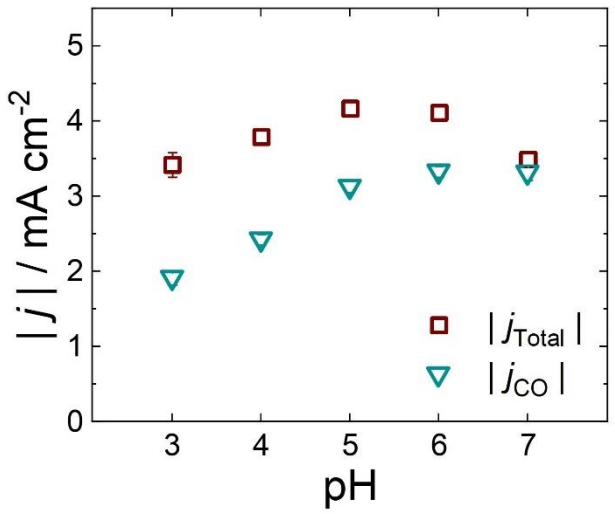

Figure 3.5 Total activity of CoPc-P4VP/GP/GCE (j_{Total} , red square) and activity corrected for CO production (j_{CO}, blue triangle) showing a peak in total activity near pH 5 and a plateau in activity for CO production that begins near pH 5. Activity measurements were taken under rotation at 1600 rpm via a 6-min CA step at -0.647 V vs. RHE in 0.4 M phosphate 0.5 M perchlorate electrolyte.

To show that axial coordination is retained across the pH range discussed herein, we performed a study where we compared the effects of two different polymers: P4VP and the similar poly-2-vinylpyridine (P2VP), which does not coordinate to CoPc centers due to the location of the nitrogen on the pyridyl residue and the steric hinderance of the polymer backbone. Previous studies showed decreased activity and selectivity for a system using CoPc-P4VP as a catalyst compared to CoPc-P2VP,[35,40] but we showed concrete evidence using X-ray absorbance spectroscopy that CoPc-P2VP retains an absorbance energy consistent with 4-coordinate character.[29] However, CoPc-P4VP loses that absorbance, which is consistent with axial coordination of the pyridyl residues of the polymer to the cobalt center, creating a 5-coordinate system. In that same study, we were able to measure CoPc-P4VP under a range of different pH levels discussed herein and showed that it retained an electronic structure consistent with 5-coordinate character (Figure 3.6b). However, free pyridine did not behave in the same manner (Figure 3.6c). At pH 3, the system seems to lose 5-coordinate character, which would be consistent with the protonation of pyridine off the CoPc.

We hypothesized that the CoPc remains 5-coordinate in the polymer due to the comparative lower pKa of a protonated pyridinium within the polymer in relation to a free pyridine, which would result in the pyridine being protonated off of the CoPc center at a higher pH, likely due to the hydrophobic backbone of the polymer.[29] Here, we confirm that axial coordination is still required to maintain overall activity across all pH levels. When CoPc-P2VP is prepared and tested across pH levels from 3-7, we see that total activity is lower compared to that of CoPc-P4VP (Figure 3.6). This is especially apparent at higher pH levels, as pH 4 and pH 3 show similar total activity results. It's important to note that these results are for total activity – we would expect for CoPc-P2VP, the selectivity for CO production would fall short of the metrics for a CoPc-P4VP

system, as we have shown previously. We did not find it necessary to show this result at all pH levels, but we did perform a CPE experiment at pH 5. We found that, indeed, at pH 5, CoPc-P2VP produces CO with 58% Faradaic efficiency, while CoPc-P4VP produces CO with 75% Faradaic efficiency (details found in Table 3.5). In a previous study observing the impact of graphite powder incorporation on electrochemical activity, we saw that CoPc-P2VP/GP/GCE performed with lower activity compared to CoPc-P4VP/GP/GCE across several different catalyst/polymer loadings – these results further confirm the finding that axial coordination is necessary to perform with optimal levels of activity and selectivity, even as a function of pH.

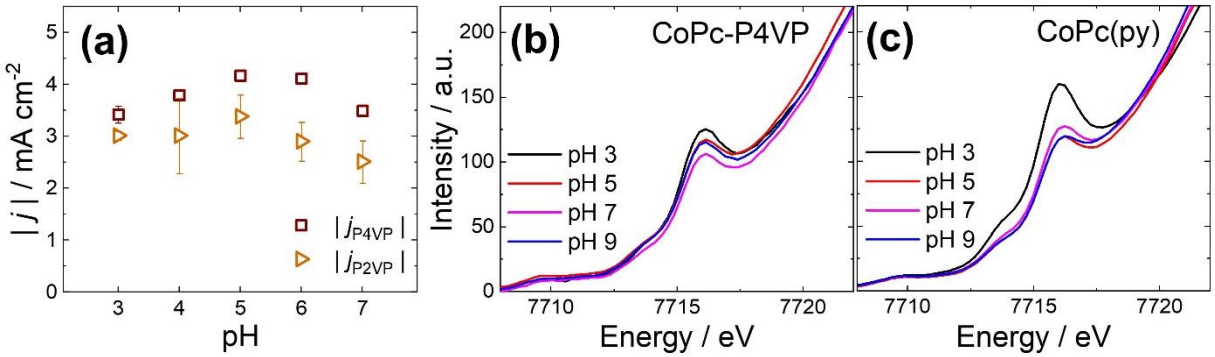

Figure 3.6 (a) Comparison of total activity under rotation for CoPc-P4VP/GP/GCE (red square) compared to CoPc-P2VP/GP/GCE (orange triangle), with CoPc-P2VP showing lower total activity compared to CoPc-P4VP at all pH levels and the differences being especially stark at higher pH levels. Activity measurements were taken under rotation at 1600 rpm via a 6-min CA step at -0.647 V vs. RHE in 0.4 M phosphate 0.5 M perchlorate electrolyte. (b) and (c) show previously published X-ray absorbance data for CoPc-P4VP and CoPc(py), where the absorbance associated with a 4-coordinate CoN_4 complex is shown to remain comparatively absent at pH 3 for CoPc-P4VP while CoPc(py) showed an increase in that absorbance, indicating the loss of 5-coordinate character of the CoPc(py) complex. (b) and (c) Are previously published data from Ref. [29] and reprinted here with permission from the Royal Society of Chemistry.

3.5.2 The impact of electrolyte concentration on the activity, selectivity, and measurement of the kinetic isotope effect

In previous studies,[29,35,40,58,59] the electrolyte used for all electrochemical studies of CoPc-P4VP was a concentration of 0.1 M sodium phosphate monobasic, with a resultant pH of approximately 4.7 after CO_2 was bubbled into the system. This pH was dictated mainly by the phosphate buffer, but was convenient as it was about one pH unit higher than the pKa of P4VP.[47] We note that the pKa of protonated pyridyl residues of a P4VP polymer is measured to be approximately 3.5 by potentiometric titration, considerably lower than the pKa of the monomeric analogue, presumably due to the hydrophobic backbone of the polymer. In this pH-dependent study, to reach a bulk pH of 7 with CO_2 in solution, we increased the concentration to 0.4 M phosphate. The higher concentration of 0.4 M phosphate was to allow for maintenance of the pH and limited buffer breakdown as CO_2 was added to the system. Additionally, being concerned about the ionic strength of the electrolyte, to maintain relatively similar ionic strength, we added sodium perchlorate into the system. The high concentration of perchlorate, 0.5 M $NaClO_4$ in addition to the 0.4 M NaH_2PO_4, prevented the presence of any confounding variables of having higher concentration of ions in solution.

This incorporation of higher levels of electrolyte caused some interesting changes in the system. One note was that the ohmic response of the system saw an overall decreased solution resistance with increased electrolyte concentration. Additionally, the reaction selectivity of the CO_2RR over the HER decreased slightly at pH 5 compared to a solution of 0.1 M phosphate. In general, a trend was that increasing electrolyte concentration at a common pH resulted in a decreasing selectivity for the CO_2RR over the HER (see Table 3.5 for a comparison of the CoPc-P4VP/GP/GCE system under different levels of electrolyte concentration). This phenomenon can

be explained by the increased ability for the local pH to be maintained at the higher concentration of electrolyte. As seen in other studies, persistent alkalinity is maintained close to the electrode surface when an electrode is performing CO_2RR, as the consumption of protons drives up the local pH.[60] A higher concentration of buffer prevents the buffer breakdown and maintains the low pH close to the electrode surface, which results in a lower pH and therefore more HER over the CO_2RR.

However, in addition to the selectivity of these systems, we saw an interesting phenomenon when considering the kinetic isotope effect (KIE) of the CO_2RR and the HER. In previous studies, we saw that the CoPc-P4VP-catalyzed CO_2RR showed a KIE of 2, meaning that the activity measured was twice as fast when the CO_2RR was performed in protonated electrolyte compared to when performed in deuterated electrolyte. In combination with some mechanistic studies, that strongly suggested that the rate-determining step of the CO_2RR was a proton transfer event which took place after the binding of the CO_2 molecule to the CoPc site. However, the four coordinate CoPc parent complex showed a KIE = 1, meaning that the RDS was not dependent on the transfer of a proton as the rate in protonated and deuterated electrolyte was the same. This suggested that the RDS could be the addition of CO_2 to the catalyst, and that the axial coordination of the pyridyl residues of the polymer promoted the binding of CO_2 by making the electrons that donate into the CO_2 more nucleophilic. The kinetic isotope effect with CoPc(py), where was equal to 3. The deflated KIE of 2 for CoPc-P4VP compared to that of 3 for CoPc(py) as a result of the proton hopping mechanism of the polymer, where a slight inverse isotope effect (pyridyl residues propensity to hold onto a deuterium with higher strength added up throughout the time to transport a proton through the polymer matrix. This inverse isotope effect and the proton hopping transport

mechanism through a long chain or pyridyl residues resulted in the KIE being equal to 2 rather than being equal to 3 in the CoPc(py) case where there is not a proton relay.

When conceiving of this project, we had hypothesized that this proton relay effect would change as a function of bulk pH. Specifically, we thought that when the pH was low or very high, we would see the operative mechanism of proton transport change from mainly proton relay to diffusion, which would result in a KIE shift from 2 at intermediate pH values (as seen in our previous study) to 3 at the extreme pH values of 3 or 7. However, what we found an unexpected response, where the KIE trended downward as the pH increased (Figure 3.7). Specifically, we saw that the KIE of these systems was 2 near pH 3 and decreased to 1 as the bulk concentration of protons decreased with an increased pH of 7. This was very different than what we had seem previously – with a comparable pH of 5, the KIE was 1.5 instead of 2.1 as we had seen in the previously studied systems.

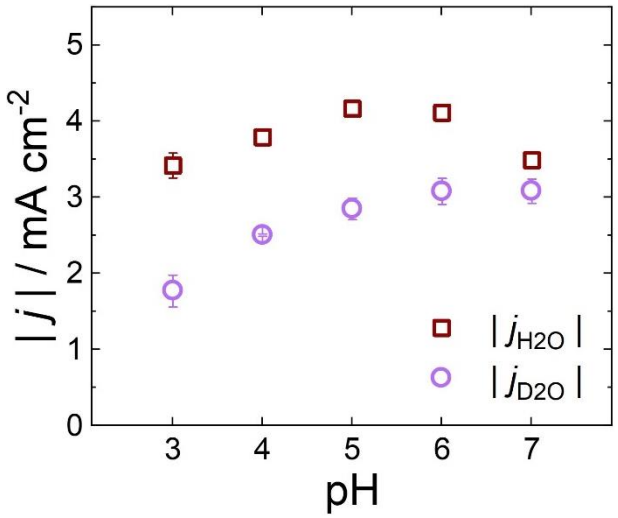

Figure 3.7 Total current density of CoPc-P4VP/GP/GCE measured under rotation in protonated (red) and deuterated (purple) electrolyte under a CO_2 atmosphere. Activity measurements were taken under rotation at 1600 rpm via a 6-min CA step at -0.647 V vs. RHE in 0.4 M phosphate 0.5 M perchlorate electrolyte.

One major consideration was the KIE of the HER. Since different levels of HER are present as a function of the pH, we knew that the overall observed KIE would be dependent on the KIE of the HER, as not all of the charge produced, and therefore fractional current density, would be going toward the production of CO. To test this, I performed a pH-dependent experiment under the same conditions but with the presence of N_2 instead of the presence of CO_2 with both systems (Figure 3.8). The results were surprising. Where the previous results had shown a KIE of 1.3 for the production of H_2 under N_2, saw that the KIE for the HER was nearly 3 under most pH levels. Importantly, the KIE at an electrolyte pH of 7 decreased and was closer to 2.

Interestingly, the activity to produce H_2 shifts as the pH changes within the tested range of pH 3-7. This should not be the case, as the chronoamperometric steps were held at the same potential against the RHE, and the RHE scale takes into consideration the concentration of protons to overcome the Nernstian response of proton activity within the electrolyte by -0.059 V for each pH unit. However, this shows that the decrease in activity as pH increases could be due to some other mechanistic step being the rate limiting step for the HER. This was the case in a study performed by Koper and coworkers,[53] where they found on a gold electrode at alkaline pH levels that an increase in pH led to an increase in activity (the opposite effect that we see here, at acidic pH, where the activity decreases with increasing pH at the same potential on the RHE scale). They attributed the change in HER activity to the kinetically rate-limiting step being independent of a proton transfer event, and instead that the RDS was dependent on cation concentration of the stabilization of the Volmer step. Additionally, they postulated that increasing pH led to an increase in the local field strength which indirectly changed the cation concentration near the surface, which was therefore leading to an increase in HER activity.

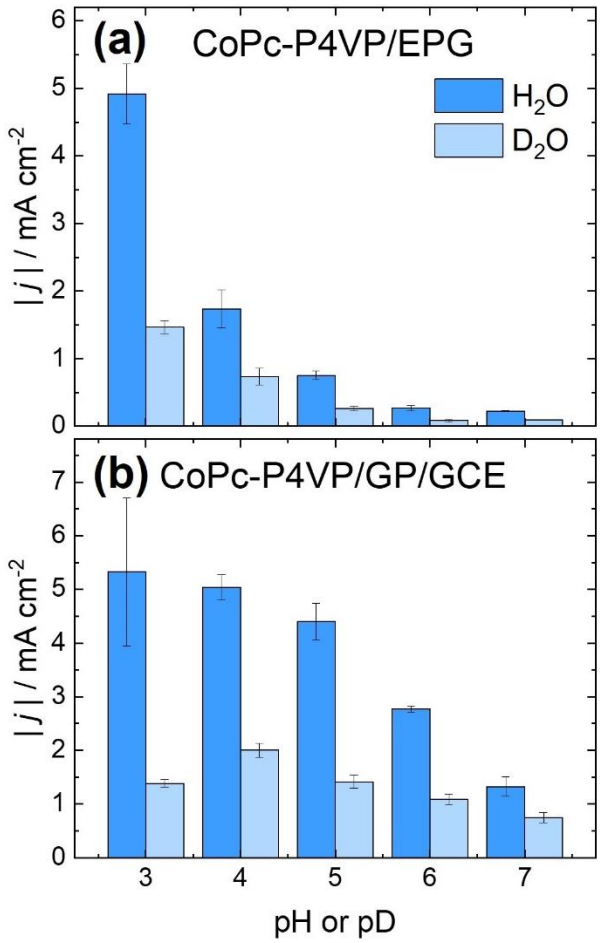

Figure 3.8 pH-dependent activity of (a) CoPc-P4VP/EPG and (b) CoPc-P4VP/GP/GCE in H_2O/ protonated electrolyte (dark blue) and D_2O/deuterated electrolyte (light blue) for the production of H_2 (HER) under an N_2 atmosphere. In both systems, activity decreases with pH and KIE is ≥ 2.5 for all pH levels except pH 7. Activity measurements were taken under rotation at 1600 rpm via a 6-min CA step at -0.647 V vs. RHE in 0.4 M phosphate 0.5 M perchlorate electrolyte.

It's possible that there is something similar occurring here, but the KIE results show that the RDS likely does involve a proton transfer event, as the KIE is ≥ 2.5 at all pH levels except for pH 7, where the KIE ~ 2. Interestingly, these results were somewhat consistent across two different systems tested: CoPc-P4VP/GP/GCE and CoPc-P4VP/EPG. This ruled out the fact that either the CoPc or the GP would be the contributing factor to the kinetic isotope effect of the HER. Since the CoPc-P4VP/EPG also showed the KIE equal to three under pH three through six, and a KIE of 2 near the pH 7, we determined that the graphite powder was not the reason for the change in KIE. Instead, I turned to study the concentration of electrolyte.

To test whether this was a function of using a CoPc-P4VP/GP/GCE electrode compared to our previous EPG system, we tested the KIE of 0.1 M phosphate with CoPc-P4VP/GP/GCE, CoPc-P4VP/EPG, and CoPc-P4VP (1%)/EPG, all of which showed that the KIE was ~1.3 for the production of H_2. However, the addition of additional electrolyte caused the KIE of the HER to increase. For instance, the KIE of the HER was 2 under 0.15 M phosphate, while 0.2 M phosphate resulted in a KIE of 3. This was also the case for 0.4 M phosphate. These experiments were each performed at pH 5, where the increased electrolyte concentration was how the high activity. Interestingly, it seems that the KIE of this system does not increase past 3, even after the concentration of electrolyte increases past 0.2 M. While these tools cannot confirm whether the anion or cation is causing this interesting phenomenon, we suggest that measuring the activity or selectivity dependence of different ions or cations (as have been performed in numerous studies) could be useful for further understanding of this phenomenon, but is out of the scope of this study.

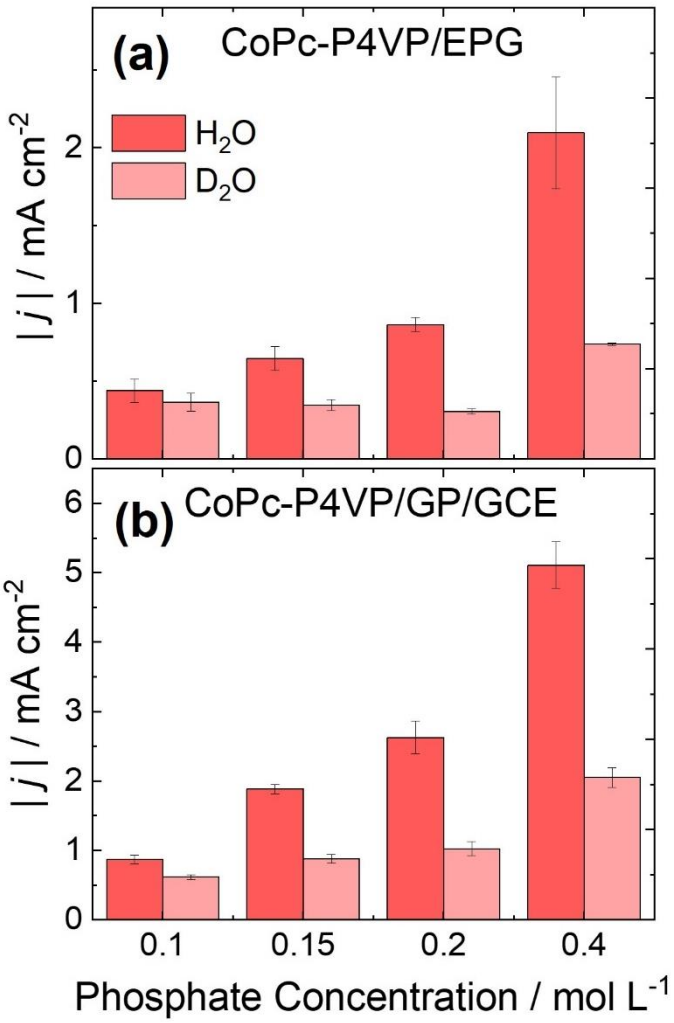

Figure 3.9 Electrolyte-dependent activity of (a) CoPc-P4VP/EPG and (b) CoPc-P4VP/GP/GCE in H_2O/ protonated electrolyte (dark red) and D_2O/deuterated electrolyte (light red) for the production of H_2 (HER) under an N_2 atmosphere. Both systems show an increase in activity with an increase in the electrolyte concentration, and both systems show an increase in the KIE from ~ 1.3 to ~2.7 as the concentration of phosphate increases. Activity measurements were taken under rotation at 1600 rpm via a 6-min CA step at -0.647 V vs. RHE in 0.4 M phosphate 0.5 M perchlorate electrolyte.

Since the change in KIE occurs with increased electrolyte concentration, we hypothesize that intercalation of protons into the polymer layer could be rate limiting due to the lack of anion counterion balance. To study whether the increasing phosphate concentration was leading to a difference in the fractional protonation of the system, we performed IR spectroscopy to determine the protonation as a function of electrolyte concentration (Figure 3.10). In this study, we exposed P4VP to different phosphate concentration buffers at the same pH in order to determine the fractional protonation of the polymer as a function of electrolyte concentration.

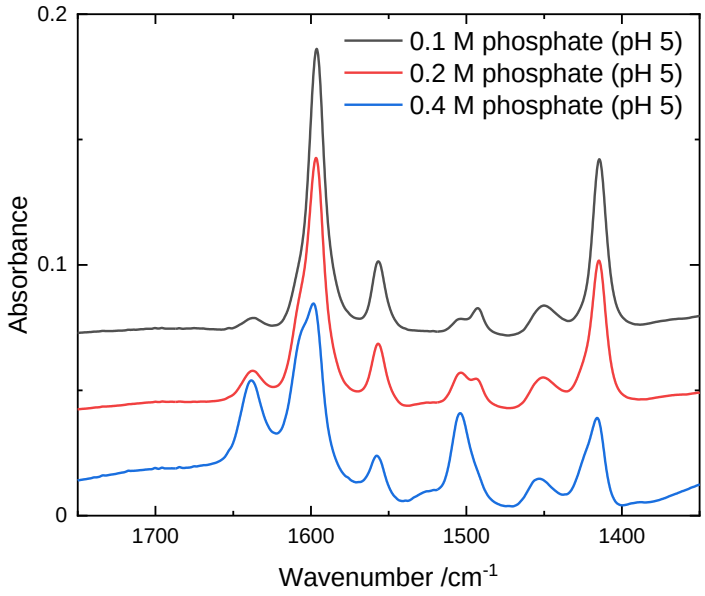

Figure 3.10 Infrared spectroscopy of a P4VP layer after exposure to pH 5 phosphate at different electrolyte concentrations.

At the constant pH of 5, the increasing electrolyte concentration resulted in an increase in protonation as seen in the 1640 cm^{-1} frequency absorbance, which is highest for the 0.4 M phosphate sample (blue), and second highest for the 0.2 M phosphate sample. This could mean that the increase in electrochemical activity with increasing electrolyte concentration could have to do with increased partial protonation of the polymer and suggests that a counterion must be associated in order for a proton to be wicked from the solution into the polymer film. Combined with the KIE data showing that the proton-related RDS occurs at higher concentrations of electrolyte, it could be that the *transport* of protons is rate-limiting at low concentrations of electrolyte or protons – both experimental parameters that contribute to low overall fractional protonation of the polymer.

Interestingly, we see that the KIE does not necessarily align with our expectations – when there are more protons around, there is a KIE, meaning the mechanism is dependent on a proton transfer event. This *could* be true when there is a lower concentration of electrolyte, and it would make sense that a proton transfer event is the chemical RDS for the HER, when the only chemical steps are pronation events. However, it seems that since the transport of the proton is rate-impacting, the rate-limiting step of the proton transfer event is not reflected via electrochemical KIE when there is a small concentration of electrolyte to wick protons from the bulk electrolyte into the polymer layer. These insights are extremely important to consider when evaluating whether electrochemical KIE is a proper tool for understanding catalytic pathways.

3.6 Conclusions

Here, we present results that show the activity, selectivity, and measured rate-limiting step of the CO_2 reduction reaction (CO_2RR) and hydrogen evolution reaction (HER) can be impacted by bulk pH and electrolyte concentration. What began as a study measuring the impacts of electrolyte pH on the activity, selectivity, and proton transport mechanism of the CoPc-electrocatalyzed CO_2RR brought unexpected results, as there was a kinetic isotope effect (KIE) present for the production of hydrogen when the electrolyte concentration was higher than what was used in prior studies of this system. An in-depth study of the dependence of electrolyte concentration on the KIE of HER showed that even a small 50% increase in electrolyte concentration resulted in a KIE of ~ 2, and that a 100% increase in electrolyte concentration showed a KIE of ~ 3.

Interested in these results, we performed *ex-situ* IR spectroscopy to determine the extent to which the polymer film became protonated upon exposure to electrolyte, measuring the qualitative protonation of the pyridyl residues of the polymer as a function of pH and electrolyte concentration. We showed that a decrease in pH resulted in an increase in fractional protonation of the polymer, while an increase in electrolyte concentration also resulted in an increase in fractional protonation of the pyridyl residues. From these results, we present compelling evidence that intercalation of anions into a polymer film is necessary for protonation of the polymer. This result has crucial consequences for the way we think about polymer-coated electrode systems in aqueous electrolyte, especially when the polymer contains a moiety that has a pKa value. While the direct results of these experiments are interesting for this system as CoPc is a popular electrocatalyst for the CO_2RR, in particular showing that fractional protonation increases with decreasing pH or increasing electrolyte concentration, we also lay out a procedure for measuring

the effects of fractional protonation through electrochemical and spectroscopic means. These procedures can be used in other polymer-coated electrode or polymer-encapsulated electrocatalyst systems. We suggest that these methods be used to probe the microenvironment in other systems and propose that further studies could attempt in situ IR spectroscopy to determine how the fractional protonation changes as the electrochemical catalysis takes place. Additionally, an interesting study could look at different buffer systems, such as bicarbonate or acetate. Alternatively, a studying the size dependence of the cation or anion could provide useful insight to whether this phenomenon is universal.

3.7 Supplementary Information

3.7.1 Supplementary Tables

Table 3.1. CoPc preparation methods and loadings for deposition ink used for the all graphite powder systems (CoPc-P4VP/GP and CoPc-P2VP/GP), where columns 1-3 detail the concentrations of cobalt phthalocyanine (CoPc), poly-(4-vinylpyridine) (P4VP), and graphite powder (GP) in the preparation suspension 4-6 detail the measured conditions of the preparation conditions of the CoPc loading, P4VP loading, and GP loading, with errors being the standard deviation of at least 3 individually prepared measurements. Columns 7-9 detail the catalyst, polymer, and GP loading on the 0.196 cm^2 glassy carbon electrodes (GCEs). Additionally, this includes the data for CoPc-P4VP/EPG that was used as a control. There was no centrifugation in this system, so columns 4-6 detail the measured conditions of the preparation conditions of the CoPc loading and P4VP loading as directly prepared for the deposition ink. Columns 7-9 detail the CoPc, polymer, and GP loading on the total surface area of the electrode surface, 0.196 cm^2 (conductive surface area: 0.114 cm^2 due to encapsulating non-conductive polymer epoxy).

	Before Centrifugation			After Centrifugation			Electrode Loading		
	Preparation Suspension			Deposition Ink			Deposition Ink Dropcasted		
	CoPc loading / mM	Polymer loading / mg mL^{-1}	GP loading / mg mL^{-1}	CoPc loading / mM	Polymer loading / mg mL^{-1}	GP loading / mg mL^{-1}	CoPc loading / 10^{-9} mol cm^{-2}	Polymer loading / mg cm^{-2}	GP loading / mg cm^{-2}
CoPc-P4VP/ GP/GCE	0.05	30	10	0.026 ± 0.003	3.01 ± 0.97	10	1.30 ± 0.16	0.117 ± 0.049	0.513
CoPc-P2VP/ GP/GCE	0.05	30	10	0.035 ± 0.003	9.03 ± 2.54	10	1.79 ± 0.17	0.463 ± 0.1306	0.513
CoPc-P4VP/EPG	No centrifugation			0.05	3.0	0	1.27	0.076	0

Table 3.2 CPE Results for data presented in Figure 3.4a of CoPc-P4VP/GP/GCE electrocatalyzed 2 hour experiments run under CO_2 atmosphere at a potential of -0.646 V vs RHE. The experiments were run at the specified pH after the addition of CO_2 and the reported errors are standard deviations of at least 3 measurements.

	Charge / C	FE_{CO} / %	FE_{H2} / %	FE_{Total} / %
pH 3	2.8 ± 0.6	55 ± 2	37 ± 4	93 ± 3
pH 4	2.8 ± 0.5	64 ± 3	28 ± 3	93 ± 3
pH 5	3.9 ± 0.5	75 ± 2	20 ± 1	96 ± 2
pH 6	3.2 ± 0.2	81 ± 2	14 ± 3	96 ± 2
pH 7	3.2 ± 0.6	93 ± 1	11 ± 2	101 ± 5

Table 3.3 CPE Results for data presented in Figure 3.4b of CoPc-P4VP/GP/GCE electrocatalyzed 2 hour experiments run under CO_2 atmosphere at a potential of -0.706 V vs RHE. The experiments were run at the specified pH after the addition of CO_2 and the reported errors are standard deviations of at least 3 measurements.

	Charge / C	FE_{CO} / %	FE_{H2} / %	FE_{Total} / %
pH 3	1.9 ± 0.3	48 ± 1	47 ± 4	92 ± 5
pH 4	3.6 ± 1.1	72 ± 1	26 ± 4	98 ± 2
pH 5	2.6 ± 0.3	76 ± 3	20 ± 3	97 ± 1
pH 6	2.9 ± 0.5	85 ± 5	13 ± 1	98 ± 4
pH 7	3.0 ± 0.1	95 ± 4	7 ± 1	103 ± 6

Table 3.4 Activity results as seen in Figure 3.5 of rotating disk chronoamperometry (RDE-CA) step experiment at --0.647 V vs RHE, conducted under 1 atm CO_2 in 0.4 M NaH_2PO_4 and 0.5 M $NaClO_4$ at the specified pH under 1600 rpm rotation rate for CoPc-P4VP/GP/GCE with 10 mg/mL graphite powder in the catalyst ink solution, corresponding to a loading of 0.51 mg cm^{-2}. The $|j_{CO}|$ value is the activity multiplied by the product distribution as measured by controlled potential electrolysis (see Table 3.2) and the standard error is the combination of the standard deviations of the two measurements.

pH	**$\|j\|$ @ -0.647 V vs RHE / mA cm^{-2}**	**Standard Deviation ± $\|j\|$ @ -0.647 V vs RHE / mA cm^{-2}**	**$\|j_{CO}\|$ @ -0.647 V vs RHE / mA cm^{-2}**	**Standard Error ± $\|j_{CO}\|$ @ -0.647 V vs RHE / mA cm^{-2}**
3	3.4	0.1	1.9	0.1
4	3.8	0.1	2.4	0.1
5	4.1	0.1	3.1	0.1
6	4.1	0.1	3.3	0.1
7	3.5	0.1	3.3	0.1

Table 3.5 CPE Results: CO_2 CoPc-P4VP/GP/GCE and CoPc-P2VP/GP/GCE pH 5 CPE Data -0.647 V vs RHE. electrocatalyzed by CoPc-P4VP/GP/GCE and CoPc-P2VP/GP/GCE and measured as a function of pH. The standard deviations are also presented (the average of at least 3 measurements). Electrolyte concentration is specified within the table and was run under CO_2 atmosphere

System	**Phosphate / M**	**Perchlorate / M**	**Charge / C**	**FE_{CO} / %**	**FE_{H2} / %**	**FE_{Total} / %**
CoPc-P4VP/GP/GCE pH 4.7	0.1	0.5	4.0 ± 0.5	81 ± 3	16 ± 2	98 ± 1
CoPc-P4VP/GP/GCE pH 5	0.4	0.5	3.9 ± 0.5	75 ± 2	20 ± 1	96 ± 2
CoPc-P4VP/GP/GCE pH 4.7	0.1	0	2.8 ± 0.8	83 ± 1	14 ± 4	97 ± 3
CoPc-P2VP/GP/GCE pH 5	0.4	0.5	2.8 ± 0.5	58 ± 1	36 ± 3	94 ± 3
CoPc-P2VP/GP/GCE pH 5	0.1	0	2.6 ± 0.2	74 ± 5	21 ± 3	95 ± 3

Table 3.6 Activity data for the RDE-CAs measurements as shown in Figure 3.6a. These studies show the total activity under CO_2 atmosphere (where both CO_2RR and HER were possible) as electrocatalyzed by CoPc-P4VP/GP/GCE and CoPc-P2VP/GP/GCE and measured as a function of pH. The standard deviations are also presented (the average of at least 3 measurements). Electrolyte concentration was 0.4 M phosphate/0.5M perchlorate and was run under CO_2 atmosphere.

pH	$\|j\|$ @ -0.647 V vs RHE / mA cm^{-2}	Standard Deviation $\pm \|j\|$ @ -0.647 V vs RHE / mA cm^{-2}	$\|j_{P2VP}\|$ @ -0.647 V vs RHE / mA cm^{-2}	Standard Deviation $\pm \|j_{P2VP}\|$ @ -0.647 V vs RHE / mA cm^{-2}
3	3.4	0.1	3.0	0.1
4	3.8	0.1	3.0	0.7
5	4.1	0.1	3.4	0.4
6	4.1	0.1	2.9	0.4
7	3.5	0.1	2.5	0.4

Table 3.7 Activity data for the RDE-CAs measurements as shown in Figure 3.7. These studies show the total activity under CO_2 atmosphere (where both CO_2RR and HER were possible) as electrocatalyzed by CoPc-P4VP/GP/GCE and measured as a function of pH in both protonated and deuterated electrolyte. The standard deviations are also presented (the average of at least 3 measurements). Electrolyte concentration was 0.4 M phosphate/0.5M perchlorate and was run under CO_2 atmosphere.

pH	$\|j\|$ @ -0.647 V vs RHE / mA cm^{-2}	Standard Deviation $\pm \|j\|$ @ -0.647 V vs RHE / mA cm^{-2}	$\|j_{D2O}\|$ @ -0.647 V vs RHE / mA cm^{-2}	Standard Deviation $\pm \|j_{D2O}\|$ @ -0.647 V vs RHE / mA cm^{-2}	KIE
3	3.4	0.1	1.8	0.2	1.9 ± 0.2
4	3.8	0.1	2.5	0.1	1.5 ± 0.1
5	4.1	0.1	2.8	0.1	1.5 ± 0.1
6	4.1	0.1	3.1	0.2	1.3 ± 0.1
7	3.5	0.1	3.1	0.2	1.1 ± 0.1

Table 3.8 Activity data for the RDE-CAs measurements as shown in Figure 3.8a. These studies show the HER activity as electrocatalyzed by CoPc-P4VP/EPG and measured as a function of pH. Electrolyte concentration was 0.4 M phosphate/0.5M perchlorate and was run under N_2 atmosphere.

pH	$\|j\|$ @ -0.647 V vs RHE / mA cm^{-2}	Standard Deviation $\pm \|j\|$ @ -0.647 V vs RHE / mA cm^{-2}	$\|j_{D2O}\|$ @ -0.647 V vs RHE / mA cm^{-2}	Standard Deviation $\pm \|j_{D2O}\|$ @ -0.647 V vs RHE / mA cm^{-2}	KIE
3	4.92	0.44	1.47	0.09	3.3 ± 0.4
4	1.74	0.28	0.73	0.12	2.4 ± 0.5
5	0.75	0.07	0.26	0.03	2.9 ± 0.4
6	0.27	0.04	0.08	0.02	3.2 ± 1.0
7	0.23	0.01	0.09	0.01	2.3 ± 0.1

Table 3.9 Activity data for the RDE-CAs measurements as shown in Figure 3.8b. These studies show the HER activity as electrocatalyzed by CoPc-P4VP/GP/GCE and measured as a function of pH. Electrolyte concentration was 0.4 M phosphate/0.5M perchlorate and was run under N_2 atmosphere.

pH	$\|j\|$ @ -0.647 V vs RHE / mA cm^{-2}	Standard Deviation $\pm \|j\|$ @ -0.647 V vs RHE / mA cm^{-2}	$\|j_{D2O}\|$ @ -0.647 V vs RHE / mA cm^{-2}	Standard Deviation $\pm \|j_{D2O}\|$ @ -0.647 V vs RHE / mA cm^{-2}	KIE
3	5.3	1.4	1.4	0.1	3.8 ± 1.0
4	5.0	0.2	2.0	0.1	2.5 ± 0.2
5	4.4	0.3	1.4	0.1	3.1 ± 0.3
6	2.8	0.1	1.1	0.1	2.6 ± 0.3
7	1.3	0.2	0.7	0.1	1.8 ± 0.3

Table 3.10 Activity data for the RDE-CAs measurements as shown in in Figure 3.9b. These studies show the HER activity as electrocatalyzed by CoPc-P4VP/GP/GCE and measured as a function of electrolyte concentration. All experiments run at pH 5 with specified electrolyte concentration under N_2 atmosphere.

[Phosphate] / M	[Perchlorate] / M	$\lvert j \rvert$ @ -0.647 V vs RHE / mA cm^{-2}	Standard Deviation ± $\lvert j \rvert$ @ -0.647 V vs RHE / mA cm^{-2}	$\lvert j_{D2O} \rvert$ @ -0.647 V vs RHE / mA cm^{-2}	Standard Deviation ± $\lvert j_{D2O} \rvert$ @ -0.647 V vs RHE / mA cm^{-2}	KIE
0.1	0	0.87	0.06	0.62	0.03	1.4 ± 0.1
0.15	0	1.88	0.07	0.88	0.06	2.1 ± 0.2
0.2	0	2.63	0.24	1.02	0.10	2.6 ± 0.3
0.4	0	5.11	0.33	2.05	0.14	2.5 ± 0.2

Table 3.11 Activity data for the RDE-CAs measurements as shown in in Figure 3.9a. These studies show the HER activity as electrocatalyzed by CoPc-P4VP/EPG and measured as a function of electrolyte concentration. All experiments run at pH 5 with specified electrolyte concentration under N_2 atmosphere.

[Phosphate] / M	[Perchlorate] / M	$\lvert j \rvert$ @ -0.647 V vs RHE / mA cm^{-2}	Standard Deviation ± $\lvert j \rvert$ @ -0.647 V vs RHE / mA cm^{-2}	$\lvert j_{D2O} \rvert$ @ -0.647 V vs RHE / mA cm^{-2}	Standard Deviation ± $\lvert j_{D2O} \rvert$ @ -0.647 V vs RHE / mA cm^{-2}	KIE
0.1	0	0.44	0.07	0.36	0.06	1.2 ± 0.3
0.15	0	0.64	0.08	0.35	0.04	1.9 ± 0.3
0.2	0	0.86	0.05	0.30	0.02	2.8 ± 0.2
0.4	0	2.10	0.36	0.74	0.01	2.8 ± 0.4

3.7.2 Supplementary Figures

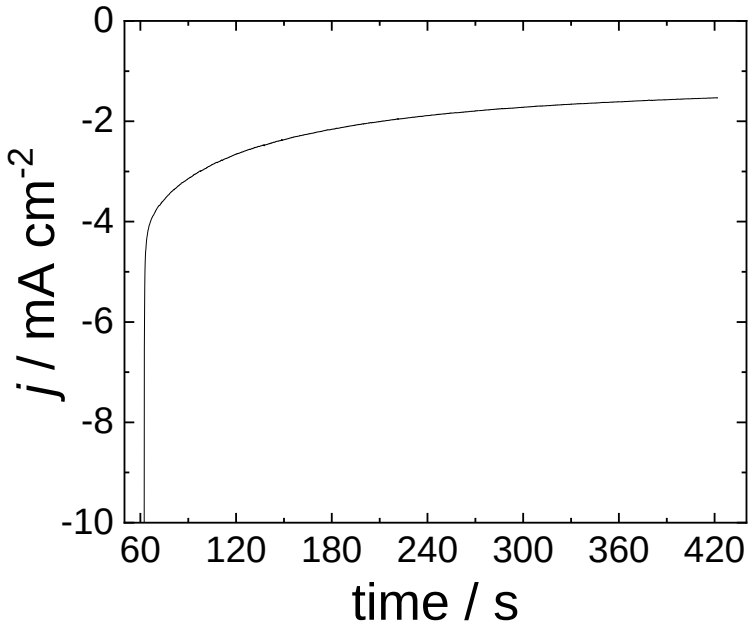

Figure 3.11 pD 3 CO_2 representative RDE-CA (1600 rpm held for 6 minutes at -1.183 V vs. SCE) CoPc-P4VP/GP/GCE in pD 3 deuterated electrolyte (0.4 M NaD_2PO_4/0.5 $NaClO_4$).

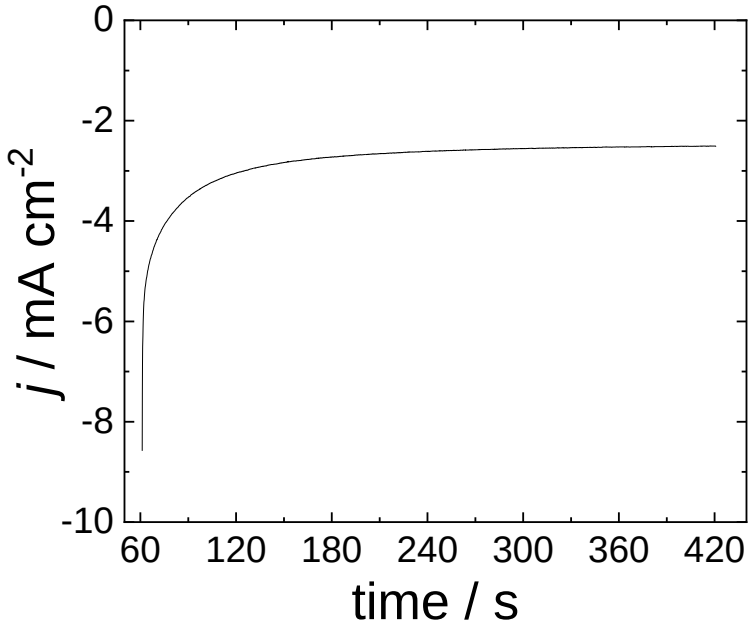

Figure 3.12 pD 4 CO_2 representative RDE-CA (1600 rpm held for 6 minutes at -1.183 V vs. SCE) CoPc-P4VP/GP/GCE in pD 4 deuterated electrolyte (0.4 M NaD_2PO_4/0.5 $NaClO_4$).

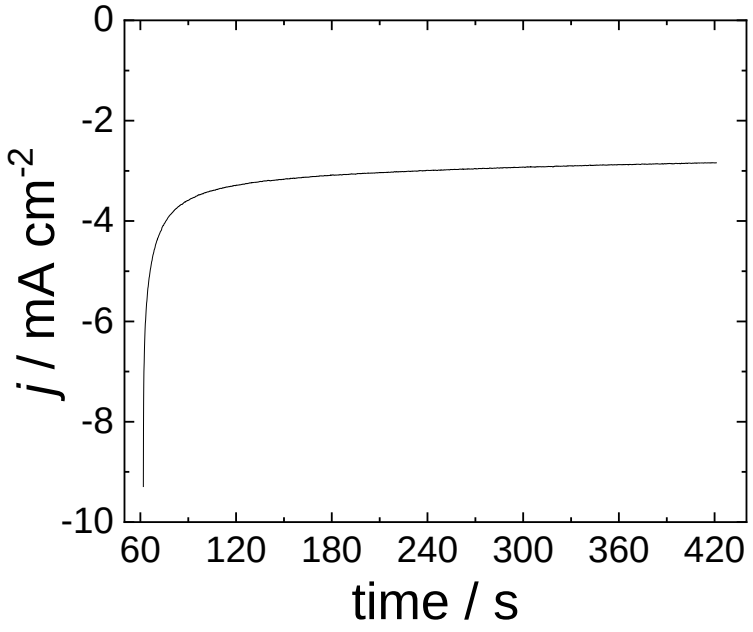

Figure 3.13 pD 5 CO_2 representative RDE-CA (1600 rpm held for 6 minutes at -1.183 V vs. SCE) CoPc-P4VP/GP/GCE in pD 5 deuterated electrolyte (0.4 M NaD_2PO_4/0.5 $NaClO_4$).

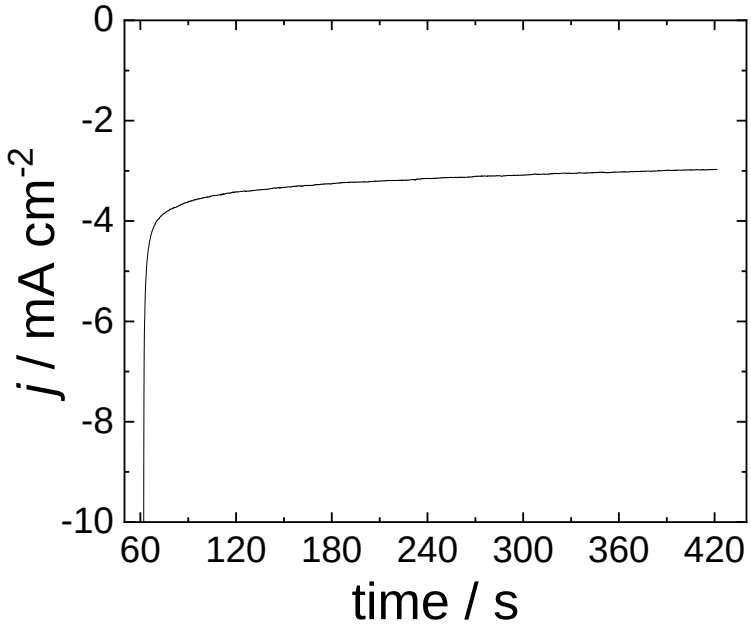

Figure 3.14 pD 6 CO_2 representative RDE-CA (1600 rpm held for 6 minutes at -1.183 V vs. SCE) CoPc-P4VP/GP/GCE in pD 6 deuterated electrolyte (0.4 M NaD_2PO_4/0.5 $NaClO_4$).

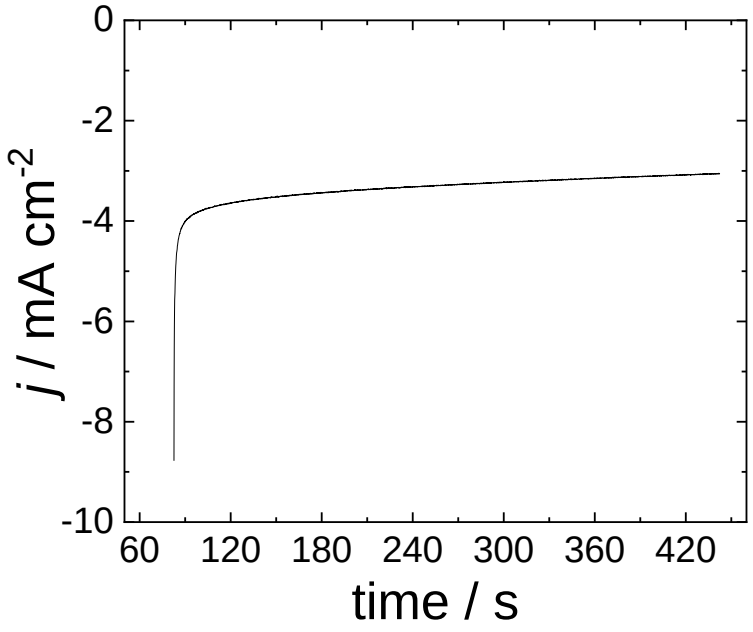

Figure 3.15 pD 7 CO_2 representative RDE-CA (1600 rpm held for 6 minutes at -1.183 V vs. SCE) CoPc-P4VP/GP/GCE in pD 7 deuterated electrolyte (0.4 M NaD_2PO_4/0.5 $NaClO_4$).

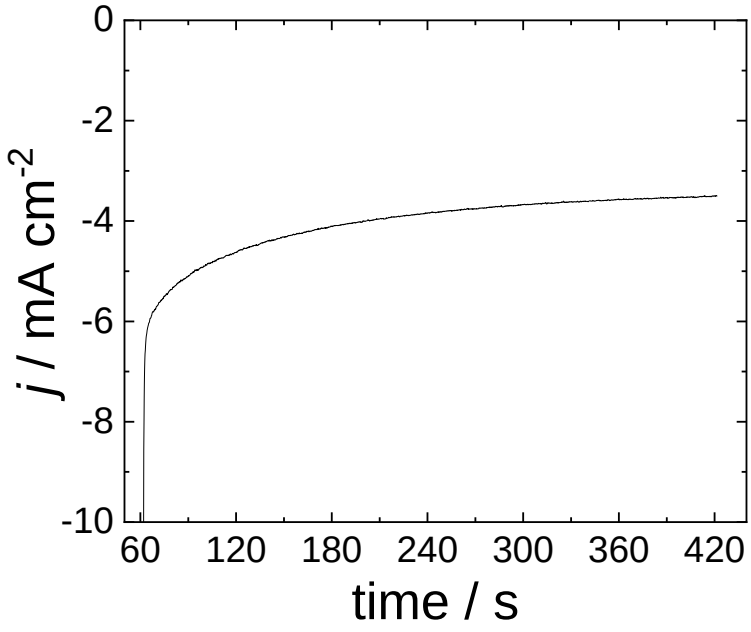

Figure 3.16 pH 3 CO_2 representative RDE-CA (1600 rpm held for 6 minutes at -1.183 V vs. SCE) CoPc-P4VP/GP/GCE in pH 3 protonated electrolyte (0.4 M NaH_2PO_4/0.5 $NaClO_4$).

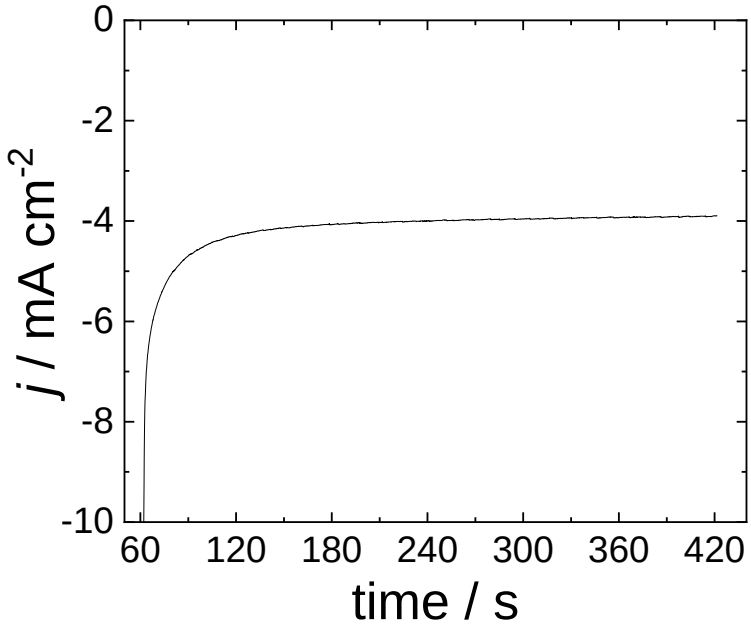

Figure 3.17. pH 4 CO_2 representative RDE-CA (1600 rpm held for 6 minutes at -1.183 V vs. SCE) CoPc-P4VP/GP/GCE in pH 4 protonated electrolyte (0.4 M NaH_2PO_4/0.5 $NaClO_4$).

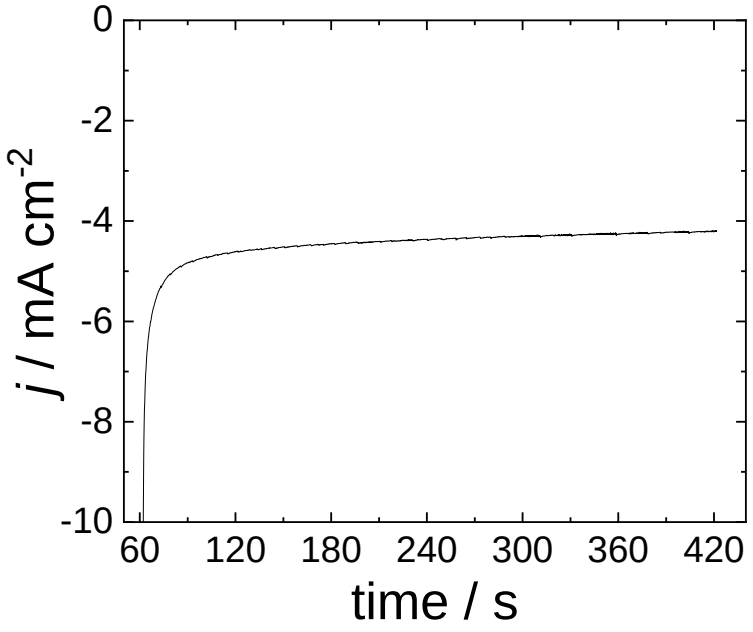

Figure 3.18 pH 5 CO_2 representative RDE-CA (1600 rpm held for 6 minutes at -1.183 V vs. SCE) CoPc-P4VP/GP/GCE in pH 5 protonated electrolyte (0.4 M NaH_2PO_4/0.5 $NaClO_4$).

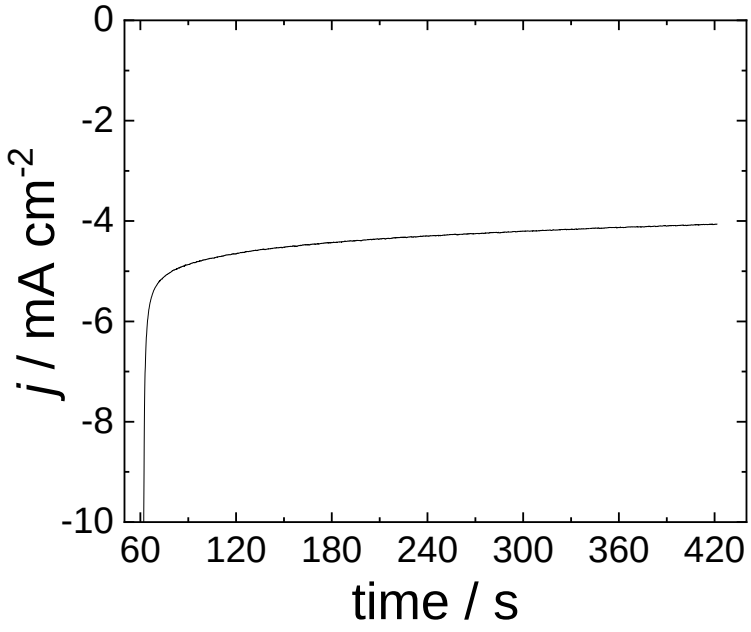

Figure 3.19 pH 6 CO_2 representative RDE-CA (1600 rpm held for 6 minutes at -1.183 V vs. SCE) CoPc-P4VP/GP/GCE in pH 6 protonated electrolyte (0.4 M NaH_2PO_4/0.5 $NaClO_4$).

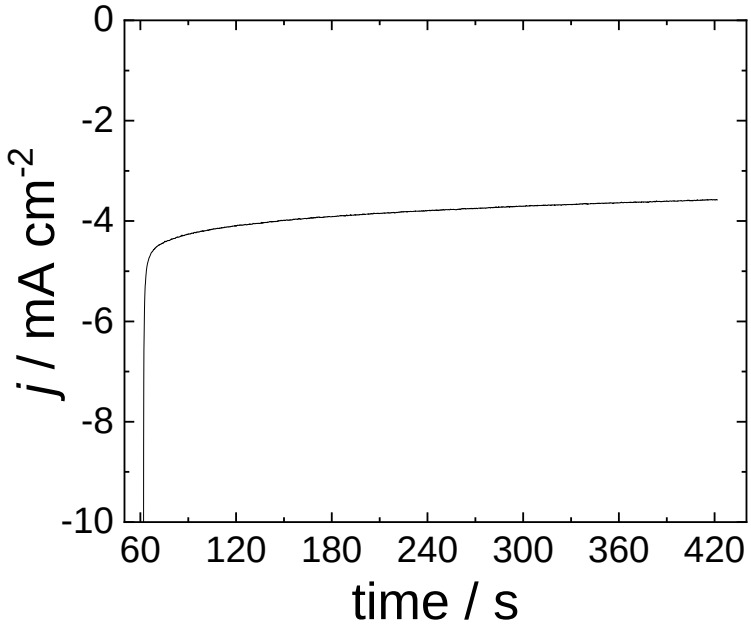

Figure 3.20 pH 7 CO_2 representative RDE-CA (1600 rpm held for 6 minutes at -1.183 V vs. SCE) CoPc-P4VP/GP/GCE in pH 7 protonated electrolyte (0.4 M NaH_2PO_4/0.5 $NaClO_4$).

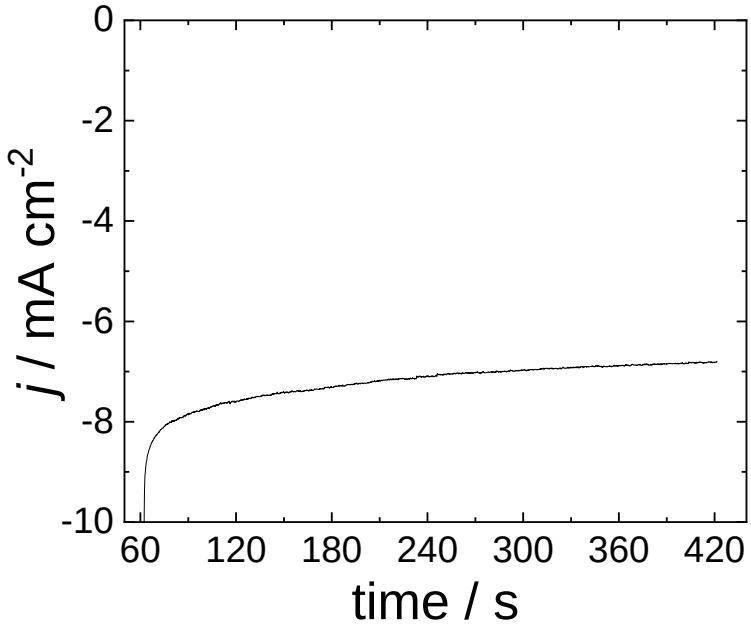

Figure 3.21 pH 3 N_2 representative RDE-CA (1600 rpm held for 6 minutes at -1.183 V vs. SCE) CoPc-P4VP/GP/GCE in pH 3 protonated electrolyte (0.4 M NaH_2PO_4/0.5 $NaClO_4$).

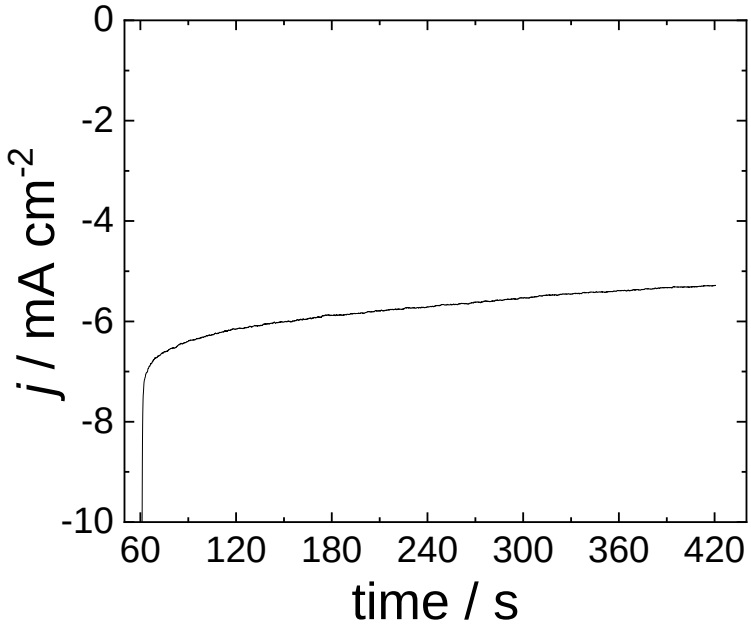

Figure 3.22 pH 4 N_2 representative RDE-CA (1600 rpm held for 6 minutes at -1.124 V vs. SCE) CoPc-P4VP/GP/GCE in pH 4 protonated electrolyte (0.4 M NaH_2PO_4/0.5 $NaClO_4$).

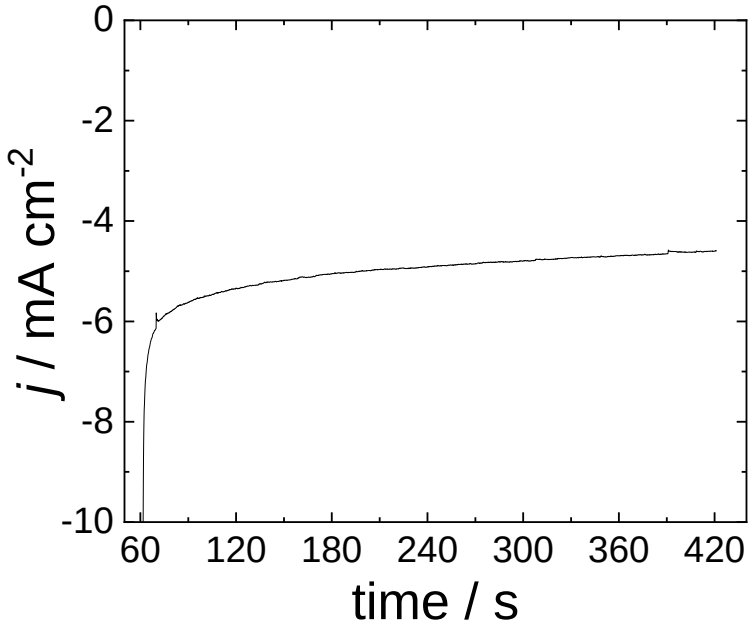

Figure 3.23 pH 5 N_2 representative RDE-CA (1600 rpm held for 6 minutes at -1.183 V vs. SCE) CoPc-P4VP/GP/GCE in pH 5 protonated electrolyte (0.4 M NaH_2PO_4/0.5 $NaClO_4$).

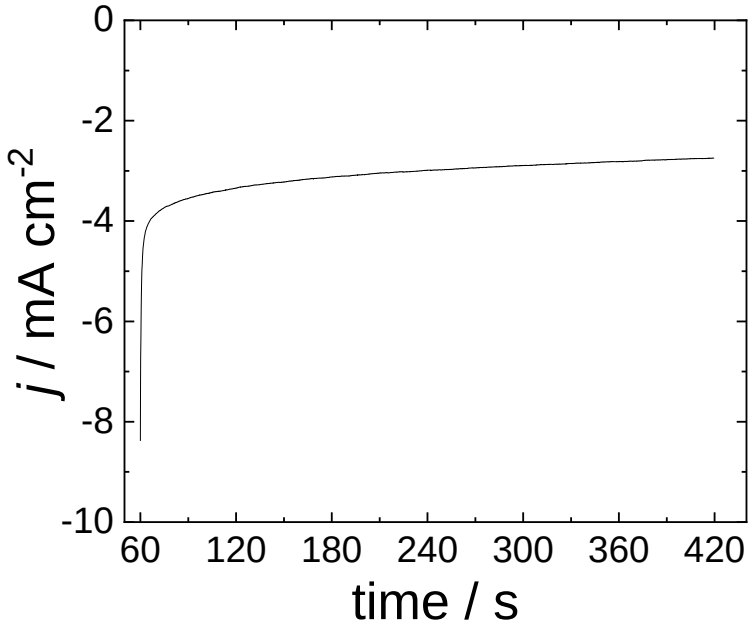

Figure 3.24 pH 6 N_2 representative RDE-CA (1600 rpm held for 6 minutes at -1.183 V vs. SCE) CoPc-P4VP/GP/GCE in pH 6 protonated electrolyte (0.4 M NaH_2PO_4/0.5 $NaClO_4$).

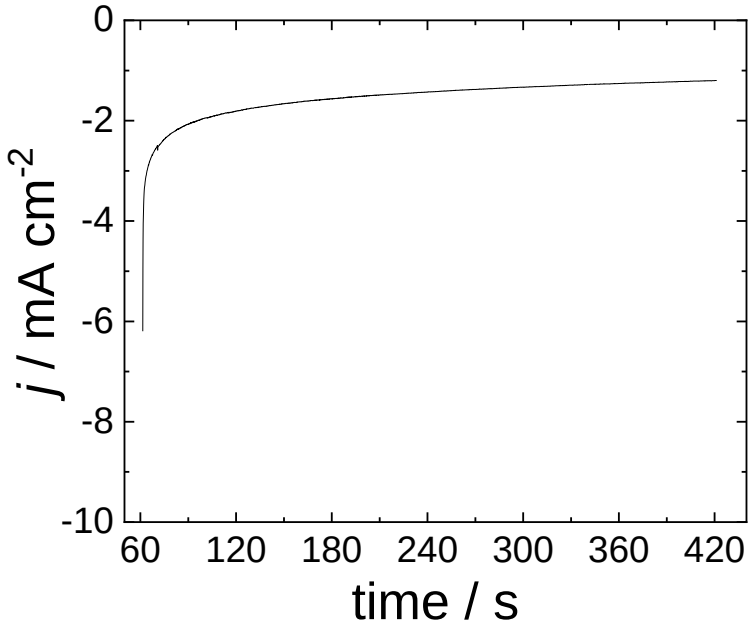

Figure 3.25 pH 7 N_2 representative RDE-CA (1600 rpm held for 6 minutes at -1.183 V vs. SCE) CoPc-P4VP/GP/GCE in pH 7 protonated electrolyte (0.4 M NaH_2PO_4/0.5 $NaClO_4$).

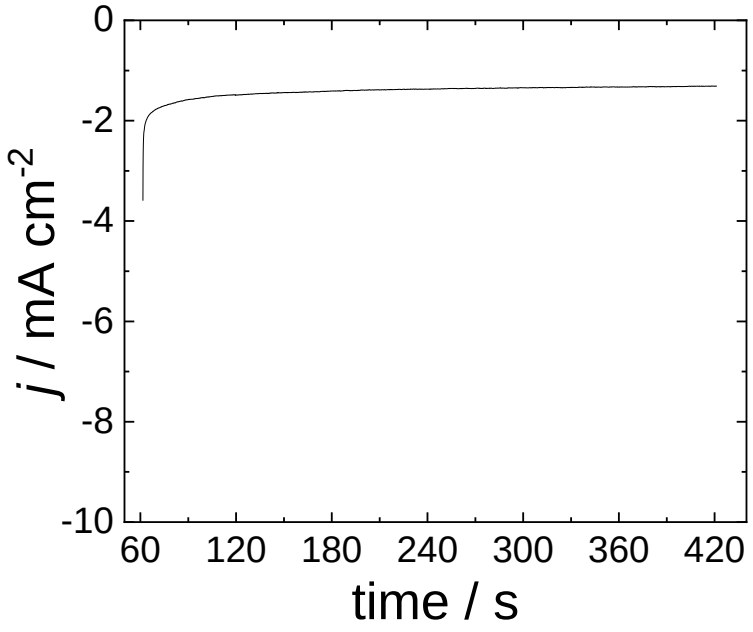

Figure 3.26 pD 3 N_2 representative RDE-CA (1600 rpm held for 6 minutes at -1.183 V vs. SCE) CoPc-P4VP/GP/GCE in pD 3 deuterated electrolyte (0.4 M NaD_2PO_4/0.5 $NaClO_4$).

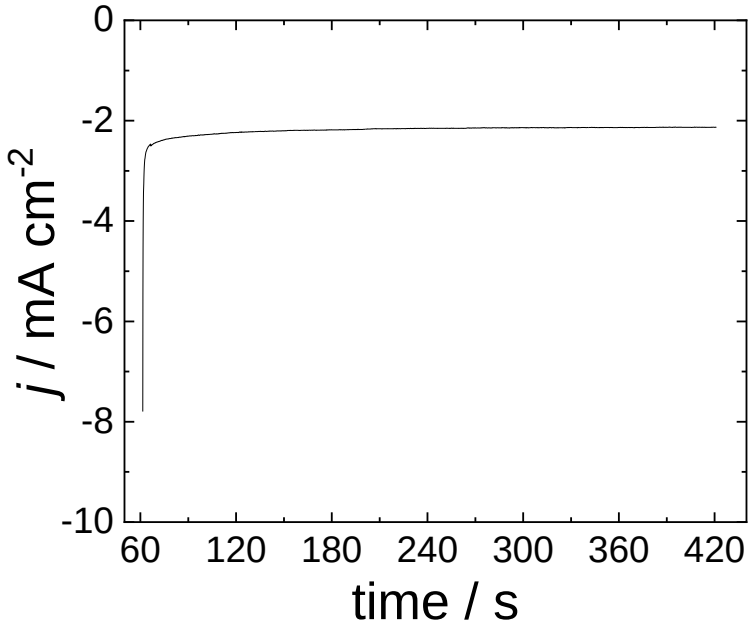

Figure 3.27 pD 4 N_2 representative RDE-CA (1600 rpm held for 6 minutes at -1.183 V vs. SCE) CoPc-P4VP/GP/GCE in pD 4 deuterated electrolyte (0.4 M NaD_2PO_4/0.5 $NaClO_4$).

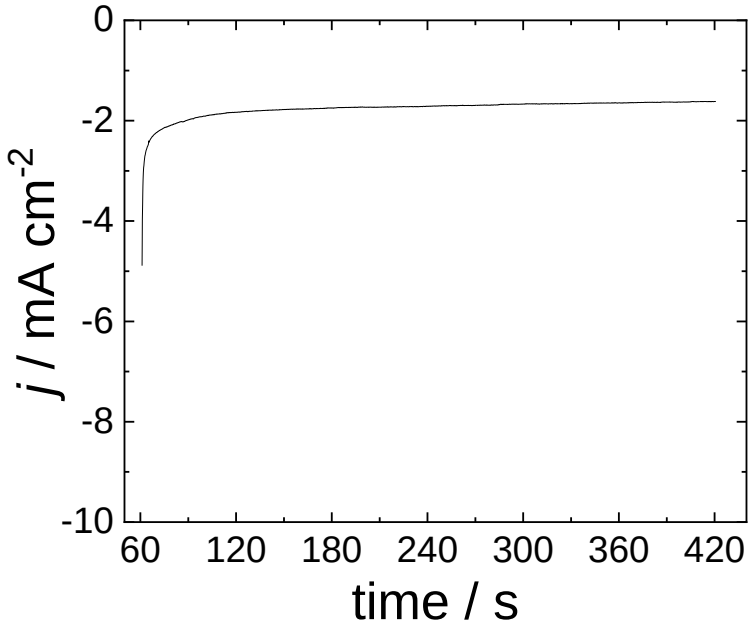

Figure 3.28 pD 5 N_2 representative RDE-CA (1600 rpm held for 6 minutes at -1.183 V vs. SCE) CoPc-P4VP/GP/GCE in pD 5 deuterated electrolyte (0.4 M NaD_2PO_4/0.5 $NaClO_4$).

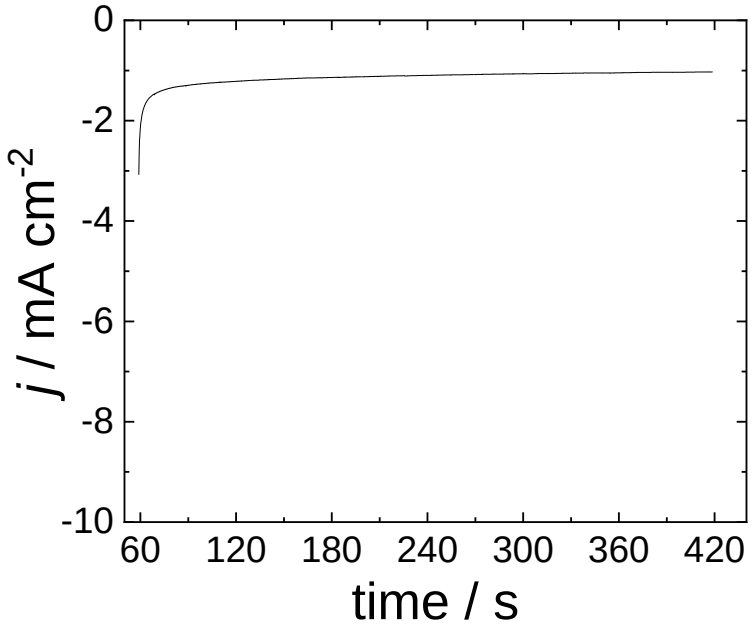

Figure 3.29 pD 6 N_2 representative RDE-CA (1600 rpm held for 6 minutes at -1.183 V vs. SCE) CoPc-P4VP/GP/GCE in pD 6 deuterated electrolyte (0.4 M NaD_2PO_4/0.5 $NaClO_4$).

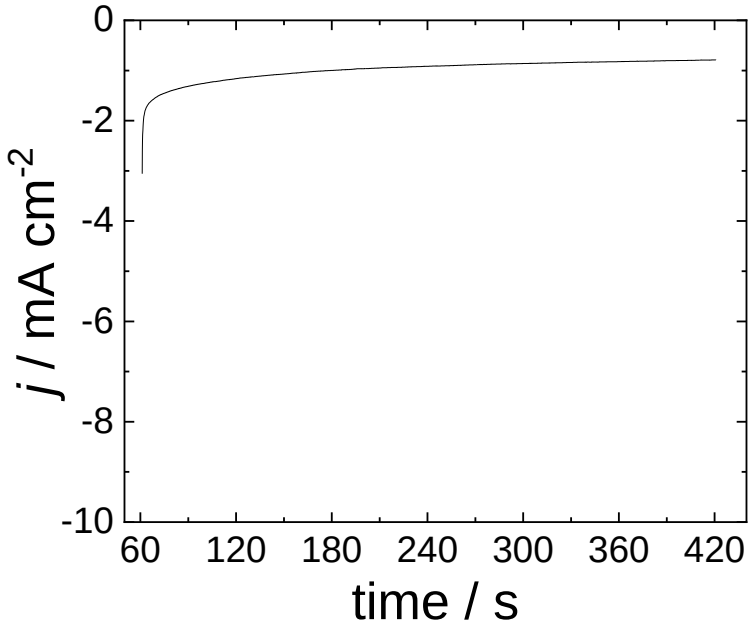

Figure 3.30 pD 7 N_2 representative RDE-CA (1600 rpm held for 6 minutes at -1.183 V vs. SCE) CoPc-P4VP/GP/GCE in pD 7 deuterated electrolyte (0.4 M NaD_2PO_4/0.5 $NaClO_4$).

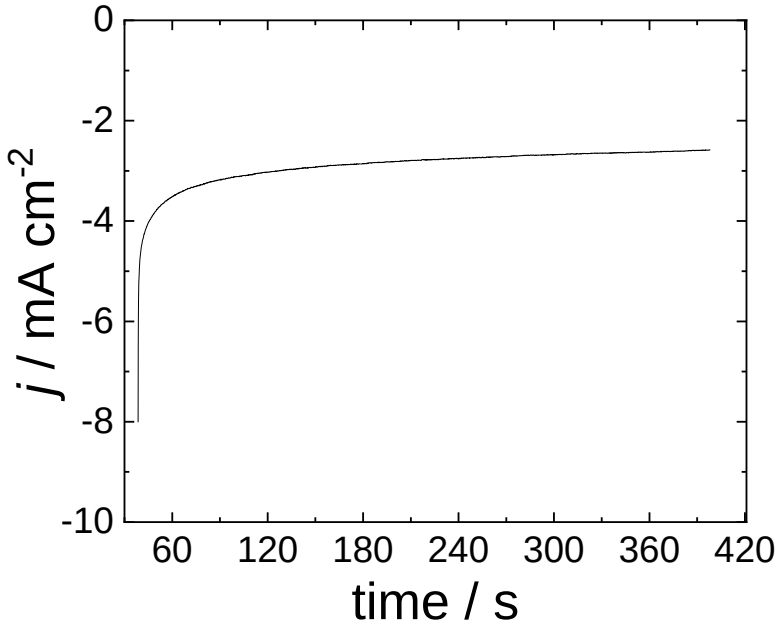

Figure 3.31 pH 3 N_2 representative RDE-CA (1600 rpm held for 6 minutes at -1.183 V vs. SCE) CoPc-P4VP/EPG in pH 3 protonated electrolyte (0.4 M NaH_2PO_4/0.5 $NaClO_4$).

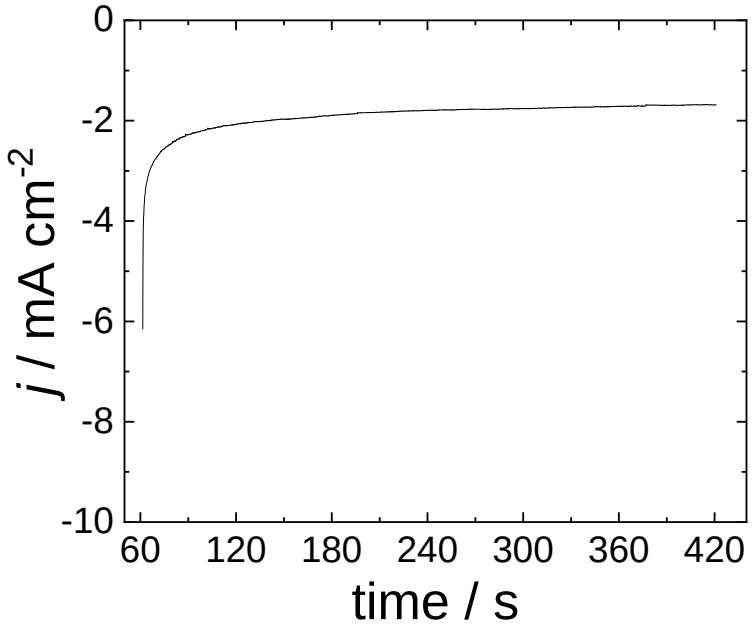

Figure 3.32 pH 4 N_2 representative RDE-CA (1600 rpm held for 6 minutes at -1.183 V vs. SCE) CoPc-P4VP/EPG in pH 4 protonated electrolyte (0.4 M NaH_2PO_4/0.5 $NaClO_4$).

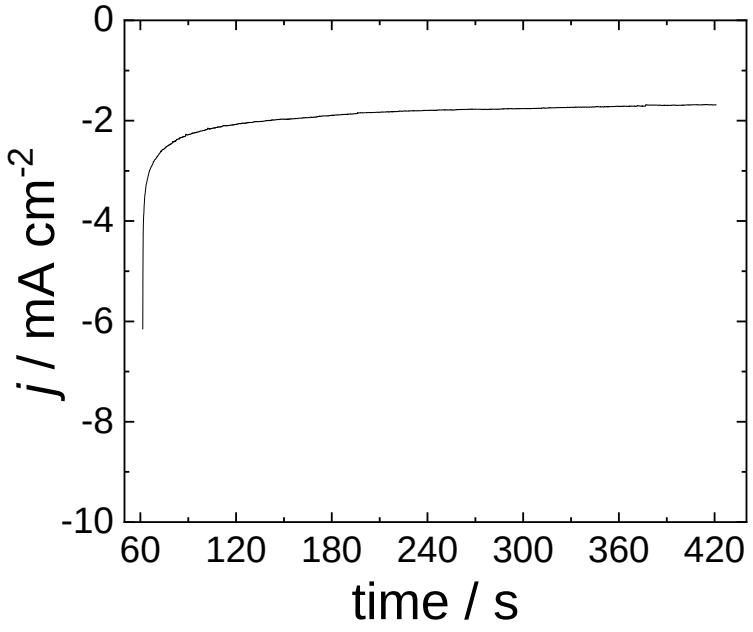

Figure 3.33 pH 5 N_2 representative RDE-CA (1600 rpm held for 6 minutes at -1.183 V vs. SCE) CoPc-P4VP/EPG in pH 5 protonated electrolyte (0.4 M NaH_2PO_4/0.5 $NaClO_4$).

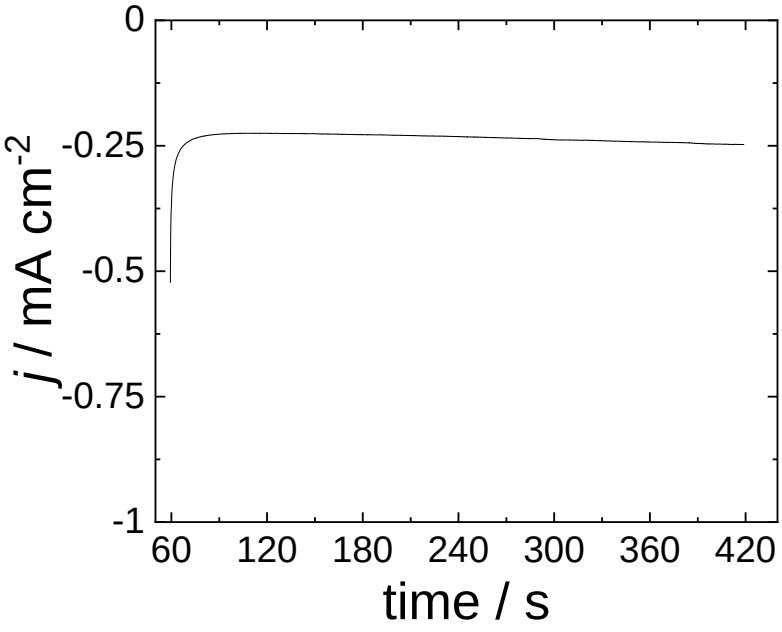

Figure 3.34 pH 6 N_2 representative RDE-CA (1600 rpm held for 6 minutes at -1.183 V vs. SCE) CoPc-P4VP/EPG in pH 6 protonated electrolyte (0.4 M NaH_2PO_4/0.5 $NaClO_4$).

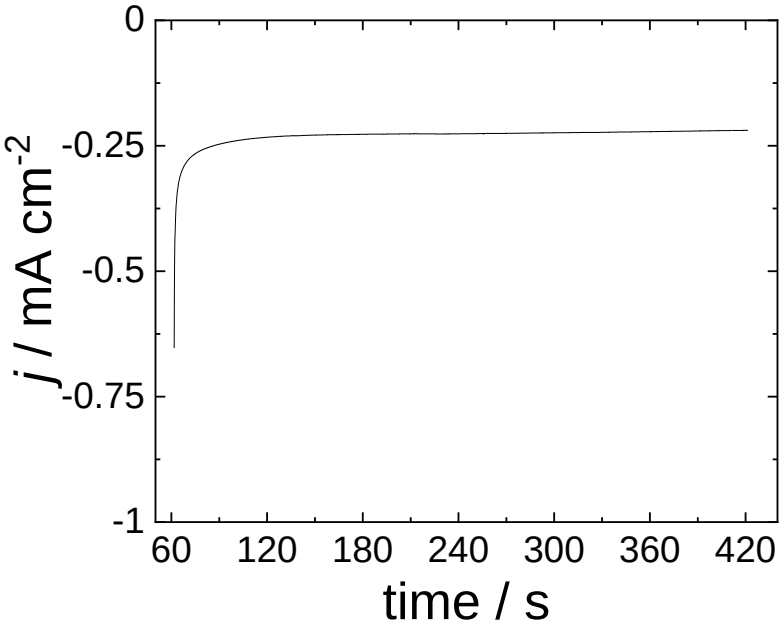

Figure 3.35 pH 7 N_2 representative RDE-CA (1600 rpm held for 6 minutes at -1.183 V vs. SCE) CoPc-P4VP/EPG in pH 7 protonated electrolyte (0.4 M NaH_2PO_4/0.5 $NaClO_4$).

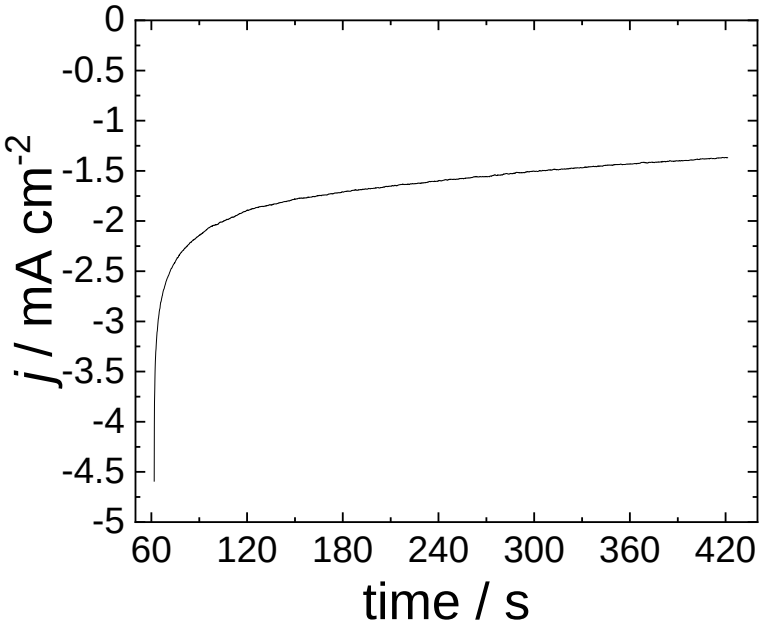

Figure 3.36 pD 3 N_2 representative RDE-CA (1600 rpm held for 6 minutes at -1.183 V vs. SCE) CoPc-P4VP/EPG in pD 3 deuterated electrolyte (0.4 M NaD_2PO_4/0.5 $NaClO_4$).

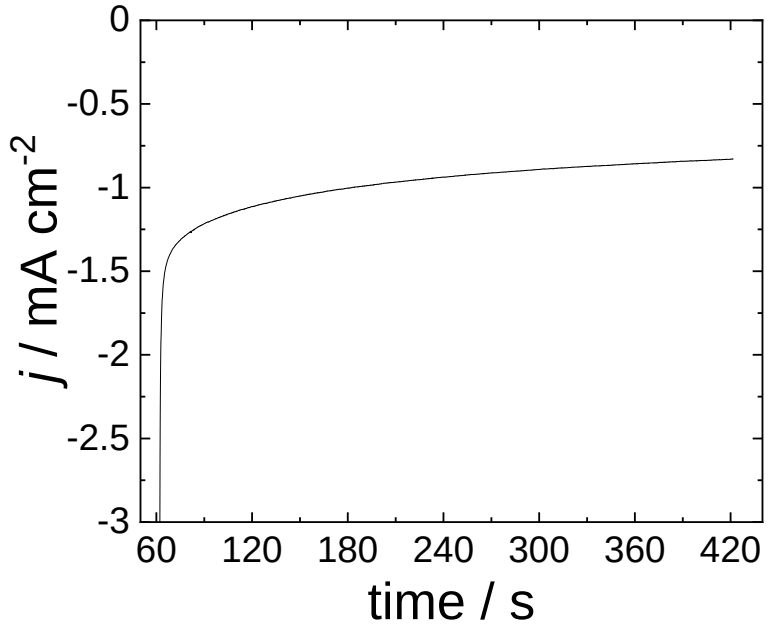

Figure 3.37 pD 4 N_2 representative RDE-CA (1600 rpm held for 6 minutes at -1.183 V vs. SCE) CoPc-P4VP/EPG in pD 4 deuterated electrolyte (0.4 M NaD_2PO_4/0.5 $NaClO_4$).

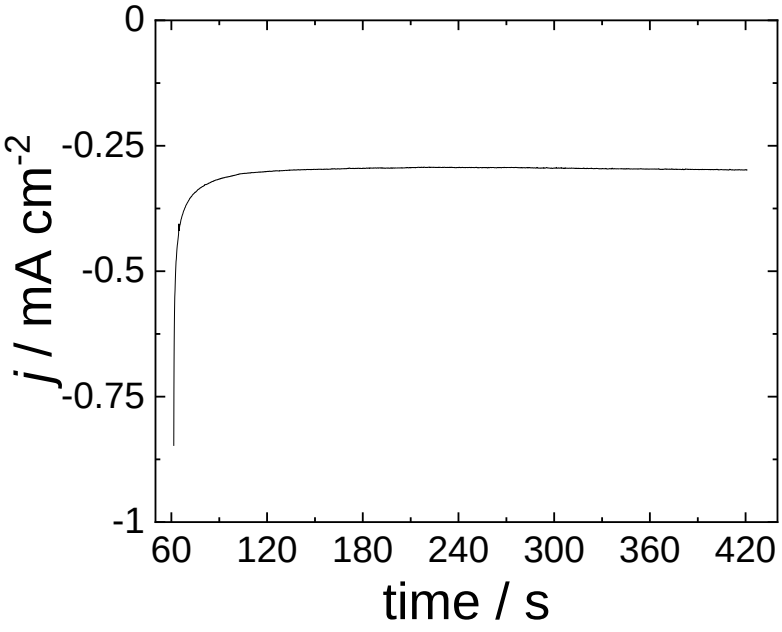

Figure 3.38 pD 5 N_2 representative RDE-CA (1600 rpm held for 6 minutes at -1.183 V vs. SCE) CoPc-P4VP/EPG in pD 5 deuterated electrolyte (0.4 M NaD_2PO_4/0.5 $NaClO_4$).

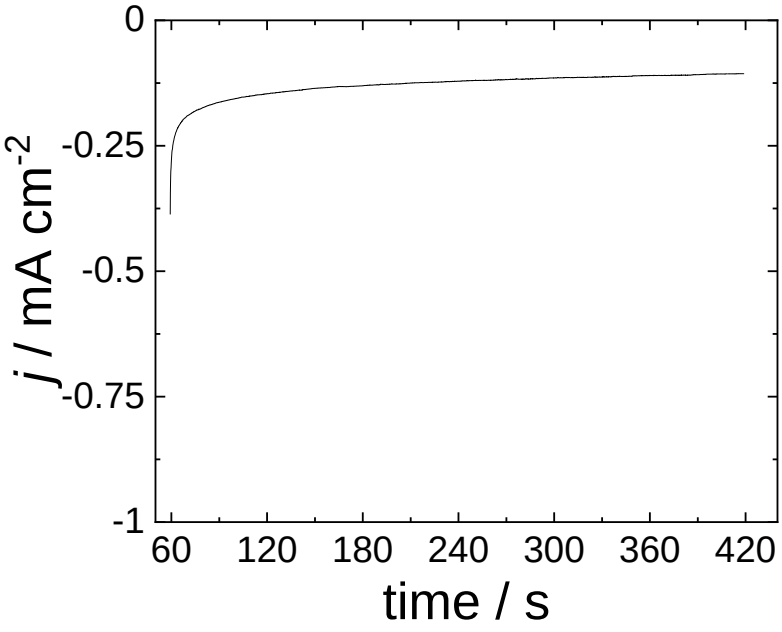

Figure 3.39 pD 6 N_2 representative RDE-CA (1600 rpm held for 6 minutes at -1.183 V vs. SCE) CoPc-P4VP/EPG in pD 6 deuterated electrolyte (0.4 M NaD_2PO_4/0.5 $NaClO_4$).

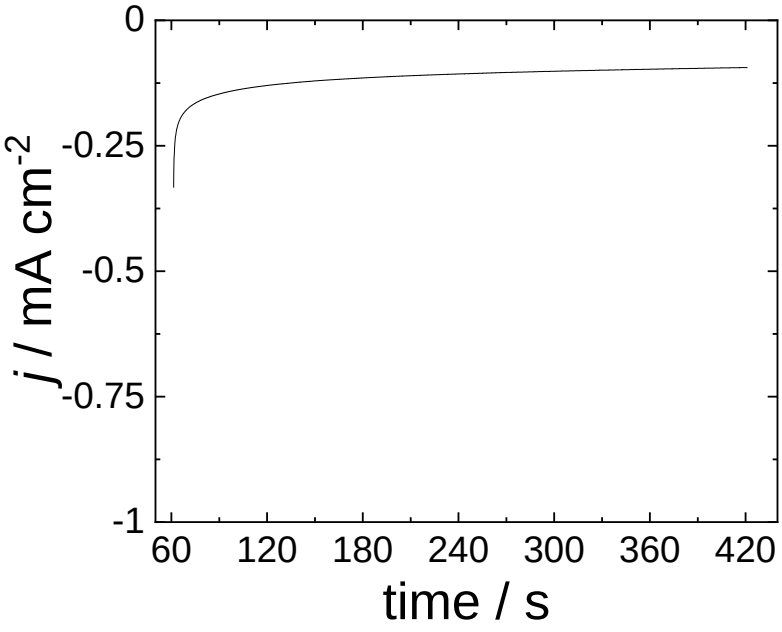

Figure 3.40. pD 7 N_2 representative RDE-CA (1600 rpm held for 6 minutes at -1.183 V vs. SCE) CoPc-P4VP/GP/GCE in pD 7 deuterated electrolyte (0.4 M NaD_2PO_4/0.5 $NaClO_4$).

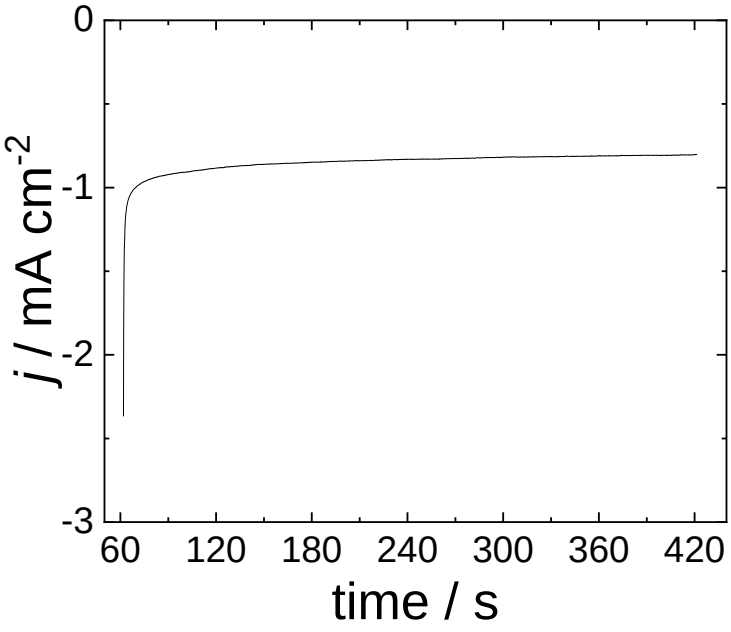

Figure 3.41 pH 5 N_2 representative RDE-CA (1600 rpm held for 6 minutes at -1.183 V vs. SCE) CoPc-P4VP/GP/GCE in pH 5 protonated electrolyte (0.1 M NaH_2PO_4).

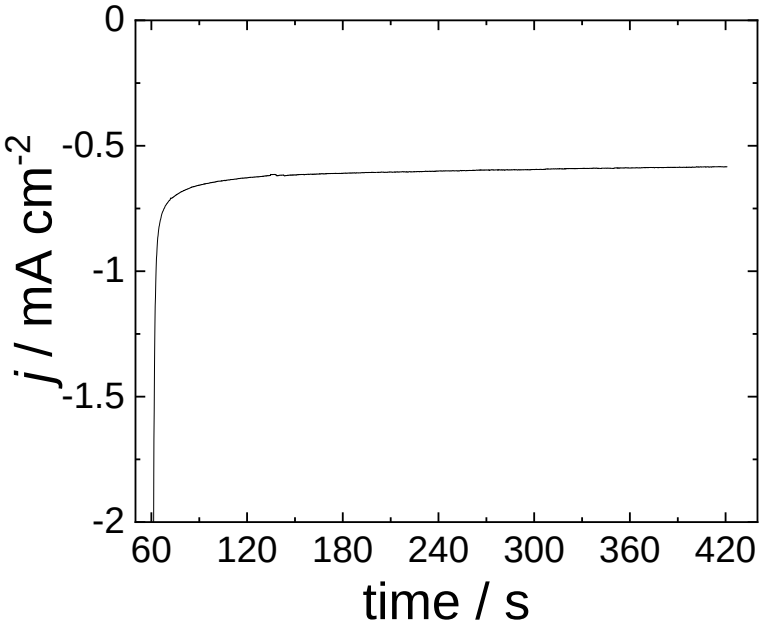

Figure 3.42 pD 5 N_2 representative RDE-CA (1600 rpm held for 6 minutes at -1.183 V vs. SCE) CoPc-P4VP/GP/GCE in pD 5 deuterated electrolyte (0.1 M NaD_2PO_4).

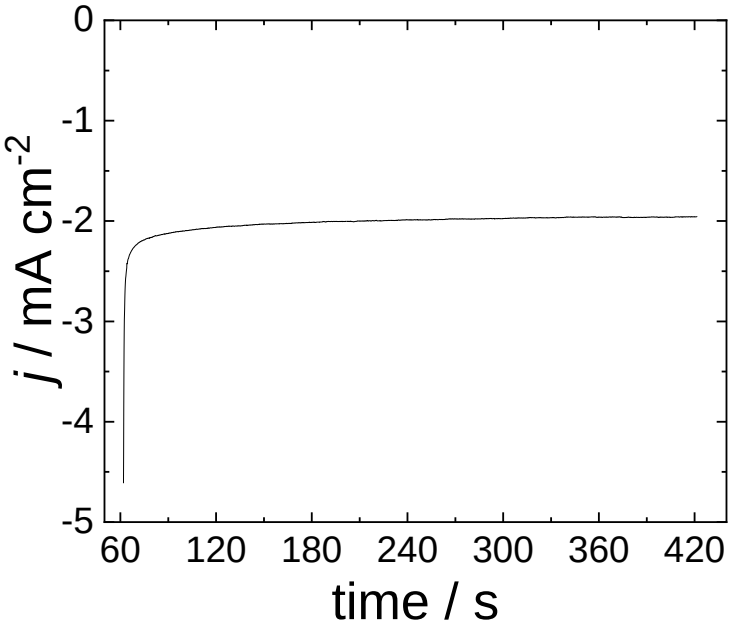

Figure 3.43 pH 5 N_2 representative RDE-CA (1600 rpm held for 6 minutes at -1.183 V vs. SCE) CoPc-P4VP/GP/GCE in pH 5 protonated electrolyte (0.15 M NaH_2PO_4).

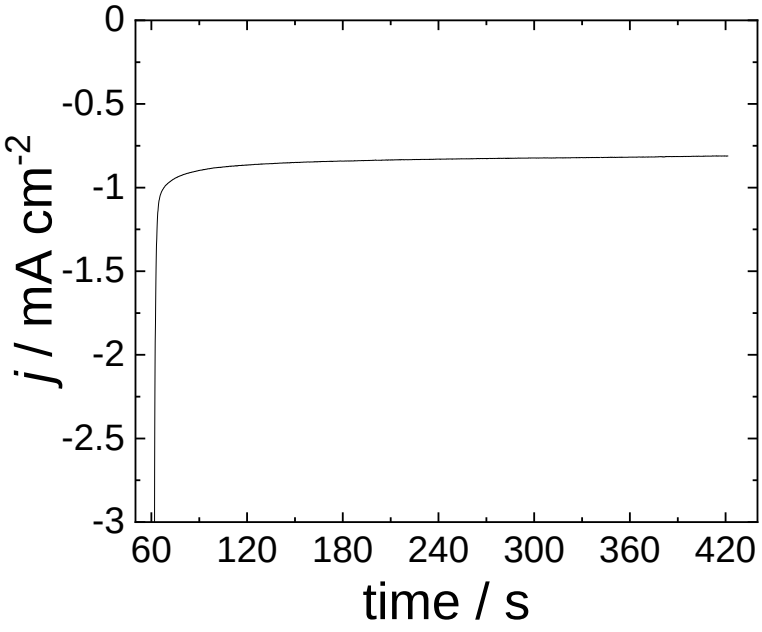

Figure 3.44 pD 5 N_2 representative RDE-CA (1600 rpm held for 6 minutes at -1.183 V vs. SCE) CoPc-P4VP/GP/GCE in pD 5 deuterated electrolyte (0.15 M NaD_2PO_4).

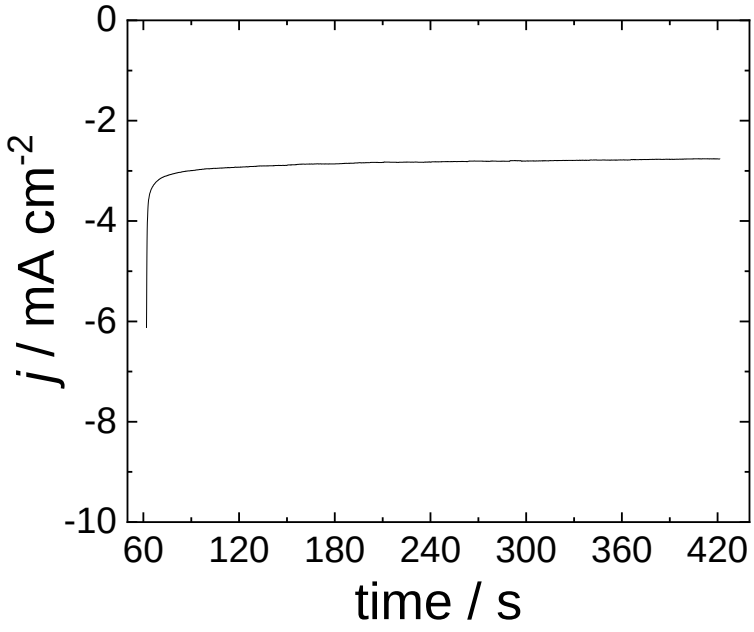

Figure 3.45 pH 5 N_2 representative RDE-CA (1600 rpm held for 6 minutes at -1.183 V vs. SCE) CoPc-P4VP/GP/GCE in pH 5 protonated electrolyte (0.2 M NaH_2PO_4).

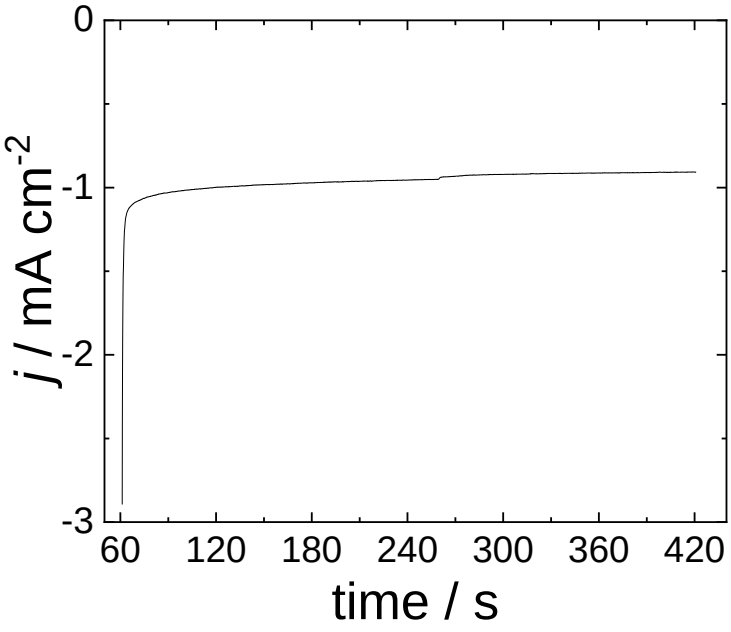

Figure 3.46 pD 5 N_2 representative RDE-CA (1600 rpm held for 6 minutes at -1.183 V vs. SCE) CoPc-P4VP/GP/GCE in pD 5 deuterated electrolyte (0.2 M NaD_2PO_4).

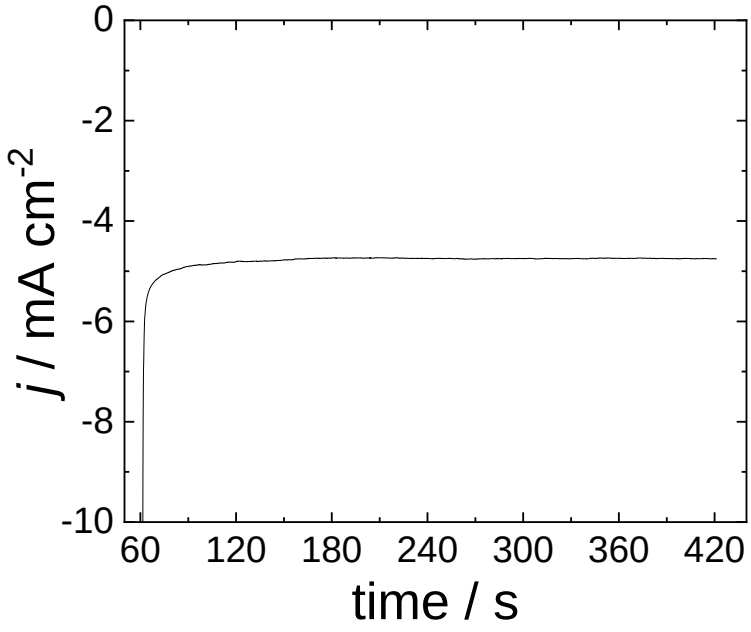

Figure 3.47 pH 5 N_2 representative RDE-CA (1600 rpm held for 6 minutes at -1.183 V vs. SCE) CoPc-P4VP/GP/GCE in pH 5 protonated electrolyte (0.4 M NaH_2PO_4).

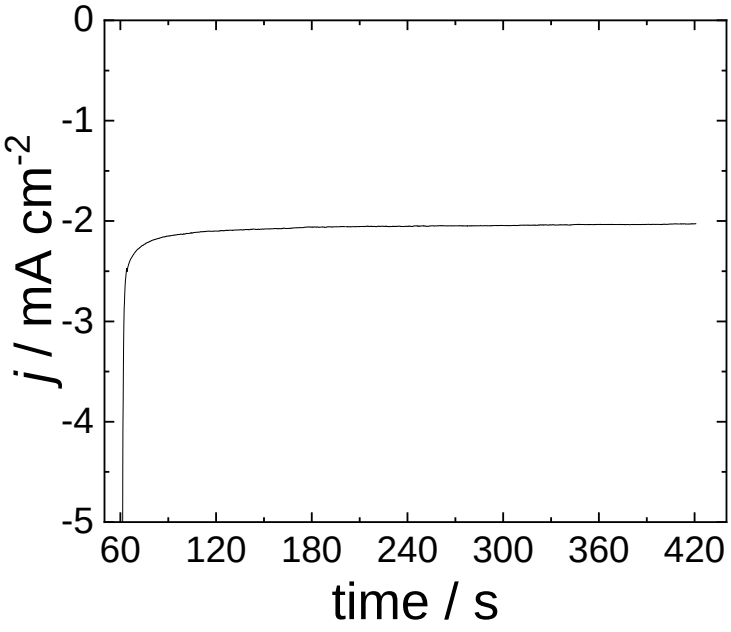

Figure 3.48 pD 5 N_2 representative RDE-CA (1600 rpm held for 6 minutes at -1.183 V vs. SCE) CoPc-P4VP/GP/GCE in pD 5 deuterated electrolyte (0.4 M NaD_2PO_4).

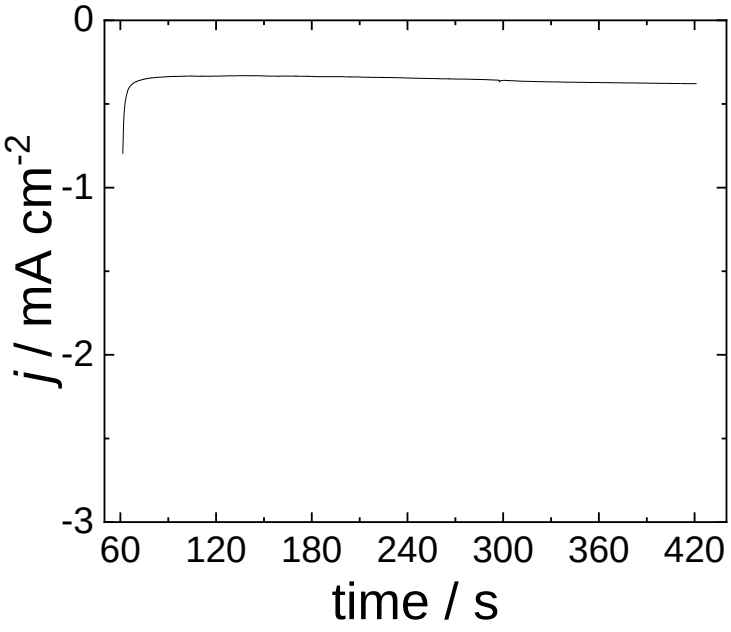

Figure 3.49 pH 5 N_2 representative RDE-CA (1600 rpm held for 6 minutes at -1.183 V vs. SCE) CoPc-P4VP/EPG in pH 5 protonated electrolyte (0.1 M NaH_2PO_4).

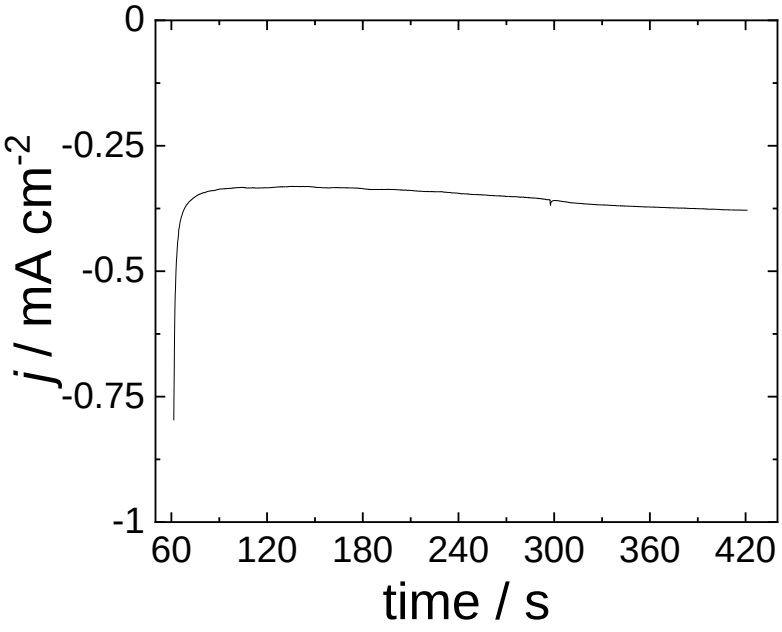

Figure 3.50 pD 5 N_2 representative RDE-CA (1600 rpm held for 6 minutes at -1.183 V vs. SCE) CoPc-P4VP/EPG in pD 5 deuterated electrolyte (0.1 M NaD_2PO_4).

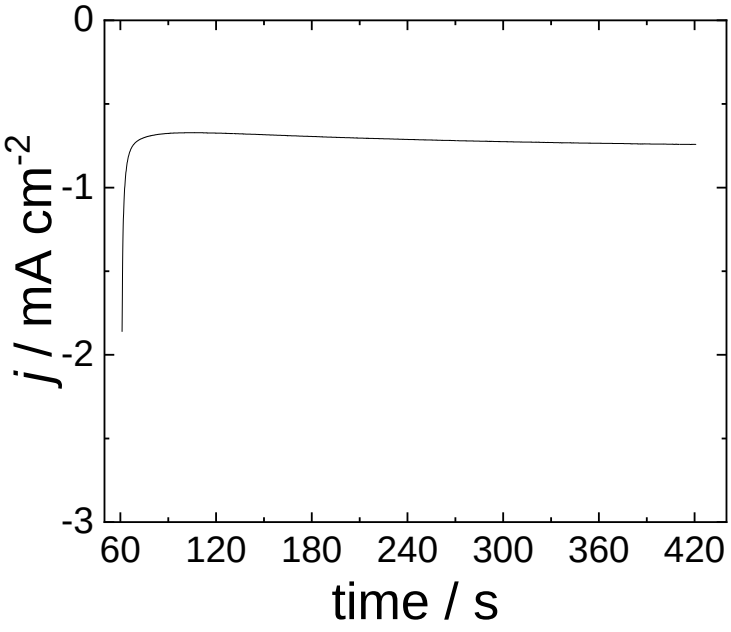

Figure 3.51 pH 5 N_2 representative RDE-CA (1600 rpm held for 6 minutes at -1.183 V vs. SCE) CoPc-P4VP/EPG in pH 5 protonated electrolyte (0.15 M NaH_2PO_4).

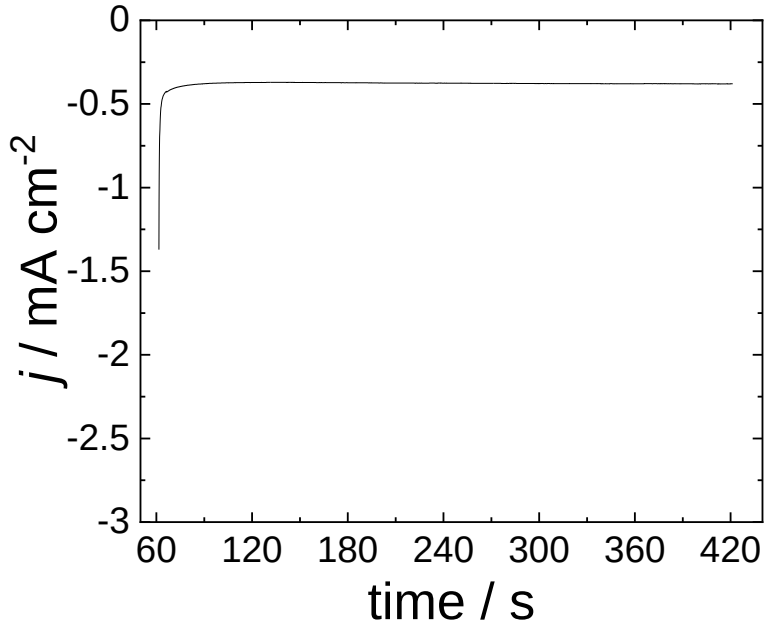

Figure 3.52 pD 5 N_2 representative RDE-CA (1600 rpm held for 6 minutes at -1.183 V vs. SCE) CoPc-P4VP/EPG in pD 5 deuterated electrolyte (0.15 M NaD_2PO_4).

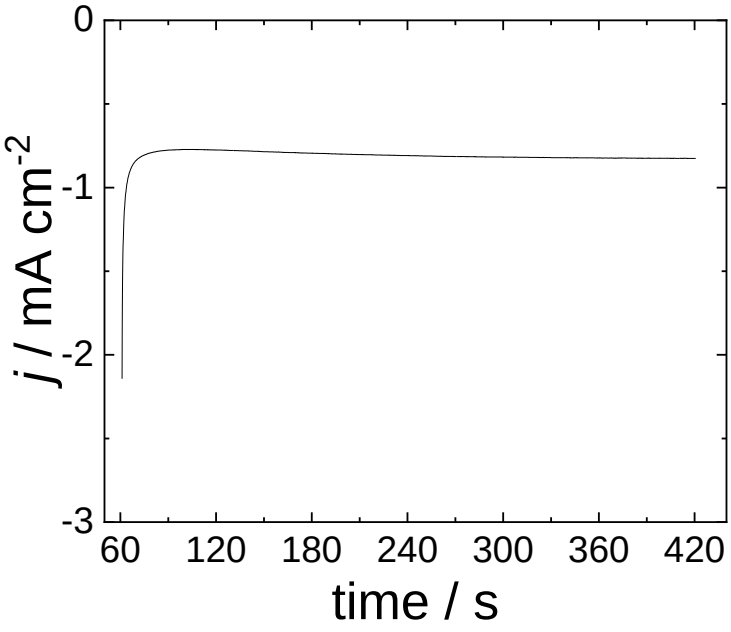

Figure 3.53 pH 5 N_2 representative RDE-CA (1600 rpm held for 6 minutes at -1.183 V vs. SCE) CoPc-P4VP/EPG in pH 5 protonated electrolyte (0.2 M NaH_2PO_4).

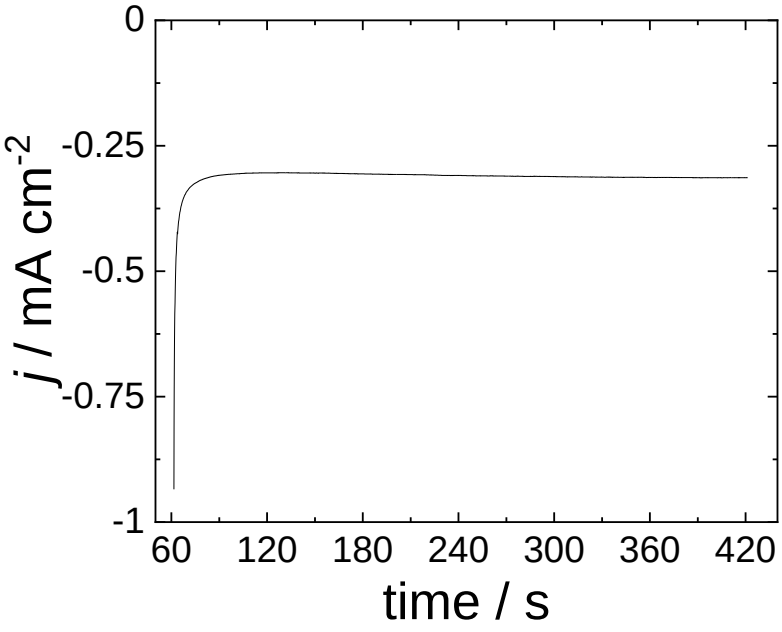

Figure 3.54 pD 5 N_2 representative RDE-CA (1600 rpm held for 6 minutes at -1.183 V vs. SCE) CoPc-P4VP/ EPG in pD 5 deuterated electrolyte (0.2 M NaD_2PO_4).

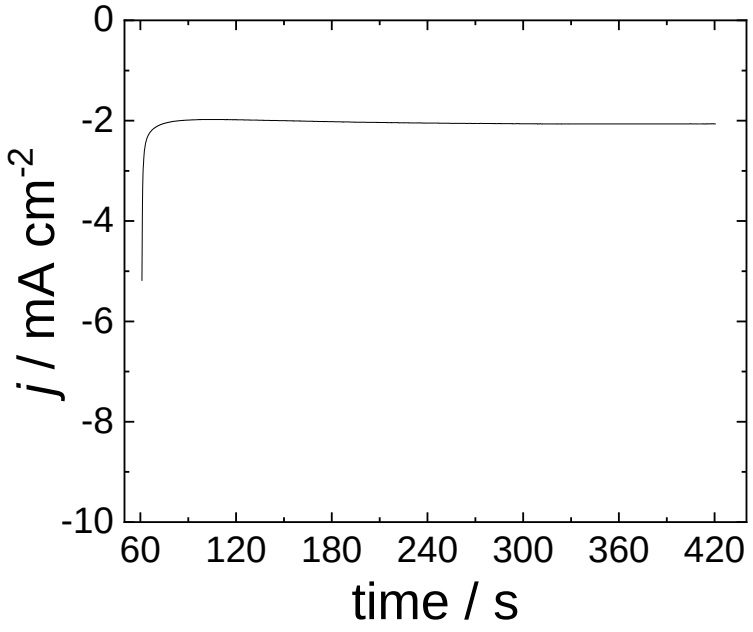

Figure 3.55 pH 5 N_2 representative RDE-CA (1600 rpm held for 6 minutes at -1.183 V vs. SCE) CoPc-P4VP/ EPG in pH 5 protonated electrolyte (0.4 M NaH_2PO_4).

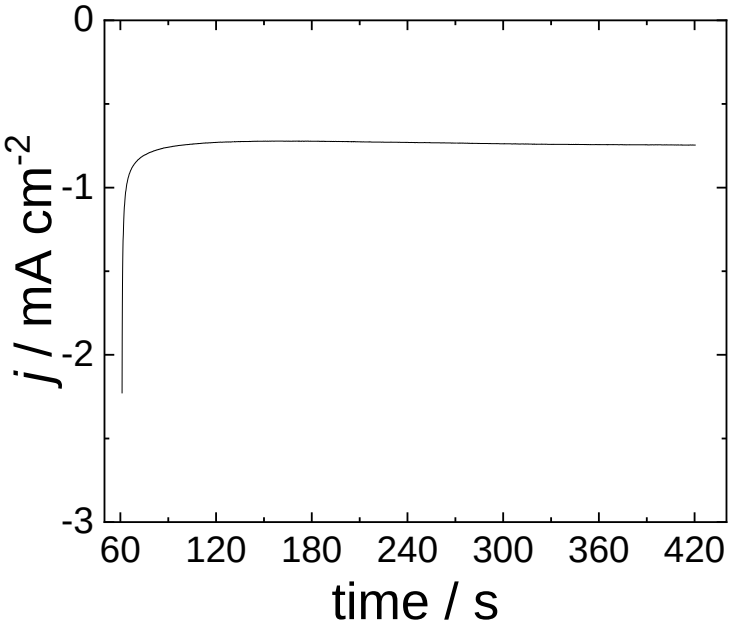

Figure 3.56 pD 5 N_2 representative RDE-CA (1600 rpm held for 6 minutes at -1.183 V vs. SCE) CoPc-P4VP/EPG in pD 5 deuterated electrolyte (0.4 M NaD_2PO_4).

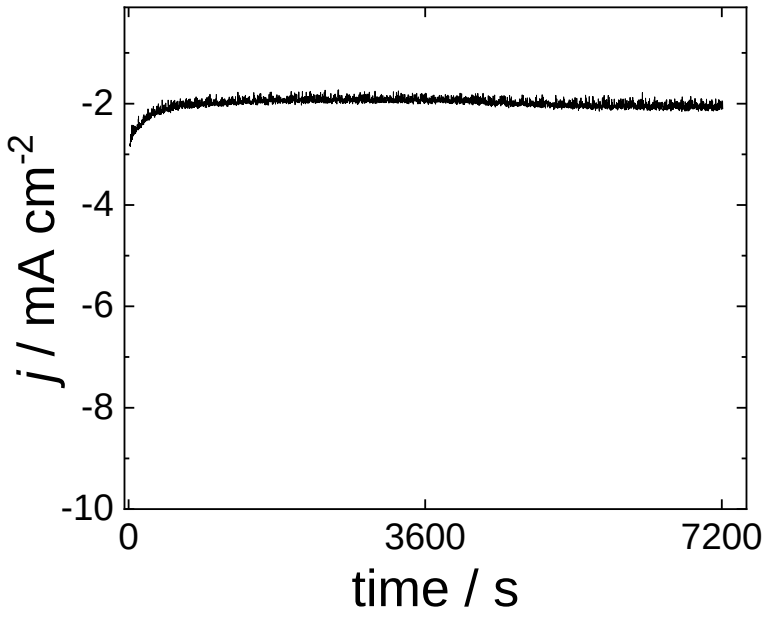

Figure 3.57 Representative current trace of a 2-hour controlled potential electrolysis at pH 3 under CO_2 at -1.065 V vs. SCE (-0.647 V vs. RHE) catalyzed by CoPc-P4VP/GP/GCE in protonated electrolyte (0.4 M NaH_2PO_4/0.5 M $NaClO_4$).

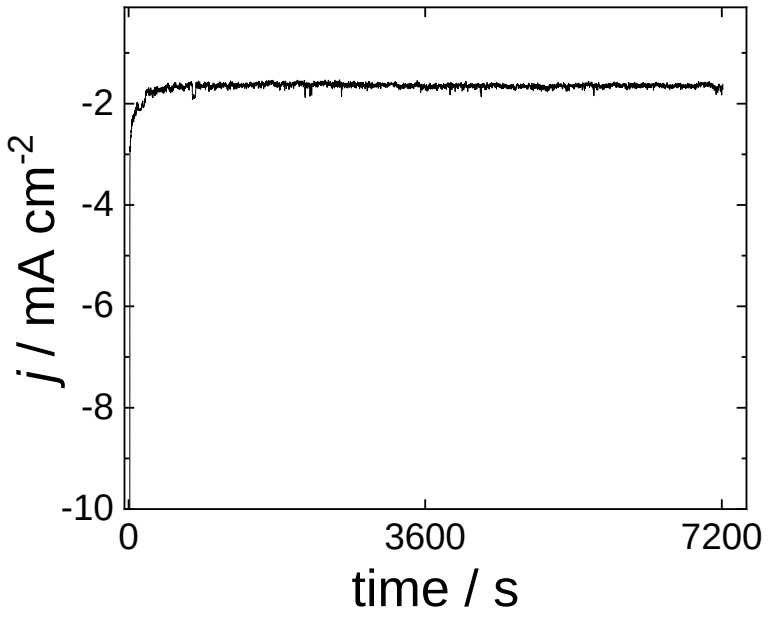

Figure 3.58 Representative current trace of a 2-hour controlled potential electrolysis at pH 4 under CO_2 at -1.124 V vs. SCE (-0.647 V vs. RHE) catalyzed by CoPc-P4VP/GP/GCE in protonated electrolyte (0.4 M NaH_2PO_4/0.5 M $NaClO_4$).

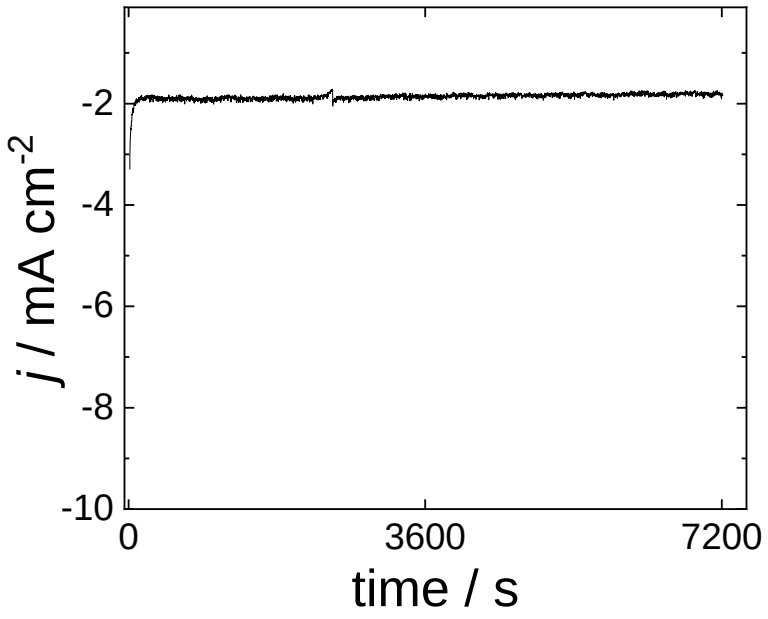

Figure 3.59 Representative current trace of a 2-hour controlled potential electrolysis at pH 5 under CO_2 at -1.183 V vs. SCE (-0.647 V vs. RHE) catalyzed by CoPc-P4VP/GP/GCE in protonated electrolyte (0.4 M NaH_2PO_4/0.5 M $NaClO_4$).

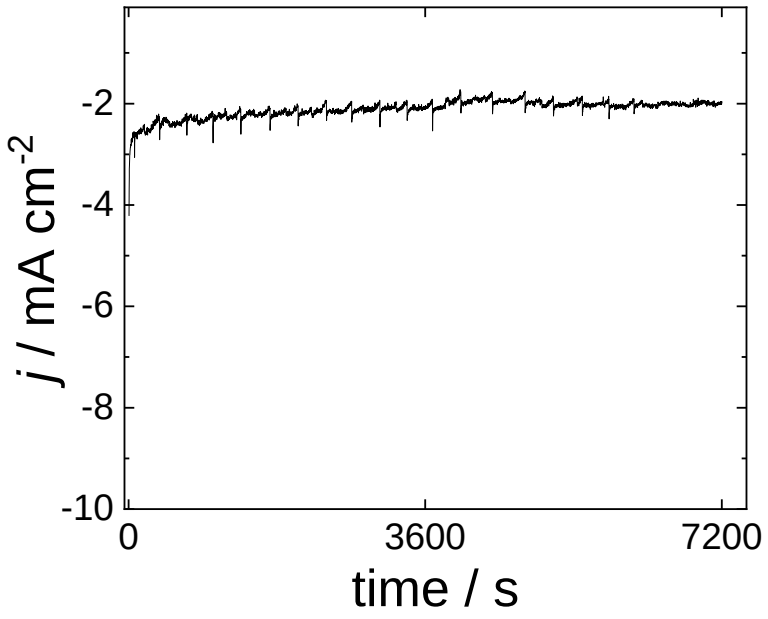

Figure 3.60 Representative current trace of a 2-hour controlled potential electrolysis at pH 6 under CO_2 at -1.242 V vs. SCE (-0.647 V vs. RHE) catalyzed by CoPc-P4VP/GP/GCE in protonated electrolyte (0.4 M NaH_2PO_4/0.5 M $NaClO_4$).

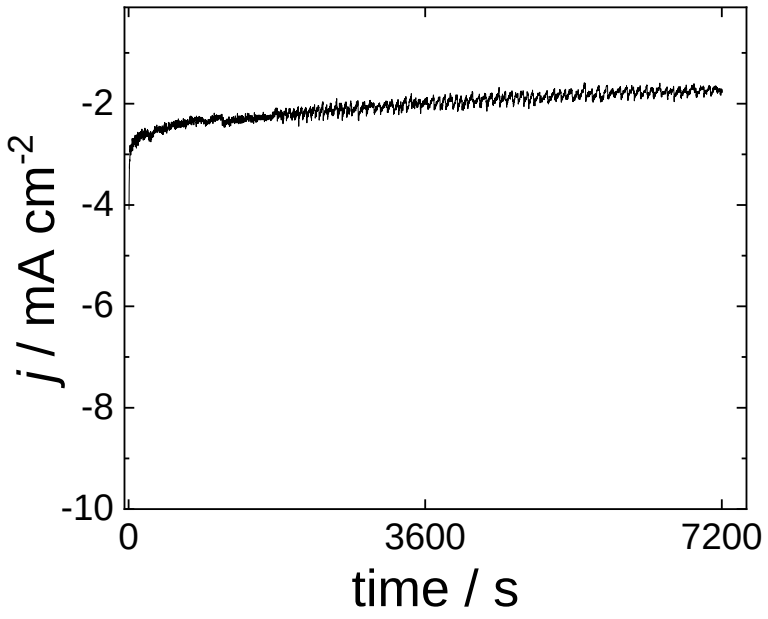

Figure 3.61 Representative current trace of a 2-hour controlled potential electrolysis at pH 7 under CO_2 at -1.301 V vs. SCE (-0.647 V vs. RHE) catalyzed by CoPc-P4VP/GP/GCE in protonated electrolyte (0.4 M NaH_2PO_4/0.5 M $NaClO_4$).

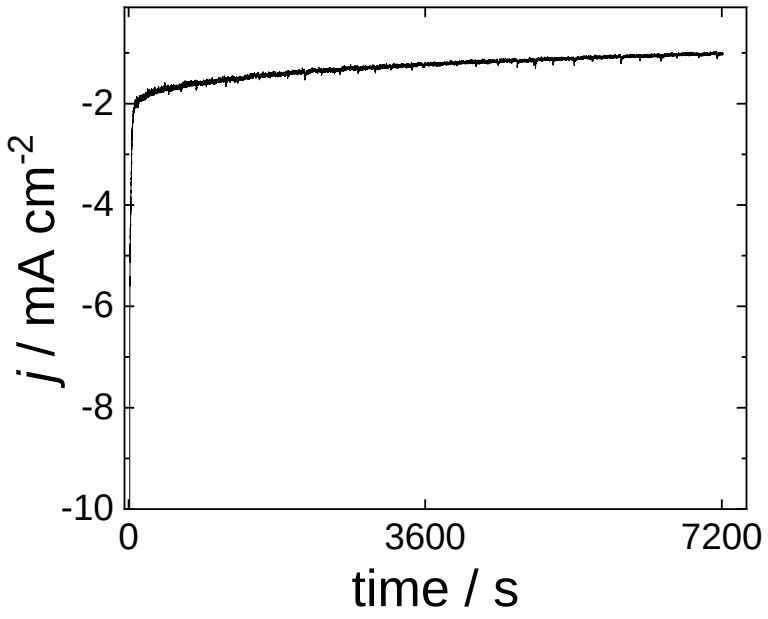

Figure 3.62 Representative current trace of a 2-hour controlled potential electrolysis at pH 3 under CO_2 at -1.125 V vs. SCE (-0.707 V vs. RHE) catalyzed by CoPc-P4VP/GP/GCE in protonated electrolyte (0.4 M NaH_2PO_4/0.5 M $NaClO_4$).

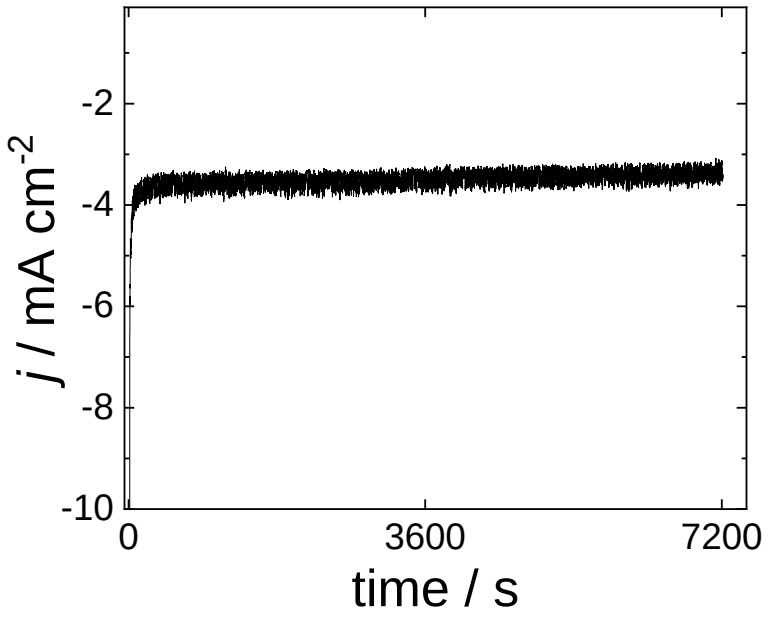

Figure 3.63 Representative current trace of a 2-hour controlled potential electrolysis at pH 4 under CO_2 at -1.184 V vs. SCE (-0.707 V vs. RHE) catalyzed by CoPc-P4VP/GP/GCE in protonated electrolyte (0.4 M NaH_2PO_4/0.5 M $NaClO_4$).

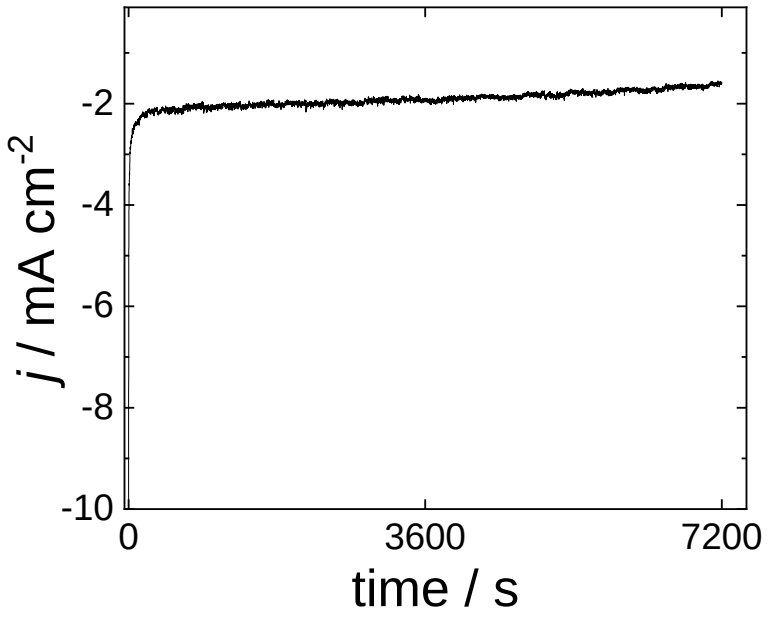

Figure 3.64 Representative current trace of a 2-hour controlled potential electrolysis at pH 5 under CO_2 at -1.243 V vs. SCE (-0.707 V vs. RHE) catalyzed by CoPc-P4VP/GP/GCE in protonated electrolyte (0.4 M NaH_2PO_4/0.5 M $NaClO_4$).

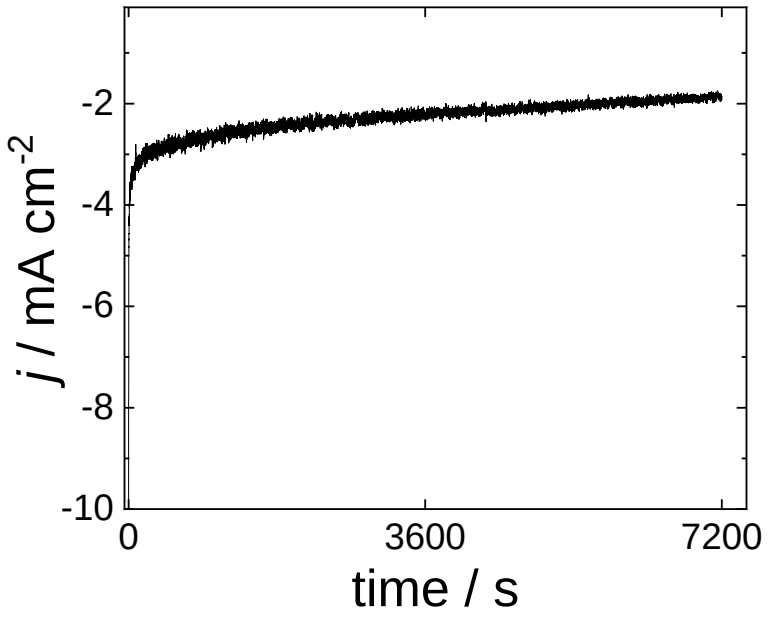

Figure 3.65 Representative current trace of a 2-hour controlled potential electrolysis at pH 6 under CO_2 at -1.302 V vs. SCE (-0.707 V vs. RHE) catalyzed by CoPc-P4VP/GP/GCE in protonated electrolyte (0.4 M NaH_2PO_4/0.5 M $NaClO_4$).

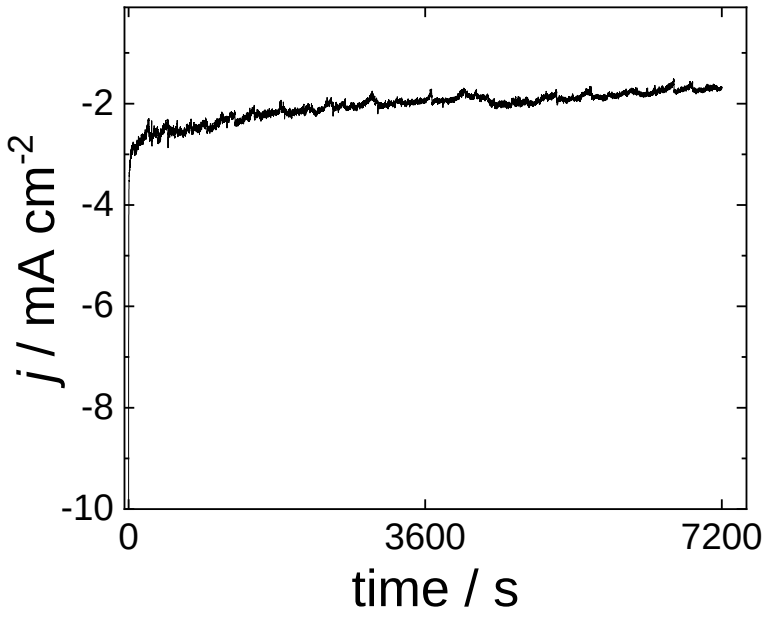

Figure 3.66 Representative current trace of a 2-hour controlled potential electrolysis at pH 7 under CO_2 at -1.361 V vs. SCE (-0.707 V vs. RHE) catalyzed by CoPc-P4VP/GP/GCE in protonated electrolyte (0.4 M NaH_2PO_4/0.5 M $NaClO_4$).

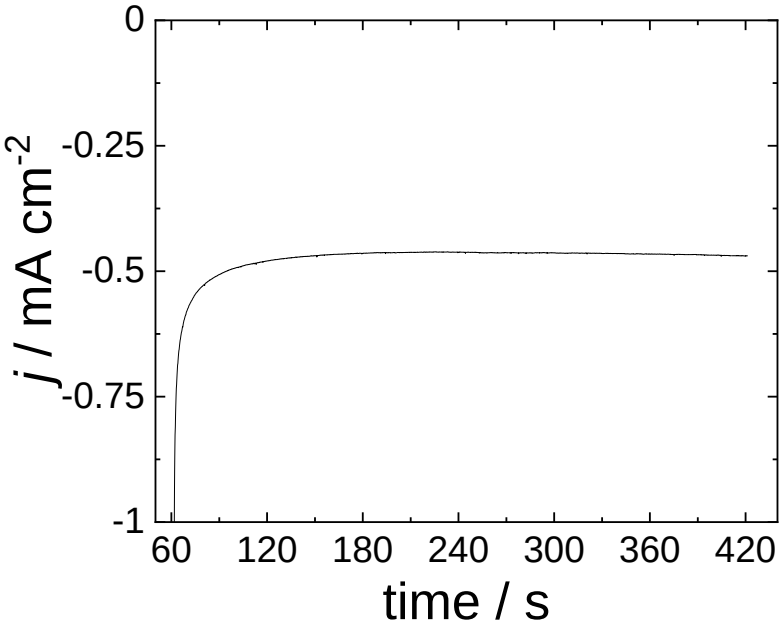

Figure 3.67 pH 5 N_2 representative RDE-CA (1600 rpm held for 6 minutes at -1.183 V vs. SCE) CoPc-P4VP/EPG in pH 5 protonated electrolyte (0.1 M NaH_2PO_4 /0.5 M $NaClO_4$).

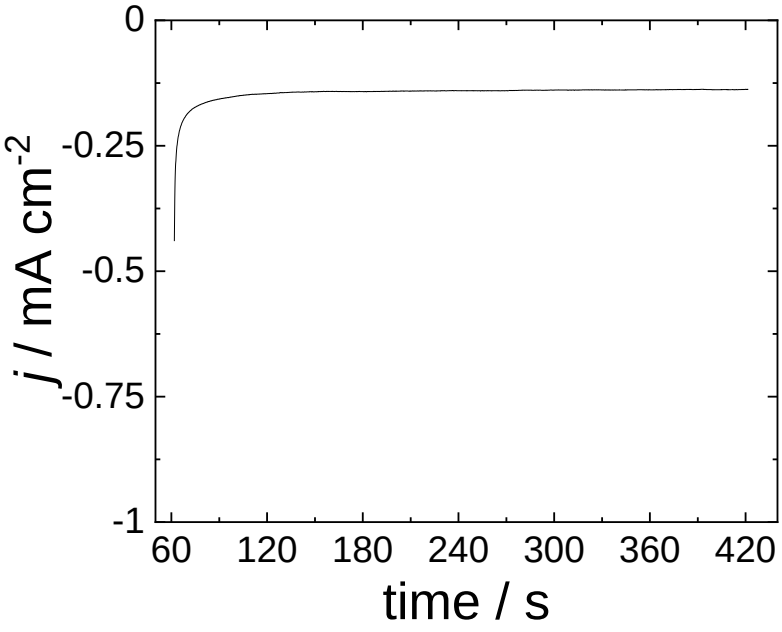

Figure 3.68 pD 5 N_2 representative RDE-CA (1600 rpm held for 6 minutes at -1.183 V vs. SCE) CoPc-P4VP/EPG in pD 5 deuterated electrolyte (0.1 M NaD_2PO_4 /0.5 M $NaClO_4$).

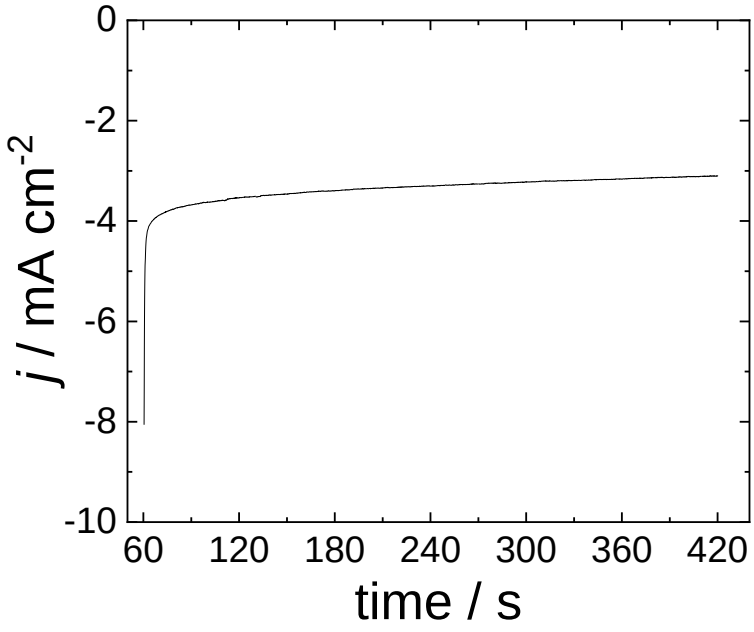

Figure 3.69 pH 5 N_2 representative RDE-CA (1600 rpm held for 6 minutes at -1.183 V vs. SCE) CoPc-P4VP/GP/GCE in pH 5 protonated electrolyte (0.1 M NaH_2PO_4 /0.5 M $NaClO_4$).

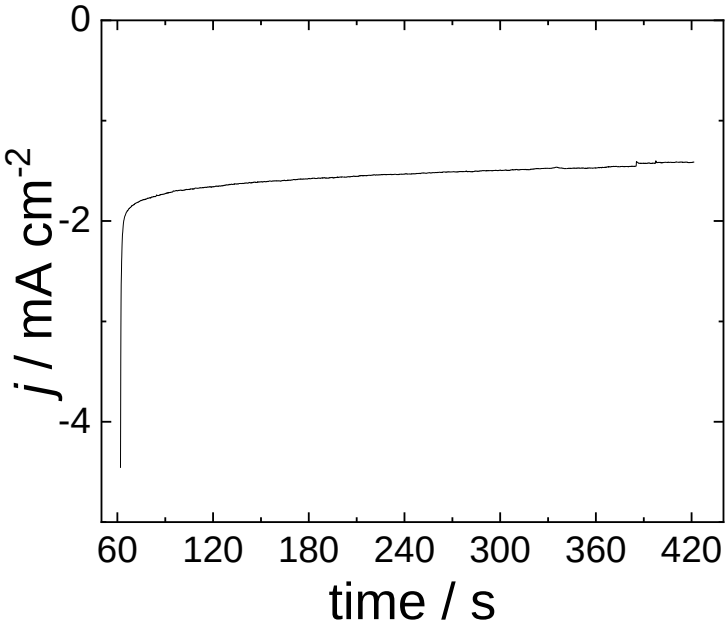

Figure 3.70 pD 5 N_2 representative RDE-CA (1600 rpm held for 6 minutes at -1.183 V vs. SCE) CoPc-P4VP/GP/GCE in pD 5 deuterated electrolyte (0.1 M NaD_2PO_4 /0.5 M $NaClO_4$).

3.8 References

(1) Roy, S. C.; Varghese, O. K.; Paulose, M.; Grimes, C. A. "Toward Solar Fuels: Photocatalytic Conversion of Carbon Dioxide to Hydrocarbons," *ACS Nano* **2010**, *4*, 1259-1278. http://dx.doi.org/10.1021/nn9015423

(2) Verma, S.; Kim, B.; Jhong, H.-R. M.; Ma, S.; Kenis, P. J. A. "A Gross-Margin Model for Defining Technoeconomic Benchmarks in the Electroreduction of CO2," *ChemSusChem* **2016**, *9*, 1972-1979. http://dx.doi.org/https://doi.org/10.1002/cssc.201600394

(3) Nocera, D. G. "Solar Fuels and Solar Chemicals Industry," *Accounts of Chemical Research* **2017**, *50*, 616-619. http://dx.doi.org/10.1021/acs.accounts.6b00615

(4) Spurgeon, J. M.; Kumar, B. "A comparative technoeconomic analysis of pathways for commercial electrochemical CO2 reduction to liquid products," *Energy & Environmental Science* **2018**, *11*, 1536-1551. http://dx.doi.org/10.1039/C8EE00097B

(5) Luna, P. D.; Hahn, C.; Higgins, D.; Jaffer, S. A.; Jaramillo, T. F.; Sargent, E. H. "What would it take for renewably powered electrosynthesis to displace petrochemical processes?," *Science* **2019**, *364*, eaav3506. http://dx.doi.org/doi:10.1126/science.aav3506

(6) Crabtree, R. H. "Alternate Strategies for Solar Fuels from Carbon Dioxide," *ACS Energy Letters* **2020**, *5*, 2505-2507. http://dx.doi.org/10.1021/acsenergylett.0c01359

(7) Mustafa, A.; Lougou, B. G.; Shuai, Y.; Wang, Z.; Tan, H. "Current technology development for CO2 utilization into solar fuels and chemicals: A review," *Journal of Energy Chemistry* **2020**, *49*, 96-123. http://dx.doi.org/https://doi.org/10.1016/j.jechem.2020.01.023

(8) Jin, S.; Hao, Z.; Zhang, K.; Yan, Z.; Chen, J. "Advances and Challenges for the Electrochemical Reduction of CO2 to CO: From Fundamentals to Industrialization," *Angewandte Chemie International Edition* **2021**, *60*, 20627-20648. http://dx.doi.org/https://doi.org/10.1002/anie.202101818

(9) Park, S.; Wijaya, D. T.; Na, J.; Lee, C. W. "Towards the Large-Scale Electrochemical Reduction of Carbon Dioxide," *Catalysts* **2021**, *11*, 253.

(10) Senftle, T. P.; Carter, E. A. "The Holy Grail: Chemistry Enabling an Economically Viable CO2 Capture, Utilization, and Storage Strategy," *Accounts of Chemical Research* **2017**, *50*, 472-475. http://dx.doi.org/10.1021/acs.accounts.6b00479

(11) Abe, T.; Imaya, H.; Yoshida, T.; Tokita, S.; Schlettwein, D.; Wöhrle, D.; Kaneko, M. "Electrochemical CO 2 reduction catalysed by cobalt octacyanophthalocyanine and its mechanism," *Journal of Porphyrins and Phthalocyanines* **1997**, *1*, 315-321.

(12) Torbensen, K.; Joulié, D.; Ren, S.; Wang, M.; Salvatore, D.; Berlinguette, C. P.; Robert, M. "Molecular Catalysts Boost the Rate of Electrolytic CO2 Reduction," *ACS Energy Letters* **2020**, *5*, 1512-1518. http://dx.doi.org/10.1021/acsenergylett.0c00536

(13) Zhang, S.; Fan, Q.; Xia, R.; Meyer, T. J. "CO2 Reduction: From Homogeneous to Heterogeneous Electrocatalysis," *Accounts of Chemical Research* **2020**, *53*, 255-264. http://dx.doi.org/10.1021/acs.accounts.9b00496

(14) Abdinejad, M.; Hossain, M. N.; Kraatz, H.-B. "Homogeneous and heterogeneous molecular catalysts for electrochemical reduction of carbon dioxide," *RSC Advances* **2020**, *10*, 38013-38023. http://dx.doi.org/10.1039/D0RA07973A

(15) Costentin, C.; Robert, M.; Saveant, J. M. "Catalysis of the electrochemical reduction of carbon dioxide," *Chem Soc Rev* **2013**, *42*, 2423-2436. http://dx.doi.org/10.1039/c2cs35360a
(16) Smith, P. T.; Nichols, E. M.; Cao, Z.; Chang, C. J. "Hybrid Catalysts for Artificial Photosynthesis: Merging Approaches from Molecular, Materials, and Biological Catalysis," *Accounts of Chemical Research* **2020**, *53*, 575-587. http://dx.doi.org/10.1021/acs.accounts.9b00619
(17) Costentin, C.; Robert, M.; Savéant, J.-M. "Molecular catalysis of electrochemical reactions," *Current Opinion in Electrochemistry* **2017**, *2*, 26-31. http://dx.doi.org/https://doi.org/10.1016/j.coelec.2017.02.006
(18) Sun, L.; Reddu, V.; Fisher, A. C.; Wang, X. "Electrocatalytic reduction of carbon dioxide: opportunities with heterogeneous molecular catalysts," *Energy & Environmental Science* **2020**, *13*, 374-403. http://dx.doi.org/10.1039/C9EE03660A
(19) Nam, D. H.; De Luna, P.; Rosas-Hernandez, A.; Thevenon, A.; Li, F.; Agapie, T.; Peters, J. C.; Shekhah, O.; Eddaoudi, M.; Sargent, E. H. "Molecular enhancement of heterogeneous CO2 reduction," *Nat Mater* **2020**, *19*, 266-276. http://dx.doi.org/10.1038/s41563-020-0610-2
(20) Lee, M.-Y.; Park, K. T.; Lee, W.; Lim, H.; Kwon, Y.; Kang, S. "Current achievements and the future direction of electrochemical CO2 reduction: A short review," *Critical Reviews in Environmental Science and Technology* **2020**, *50*, 769-815. http://dx.doi.org/10.1080/10643389.2019.1631991
(21) Long, C.; Li, X.; Guo, J.; Shi, Y.; Liu, S.; Tang, Z. "Electrochemical Reduction of CO2 over Heterogeneous Catalysts in Aqueous Solution: Recent Progress and Perspectives," *Small Methods* **2019**, *3*, 1800369. http://dx.doi.org/https://doi.org/10.1002/smtd.201800369
(22) Ma, T.; Fan, Q.; Tao, H.; Han, Z.; Jia, M.; Gao, Y.; Ma, W.; Sun, Z. "Heterogeneous electrochemical CO2 reduction using nonmetallic carbon-based catalysts: current status and future challenges," *Nanotechnology* **2017**, *28*, 472001. http://dx.doi.org/10.1088/1361-6528/aa8f6f
(23) Herranz, J.; Pătru, A.; Fabbri, E.; Schmidt, T. J. "Co-electrolysis of CO2 and H2O: From electrode reactions to cell-level development," *Current Opinion in Electrochemistry* **2020**, *23*, 89-95. http://dx.doi.org/https://doi.org/10.1016/j.coelec.2020.05.004
(24) Zheng, T.; Jiang, K.; Wang, H. "Recent Advances in Electrochemical CO2-to-CO Conversion on Heterogeneous Catalysts," *Advanced Materials* **2018**, *30*, 1802066. http://dx.doi.org/https://doi.org/10.1002/adma.201802066
(25) Kuhl, K. P.; Cave, E. R.; Abram, D. N.; Jaramillo, T. F. "New insights into the electrochemical reduction of carbon dioxide on metallic copper surfaces," *Energy & Environmental Science* **2012**, *5*, 7050-7059. http://dx.doi.org/10.1039/C2EE21234J
(26) Boutin, E.; Wang, M.; Lin, J. C.; Mesnage, M.; Mendoza, D.; Lassalle-Kaiser, B.; Hahn, C.; Jaramillo, T. F.; Robert, M. "Aqueous Electrochemical Reduction of Carbon Dioxide and Carbon Monoxide into Methanol with Cobalt Phthalocyanine," *Angewandte Chemie International Edition* **2019**, *58*, 16172-16176. http://dx.doi.org/https://doi.org/10.1002/anie.201909257
(27) Rivera Cruz, K. L., Y.; Soucy, T. L.; Zimmerman, P. M.; McCrory, C. "Increasing the CO2 Reduction Activity of Cobalt Phthalocyanine by Modulating the σ-Donor Strength of Axially Coordinating Ligands," *ChemRxiv* **2021**. http://dx.doi.org/https://doi.org/10.26434/chemrxiv.14555841.v2
(28) Soucy, T. L.; Liu, Y.; Eisenberg, J. B.; McCrory, C. C. L. "Enhancing Electrochemical Carbon Dioxide Reduction by Polymer-Encapsulated Cobalt Phthalocyanine through Incorporation of Graphite Powder.," *ChemRxiv* **2021**. http://dx.doi.org/10.33774/chemrxiv-2021-bz00c

(29) Liu, Y.; Deb, A.; Leung, K. Y.; Nie, W.; Dean, W. S.; Penner-Hahn, J. E.; McCrory, C. C. L. "Determining the coordination environment and electronic structure of polymer-encapsulated cobalt phthalocyanine under electrocatalytic CO2 reduction conditions using in situ X-Ray absorption spectroscopy," *Dalton Trans* **2020**, *49*, 16329-16339. http://dx.doi.org/10.1039/d0dt01288b
(30) Zhang, H.; Min, S.; Wang, F.; Zhang, Z. "Immobilizing cobalt phthalocyanine into a porous carbonized wood membrane as a self-supported heterogenous electrode for selective and stable CO2 electroreduction in water," *Dalton Transactions* **2020**, *49*, 15607-15611. http://dx.doi.org/10.1039/D0DT03304A
(31) Lin, L.; Liu, T.; Xiao, J.; Li, H.; Wei, P.; Gao, D.; Nan, B.; Si, R.; Wang, G.; Bao, X. "Enhancing CO2 Electroreduction to Methane with a Cobalt Phthalocyanine and Zinc–Nitrogen–Carbon Tandem Catalyst," *Angewandte Chemie International Edition* **2020**, *59*, 22408-22413. http://dx.doi.org/https://doi.org/10.1002/anie.202009191
(32) De Riccardis, A.; Lee, M.; Kazantsev, R. V.; Garza, A. J.; Zeng, G.; Larson, D. M.; Clark, E. L.; Lobaccaro, P.; Burroughs, P. W. W.; Bloise, E.; Ager, J. W.; Bell, A. T.; Head-Gordon, M.; Mele, G.; Toma, F. M. "Heterogenized Pyridine-Substituted Cobalt(II) Phthalocyanine Yields Reduction of CO2 by Tuning the Electron Affinity of the Co Center," *ACS Applied Materials & Interfaces* **2020**, *12*, 5251-5258. http://dx.doi.org/10.1021/acsami.9b18924
(33) Wu, Y.; Hu, G.; Rooney, C. L.; Brudvig, G. W.; Wang, H. "Heterogeneous Nature of Electrocatalytic CO/CO2 Reduction by Cobalt Phthalocyanines," *ChemSusChem* **2020**, *13*, 6296-6299. http://dx.doi.org/10.1002/cssc.202001396
(34) Xia, Y.; Kashtanov, S.; Yu, P.; Chang, L.-Y.; Feng, K.; Zhong, J.; Guo, J.; Sun, X. "Identification of dual-active sites in cobalt phthalocyanine for electrochemical carbon dioxide reduction," *Nano Energy* **2020**, *67*, 104163. http://dx.doi.org/https://doi.org/10.1016/j.nanoen.2019.104163
(35) Liu, Y.; McCrory, C. C. L. "Modulating the mechanism of electrocatalytic CO2 reduction by cobalt phthalocyanine through polymer coordination and encapsulation," *Nature Communications* **2019**, *10*, 1683. http://dx.doi.org/10.1038/s41467-019-09626-8
(36) Wu, Y.; Jiang, Z.; Lu, X.; Liang, Y.; Wang, H. "Domino electroreduction of CO2 to methanol on a molecular catalyst," *Nature* **2019**, *575*, 639-642. http://dx.doi.org/10.1038/s41586-019-1760-8
(37) Zhu, M.; Chen, J.; Guo, R.; Xu, J.; Fang, X.; Han, Y.-F. "Cobalt phthalocyanine coordinated to pyridine-functionalized carbon nanotubes with enhanced CO2 electroreduction," *Applied Catalysis B: Environmental* **2019**, *251*, 112-118. http://dx.doi.org/https://doi.org/10.1016/j.apcatb.2019.03.047
(38) Lieber, C. M.; Lewis, N. S. "Catalytic reduction of carbon dioxide at carbon electrodes modified with cobalt phthalocyanine," *Journal of the American Chemical Society* **1984**, *106*, 5033-5034. http://dx.doi.org/10.1021/ja00329a082
(39) Meshitsuka, S.; Ichikawa, M.; Tamaru, K. "Electrocatalysis by metal phthalocyanines in the reduction of carbon dioxide," *Journal of the Chemical Society, Chemical Communications* **1974**, 158-159. http://dx.doi.org/10.1039/C39740000158
(40) Kramer, W. W.; McCrory, C. C. L. "Polymer coordination promotes selective CO2 reduction by cobalt phthalocyanine," *Chemical Science* **2016**, *7*, 2506-2515. http://dx.doi.org/10.1039/C5SC04015A
(41) Abe, T.; Yoshida, T.; Tokita, S.; Taguchi, F.; Imaya, H.; Kaneko, M. "Factors affecting selective electrocatalytic co2 reduction with cobalt phthalocyanine incorporated in a

polyvinylpyridine membrane coated on a graphite electrode," *Journal of Electroanalytical Chemistry* **1996**, *412*, 125-132. http://dx.doi.org/https://doi.org/10.1016/0022-0728(96)04631-1
(42) Yoshida, T.; Kamato, K.; Tsukamoto, M.; Iida, T.; Schlettwein, D.; Wöhrle, D.; Kaneko, M. "Selective electroacatalysis for CO2 reduction in the aqueous phase using cobalt phthalocyanine/poly-4-vinylpyridine modified electrodes," *Journal of Electroanalytical Chemistry* **1995**, *385*, 209-225. http://dx.doi.org/https://doi.org/10.1016/0022-0728(94)03762-R
(43) Shook, R. L.; Borovik, A. S. "Role of the secondary coordination sphere in metal-mediated dioxygen activation," *Inorg Chem* **2010**, *49*, 3646-3660. http://dx.doi.org/10.1021/ic901550k
(44) Loewen, N. D.; Berben, L. A. "Secondary Coordination Sphere Design to Modify Transport of Protons and CO2," *Inorganic Chemistry* **2019**, *58*, 16849-16857. http://dx.doi.org/10.1021/acs.inorgchem.9b03102
(45) Li, J.; Zhang, Y.; Kornienko, N. "Heterogeneous electrocatalytic reduction of CO2 promoted by secondary coordination sphere effects," *New Journal of Chemistry* **2020**, *44*, 4246-4252. http://dx.doi.org/10.1039/C9NJ05892C
(46) Liu, G.; Fan, Y.-J.; Zhang, J.-L. "Construction of secondary coordination sphere boosts electrochemical CO2 reduction of iron porphyrins," *Journal of Porphyrins and Phthalocyanines* **2020**, *24*, 465-472. http://dx.doi.org/10.1142/s1088424619501608
(47) Kirsh, Y. E.; Komarova, O. P. "Protonization in aqueous solutions of poly-4-vinylpyridine and poly-2-vinylpyridine partially quaternized with dimethyl sulphate," *Polymer Science U.S.S.R.* **1976**, *18*, 223-228. http://dx.doi.org/https://doi.org/10.1016/0032-3950(76)90078-2
(48) Varela, A. S.; Kroschel, M.; Reier, T.; Strasser, P. "Controlling the selectivity of CO2 electroreduction on copper: The effect of the electrolyte concentration and the importance of the local pH," *Catalysis Today* **2016**, *260*, 8-13. http://dx.doi.org/https://doi.org/10.1016/j.cattod.2015.06.009
(49) Jiang, X.; Li, H.; Yang, Y.; Gao, D. "pH dependence of CO2 electroreduction selectivity over size-selected Au nanoparticles," *Journal of Materials Science* **2020**, *55*, 13916-13926. http://dx.doi.org/10.1007/s10853-020-04983-y
(50) Zhang, Z.; Melo, L.; Jansonius, R. P.; Habibzadeh, F.; Grant, E. R.; Berlinguette, C. P. "pH Matters When Reducing CO2 in an Electrochemical Flow Cell," *ACS Energy Letters* **2020**, *5*, 3101-3107. http://dx.doi.org/10.1021/acsenergylett.0c01606
(51) Henckel, D. A.; Counihan, M. J.; Holmes, H. E.; Chen, X.; Nwabara, U. O.; Verma, S.; Rodríguez-López, J.; Kenis, P. J. A.; Gewirth, A. A. "Potential Dependence of the Local pH in a CO2 Reduction Electrolyzer," *ACS Catalysis* **2020**, *11*, 255-263. http://dx.doi.org/10.1021/acscatal.0c04297
(52) Lu, X.; Zhu, C.; Wu, Z.; Xuan, J.; Francisco, J. S.; Wang, H. "In Situ Observation of the pH Gradient near the Gas Diffusion Electrode of CO2 Reduction in Alkaline Electrolyte," *Journal of the American Chemical Society* **2020**, *142*, 15438-15444. http://dx.doi.org/10.1021/jacs.0c06779
(53) Goyal, A.; Koper, M. T. M. "The Interrelated Effect of Cations and Electrolyte pH on the Hydrogen Evolution Reaction on Gold Electrodes in Alkaline Media," *Angewandte Chemie International Edition* **2021**, *60*, 13452-13462. http://dx.doi.org/https://doi.org/10.1002/anie.202102803
(54) Lim, C. F. C.; Harrington, D. A.; Marshall, A. T. "Effects of mass transfer on the electrocatalytic CO2 reduction on Cu," *Electrochimica Acta* **2017**, *238*, 56-63. http://dx.doi.org/https://doi.org/10.1016/j.electacta.2017.04.017
(55) Hashiba, H.; Weng, L.-C.; Chen, Y.; Sato, H. K.; Yotsuhashi, S.; Xiang, C.; Weber, A. Z. "Effects of Electrolyte Buffer Capacity on Surface Reactant Species and the Reaction Rate of CO2

in Electrochemical CO2 Reduction," *The Journal of Physical Chemistry C* **2018**, *122*, 3719-3726. http://dx.doi.org/10.1021/acs.jpcc.7b11316
(56) Moura de Salles Pupo, M.; Kortlever, R. "Electrolyte Effects on the Electrochemical Reduction of CO2," *ChemPhysChem* **2019**, *20*, 2926-2935. http://dx.doi.org/https://doi.org/10.1002/cphc.201900680
(57) Fife, T. H.; Bruice, T. C. "THE TEMPERATURE DEPENDENCE OF THE ΔpD CORRECTION FOR THE USE OF THE GLASS ELECTRODE IN D2O," *The Journal of Physical Chemistry* **1961**, *65*, 1079-1080. http://dx.doi.org/10.1021/j100824a525
(58) Soucy, T. L.; Liu, Y.; Eisenberg, J. B.; McCrory, C. C. L. "Enhancing the Electrochemical CO2 Reduction Activity of Polymer-Encapsulated Cobalt Phthalocyanine Films by Modulating the Loading of Catalysts, Polymers, and Carbon Supports," *ACS Applied Energy Materials* **2021**. http://dx.doi.org/10.1021/acsaem.1c02689
(59) Rivera Cruz, K. E.; Liu, Y.; Soucy, T. L.; Zimmerman, P. M.; McCrory, C. C. L. "Increasing the CO2 Reduction Activity of Cobalt Phthalocyanine by Modulating the σ-Donor Strength of Axially Coordinating Ligands," *ACS Catalysis* **2021**, 13203-13216. http://dx.doi.org/10.1021/acscatal.1c02379
(60) Yang, K.; Kas, R.; Smith, W. A. "In Situ Infrared Spectroscopy Reveals Persistent Alkalinity near Electrode Surfaces during CO2 Electroreduction," *Journal of the American Chemical Society* **2019**, *141*, 15891-15900. http://dx.doi.org/10.1021/jacs.9b07000

Chapter 4 Studies of the CO_2 Reduction Reaction by Poly-(4-vinylpyridine-*co*-styrene) Encapsulated Cobalt Phthalocyanine

4.1 Preface

This chapter presents how the use of copolymers made up of styrene and 4-vinylpyridine monomers at different ratios can encapsulate cobalt phthalocyanine and how the polymer identity impacts the CO_2 reduction activity and mechanism. This chapter of my dissertation is derived from a manuscript that is in preparation for submission. I am the primary author on the manuscript, with the other authors being Jonah B. Eisenberg, Dr. Leila M. Foroughi, Prof. Adam J. Matzger, and Prof. Charles C. L. McCrory. I was responsible for all electrochemical measurements and all sample preparation for the collection of the electrochemical data in addition to the ICP-MS characterization and interpretation of all data, creation of figures, and writing of the manuscript. Jonah B. Eisenberg was responsible for the collection of some electrochemical data and assisted with sample/electrode preparation along with electrochemical method development. Dr. Leila Foroughi performed the synthesis and characterization of the copolymers. Professor Adam Matzger provided expertise in macromolecular synthesis, characterization, and conceived of the idea along with Professor Charles C. L. McCrory, who also provided significant insight and expertise in electroanalytical techniques and analysis.

4.2 Abstract

Cobalt phthalocyanine (CoPc) encapsulated within a polymer has been shown to be an interesting electrocatalyst for the CO_2 reduction reaction. Previous work has shown that the transport of protons has been an interesting aspect and important reason for enhanced activity and selectivity when molecular catalysts have been encapsulated by a polymer (and could be possible in other, similar membrane coated electrode systems). In this study, we perform CoPc-electrocatalyzed CO_2 reduction with copolymers of 4-vinylpyridine and styrene monomers in varying ratios in order to purposefully inhibit the transport of protons and determine the extent to which pyridyl residues are necessary for the swift and controlled transport of protons from the bulk electrolyte to the catalytic active sites within the polymer. This work studies the activity and kinetic isotope effect as a function of the concentration of styrene within the copolymer, showing that activity decreases substantially with just 10% of the copolymer being made up of styrene. I show through these studies that there may be impacts from the folding of the copolymer or aggregation of the CoPc, because the addition of pyridine within the CoPc-polymer complex results in higher activity for CoPc-copolymers with low levels of styrene in the copolymer. Finally, I discuss the opportunity of performing proton inventory studies with these polymers for future studies. These results are important for considerations of polymer-catalyst interactions where there is a heteropolymer involved in binding a catalyst to an electrode surface.

4.3 Introduction

The use of polymer-coated and polymer-encapsulated electrodes and electrocatalysts for small molecule transformations has become more common in recent years as the benefits of increased reaction or product selectivity and improved tunability with prevention of poisoning have become well known.[1,2] The McCrory group[3,4] and others[5-7] have reviewed how membrane coated electrode systems are interesting alternatives to traditional heterogeneous catalysts, and specifically how reactant, charge, and product transport can all impact the overall rates of reaction and the product/reaction selectivity for reactions such as the CO_2 reduction reaction (CO_2RR) where CO_2 can be reduced to many carbon-containing products in addition to H_2 by the competing proton reduction (shown in Figure 4.1).

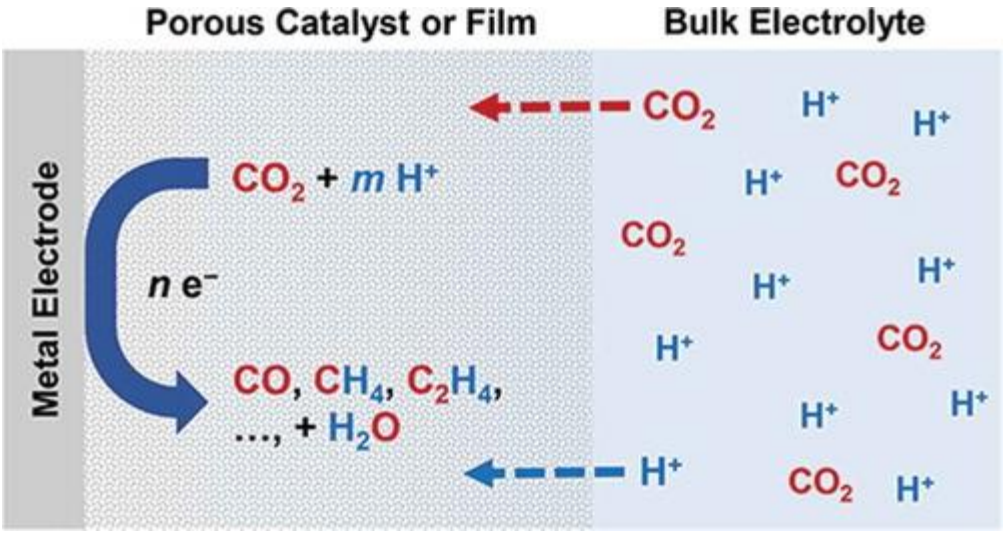

Figure 4.1 Representation of the transport into and out of a porous catalyst or film from the bulk electrolyte. Figure is reproduced from Ref. 4 with permission from Taylor & Francis.[4]

The McCrory group has worked on this concept by focusing on systematically studying a single polymer-encapsulated catalyst: Cobalt phthalocyanine (CoPc) encapsulated by poly-4-vinylpyirine, resulting in a CoPc-P4VP catalyst-polymer complex that is then dropcasted onto the surface of an electrode. The use of polymers as a binder for polymer-encapsulated cobalt phthalocyanine catalyzed CO_2RR is a concept that was used from the very first report about CoPc-catalyzed CO_2RR.[8] The authors used styrene to adhere CoPc to a graphitic electrode surface for CO_2 reduction and found that the activity was <10% what it had been without the polymer – at the time, this was attributed to the increased resistance of the system.[8] This idea of the use of polymers in this system was expanded upon in 1995, with Kaneko and coworkers recognizing the possibilities of using polymers as both a binding agent and as a tool to enhance catalytic performance. Previously, the group had studied the impact of incorporating other molecular catalysts within Nafion polymer coated molecular catalysts in aqueous systems, with the idea being that creating an artificially hydrophobic environment around the catalysts would improve reaction selectivity for the CO_2RR over the competing HER as they performed CO_2RR in aqueous systems, and they found that both a rhenium and cobalt inorganic complex could be incorporated into a polymer membrane, which would yield improvements in activity and selectivity.[9,10]

The group then studied CoPc and how its properties changed when the catalyst was encapsulated in a polymer made up of a 90% 4-vinylpyridine/10% styrene (PVP).[11] They were specifically interested in the product distribution of two competing reactions: the CO_2 reduction reaction (CO_2RR) and the hydrogen evolution reaction (HER). Since reaction selectivity is important for effective CO_2RR, they were interested in how the product distribution changed from relatively high H_2 products toward CO_2RR-dominated upon encapsulation by the PVP

polymer. Upon further investigation focusing only on a polymer made up of 4VP (and no styrene), the authors concluded that the coordinative properties of the pyridyl residues toward the CoPc combined with the weakly basic properties of the polymer contributed to the changing selectivity metrics.[12] Additionally, they studied the changing selectivity as a function of applied electrochemical potential and catalyst loading. In these studies, they found that there was a "sweet spot" for both of these experimental conditions. With a potential too positive, there was not the maximum amount of CO produced; with a potential too negative, the HER showed higher production compared to the CO_2RR at less negative potentials, but the authors noted that the HER may be taking place on the electrode surface and not on the catalytic sites due to the HER's independence of catalyst loading. At more negative potentials, the CO production increases with increasing catalyst loading.[12]

Inspired by the interesting findings of Kaneko and coworkers, our group systematically studied the impacts of the primary and outer coordination sphere between CoPc and the P4VP polymer. The primary sphere was defined by the interaction between the nitrogen of pyridyl groups and the Co center, and the outer coordination sphere was defined as the transport mechanism of protons through the polymer film to the CoPc catalytic sites.[13] To do this, we studied the activity and selectivity of CoPc under multiple coordination/polymer environments (Figure 4.2).

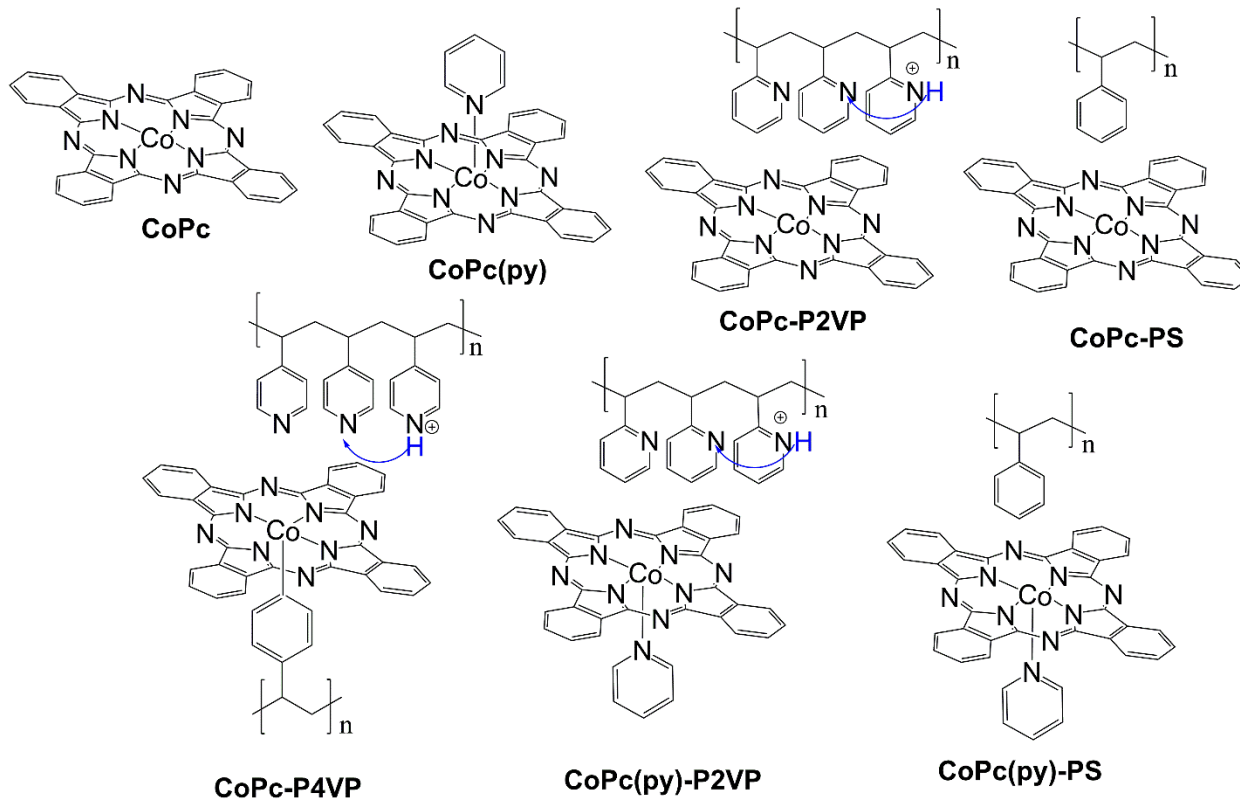

Figure 4.2 CoPc under different polymer or coordination environments, highlighting whether the polymer moiety has the ability to coordinate and/or perform the characteristics of a proton relay. Figure adapted from Ref. [14]

First, we consider the 4-coordinate CoPc parent complex; CoPc coordinated by free pyridine (CoPc(py)); and CoPc encapsulated in the non-coordinating polymer poly-2-vinylpyridine (CoPc-P2VP). Finally, we studied CO_2 reduction by CoPc-P4VP, where primary, secondary, and outer coordination sphere effects were combined by the polymer. In separate studies, we expanded upon the idea of axial coordination from the polymer – providing X-ray spectroscopy evidence to show that there was likely an axial interaction between the pyridyl residues and the Co center,[15] and showing that the donating strength of the σ-electrons of the nitrogen of an axial ligand would influence overall catalytic CO_2RR activity.[16] These studies were important to determine that the primary (axial coordination) of pyridine combined with the outer sphere-controlled proton delivery and hydrogen bonding stabilization of the reactive carboxylate intermediate by protonated pyridyl residues were important to take full advantage of activity and selectivity in these systems.

In particular, the transport of reactants (protons and CO_2) from the bulk electrolyte through the polymer film to catalyst sites has been an interesting concept to consider, as electron transfer from an electrode must take place close to the electrode surface. In addition to considering charge transport (as our group did when looking to incorporate graphite powder into the CoPc-polymer system, discussed at length in Chapter 2 and Ref.[17]), we consider that transport of the CO_2 and protons from the bulk electrolyte through the polymer to catalytic sites must take place in order to perform the electrochemical reaction. Initially, we proposed that a proton hopping mechanism between pyridyl moieties of the polymer resulted in a controlled and swift proton delivery, contributing to the interesting activity and selectivity effects observed when the parent complex was encapsulated in the P4VP film. Since protons and deuterons have such different masses, the technique of kinetic isotope effect analysis has been very useful to us.

This technique, which allows for measurement of overall current (directly proportion to rate of reaction in the catalytic mechanism) in protonated and deuterated electrolyte, allowed us to determine whether the rate-limiting step of the mechanism was impacted by the proton transfer event. This is a unique aspect of the isotope effect for proton-related reactions: since the masses of a proton or deuteron are substantially different, the KIE will be large if the RDS contains a proton transfer event, as the kinetics of the transfer event will be slower for a heavier atom. Our group specifically found that the axial coordination of the pyridyl residues from the polymer impact he overall rate of reaction. These insights were crucial for the confirmation that axial coordination of the pyridyl residues were causing enhanced catalysis by changing the RDS from a CO_2-binding step to a H^+ transfer event, which contributed to the increased activity and selectivity in the CoPc-P4VP or CoPc(py) systems over the parent CoPc complex.

In order to provide evidence for the existence of proton relays that provide controlled delivery of protons through the polymer matrix to the catalytic active sites, we adapted a technique that is commonly used in enzymology to prove the presence of a proton relay. In the first electrochemical study of proton inventory analysis,[14] our group showed evidence that for the presence of a proton relay due to the pyridyl moieties of the polymer. The results of this study can be seen in Figure 4.3, along with an explanation for understanding the proton inventory results in Figure 4.3c. These figures highlight the results of this study, specifically that current density in a fractionally deuterated (Equation 4.1) electrolyte can yield a dome-shaped curve when plotted against the concentration of deuterium oxide in the electrolyte. These curves, which are the absence of a straight line along the activity vs. fractional deuteration curve, can be modeled from the Kresge-Gross-Butler relationship shown in Equation 4.2.[18-20]

$$n_{D2O} = \frac{[D_2O]}{[D_2O] + [H_2O]}$$

Equation 4.1 Equation for determining the fractional deuteration of the electrolyte

$$\frac{j_{nD2O}}{j_0} = \frac{\nu_{nD2O}}{\nu_0} = (1 - n_{D2O} + n_{D2O}\varphi)Z^{nD2O}$$

Equation 4.2 Relative current density in fractionally deuterated electrolyte (j_{D2O}, with n_{D2O} defined in Equation 4.1) compared to the current density in 100% H_2O (j_0) which is impacted by φ, the relationship between isotope fractionation factor for a hydrogenic site, and Z, which is the solvent isotope effect that results from the contribution of many hydrogenic sites (in this case, protonated pyridyl residues would be identical hydrogenic sites).

In Figure 4.3a, the electrochemical results of the proton inventory are presented for CoPc (where the KIE = 1), CoPc(py) (where the KIE = 3) and CoPc-P4VP (where the KIE ~2.1). The KIE is one indiator of the presence of a proton relay, as CoPc-P4VP has a slightly deflated KIE from the CoPc(py) KIE of 3, due to the slight inverse isotope effect of the pyridyl residue that favors protonation by a deuteron compared to a proton. These KIEs are not observed within polystyrene (PS), which is run as a control to confirm that the KIE and proton inventory effects are not inherent to any polymer but require the pyridyl moiety to promote proton transport via the proton relay (results seen in Figure 4.3b). Specifically, the deviation from linearity and the corresponding KIE change for CoPc-P4VP is not present for the case of CoPc(py)-PS, where CoPc(py) is 5 coordinate and the RDS is therefore a proton transfer event (as opposed to the CoPc or CoPc-PS cases where the CO_2 binding is likely the RDS). This deviation from linearity is indicative of multiple hydrogenic sites contributing to this effect and is shown in Figure 4.3c, which highlights that the relative rates of reaction (in this case measured by current density) plotted against the fractional deuteration of the electrolyte result in a dome shaped curve where

there is evidence for a proton relay, and a linear curve (observed in the case of CoPc(py) and CoPc(py)-PS) supports the hypothesis that there is no proton relay in these systems.

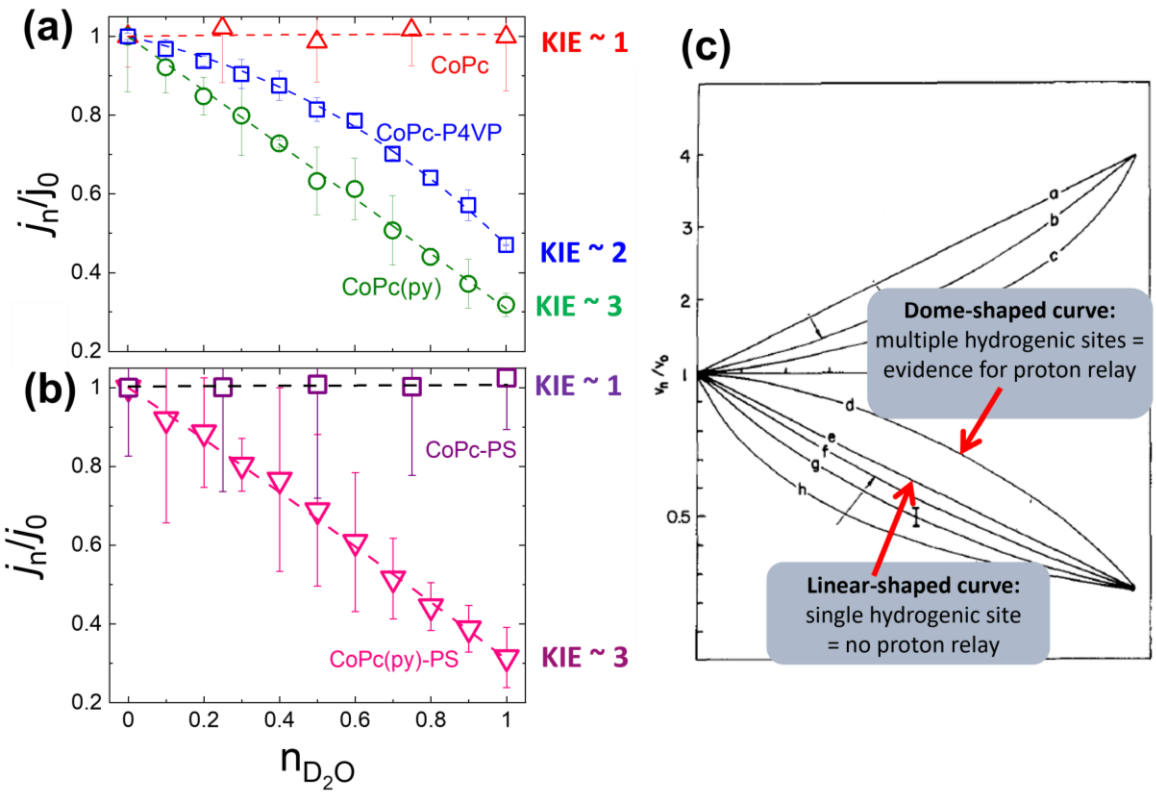

Figure 4.3 Electrochemical proton inventory studies for (a) CoPc, CoPc-P4VP, and CoPc(py) and (b) CoPc-PS and CoPc(py)-PS. (c) shows typical proton inventory studies as performed in enzymology, where a dome-shaped curve is indicative of multiple hydrogenic sites contributing to the transport of a proton, and a linear shaped curve is indicative of a single hydrogenic site and therefore does not provide evidence of a proton relay. (a) and (b) are reproduced with permission by Springer Nature.. (c) is adapted and reproduced with permission from Venkatasubban, K. & Schowen, R. L. The Proton Inventory Technique. Crit. Rev. Biochem. 17, 1-44 (1984).

While it is well known that polymer matrices or other membranes can contribute to certain characteristics within an electrocatalysis system, understanding the microenvironment and modulating some of the effects of these polymers has not been well studied other than a few key works highlighted in the Introduction and in other places throughout this dissertation. To understand this proton relay mechanism further (highlighted in the inset of Figure 4.4a) we proposed that limiting these proton relays by incorporating styrene moieties within a copolymer system could break down this proton relay (highlighted in the inset of Figure 4.4b).

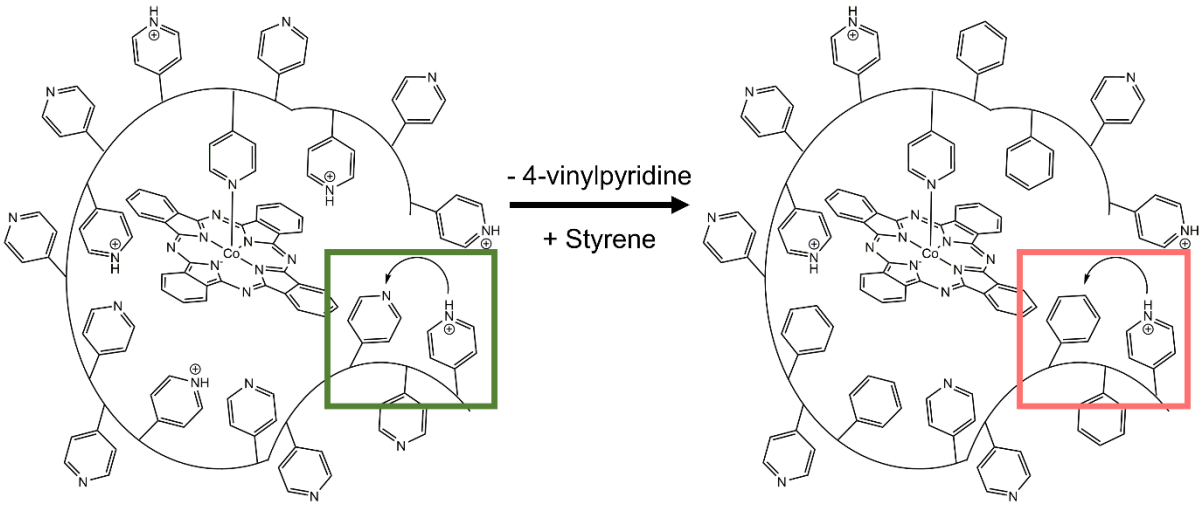

Figure 4.4 (a) the proposed encapsulation of cobalt phthalocyanine by poly-4-vinylpyridine, where the proton hopping mechanism is highlighted; (b) the 4-vinylpyridine moieties are replaced by styrene components. We hypothesize that this shuts down the proton hopping mechanism and therefore may impact activity. Figure 4.3(a) adapted from Ref . .[13]

The proton inventory studies assisted in our understanding of the proton delivery method, and the kinetic isotope effect studies were crucial for the understanding of the RDS of the mechanism. In this work, we attempt to break down the proton relays by incorporating styrene residues within the polymer to create poly-(4-vinylpyridine *co* styrene) (P(4VP-*c*-Sty), Figure 4.4). We found that with just 10% of the molar fraction of the copolymer being styrene moieties, the activity decreased by 90%, but that when CoPc was combined with a pyridyl residue prior to polymer encapsulation, the activity drop was very minor and with 25% of the molar mass being styrene, the activity dropped by 50%. These results showed that axial coordination of pyridyl residues within the polymer may be lost with low levels of styrene added within the copolymer, and that aggregation or polymer folding could contribute to the loss in activity when there was no free pyridine within the system. These results have implications for similar electrocatalytic systems where there are heteropolymers used as a binding agent, or where there are molecular catalysts that require the use of a primary coordination sphere to ensure maximum activity. We propose that future studies could use the proton inventory technique to understand the proton transport of this system. In addition to these results, we show preliminary results that imply that other polymers with other moieties have the possibility to perform proton or CO_2 transport through the polymer to promote swift electrocatalysis.

4.4 Experimental

4.4.1 Materials

All chemicals were used as received without further purification, unless specified. All water used in this study was ultrapure water purified with a Thermo Scientific GenPure UV-TOC/UF x CAD-plus water purification system, with a resistivity of 18.2 MΩ cm. Carbon dioxide (CO_2, 99.8%) was purchased from Cryogenic Gases. Nitrogen (N_2) was boil-off gas from a liquid nitrogen source. Cobalt phthalocyanine (CoPc, 97%), *N,N*-dimethylformamide (DMF, ACS grade), sodium phosphate monobasic (NaH_2PO_4, BioXtra, >99.0%), and Nafion-117 cation exchange membrane (Nafion) were purchased from Sigma Aldrich. Sodium hydroxide (NaOH, TraceMetal grade) and nitric acid (HNO_3, TraceMetal grade, 67-70%) were obtained from Fisher Scientific. Phosphoric acid (H_3PO_4, 85%), 4-vinylpyridine (4VP, 95%), 2,2—Azobis(2-methylpropionitrile) (98%) were purchased from Sigma Aldrich. Deuterium oxide (D_2O, 99.9%) and deuterated phosphoric acid (D_3PO_4, 85%) were obtained from Cambridge Isotope Laboratories, Inc. Deuterated sodium hydroxide (NaOD, 40%) was purchased from Acros Organics.

4.4.2 Electrolyte Solution Preparation and pH Measurements

Protonated Electrolyte. All protonated electrolyte solutions were prepared using ultrapure water. All protonated experiments were performed in solutions of 0.1 M NaH_2PO_4 adjusted to pH 5 by the dropwise addition of 1 M NaOH and 85% H_3PO_4. After the purging of the electrolyte by gaseous CO_2, the pH was ~4.7.

Deuterated Electrolyte. Deuterated electrolyte was prepared using oven-dried glassware. The electrolyte 0.1 M NaD_2PO_4 was prepared by dissolving 0.3565 g 85% D_3PO_4 and

0.3075 g 40% NaOD in 30 mL D_2O. This electrolyte was adjusted to pD 5 (which corresponds to $pH_{meter\ reading}$ = 4.6) via dropwise addition of additional 1 M D_3PO_4 and NaOD. After the purging of CO_2, the pD of the system was ~ 4.7 (which corresponds to $pH_{meter\ reading}$ = 4.3).

The electrolyte pH was measured with a Fisher Scientific Accumet AB200 pH meter with an Atlas Scientific pH probe electrode calibrated with a three-point calibration curve at pH 4.01, 7.00, and 10.01. Before each experiment, the electrolyte in the working chamber of the cell was sparged by CO_2 or N_2 for at least 30 minutes. The gas was bubbled through the appropriate electrolyte solvent and into the cell solution via Tygon tubing.

4.4.3 Polymer Synthesis & Characterization

Poly(4-vinylypridine-*co*-styrene) polymers and the corresponding homopolymers were synthesized by free radical polymerization in dimethylformamide as shown in Figure 4.5.

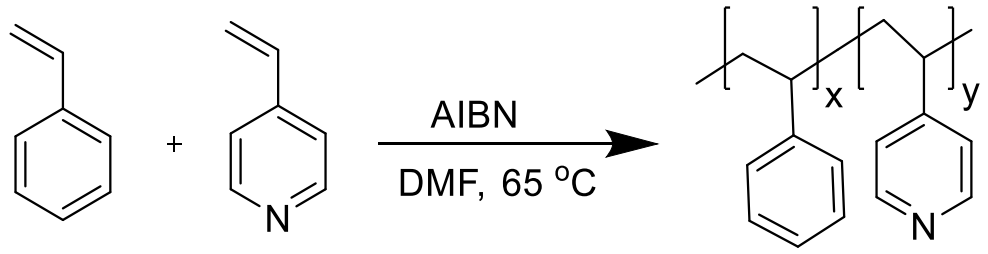

Figure 4.5 Synthesis scheme for poly(4-vinylpyridine-ran-styrene).

The monomers, styrene (Acros Organics, 99%) and 4-vinylpyridine (Sigma-Aldrich, 95%) were purified with stabilizer removal columns (tert-butylcatechol and methyl ether hydroquinone, respectively). The monomers (see Table 4.1 for the moles of each monomer) were dissolved in 500 μL dimethylformamide in a 4 mL Teflon screw capped vial. The vial was purged with nitrogen before and after the addition of the initiator, 2,2'-Azobis(2-methylpropionitrile) (0.235

mmol, Sigma-Aldrich, 98%), capped, and heated at 65 °C overnight to allow for polymerization. After polymerization the polymers were moved to a 50 mL centrifuge tube, precipitated with ether and centrifuged (4200 RPM, 20 minutes). Due to differences in composition poly(4-vinylpyridine) and poly(4-vinylpyridine-*ran*-styrene) 90:10, 75:25, and 50:50 was further dissolved and precipitated (2x) in dimethylformamide and ether (respectively), while poly(styrene), poly(4-vinylpyridine-*ran*-styrene) 25:75, and 10:90 was dissolved and precipitated (2x) in THF and hexanes (respectively). The polymers were dried in vacuo at room temperature overnight and then further dried in vacuo at 80 °C. The incorporation of the monomers was verified using attenuated total reflection infrared spectroscopy (ThermoFisher Nicolet IS50 Infrared spectrophotometer).

Table 4.1 Monomer ratios (v/v%) and the quantity of monomers used in the synthesis of poly(4-vinylpyridine-ran-styrene) (various monomer ratios), poly(4-vinylpyridine), poly(styrene).

Monomer ratios of 4-vinylpyridine: styrene (v/v%)	Volume/moles (4-vinylpyridine: styrene)
100:00	500 μL (4.6 mmol) 4-vinylpyridine
90:10	450 μL (4.2 mmol): 50 μL (0.48 mmol)
75:25	375 μL (3.5 mmol): 125 μL (1.2 mmol)
50:50	250 μL (2.3 mmol): 250 μL (2.4 mmol)
25:75	125 μL (1.2 mmol): 375 μL (3.6 mmol)
10:90	50 μL (.46 mmol): 450 μL (4.3 mmol)
0:100	500 μL (4.8 mmol) styrene

4.4.4 Preparation of Deposition Solutions

CoPc/DMF and CoPc(py)/DMF. The 0.05 mM CoPc/DMF deposition solution was prepared by dissolving 0.0016 g CoPc in 50 mL of DMF in a 100 mL glass media jar (Fisher Scientific). The CoPc(py)/DMF deposition solution was prepared by dissolving 0.0016 g CoPc in 47.5 mL DMF in a 100 mL glass bottle and adding 2.5 mL pyridine. CoPc deposition solutions were sonicated for at least 60 minutes to ensure dispersion of the catalyst. All glass containers used to store CoPc solutions were wrapped in duct tape jackets to protect the catalyst from any photodegradation.

CoPc-polymer and CoPc(py)-polymer. After sonication, the catalyst solution was vortexed at 3000 rpm for 30 seconds to ensure additional dispersion of CoPc. 0.010 g of polymer and 1 mL of CoPc/DMF or CoPc(py)/DMF were added to a 20 mL scintillation vial. The vial was capped, jacketed in duct tape, and sonicated for at least 30 minutes to disperse the polymer.

4.4.5 Preparation of Modified Electrodes

5 mm pyrolytic edge-plane graphite (EPG) electrodes (3.81 mm EPG disk enclosed in epoxy, 0.114 cm^2 effective surface area, Pine Research Instrumentation) or 5 mm glassy carbon

electrodes (GCEs, 4 mm thick, 0.196 cm^2 surface area, Sigradur G, HTW Hochtemperatur-Werkstoffe GmbH) were used as working electrodes. EPG electrodes were polished manually with water on 600 grit silicon carbide polishing paper (Buehler CarbiMet). For studies that were performed with rough polished glassy carbon electrodes (RPGCEs), electrodes were polished manually with ultrapure water on 240, 400, and 600 grit silicon carbide polishing paper (Norton Blue-Bak, Finish 1^{st}, and Buehler CarbiMet, respectively). After polishing, EPGs or RPGCEs were rinsed thoroughly with water and then individually sonicated in isopropyl alcohol and water for at least one minute each, before being rinsed with additional water and dried with N_2. CoPc deposition solutions were vortexed for 30 seconds and 5 µL was dropcasted onto the polished electrodes. The electrodes were dried in a 70 ºC oven for 20 minutes.

4.4.6 Electrochemical Measurements: Rotating Disk Electrovoltammetry – Chronoamperometric Steps

Electrochemical measurements were conducted using a Bio-Logic SP200 potentiostat/galvanostat and accompanying Bio-Logic EC-Lab software. Working electrodes were the CoPc-polymer- or CoPc(py)-polymer modified EPGs described above. Reference electrodes were commercial saturated calomel electrodes (SCEs) that were externally referenced to ferrocenecarboxylic acid in 0.2 M pH 7 phosphate buffer (reference potential is 0.284 V vs. SCE). Auxiliary electrodes were carbon rods (99.999%, Strem Chemicals Inc.). The working electrode and auxiliary electrode were separated by a Nafion membrane. In all cases, unless otherwise noted, each electrochemical experiment was performed at least three times on three independently prepared electrodes. All reported values are the averages of those measurements, and all reported errors are standard deviations or standard errors calculated from standard deviations of measurements.

Rotating disk electrode voltammetry-chronoamperometry experiments were conducted using a custom two-compartment glass cell. The working chamber contained a chamber for the rotating shaft for the working electrode, three gas inlets, and a reference electrode inlet. This chamber contained approximately 30 mL of 0.1 M NaH_2PO_4 electrolyte. The auxiliary electrode chamber contained approximately 15 mL of 0.1 M NaH_2PO_4 electrolyte. The working electrode was assembled using Pine Research Instrumentation E6-series rotating disk electrode (RDE) assembly, attached to an MSR rotator. RDE-CA experiments were conducted under 1600 rpm rotation with CA steps of 0.05 V between -1.00 to -1.25 V vs. SCE. Rotation was carried out to ensure steady-state proton and CO_2 delivery to the surface of the modified electrode. During measurements, the electrolyte was blanketed with CO_2 in addition to the sparging done prior to the experiment to prevent contamination by other gases which could result in other reductive processes occurring. Electrolyte evaporation was minimized in this blanketing process by bubbling CO_2 through the electrolyte's corresponding solvent (H_2O or D_2O). For proton inventory studies, the bubbling solvent was the fraction of protonated solvent that was used in the electrolyte. Before chronoamperometry and cyclic voltammetry steps were completed, the iR drop was measured and compensated at 85%. Ru of most measurements fell in the range of 250-700 Ω.

4.4.7 Electrochemical Measurements: Controlled Potential Electrolysis

Controlled potential electrolysis (CPE) was performed in a custom, gastight, two-chamber U cell as used in prior studies,[14] where the working cell portion was sealed after being purged of all air with CO_2. The modified working electrode (EPG, as described above) was loaded into an RDE internal hardware kit (Pine Research Instrumentation). It was loaded into a custom PEEK sleeve and was a part of the working electrode cell component along with the reference electrode

(SCE) and ~20-30 mL of electrolyte. All inlets of the working chamber were wrapped in Teflon tape to minimize gas escape. The auxiliary chamber was open to air and held ~ 20 mL of electrolyte and the graphitic rod. The two chambers were separated by a Nafion cation exchange membrane. Prior to the experiment, the working chamber was sparged with CO_2 and then was sealed under CO_2 atmosphere. The uncompensated resistance of the cell was measured prior to CPE but was the applied potential was not compensated for iR drop during the CPE measurements. Generally, the resistance of the CPE cell was Ru < 400 Ω. CPE measurements were 2 hours long and held at a potential of -1.25 V vs. SCE.

4.4.8 Product Detection and Quantification

After CPE, gaseous products were detected using gas chromatography (GC) on a Thermo Scientific Trace 1310 system. There were two separate analyzer channels: one for H_2 and one for C_1-C_2 products, and the custom valve system, column configuration, and methods were provided by Thermo Scientific. Gas separation occurred such that H_2 was detected on the first channel using Ar carrier gas and thermal conductivity detector (TCD) and all other gases were detected on the second channel using He carrier gas and separate TCD. Calibration was performed using calibration gas mixtures (SCOTTY Specialty Gas) at H_2 = 0.01%, 0.02%, 0.05%, 0.5%, 1% v/v; CO was calibrated using calibration standards where CO = 0.02%, 0.05%, 0.5%, 1% v/v. Chromatographs were analyzed using the Chromeleon Console WorkStation software.

Faradaic efficiencies of the products were determined by using Equation 4.3

$$FE = \frac{\frac{V_{HS}}{V_g} \times G \times n \times F}{Q}$$

Equation 4.3 Faradaic efficiency as calculated for production of H_2 or CO

In this equation, V_{HS} is the headspace volume in mL of the working chamber, V_g is the molar volume of gas at 25ºC and 1.0 atm (24,500 mL/mol), G is the volume percent of gaseous product determined by GC (%), n is the number of electrons required for each product (n = 2 for H_2 and CO), F is the Faraday constant (C/mol) and Q is the charge passed in Coulombs.

4.4.9 Testing of Metal Contamination Using ICP-MS

In addition to electrochemical characterization, we performed ICP-MS to confirm that there was no metal contamination within the system. The loading of copper, cobalt, iron, chromium, and nickel was determined by digesting the polymer and analyzing the digestate via inductively coupled plasma-mass spectrometry (ICP-MS, PerkinElmer Nexion 2000) in a 15 mL polypropylene centrifuge tube. A mass of 0.01 g of the P4VP was added to 5 mL of 1 M HNO_3 (TraceMetal grade). The mixture was allowed to be shaken overnight (15 h) and then the same polymer-nitric acid mixture was sonicated for 6 h. The polymer/nitric acid mixture was then centrifuged at 4500 rpm for 30 min at 11 ºC in an Eppendorf 5430R refrigerated centrifuge. The nitric acid was then decanted by plastic micropipette, and the decanted nitric acid was injected directly into the ICP-MS without further dilution. The ICP-MS was calibrated using calibration standards for each of the metals (Ricca Chemical). The conversion between the calculated parts per billion measurement and the mass % can be found in Equation 4.4 – Equation 4.6. All metals showed very low detection and likely did not contribute to overall electrocatalysis, and there were no unexpected redox peaks that showed that there was any metal contamination.

$$X \text{ ppb} \times \frac{\frac{1\ \mu\text{g}}{\text{L}}}{1 \text{ ppb}} \times 0.003 \text{ L} = \text{mass of metal in } \mu\text{g}$$

Equation 4.4 Mass of metal in analyte solution (µL)

$$\text{mass in } \mu\text{g} \times \frac{10^{-6}\ \text{g}}{1\ \mu\text{g}} = \text{mass in g}$$

Equation 4.5Mass of metal in analyte solution (g)

$$\frac{\text{mass in g}}{0.01\ \text{g digested}} \times 100\% = \text{mass \% of metal content}$$

Equation 4.6 Percentage mass content within mass of polymer

4.5 Results and Discussion

As discussed in the introduction, we provided evidence for the presence of a proton relay due to the pyridyl residues of the encapsulating polymer by performing electrochemical proton inventory studies, which measured the relative rate of reaction in fractionally deuterated electrolyte. These measurements, similar to rate comparisons proving proton relays in enzymatic systems, were able to show that there was a slight inverse isotope effect where a deuteron has a slight preference to be bonded to a nitrogen from the pyridyl residue. We had an initial hypothesis that we could break down these relays by incorporating a moiety within the polymer that did not show proton hopping ability. As we measured in a previous study, polystyrene did not show a proton relay effect and showed an overall low activity. However, an issue with this method was that CoPc with polystyrene did not have any axial coordination to the Co center, which resulted in the CO_2 addition being the RDS and not the subsequent proton transfer. This resulted in the KIE being equal to 1. In this situation, when the RDS is not dependent on the proton transfer, the proton relay cannot be measured using the proton inventory technique (this is the case for a system such as CoPc-P2VP, where CoPc is a 4-coordinate complex with no axial coordination to the metal center so the KIE = 1, but there is likely a proton relay from the pyridyl residues in the polymer). When CoPc was combined with pyridine (rendering the RDS a proton transfer event) and then further encapsulated in polystyrene (CoPc(py)-PS), the KIE was equal to ~ 3, indicating that the subsequent proton transfer event was the RDS for this system. However, in this case, where there was polystyrene in the polymer film, there was no indication of a proton relay as measured by proton inventory studies.

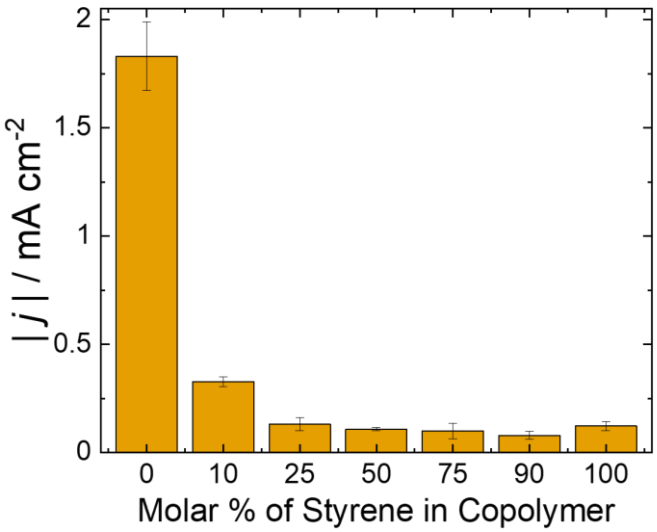

Figure 4.6 Overall current density when CoPc is encapsulated in the P(4VP-c-Sty) as a function of styrene molar % in the copolymer. Data taken in 0.1 M NaH_2PO_4 under 1 atm CO_2 at pH 4.7, where the applied potential was -1.25 V vs. SCE in a 2 minute RDE-CA step with rotation to ensure steady-state substrate delivery at 1600 rpm.

The first experiment goal involved studying activity as a function of styrene concentration in the copolymer (Figure 4.6). We saw that activity decreases as a function of styrene concentration within the copolymer, but that when the styrene concentration is just 10% of the total copolymer concentration, the activity decreases substantially (by nearly 90%). These results were interesting, because other groups in the community, notably the Kaneko studies, used copolymers of 4-vinylpyridine and styrene that matched these concentrations, which may have been artificially inhibiting the overall measured activity that they saw at that time.[21] In another study, they used encapsulated CoPc derivative catalysts (with both substituted cyano groups and sulfano groups) to perform proton reduction. These studies used P(4VP-*c*-Sty) that was synthesized with a molar ratio of 9:1, comparable to the P(90% 4VP-*c*-10%Sty) copolymer.[21] The reasoning for the use of this copolymer was not discussed, but it could be because prior studies that had used the homopolymer of polystyrene as a binding agent to ensure catalyst stability on the surface of a graphitic electrode.

Furthermore, we were interested in the catalytic mechanism and whether it changed based on the concentration of styrene in the polymer. As mentioned in the introduction, the kinetic isotope effect (KIE) assists in understanding whether the rate determining step (RDS) involves a proton transfer event. In general, a KIE = 1 is consistent the RDS being independent of a proton transfer event, while a KIE > 1 is consistent with a proton transfer event being involved in the RDS, due to the enhanced kinetic barrier that is involved in the breaking and reformation of a bond involving an atom that is 100% heavier. The results of this study are outlined in Figure 4.7.

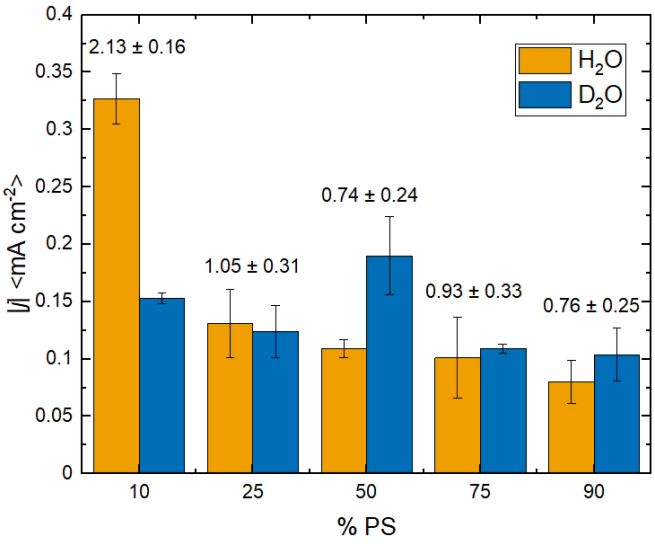

Figure 4.7 Activity of CoPc-P(4VP-c-Sty) in protonated and deuterated electrolyte as a function of styrene molar % within the copolymer, with the kinetic isotope effect listed above each copolymer (KIE, activity in protonated electrolyte divided by activity in deuterated electrolyte).

The results presented in Figure 4.7 were somewhat unexpected. In previous studies (summarized in Table 4.2) we showed that CoPc-P4VP had a KIE ~2.1; CoPc-Polystyrene (CoPc-PS) had a KIE of 1, and CoPc(py)-PS had a KIE of 3. Importantly, the coordination environment was crucial for the RDS – 4-coordinate CoPc environments (CoPc, CoPc-P2VP, and CoPc-PS) all showed KIE of 1, while 5-coordinate CoPc (with axial coordination coming from either the pyridyl residues of the polymer or from a free pyridyl ligand that was added without or prior to polymer encapsulation) showed a KIE of at least 2.1. Since the KIE of CoPc-P(4VP-*c*-Sty) polymers with at least 25% styrene in the copolymer showed a KIE ~ 1, we hypothesized that there may be a loss of axial coordination within the polymer. The results of these KIE studies give us possible insight into the coordination environment, but this loss of coordination could be confirmed using spectroscopic methods. UV-Vis has been used to show evidence for axial coordination, but X-ray absorbance spectroscopy in particular would provide concrete evidence of a dried CoPc-polymer system on an electrode surface (discussed throughout this dissertation, but example data for the CoPc system shown in Figure 1.3 and Figure 3.6. In order to ensure that we were obtaining a 5-coordinate CoPc system, we postulated that performing coordination with pyridine prior to polymer encapsulation would be important. The results of that study are presented in Figure 4.8.

Table 4.2 Summary of KIEs for CoPc within differing environments coordination environments (the 4-coordinate parent complex, with a fifth axial pyridyl ligand, or encapsulated in either coordinating or non-coordinating polymers. Data from Ref. [14]

	Co coordination	KIE
CoPc	4	~1
CoPc-P2VP	4	~1
CoPc-PS	4	~1
CoPc(py)	5	~3
CoPc(py)-PS	5	~3.2
CoPc-P4VP	5	~2.1

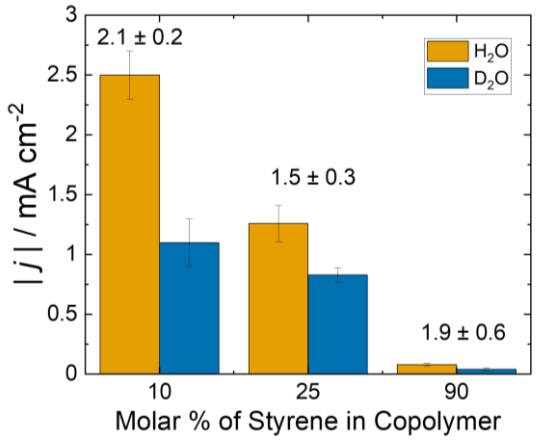

Figure 4.8 Activity in protonated and deuterated electrolyte with the corresponding kinetic isotope effect measurements for CoPc(py) encapsulated by a copolymer comprised of the specified molar % of styrene.

The results presented in Figure 4.8 suggest that axial coordination may have been lost, because the KIEs are different when the 5-coordinate CoPc(py) is encapsulated by the copolymers. It's possible that this loss of axial coordination could be due to the folding of the copolymer, as the sheer number of pyridyl residues far outnumber the number of CoPc sites even within a copolymer consisting of 90% styrene. The data shows that the KIEs for the encapsulating copolymers with the molar styrene concentration equaling 10%, 25%, and 90% were all substantially different from the same KIEs measured without pyridine as an axial ligand. Additionally, the activity is much higher for 10% styrene and 25% styrene, as seen in Table 4.3.

Table 4.3 Comparison of activity CoPc-P(90%4VP-c-10%Sty) CoPc-P(75%4VP-c-25%Sty)

	CoPc activity / mA cm^{-2}	CoPc(py) activity / mA cm^{-2}
CoPc-P(90%4VP-c-10%Sty)	0.33 ± 0.02	2.53 ± 0.18
CoPc-P(75%4VP-c-25%Sty)	0.15 ± 0.03	1.26 ± 0.15

These results are highly interesting because it may suggest that some sort of aggregation or polymer folding that is impacting the overall activity of this system. The KIEs actually suggest that there is still a proton relay mechanism in place (recall that the 5-coordinate CoPc(py)-PS system showed a KIE of 3, while the 5 coordinate CoPc-P4VP system showed a KIE of 2 when there was a proton relay in place via the pyridyl residues of the polymer). In order to confirm this, proton inventory studies must be done to show that there is a deviation from linearity when the relative rates of reaction is plotted against the corresponding fractional deuteration of the electrolyte (for electrochemical studies, this involves the use of measured current densities as the relative rates of reaction). Preliminary results of proton inventory for CoPc(py) encapsulated by P(90%4VP-c-10%Sty) and P(75%4VP-c-w5%Sty) are presented in Figure 4.9a and b, respectively.

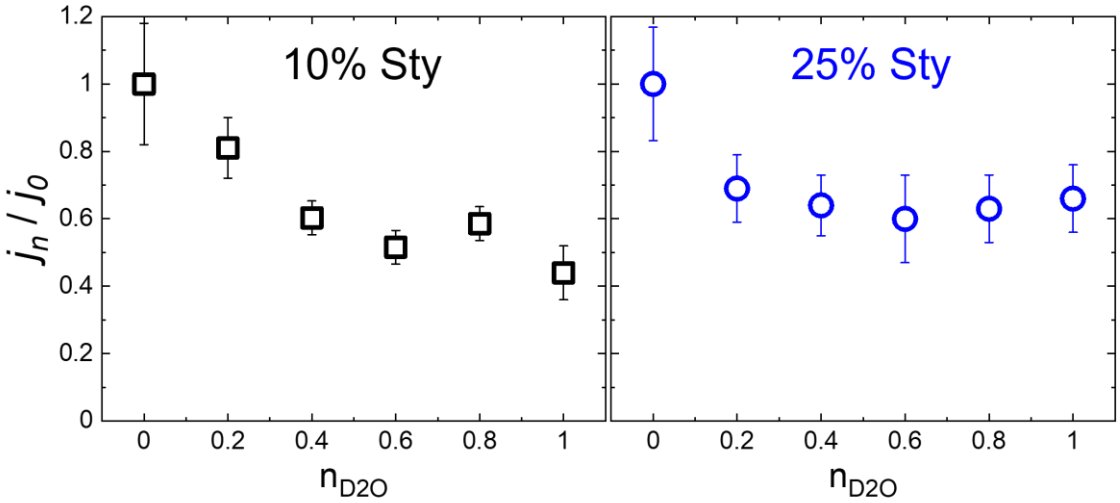

Figure 4.9 Electrochemical proton inventory studies measuring comparative current densities in fractionally deuterated electrolyte compared to 0% deuterated electrolyte plotted against the corresponding fractional deuteration for CoPc(py) with (a) 10% molar styrene within the copolymer and (b) 25% molar styrene within the copolymer.

4.6 Conclusions

Most of the work conducted in the area of polymer-coated electrode catalyst systems has involved the use of homopolymers and has not entirely considered the environment around catalytic sites to tune functionality of the systems. After understanding the importance of the proton delivery system of a proton relay mechanism, we were curious about the impact of shutting down this outer coordination sphere effect using a copolymer where the moieties incorporated into the polymer would not have the ability to transport protons (we chose styrene, as the benzene functional group, where the structure of the moiety would be similar to that of pyridine without having any proton transport abilities). I found that with just 10% of styrene in the copolymer, the activity shut down and that with just 25% styrene within the copolymer, the activity matched that of 100% polystyrene (Figure 4.6). When observing the kinetic isotope effect (KIE), I saw that the KIE for copolymers > 10% showed a KIE of ~ 1 with large errors, which somewhat indicated that axial coordination by the pyridyl moieties within the polymer was being lost (Figure 4.7). To confirm this, I performed polymer encapsulation by CoPc(py), ensuring 5-coordinate character by the free pyridyl residue. At 10% styrene, 25% styrene, and 90% styrene, the CoPc-copolymer, the KIE was closer to 2 (again, with large errors), but the activity for 10% and 25% styrene was substantially higher than without the free pyridine (Figure 4.8). The clear next steps for this project would be rigid proton inventory studies, but preliminary results (Figure 4.9) showed deviation from linearity for CoPc(py)-P(90%4VP-c-10% Sty) and CoPc(py)-P(75%4VP-c-25%Sty), and would indicate that the proton relay is still intact. Future work in this area should discuss whether other polymers with moieties of varying pKa still exhibit the proton relay.

4.7 Recommendations for Future Work

In addition to continuing to study the proton inventory work shown in Figure 4.9 (specifically performing activity studies at other n_{D2O} values), I suggest that the use of other polymers as encapsulating or binding agents may be useful to this community. I performed activity studies with homopolymers synthesized in collaboration with Professor Matzgfer's lab (shown in Figure 4.10). Two polymers had not been studied for CoPc CO2RR: polytriazole and polyethyleneimine). They were studied with the parent CoPc complex and the 5-coordinate CoPc(py). They each showed an increase in activity when CoPc had first been coordinated by the pyridyl ligand but showed similar or enhanced activity compared to P4VP. It would be highly interesting to test these polymers further for proton relay ability or the activity/selectivity effects of the pKa of the protonated moieties within the polymer.

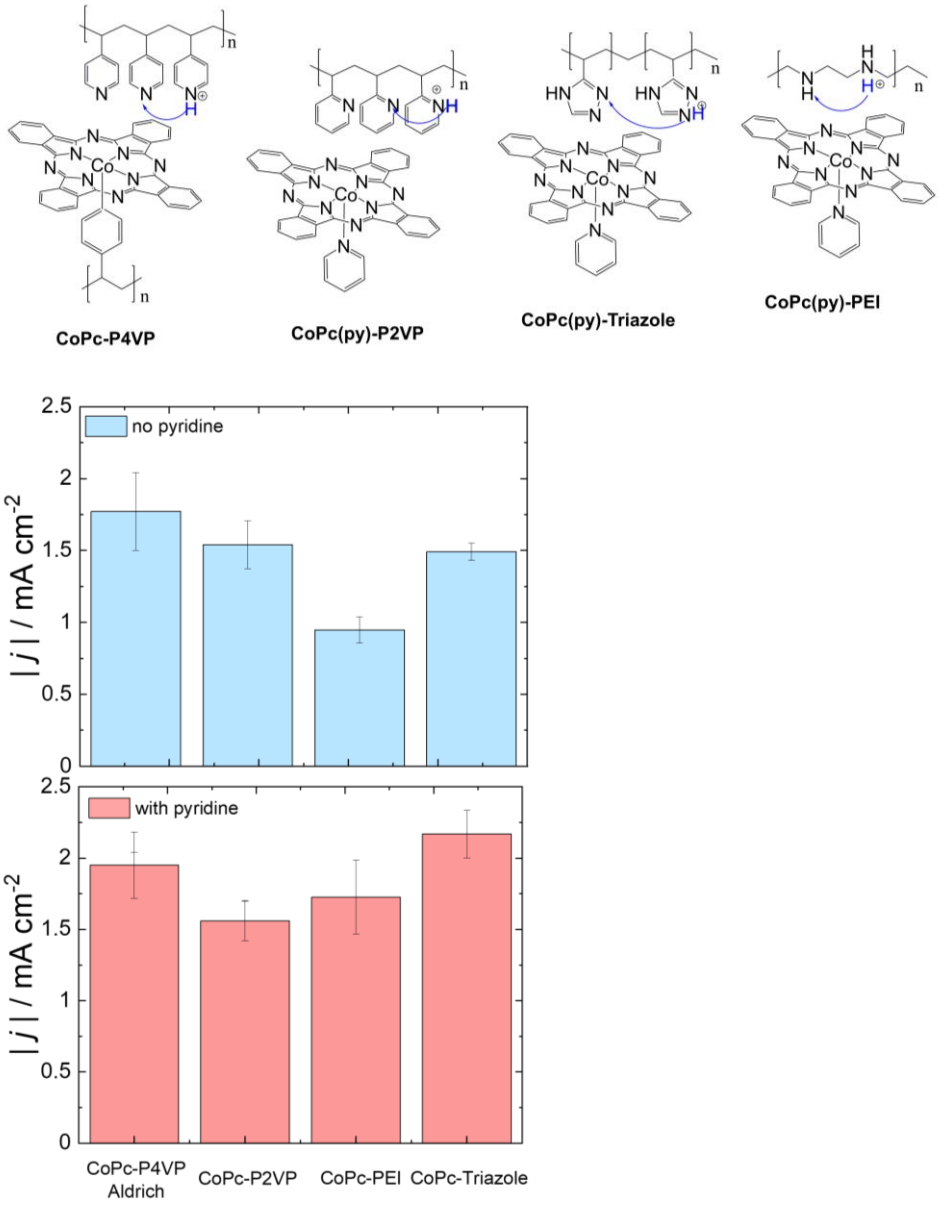

Figure 4.10 (a) Polymers encapsulating CoPc for CO_2RR: P4VP, poly(2-vinylpyridine) (P2VP), poly vinyl triazole (Triazole), and poly-(ethyleneimine) (PEI) (b) Activity by polymer-encapsulated CoPc (c) Activity for CO_2RR by CoPc(py) encapsulated by the corresponding polymer. Experiments performed on RP-GCE as described in the experimental section and activity data are from RDE-CAs at -1.25 V vs. SCE in pH 4.7 NaH_2PO4.

4.8 Supplementary Information

4.8.1 Supplementary Tables

Table 4.4 Activity data of CoPc-copolymer as shown in Figure 4.6. Activity data were taken using rotating disk electrode chronoamperometry steps (RDE-CAs) where the electrode was under constant rotation at 1600 rpm to ensure steady substrate delivery from the electrolyte, which was 0.1 M NaH_2PO_4 at pH 5 in 100% H_2O. The electrodes were edge-plane graphite and modified according to the Experimental Section.

Molar % Styrene in Copolymer / %	$\lvert j \rvert$ / mA cm^{-2}
0	1.98 ± 0.32
10	0.33 ± 0.02
25	0.13 ± 0.03
50	0.11 ± 0.01
75	0.10 ± 0.03
90	0.08 ± 0.02
100	0.12 ± 0.02

Table 4.5 Activity data of CoPc-copolymer as shown in Figure 4.7. Activity data were taken using rotating disk electrode chronoamperometry steps (RDE-CAs) where the electrode was under constant rotation at 1600 rpm to ensure steady substrate delivery from the electrolyte, which was 0.1 M NaH_2PO_4 at pH 5 in 100% H_2O or 100% D_2O. The electrodes were edge-plane graphite and modified according to the Experimental Section.

Molar % Styrene in Copolymer / %	$\lvert j \rvert$ in H_2O / mA cm^{-2}	$\lvert j \rvert$ in D_2O / mA cm^{-2}
10	0.33 ± 0.02	0.15 ± 0.01
25	0.13 ± 0.03	0.12 ± 0.02
50	0.11 ± 0.01	0.15 ± 0.08
75	0.10 ± 0.03	0.11 ± 0.01
90	0.08 ± 0.02	0.10 ± 0.03

Table 4.6 Activity data of CoPc (py)-copolymer as shown in Figure 4.8. Activity data were taken using rotating disk electrode chronoamperometry steps (RDE-CAs) where the electrode was under constant rotation at 1600 rpm to ensure steady substrate delivery from the electrolyte, which was 0.1 M NaH_2PO_4 at pH 5 in 100% H_2O or 100% D_2O. The electrodes were edge-plane graphite and modified according to the Experimental Section.

Molar % Styrene in Copolymer / %	**$\lvert j \rvert$ in H_2O / mA cm^{-2}**	**$\lvert j \rvert$ in D_2O / mA cm^{-2}**
10	2.53 ± 0.18	1.11 ± 0.20
25	1.26 ± 0.15	0.83 ± 0.06
90	0.08 ± 0.01	0.04 ± 0.01

Table 4.7 Activity data of CoPc-poly(90%4VP-co-10%Sty) as shown in Figure 4.9a. Activity data were taken using rotating disk electrode chronoamperometry steps (RDE-CAs) where the electrode was under constant rotation at 1600 rpm to ensure steady substrate delivery from the electrolyte, which was 0.1 M NaH_2PO_4 at pH 5 in fractionally deuterated electrolyte. The electrodes were edge-plane graphite and modified according to the Experimental Section. Relative rates of reaction were activity as measured by current density in the corresponding fractionally deuterated electrolyte (j_n) divided by the current density in 0% deuterated electrolyte (j_0).

n_{D2O}	$\lvert j_n/j_0 \rvert$
0	1 ± 0.18
0.2	0.81 ± 0.09
0.4	0.60 ± 0.05
0.6	0.52 ± 0.05
0.8	0.58 ± 0.05
1	0.44 ± 0.08

Table 4.8 Activity data of CoPc-poly(75%4VP-co-25%Sty) as shown in Figure 4.9b. Activity data were taken using rotating disk electrode chronoamperometry steps (RDE-CAs) where the electrode was under constant rotation at 1600 rpm to ensure steady substrate delivery from the electrolyte, which was 0.1 M NaH_2PO_4 at pH 5 in fractionally deuterated electrolyte. The electrodes were edge-plane graphite and modified according to the Experimental Section. Relative rates of reaction were activity as measured by current density in the corresponding fractionally deuterated electrolyte (j_n) divided by the current density in 0% deuterated electrolyte (j_0).

n_{D2O}	$\lvert j_n/j_0 \rvert$
0	1 ± 0.17
0.2	0.69 ± 0.10
0.4	0.64 ± 0.09
0.6	0.60 ± 0.13
0.8	0.63 ± 0.10
1	0.66 ± 0.10

Table 4.9 Inductively coupled plasma mass spectrometry (ICP-MS) results which rendered a mass % of metal content within the polymer. Digestion performed according to the Experimental Section. Error was the standard deviation of three measurements. All tests resulted in very low metal contamination.

	Cobalt	Copper	Chromium	Nickel	Iron
Mass % Metal Content / %	0.000145	0.000309	0.001392	-0.00018	0.002289
Standard Deviation / %	0.000134	9.71E-05	8.44E-05	0.000154	0.000624

Table 4.10 Results of controlled potential electrolysis experiments (CPEs) for CoPc encapsulated by the lab-synthesized P4VP and CoPc(py) encapsulated by copolymers P(90%4VP-c-10%Sty) and P(75%4VP-c-25%Sty), showing high levels of selectivity for CO_2RR in each case.

	FE CO	Std Dev	FE H2	Std Dev	Q	Std Dev
100%P4VP	89.5	5.7	7.02	0.32	1.15	0.2
(py)90%4VP10%Sty	87.7	0.5	5	1.1	1.2	0.15
(py)75%P4VP25%Sty	87.6	2.7	4.8	0.8	0.8	0.07

4.8.2 Supplementary Figures

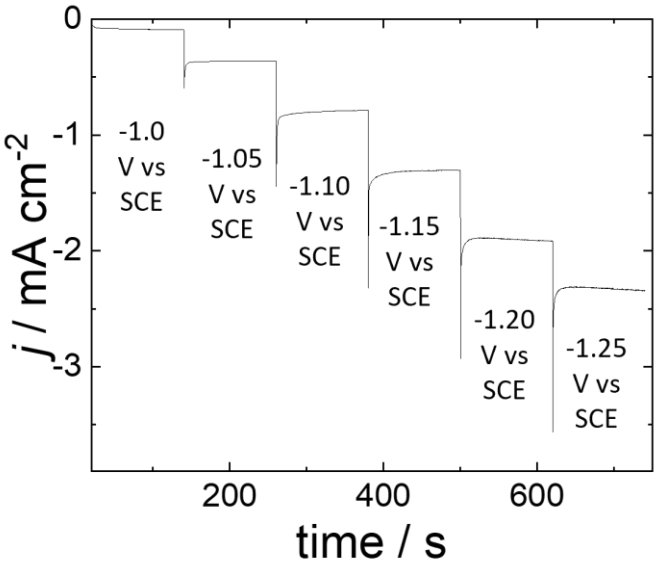

Figure 4.11 CoPc-100% P4VP in 100% H_2O as seen in Figure 4.6 representative rotating disk chronoamperometry steps with potentials listed in the figure. The 2-min RDE-CA steps at the six potentials specified were performed at 1600 rpm to ensure steady-state substrate delivery from electrolyte, which was 0.1 M NaH_2PO_4 at pH 4.7 under CO_2.

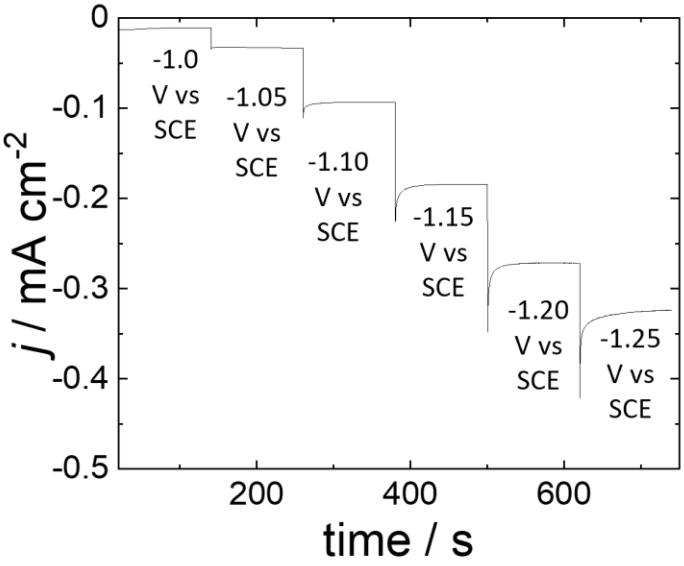

Figure 4.12 CoPc-90% P4VP in 100% H_2O as seen in Figure 4.6 representative rotating disk chronoamperometry steps with potentials listed in the figure. The 2-min RDE-CA steps at the six potentials specified were performed at 1600 rpm to ensure steady-state substrate delivery from electrolyte, which was 0.1 M NaH_2PO_4 at pH 4.7 under CO_2.

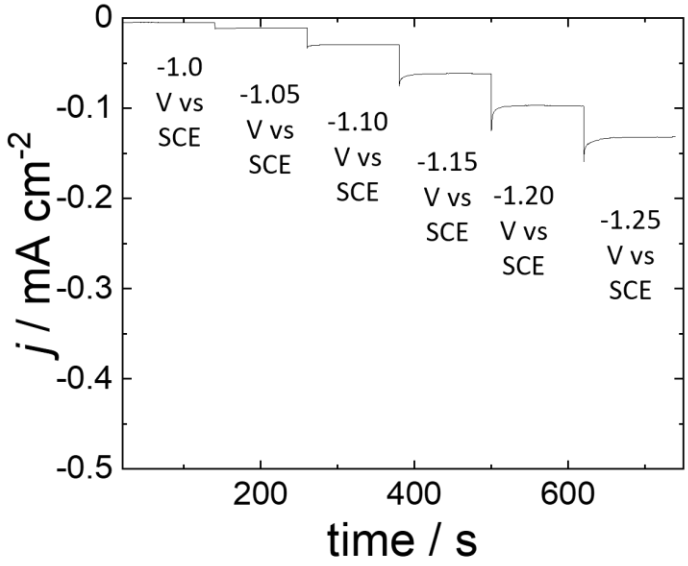

Figure 4.13 CoPc-75% P4VP in 100% H_2O as seen in Figure 4.6 representative rotating disk chronoamperometry steps with potentials listed in the figure. The 2-min RDE-CA steps at the six potentials specified were performed at 1600 rpm to ensure steady-state substrate delivery from electrolyte, which was 0.1 M NaH_2PO_4 at pH 4.7 under CO_2.

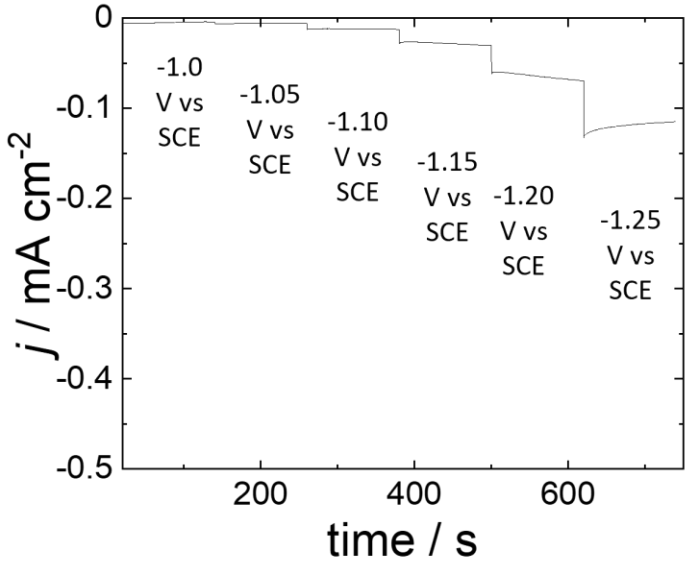

Figure 4.14 CoPc-50% P4VP in 100% H_2O as seen in Figure 4.6 representative rotating disk chronoamperometry steps with potentials listed in the figure. The 2-min RDE-CA steps at the six potentials specified were performed at 1600 rpm to ensure steady-state substrate delivery from electrolyte, which was 0.1 M NaH_2PO_4 at pH 4.7 under CO_2.

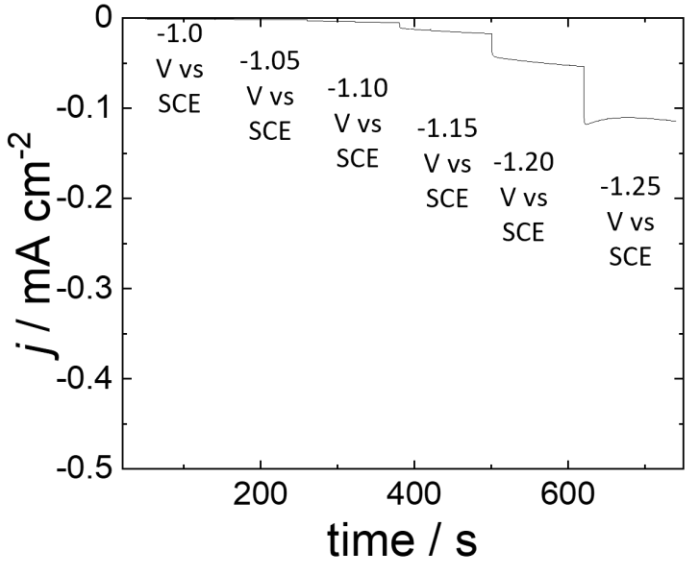

Figure 4.15 CoPc-25% P4VP in 100% H_2O as seen in Figure 4.6 representative rotating disk chronoamperometry steps with potentials listed in the figure. The 2-min RDE-CA steps at the six potentials specified were performed at 1600 rpm to ensure steady-state substrate delivery from electrolyte, which was 0.1 M NaH_2PO_4 at pH 4.7 under CO_2.

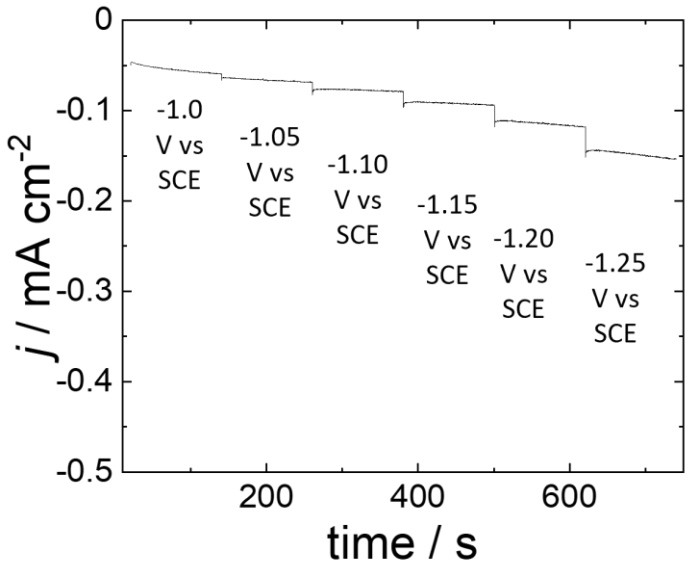

Figure 4.16 CoPc-10% P4VP in 100% H_2O as seen in Figure 4.6 representative rotating disk chronoamperometry steps with potentials listed in the figure. The 2-min RDE-CA steps at the six potentials specified were performed at 1600 rpm to ensure steady-state substrate delivery from electrolyte, which was 0.1 M NaH_2PO_4 at pH 4.7 under CO_2.

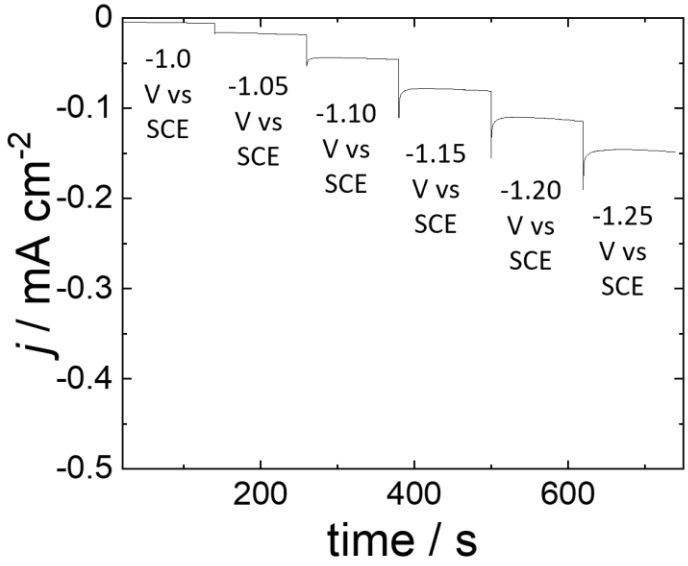

Figure 4.17 CoPc-90% P4VP in 100% D_2O as seen in Figure 4.7 representative rotating disk chronoamperometry steps with potentials listed in the figure. The 2-min RDE-CA steps at the six potentials specified were performed at 1600 rpm to ensure steady-state substrate delivery from electrolyte, which was 0.1 M NaH_2PO_4 at pH 4.7 under CO_2.

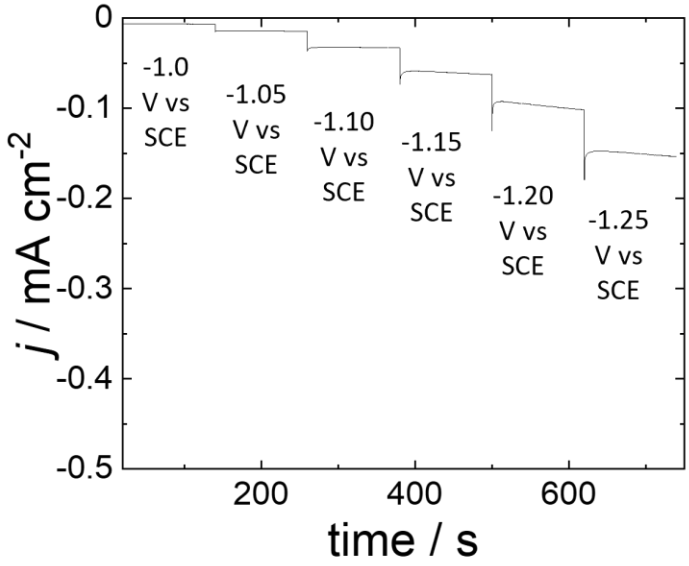

Figure 4.18 CoPc-75% P4VP in 100% D_2O as seen in Figure 4.7 representative rotating disk chronoamperometry steps with potentials listed in the figure. The 2-min RDE-CA steps at the six potentials specified were performed at 1600 rpm to ensure steady-state substrate delivery from electrolyte, which was 0.1 M NaH_2PO_4 at pH 4.7 under CO_2.

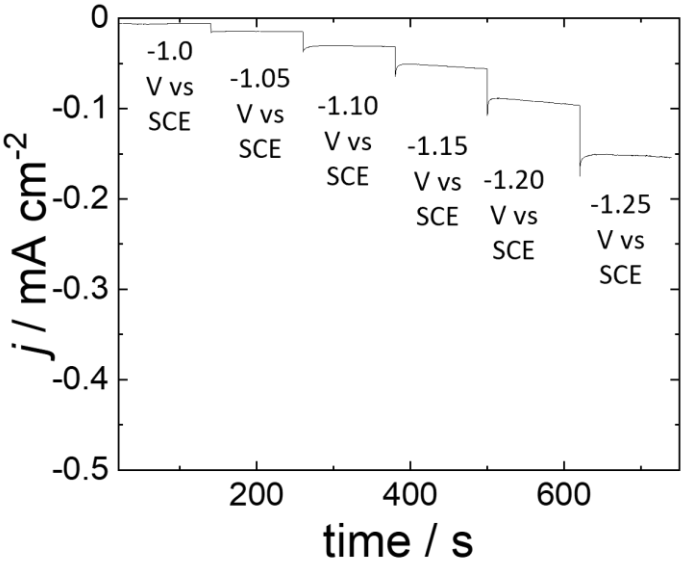

Figure 4.19 CoPc-50% P4VP in 100% D_2O as seen in Figure 4.7 representative rotating disk chronoamperometry steps with potentials listed in the figure. The 2-min RDE-CA steps at the six potentials specified were performed at 1600 rpm to ensure steady-state substrate delivery from electrolyte, which was 0.1 M NaH_2PO_4 at pH 4.7 under CO_2.

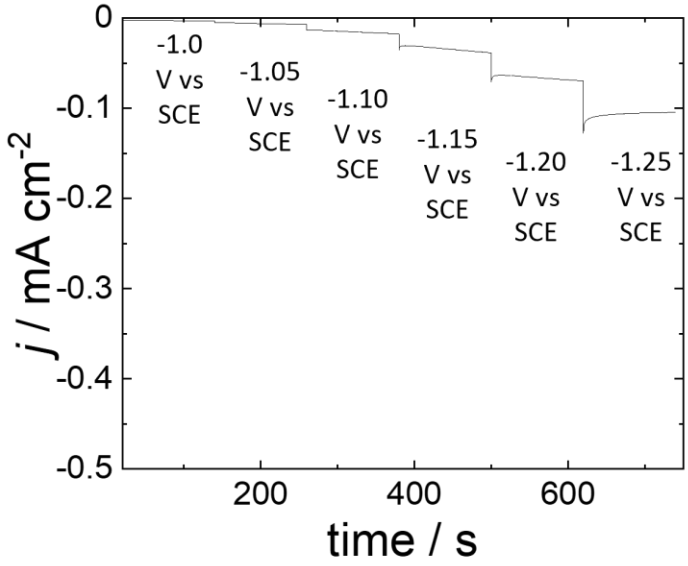

Figure 4.20 CoPc-25% P4VP in 100% D_2O as seen in Figure 4.7 representative rotating disk chronoamperometry steps with potentials listed in the figure. The 2-min RDE-CA steps at the six potentials specified were performed at 1600 rpm to ensure steady-state substrate delivery from electrolyte, which was 0.1 M NaH_2PO_4 at pH 4.7 under CO_2.

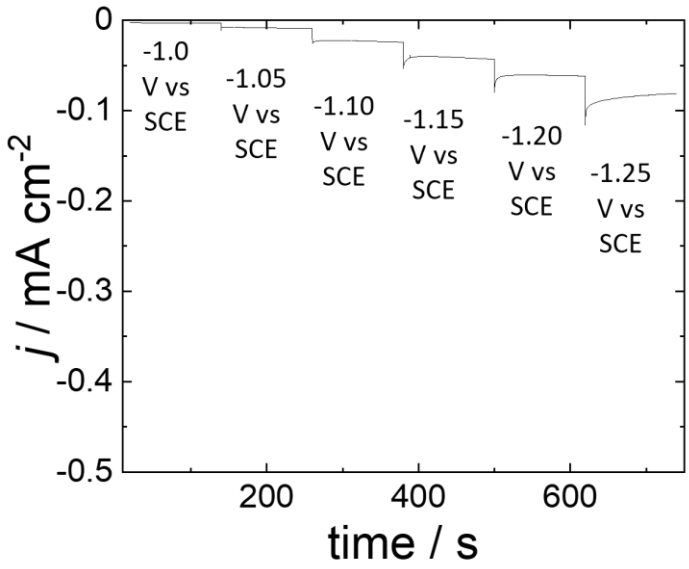

Figure 4.21 CoPc-100% P4VP in 100% D_2O as seen in Figure 4.7 representative rotating disk chronoamperometry steps with potentials listed in the figure. The 2-min RDE-CA steps at the six potentials specified were performed at 1600 rpm to ensure steady-state substrate delivery from electrolyte, which was 0.1 M NaH_2PO_4 at pH 4.7 under CO_2.

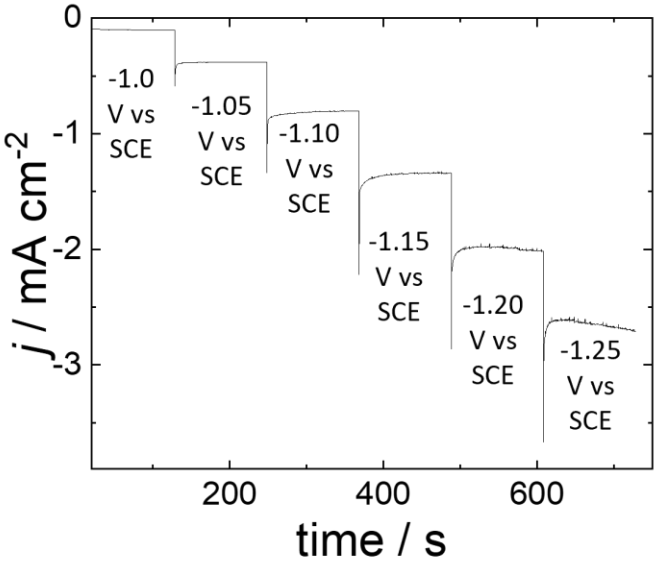

Figure 4.22 CoPc(py) 90% P4VP 100% H_2O as seen in Figure 4.8 representative rotating disk chronoamperometry steps with potentials listed in the figure. The 2-min RDE-CA steps at the six potentials specified were performed at 1600 rpm to ensure steady-state substrate delivery from electrolyte, which was 0.1 M NaH_2PO_4 at pH 4.7 under CO_2.

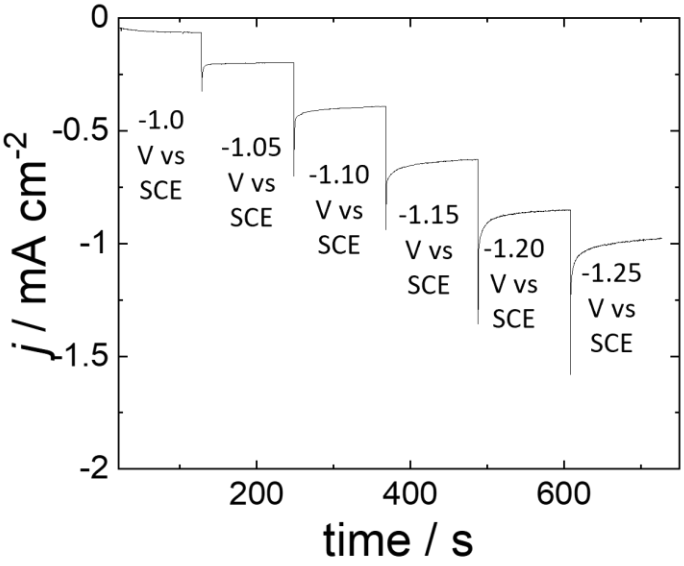

Figure 4.23 CoPc(py) 90% P4VP 100% D_2O as seen in Figure 4.8 representative rotating disk chronoamperometry steps with potentials listed in the figure. The 2-min RDE-CA steps at the six potentials specified were performed at 1600 rpm to ensure steady-state substrate delivery from electrolyte, which was 0.1 M NaH_2PO_4 at pH 4.7 under CO_2.

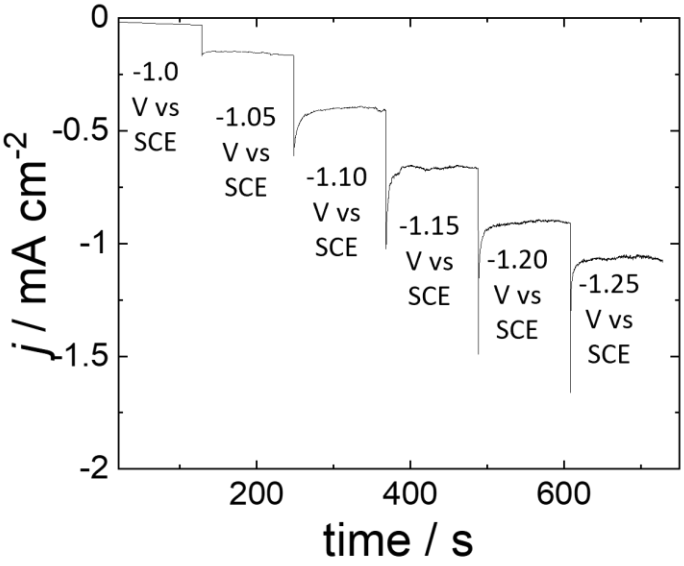

Figure 4.24 CoPc(py) 75% P4VP 100% H_2O as seen in Figure 4.8 representative rotating disk chronoamperometry steps with potentials listed in the figure. The 2-min RDE-CA steps at the six potentials specified were performed at 1600 rpm to ensure steady-state substrate delivery from electrolyte, which was 0.1 M NaH_2PO_4 at pH 4.7 under CO_2.

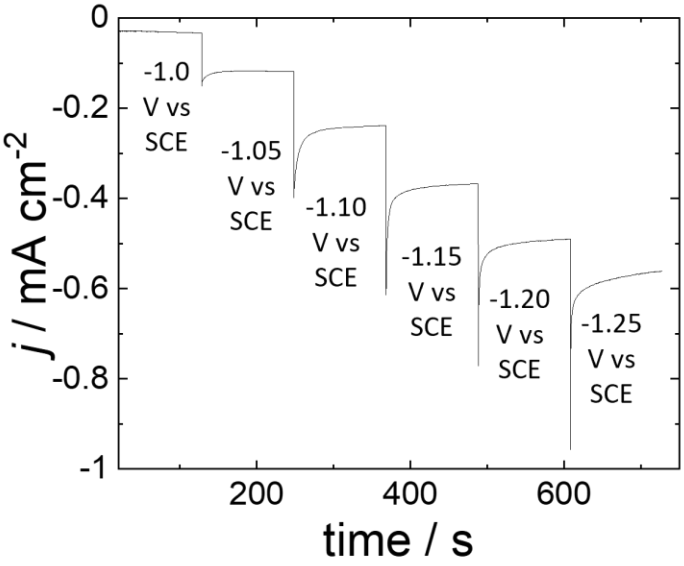

Figure 4.25 CoPc(py) 75% P4VP 100% D_2O as seen in Figure 4.8 representative rotating disk chronoamperometry steps with potentials listed in the figure. The 2-min RDE-CA steps at the six potentials specified were performed at 1600 rpm to ensure steady-state substrate delivery from electrolyte, which was 0.1 M NaH_2PO_4 at pH 4.7 under CO_2.

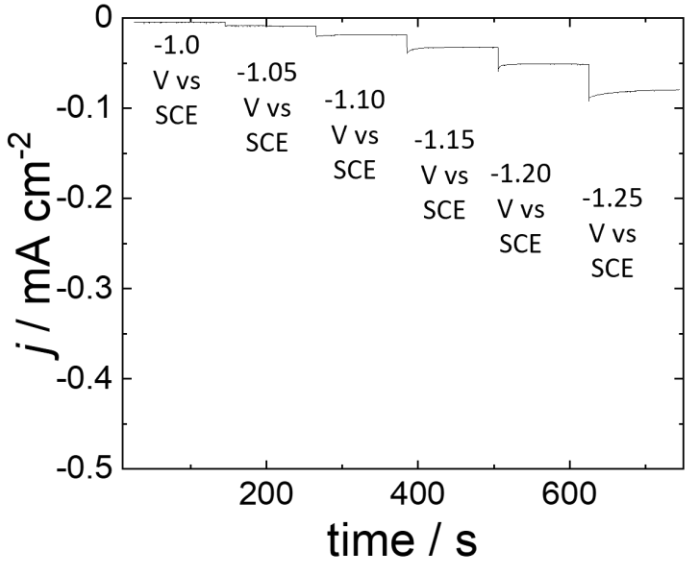

Figure 4.26 CoPc(py) 10% P4VP 100% H_2O as seen in Figure 4.8 representative rotating disk chronoamperometry steps with potentials listed in the figure. The 2-min RDE-CA steps at the six potentials specified were performed at 1600 rpm to ensure steady-state substrate delivery from electrolyte, which was 0.1 M NaH_2PO_4 at pH 4.7 under CO_2.

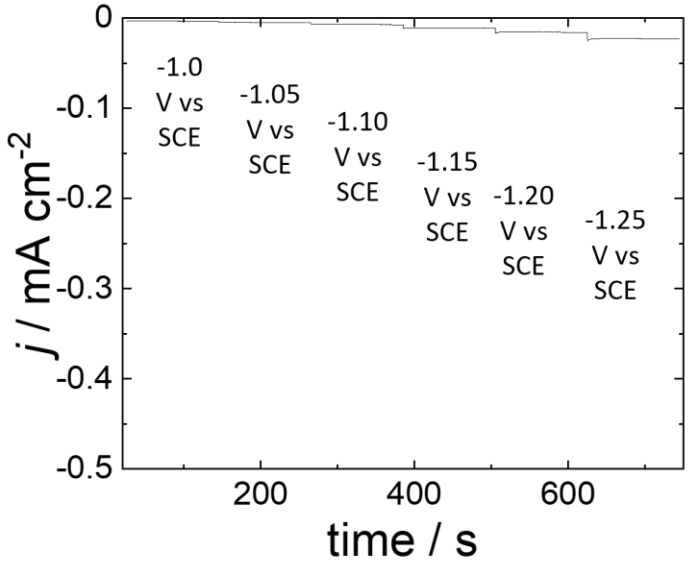

Figure 4.27 CoPc(py) 10% P4VP 100% D_2O as seen in Figure 4.8 representative rotating disk chronoamperometry steps with potentials listed in the figure. The 2-min RDE-CA steps at the six potentials specified were performed at 1600 rpm to ensure steady-state substrate delivery from electrolyte, which was 0.1 M NaH_2PO_4 at pH 4.7 under CO_2.

4.9 References

(1) Esposito, D. V. "Membrane-Coated Electrocatalysts—An Alternative Approach To Achieving Stable and Tunable Electrocatalysis," *ACS Catalysis* **2018**, *8*, 457-465. http://dx.doi.org/10.1021/acscatal.7b03374

(2) Herranz, J.; Pătru, A.; Fabbri, E.; Schmidt, T. J. "Co-electrolysis of CO2 and H2O: From electrode reactions to cell-level development," *Current Opinion in Electrochemistry* **2020**, *23*, 89-95. http://dx.doi.org/https://doi.org/10.1016/j.coelec.2020.05.004

(3) Soucy, T. L.; Dean, W. S.; Zhou, J.; Rivera Cruz, K. E.; McCrory, C. C. L. "Considering the Influence of Polymer–Catalyst Interactions on the Chemical Microenvironment of Electrocatalysts for the CO2 Reduction Reaction," *Accounts of Chemical Research* **2022**. http://dx.doi.org/10.1021/acs.accounts.1c00633

(4) Liu, Y.; Leung, K. Y.; Michaud, S. E.; Soucy, T. L.; McCrory, C. C. L. "Controlled Substrate Transport to Electrocatalyst Active Sites for Enhanced Selectivity in the Carbon Dioxide Reduction Reaction," *Comments on Inorganic Chemistry* **2019**, *39*, 242-269. http://dx.doi.org/10.1080/02603594.2019.1628025

(5) Corbin, N.; Zeng, J.; Williams, K.; Manthiram, K. "Heterogeneous molecular catalysts for electrocatalytic CO2 reduction," *Nano Research* **2019**, *12*, 2093-2125. http://dx.doi.org/10.1007/s12274-019-2403-y

(6) Casado-Coterillo, C.; Marcos-Madrazo, A.; Garea, A.; Irabien, Á. "An Analysis of Research on Membrane-Coated Electrodes in the 2001–2019 Period: Potential Application to CO2 Capture and Utilization," *Catalysts* **2020**, *10*. http://dx.doi.org/10.3390/catal10111226

(7) Costentin, C.; Savéant, J.-M. "Molecular approach to catalysis of electrochemical reaction in porous films," *Current Opinion in Electrochemistry* **2019**, *15*, 58-65. http://dx.doi.org/https://doi.org/10.1016/j.coelec.2019.03.014

(8) Meshitsuka, S.; Ichikawa, M.; Tamaru, K. "Electrocatalysis by metal phthalocyanines in the reduction of carbon dioxide," *Journal of the Chemical Society, Chemical Communications* **1974**, 158-159. http://dx.doi.org/10.1039/C39740000158

(9) Yoshida, T.; Tsutsumida, K.; Teratani, S.; Yasufuku, K.; Kaneko, M. "Electrocatalytic reduction of CO2 in water by [Re(bpy)(CO)3Br] and [Re(terpy)(CO)3Br] complexes incorporated into coated nafion membrane (bpy = 2,2′-bipyridine; terpy = 2,2′;6′,2″-terpyridine)," *Journal of the Chemical Society, Chemical Communications* **1993**, 631-633. http://dx.doi.org/10.1039/C39930000631

(10) Yoshida, T.; Iida, T.; Shirasagi, T.; Lin, R.-J.; Kaneko, M. "Electrocatalytic reduction of carbon dioxide in aqueous medium by bis(2,2′: 6′,2″-terpyridine)cobalt(II) complex incorporated into a coated polymer membrane," *Journal of Electroanalytical Chemistry* **1993**, *344*, 355-362. http://dx.doi.org/https://doi.org/10.1016/0022-0728(93)80066-Q

(11) Yoshida, T.; Kamato, K.; Tsukamoto, M.; Iida, T.; Schlettwein, D.; Wöhrle, D.; Kaneko, M. "Selective electroacatalysis for CO2 reduction in the aqueous phase using cobalt phthalocyanine/poly-4-vinylpyridine modified electrodes," *Journal of Electroanalytical Chemistry* **1995**, *385*, 209-225. http://dx.doi.org/https://doi.org/10.1016/0022-0728(94)03762-R

(12) Abe, T.; Yoshida, T.; Tokita, S.; Taguchi, F.; Imaya, H.; Kaneko, M. "Factors affecting selective electrocatalytic co2 reduction with cobalt phthalocyanine incorporated in a polyvinylpyridine membrane coated on a graphite electrode," *Journal of Electroanalytical Chemistry* **1996**, *412*, 125-132. http://dx.doi.org/https://doi.org/10.1016/0022-0728(96)04631-1

(13) Kramer, W. W.; McCrory, C. C. L. "Polymer coordination promotes selective CO2 reduction by cobalt phthalocyanine," *Chemical Science* **2016**, *7*, 2506-2515. http://dx.doi.org/10.1039/C5SC04015A
(14) Liu, Y.; McCrory, C. C. L. "Modulating the mechanism of electrocatalytic CO2 reduction by cobalt phthalocyanine through polymer coordination and encapsulation," *Nature Communications* **2019**, *10*, 1683. http://dx.doi.org/10.1038/s41467-019-09626-8
(15) Liu, Y.; Deb, A.; Leung, K. Y.; Nie, W.; Dean, W. S.; Penner-Hahn, J. E.; McCrory, C. C. L. "Determining the coordination environment and electronic structure of polymer-encapsulated cobalt phthalocyanine under electrocatalytic CO2 reduction conditions using in situ X-Ray absorption spectroscopy," *Dalton Trans* **2020**, *49*, 16329-16339. http://dx.doi.org/10.1039/d0dt01288b
(16) Rivera Cruz, K. E.; Liu, Y.; Soucy, T. L.; Zimmerman, P. M.; McCrory, C. C. L. "Increasing the CO2 Reduction Activity of Cobalt Phthalocyanine by Modulating the σ-Donor Strength of Axially Coordinating Ligands," *ACS Catalysis* **2021**, 13203-13216. http://dx.doi.org/10.1021/acscatal.1c02379
(17) Soucy, T. L.; Liu, Y.; Eisenberg, J. B.; McCrory, C. C. L. "Enhancing the Electrochemical CO2 Reduction Activity of Polymer-Encapsulated Cobalt Phthalocyanine Films by Modulating the Loading of Catalysts, Polymers, and Carbon Supports," *ACS Applied Energy Materials* **2021**. http://dx.doi.org/10.1021/acsaem.1c02689
(18) Venkatasubban, K. S.; Schowen, R. L. "The Proton Inventory Techniqu," *Critical Reviews in Biochemistry* **1984**, *17*, 1-44. http://dx.doi.org/10.3109/10409238409110268
(19) Nakano, S.-i.; Bevilacqua, P. C. "Proton Inventory of the Genomic HDV Ribozyme in Mg2+-Containing Solutions," *Journal of the American Chemical Society* **2001**, *123*, 11333-11334. http://dx.doi.org/10.1021/ja0166850
(20) Li, W.; Li, F.; Yang, H.; Wu, X.; Zhang, P.; Shan, Y.; Sun, L. "A bio-inspired coordination polymer as outstanding water oxidation catalyst via second coordination sphere engineering," *Nature Communications* **2019**, *10*, 5074. http://dx.doi.org/10.1038/s41467-019-13052-1
(21) Zhao, F.; Zhang, J.; Abe, T.; Wöhrle, D.; Kaneko, M. "Electrocatalytic proton reduction by phthalocyanine cobalt derivatives incorporated in poly(4-vinylpyridine-co-styrene) film," *Journal of Molecular Catalysis A: Chemical* **1999**, *145*, 245-256. http://dx.doi.org/https://doi.org/10.1016/S1381-1169(99)00013-8

Chapter 5 Conclusions, Recommendations, and Future Work

5.1 Conclusions

Electrocatalytic CO_2 reduction mediated by polymer-encapsulated cobalt phthalocyanine is one example of a membrane-coated electrode/electrocatalyst, where the transport of CO_2 and protons from the bulk electrolyte, across the electrolyte/membrane interface, and through the membrane to the electrocatalyst (solid-state or molecular) are each crucial for rapid reduction. This particular system offers the special case where the catalyst is dispersed within the membrane, meriting further consideration for the transport of charge from the electrode surface through the polymer film to the CoPc sites to render them catalytically active. In this work, we focused on the transport of protons and electrons by systematically modulating (i) graphite powder loading (ii) bulk pH of the electrolyte and (iii) the polymer itself.

5.1.1 Studying and Enhancing CO_2RR Activity by Modulating Graphite Powder, Polymer, and CoPc Loading

In Chapter 2, I discussed the incorporation of graphite powder into a polymer-encapsulated CoPc system to increase charge transport and therefore activity.[1] We developed a thorough understanding of the catalyst composite system by performing systematic modifications of polymer, graphite powder, and catalyst loading, and I achieved higher activity than previously seen while maintaining a high level of reaction selectivity to produce CO over the competing HER. These results were on par with the turnover frequencies observed in the literature for CoPc with carbon supports as summarized in Table 2.1. Importantly, I found that the addition of graphite powder increased activity, but that method development including centrifugation was necessary for producing optimal activity with comparable catalyst and polymer loadings.

I also developed a procedure to measure CoPc loading via ICP-MS and showed that increasing the CoPc and P4VP loading resulted in decreased activity at very high loadings, showing that charge or substrate transport could be limiting overall activity at high thickness. However, we showed that when CoPc and P4VP loading was increased along with the GP, rendering the CoPc:P4VP:GP ratio constant, there was no decrease in activity at increased loadings but rather a plateau effect, even with very low concentrations of graphite powder loading (with low levels of graphite loading when the graphite was not added along with CoPc and P4VP, the activity decreased).

The reaction selectivity for CO_2RR over the competing hydrogen evolution reaction (HER) remained high, with ~85% of Faradaic charge going toward the production of CO. The results of this study are important for members of the community developing molecular catalysts for

electrocatalytic purposes, particularly if carbon supports are being incorporated into a catalyst-polymer composite system.

5.1.2 Modulating Electrolyte pH to Understand the Impact of Bulk Proton Concentration on CO_2 Reduction Activity, Selectivity, and Mechanism

Understanding the proton transport from the electrolyte to the polymer, across the polymer, and through the polymer to CoPc sites results in a complicated system due to the buffered electrolyte and artificial buffering due to the pKa of the protonated pyridinium moieties within the polymer. One way to understand this system is by systematically changing the concentration of protons in the electrolyte. In Chapter 3, I discuss how the modulation of electrolyte pH impacts the fractional protonation of the polymer, and therefore impacted the activity, selectivity, and mechanism as measured by kinetic isotope effect studies.

First, I determined the fractional protonation of pyridyl residues within the polymer increased as the electrolyte pH decreased. Infrared spectroscopy was performed and an absorbance associated with a ring breathing mode unique to pyridinium (compared to non-protonated pyridine) was measured. We showed that the pH affected the activity, as an increase in pH resulted in a decrease in overall activity but a plateau of activity for the production of CO. This was due to the selectivity phenomenon, which saw an increase in Faradaic efficiency for CO production with an increase in pH. Finally, the kinetic isotope effect (KIE) revealed that increasing pH resulted in a decrease in measured KIE. In past studies, we have interpreted this to mean that the mechanism was not rate-limited on a proton transfer event.

In studying this phenomenon, I performed an electrolyte dependence study, finding that the KIE for the HER changed as a function of electrolyte concentration. To further understand this, IR spectroscopy was again performed to measure the fractional protonation of the pyridyl residues within the polymer, and found that at a constant pH, fractional protonation increased as a function of electrolyte concentration. This study has implications for the ways that we consider

experimental parameters such as pH and electrolyte concentration, and how they can impact the rate-limiting steps of electrocatalysis.

5.1.3 Incorporating Styrene as an Encapsulating Co-Moiety for Polymer-Encapsulated CoPc CO_2RR

In Chapter 4, I discuss the incorporation of styrene as a co-moiety within a copolymer along with 4-vinylpyridine. This model system was used to show that the proton relay effect was highly important to the efficient reduction of CO_2 to CO. These polymers were synthesized in collaboration with the Matzger group, where they used random copolymer synthesis with different concentrations of styrene monomers to create the copolymers, which rendered copolymers with corresponding molar concentrations of styrene within the polymer, as confirmed by FTIR. Interestingly, we found that even with 10% styrene in the copolymer, activity dropped by 90%, and all other styrene copolymer concentrations showed very low activity. When the 5-coordinate CoPc(pyridine) complex was synthesized and then later encapsulated in the copolymers, the loss in activity with 10% of styrene in the copolymer was less distinct, showing that there could be a decrease in coordination from the pyridyl residues of the polymer even at low styrene concentrations. Furthermore, when we tested these copolymers against a blend composite of these polymers, we found that the blend polymers performed with the same characteristics as the copolymers.

5.2 Recommendations and Future Work

Cobalt phthalocyanine is undergoing a highly intense study as an electrocatalyst for the electrocatalytic CO_2RR.[2-29] The electronic properties of CoPc in addition to its low cost and reported ability to perform a multielectron reduction of CO_2 to methanol certainly warrant its study. I propose that some additional studies might be useful to elucidate its interesting properties and apply them to other electrocatalytic systems.

5.2.1 Study of CO_2 in Commonly Used Aqueous Buffer and Electrolyte Systems

The concentration of CO_2 in aqueous electrolyte is a challenge due to its reluctance to dissolve in water as a highly nonpolar molecule. I propose that the knowledge of the concentration of CO_2 in commonly used aqueous electrolyte could benefit the electrochemical community as they study the CO_2RR. Importantly, the concentration of CO_2 in aqueous buffers and electrolytes has not been quantitatively reported across many electrolytes that are used for CO_2RR (specifically, the CO_2 concentrations within phosphate, perchlorate, acetate, and carbonate buffers have not been quantitatively reported). A recent publication did quantify the amount of carbon as a function of different electrolyte systems,[30] but there are other buffers that would be useful to study. Additionally, proving the changing CO_2 concentration as a function of pH, electrolyte concentration, and solvent (i.e. water compared to deuterium oxide). A study that measures the carbon concentration using a total carbon analyzer would be helpful for the community to report, quantitatively, the carbon concentrations within these electrolyte buffer systems.

5.2.2 Comparative Study of Carbon Supports

With the ubiquitous nature of CoPc-catalyzed CO_2RR (see Table 2.1for a literature review of the many CoPc catalyst systems used for the CO_2RR) and the incorporation of a variety of types of carbon supports to enhance the activity measured through these reactions, it could be useful for the community to have a standard approach to measuring activity and selectivity metrics in a standardized way. Although activity and selectivity have been studied as a function of different carbon supports, there are additional studies that could be useful to understand the chemical microenvironment that is present when carbon supports are added to the environment. Specifically, there is evidence that the metal centers of phthalocyanines and porphyrins can interact with heteroatoms of oxygen, nitrogen, and sulfur.[31,32] Studies that have performed X-ray absorbance spectroscopy have seen a change in absorbance at energy levels that correspond with loss of 4-coordinate character (perhaps suggesting axial coordination by heteroatoms within the carbon supports). However, this is challenging to interpret due to other electronic changes that occur during interactions with the carbon supports and the CoPc molecule. I suggest that kinetic isotope effect (KIE) studies may contribute some insight to this matter. In previous studies, we have shown that the rate-determining step changes depending on whether CoPc is axially coordinated to pyridine. These KIE studies could indicate whether the metal Co center is interacting with any heteroatoms in the carbon support.

5.2.3 Comparative Study of Polymers for CoPc Encapsulation

An interesting follow-up to the study of electrolyte pH on the activity, selectivity, and mechanism of the CO_2RR would be a systematic study of different polymer types on these characteristics. I began studying the impacts of changing the polymer in Chapter 4, by incorporating styrene residues into the polymer. However, there are a vast number of polymers that could be tested, such as nitrogen or pyridyl-like containing polymers that have varying pKas or CO_2 transport mechanisms. In Table 2.1. a review of results from CoPc-catalyzed CO_2RR and CO reduction (CORR) is presented. Most of these studies use the perfluorinated sulfonic Nafion as a polymeric binding agent, as many in the field use. However, in recent years, there have been several studies showing that Nafion may not be the optimal polymer to use for this purpose. Koper and coworkers showed that for use with their indium protoporphyrin electrocatalyst, the use of Nafion resulted in poor selectivity, activity, and stability when compared to other polymers that contained the ability to coordinate or facilitate proton transport throughout the polymer to the catalyst, which confirms studies from other groups that the use of Nafion does not always result in optimal results.[33-35] Additionally, work in our lab has shown that P4VP or even pyridine is able to disaggregate CoPc particles while Nafion does so with less efficiency.

As a part of our collaboration with the lab of Prof. Matzger, I was able to briefly study the activity of CoPc and CoPc(py) encapsulated by other polymers with possible CO_2 or H^+ transport/hopping abilities (see Figure 4.10). These are just a few examples of polymers other than P4VP that may be useful in this area. With the knowledge that other polymers may be beneficial to the overall performance of CoPc-encapsulated catalysts, a systematic study with different polymers could be interesting in order to determine the importance of the polymer and the optimal identity of polymer moieties to provide stable and active CO_2RR.

5.2.4 Using Infrared Spectroscopy to Determine Fractional Protonation of Poly(4-vinylpyridine-co-styrene)

As discussed in Chapter 4, the use of styrene as a co-moiety within a P4VP polymer layer resulted in a decrease in activity. We originally hypothesized that the addition of styrene as a comonomer would shut down activity by preventing the transport of protons through the proton hopping mechanism, and while this may have been true, we especially saw the importance of axial coordination by a free pyridyl residue in order to achieve maximum activity. However, using the knowledge from the conclusions of Chapter 3, we recognize that fractional protonation of the system could be impacted by the electrolyte concentration. A study measuring the fractional protonation of the polymer as a function of styrene concentration (and determining whether the hydrophobicity of the polymer as styrene becomes a comoiety impacts the overall protonation of the polymer) may assist in understanding this loss in activity with small amounts of styrene in the copolymer.

5.2.5 Electrolyte Identity and Concentration Studies

Chapter 3 discussed the effects of changing bulk pH on the activity and selectivity of the CO_2RR as electrocatalyzed by CoPc-P4VP. Inadvertently, I discovered that electrolyte concentration was crucial for protonation of the polymer film and therefore for proton transport of the system. From those results, I hypothesized that protonation of the polymer film required the wicking of a counteranion from the electrolyte to maintain charge balance within the polymer film. However, one way to confirm this hypothesis would be to perform a bicarbonate/cation dependence study, similar to the study performed by Koper and coworkers using a gold electrode (also in studying the electrocatalytic reduction of CO_2). In this way, the concentration of sodium cation could be held constant, and in a separate study, the sodium cation concentration could be

changing while the bicarbonate concentration is held constant. The details of the electrolyte concentration can be found in Table 2.

Table 5.1 Constant Cation: Concentrations of bicarbonate and perchlorate used to create a constant sodium ion concentration in the electrolyte. Directly adapted from Ref. [36]

$[NaHCO_3]$ / M	$[NaClO_4]$ / M	$[Na^+]$ / M	pH (CO_2 sat.)
0.01	0.49	0.50	5.7
0.05	0.45	0.50	6.2
0.10	0.40	0.50	6.7
0.25	0.25	0.50	7.0
0.50	0	0.50	7.4

Table 5.2 Constant pH and bicarbonate: Concentrations of electrolytes used for a sodium ion concentration dependent study, where the concentration of bicarbonate is constant along with the pH and the concentration of sodium ions is changing. Directly adapted from Ref.[36]

$[NaHCO_3]$ / M	$[NaClO_4]$ / M	$[Na^+]$ / M	pH (CO_2 sat.)
0.10	0	0.10	6.7
0.10	0.10	0.20	6.7
0.10	0.20	0.30	6.7
0.10	0.30	0.40	6.7

This study would involve the changing of the electrolyte cation and anion identity (most of the work discussed here involved the exclusive use of phosphate, while perchlorate was added to the system in Chapter 3 and caused some unexpected effects). This is an important note to consider, as molecular catalysts have been shown to have varying activity and selectivity metrics depending on the identity of the buffers. With this in mind, another study that could be interesting would be to measure the activity and selectivity metrics for CoPc-electrocatalyzed CO_2RR in systems with different electrolyte systems, similar to a study performed by Shafaat and coworkers.[37] In this study using a single $[Ni(cyclam)]^{2+}$ CO_2RR electrocatalyst, they found that the activity varied dramatically. This system could see similar large discrepancies in metrics, possibly due to the many different pH levels and electrolyte identities/concentrations that are present in this area of the literature (a non-exhaustive list found in Table 2.1). A study using different aqueous electrolyte for the CoPc or CoPc-P4VP-electrocatalyzed CO_2RR could be interesting in understanding how electrolyte identity can impact activity and selectivity of this electrochemical reaction.

5.2.6 Measuring the Microenvironment of Molecular Catalysts Using Different Types of Electrodes

One challenging aspect to studying these systems involves the choice of electrode. In the work discussed in this thesis, I worked with two different types of electrodes: edge plane graphite (EPG) electrodes and glassy carbon electrodes (GCEs). EPGs are manufactured in a way that allows for stacks of highly ordered pyrolytic graphite to be a part of the electrode (Figure 5.1). These graphitic sheets are then held together by a polymer epoxy. An SEM image of an EPG with CoPc-P4VP coated on its surface can be found in Figure 2.2. In electrochemical systems such as those discussed within this dissertation, this results in increased surface area to an electrolyte to increase surface area of the electrode, which can clearly be seen in the SEM image.

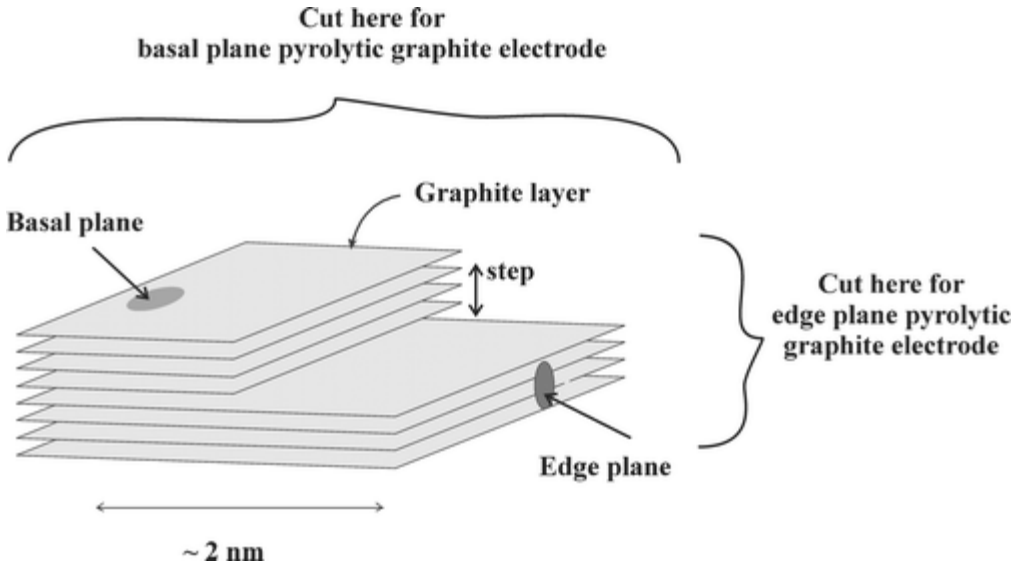

Figure 5.1 Description of the graphite planes used for edge plane and basal plane electrodes. Figure reproduced from Ref. [38]with permission from the Royal Society of Chemistry.

As discussed in Chapter 2, EPGs were extremely useful electrodes to conduct detailed study of the microenvironment systems (primary and outer coordination sphere), but there are inherent issues with the EPGs, such as their high cost and the difficulty in controlling the surface area exposed to the electrolyte, which can result in some issues with reproducibility. GCEs are a possible alternative and are structurally composed of ribbons of graphite which are interwoven, resulting in an overall harder graphitic surface compared to planar graphite structures. An SEM of CoPc-P4VP coated onto a GCE can be seen in Figure 2.1 and the ribbon-like structure of the graphite is shown in Figure 5.2.

Figure 5.2 Structure of glassy carbon comprised of interweaving ribbons of graphite. Reproduced from Ref [38] with permission from the Royal Society of Chemistry.

One issue with using GCEs is their lack of surface area, which results in extremely low activity (surface area and low activity can both be seen in Figure 2.1). By incorporating graphite powder into the catalyst-polymer complex, we saw an increase in activity as discussed at length in Chapter 2. However, the use of graphite powder makes it challenging to consider the microenvironment, and specifically to study the proton relay through proton inventory studies. One way to combat this was to rough polish the electrodes and coat the catalyst-polymer composite. I worked in collaboration with Jonah B. Eisenberg to study whether this would be possible, with experimental details following exactly those outlined in Section 4.4.5 Preparation of Modified Electrodes and Section 4.4.6 Electrochemical Measurements: Rotating Disk Electrovoltammetry – Chronoamperometric Steps. The results of this study can be seen in Figure 5.3. Unfortunately, these results also show relatively high standard deviations in measurements, so it's challenging to determine whether a proton relay can be detected using the proton inventory method. However, I propose that a study into whether it is possible to use rough polished GCEs to perform proton inventory and other studies such as activity measurements and controlled potential electrolyses may be beneficial as a long-term alternative to using EPGs.

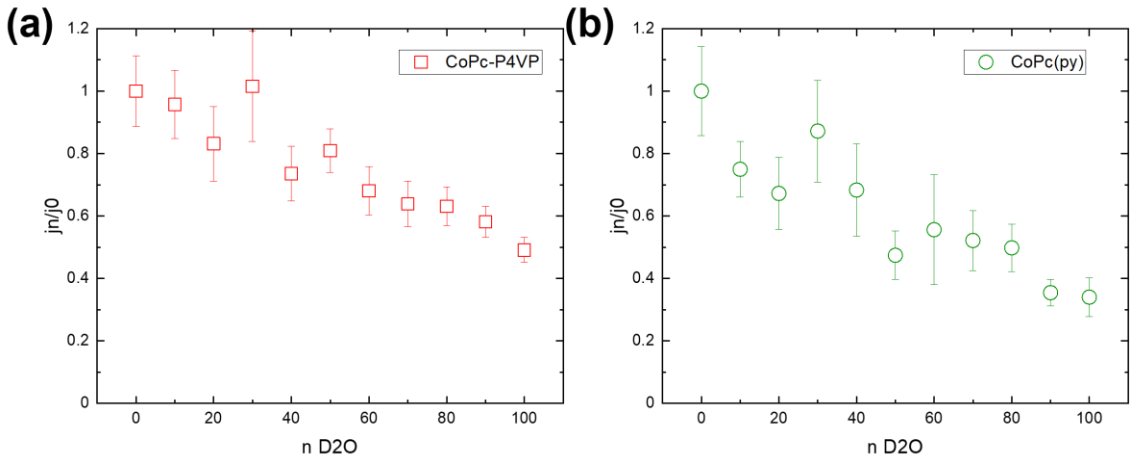

Figure 5.3 Proton inventory studies measuring the CO_2 reduction activity in fractionally deuterated electrolyte of (a) CoPc-P4VP and (b) CoPc(py) coated on rough-polished glassy carbon electrodes.

5.2.7 Confirmation of CO_2RR using $^{13}CO2$

In these systems, CO_2RR catalysis is performed by a single catalytic cobalt site, but it is surrounded by a lot of carbon – within the phthalocyanine ring, within the polymer, and within the electrode/supporting carbon materials. While I was unable to perform this experiment during my time working on this thesis, I suggest that a useful control would be to perform CO_2 electroreduction using $^{13}CO_2$ as a substrate. A controlled potential electrolysis followed by GC-MS to determine the mass of the CO produced. Because of the highly reductive potentials and the numerous controls run throughout my dissertation work of running these experiments in CO_2-free systems and only producing H_2 as a product, I believe it would be unlikely that the CO being produced could come from decomposition of the graphitic, polymeric, or phthalocyanine ring carbon atoms. However, this control would confirm that any CO produced is coming directly from the CO_2.

5.3 References

(1) Soucy, T. L.; Liu, Y.; Eisenberg, J. B.; McCrory, C. C. L. "Enhancing the Electrochemical CO2 Reduction Activity of Polymer-Encapsulated Cobalt Phthalocyanine Films by Modulating the Loading of Catalysts, Polymers, and Carbon Supports," *ACS Applied Energy Materials* **2021**. http://dx.doi.org/10.1021/acsaem.1c02689

(2) An, H.; Jeon, H.; Ji, J.; Kwon, Y.; Chung, Y. "Amine axial ligand-coordinated cobalt phthalocyanine-based catalyst for flow-type membraneless hydrogen peroxide fuel cell or enzymatic biofuel cell," *Journal of Energy Chemistry* **2021**, *58*, 463-471. http://dx.doi.org/https://doi.org/10.1016/j.jechem.2020.10.042

(3) Soucy, T. L.; Liu, Y.; Eisenberg, J. B.; McCrory, C. C. L. "Enhancing Electrochemical Carbon Dioxide Reduction by Polymer-Encapsulated Cobalt Phthalocyanine through Incorporation of Graphite Powder.," *ChemRxiv* **2021**. http://dx.doi.org/10.33774/chemrxiv-2021-bz00c

(4) Rivera Cruz, K. E.; Liu, Y.; Soucy, T. L.; Zimmerman, P. M.; McCrory, C. C. L. "Increasing the CO2 Reduction Activity of Cobalt Phthalocyanine by Modulating the σ-Donor Strength of Axially Coordinating Ligands," *ACS Catalysis* **2021**, 13203-13216. http://dx.doi.org/10.1021/acscatal.1c02379

(5) Huai, M.; Yin, Z.; Wei, F.; Wang, G.; Xiao, L.; Lu, J.; Zhuang, L. "Electrochemical CO2 reduction on heterogeneous cobalt phthalocyanine catalysts with different carbon supports," *Chemical Physics Letters* **2020**, *754*, 137655. http://dx.doi.org/https://doi.org/10.1016/j.cplett.2020.137655

(6) Chen, J.; Zhu, M.; Li, J.; Xu, J.; Han, Y.-F. "Structure–Activity Relationship of the Polymerized Cobalt Phthalocyanines for Electrocatalytic Carbon Dioxide Reduction," *The Journal of Physical Chemistry C* **2020**, *124*, 16501-16507. http://dx.doi.org/10.1021/acs.jpcc.0c04741

(7) Liu, Y.; Deb, A.; Leung, K. Y.; Nie, W.; Dean, W. S.; Penner-Hahn, J. E.; McCrory, C. C. L. "Determining the coordination environment and electronic structure of polymer-encapsulated cobalt phthalocyanine under electrocatalytic CO2 reduction conditions using in situ X-Ray absorption spectroscopy," *Dalton Trans* **2020**, *49*, 16329-16339. http://dx.doi.org/10.1039/d0dt01288b

(8) Zhang, H.; Min, S.; Wang, F.; Zhang, Z. "Immobilizing cobalt phthalocyanine into a porous carbonized wood membrane as a self-supported heterogenous electrode for selective and stable CO2 electroreduction in water," *Dalton Transactions* **2020**, *49*, 15607-15611. http://dx.doi.org/10.1039/D0DT03304A

(9) Lin, L.; Liu, T.; Xiao, J.; Li, H.; Wei, P.; Gao, D.; Nan, B.; Si, R.; Wang, G.; Bao, X. "Enhancing CO2 Electroreduction to Methane with a Cobalt Phthalocyanine and Zinc–Nitrogen–Carbon Tandem Catalyst," *Angewandte Chemie International Edition* **2020**, *59*, 22408-22413. http://dx.doi.org/https://doi.org/10.1002/anie.202009191

(10) De Riccardis, A.; Lee, M.; Kazantsev, R. V.; Garza, A. J.; Zeng, G.; Larson, D. M.; Clark, E. L.; Lobaccaro, P.; Burroughs, P. W. W.; Bloise, E.; Ager, J. W.; Bell, A. T.; Head-Gordon, M.; Mele, G.; Toma, F. M. "Heterogenized Pyridine-Substituted Cobalt(II) Phthalocyanine Yields Reduction of CO2 by Tuning the Electron Affinity of the Co Center," *ACS Applied Materials & Interfaces* **2020**, *12*, 5251-5258. http://dx.doi.org/10.1021/acsami.9b18924

(11) Zeng, J. S.; Corbin, N.; Williams, K.; Manthiram, K. "Kinetic Analysis on the Role of Bicarbonate in Carbon Dioxide Electroreduction at Immobilized Cobalt Phthalocyanine," *ACS Catalysis* **2020**, *10*, 4326-4336. http://dx.doi.org/10.1021/acscatal.9b05272

(12) Wu, Y.; Hu, G.; Rooney, C. L.; Brudvig, G. W.; Wang, H. "Heterogeneous Nature of Electrocatalytic CO/CO2 Reduction by Cobalt Phthalocyanines," *ChemSusChem* **2020**, *13*, 6296-6299. http://dx.doi.org/10.1002/cssc.202001396
(13) Xia, Y.; Kashtanov, S.; Yu, P.; Chang, L.-Y.; Feng, K.; Zhong, J.; Guo, J.; Sun, X. "Identification of dual-active sites in cobalt phthalocyanine for electrochemical carbon dioxide reduction," *Nano Energy* **2020**, *67*, 104163. http://dx.doi.org/https://doi.org/10.1016/j.nanoen.2019.104163
(14) Wang, X.; Cai, Z.-F.; Wang, Y.-Q.; Feng, Y.-C.; Yan, H.-J.; Wang, D.; Wan, L.-J. "In Situ Scanning Tunneling Microscopy of Cobalt-Phthalocyanine-Catalyzed CO2 Reduction Reaction," *Angewandte Chemie International Edition* **2020**, *59*, 16098-16103. http://dx.doi.org/https://doi.org/10.1002/anie.202005242
(15) Yang, Z.; Zhang, X.; Long, C.; Yan, S.; Shi, Y.; Han, J.; Zhang, J.; An, P.; Chang, L.; Tang, Z. "Covalently anchoring cobalt phthalocyanine on zeolitic imidazolate frameworks for efficient carbon dioxide electroreduction," *CrystEngComm* **2020**, *22*, 1619-1624. http://dx.doi.org/10.1039/C9CE01517E
(16) Liu, Y.; McCrory, C. C. L. "Modulating the mechanism of electrocatalytic CO2 reduction by cobalt phthalocyanine through polymer coordination and encapsulation," *Nature Communications* **2019**, *10*, 1683. http://dx.doi.org/10.1038/s41467-019-09626-8
(17) Choi, J.; Wagner, P.; Gambhir, S.; Jalili, R.; MacFarlane, D. R.; Wallace, G. G.; Officer, D. L. "Steric Modification of a Cobalt Phthalocyanine/Graphene Catalyst To Give Enhanced and Stable Electrochemical CO2 Reduction to CO," *ACS Energy Letters* **2019**, *4*, 666-672. http://dx.doi.org/10.1021/acsenergylett.8b02355
(18) Zhang, Z.; Xiao, J.; Chen, X.-J.; Yu, S.; Yu, L.; Si, R.; Wang, Y.; Wang, S.; Meng, X.; Wang, Y.; Tian, Z.-Q.; Deng, D. "Reaction Mechanisms of Well-Defined Metal–N4 Sites in Electrocatalytic CO2 Reduction," *Angewandte Chemie International Edition* **2018**, *57*, 16339-16342. http://dx.doi.org/https://doi.org/10.1002/anie.201808593
(19) Wu, H.; Zeng, M.; Zhu, X.; Tian, C.; Mei, B.; Song, Y.; Du, X.-L.; Jiang, Z.; He, L.; Xia, C.; Dai, S. "Defect Engineering in Polymeric Cobalt Phthalocyanine Networks for Enhanced Electrochemical CO2 Reduction," *ChemElectroChem* **2018**, *5*, 2717-2721. http://dx.doi.org/https://doi.org/10.1002/celc.201800806
(20) Zhang, X.; Wu, Z.; Zhang, X.; Li, L.; Li, Y.; Xu, H.; Li, X.; Yu, X.; Zhang, Z.; Liang, Y.; Wang, H. "Highly selective and active CO2 reduction electrocatalysts based on cobalt phthalocyanine/carbon nanotube hybrid structures," *Nature Communications* **2017**, *8*, 14675. http://dx.doi.org/10.1038/ncomms14675
(21) Han, N.; Wang, Y.; Ma, L.; Wen, J.; Li, J.; Zheng, H.; Nie, K.; Wang, X.; Zhao, F.; Li, Y.; Fan, J.; Zhong, J.; Wu, T.; Miller, D. J.; Lu, J.; Lee, S.-T.; Li, Y. "Supported Cobalt Polyphthalocyanine for High-Performance Electrocatalytic CO2 Reduction," *Chem* **2017**, *3*, 652-664. http://dx.doi.org/https://doi.org/10.1016/j.chempr.2017.08.002
(22) Kramer, W. W.; McCrory, C. C. L. "Polymer coordination promotes selective CO2 reduction by cobalt phthalocyanine," *Chemical Science* **2016**, *7*, 2506-2515. http://dx.doi.org/10.1039/C5SC04015A
(23) Abe, T.; Imaya, H.; Yoshida, T.; Tokita, S.; Schlettwein, D.; Wöhrle, D.; Kaneko, M. "Electrochemical CO 2 reduction catalysed by cobalt octacyanophthalocyanine and its mechanism," *Journal of Porphyrins and Phthalocyanines* **1997**, *1*, 315-321.
(24) Abe, T.; Yoshida, T.; Tokita, S.; Taguchi, F.; Imaya, H.; Kaneko, M. "Factors affecting selective electrocatalytic co2 reduction with cobalt phthalocyanine incorporated in a

polyvinylpyridine membrane coated on a graphite electrode," *Journal of Electroanalytical Chemistry* **1996**, *412*, 125-132. http://dx.doi.org/https://doi.org/10.1016/0022-0728(96)04631-1
(25) Yoshida, T.; Kamato, K.; Tsukamoto, M.; Iida, T.; Schlettwein, D.; Wöhrle, D.; Kaneko, M. "Selective electroacatalysis for CO2 reduction in the aqueous phase using cobalt phthalocyanine/poly-4-vinylpyridine modified electrodes," *Journal of Electroanalytical Chemistry* **1995**, *385*, 209-225. http://dx.doi.org/https://doi.org/10.1016/0022-0728(94)03762-R
(26) Nyokong, T. "Equilibrium and kinetic studies of the reaction between pyridine and cobalt(II) phthalocyanine in DMSO," *Polyhedron* **1995**, *14*, 2325-2329. http://dx.doi.org/https://doi.org/10.1016/0277-5387(95)00090-F
(27) Li, H.; Guarr, T. F. "Formation of electronically conductive thin films of metal phthalocyanines via electropolymerization," *Journal of the Chemical Society, Chemical Communications* **1989**, 832-834. http://dx.doi.org/10.1039/C39890000832
(28) Lieber, C. M.; Lewis, N. S. "Catalytic reduction of carbon dioxide at carbon electrodes modified with cobalt phthalocyanine," *Journal of the American Chemical Society* **1984**, *106*, 5033-5034. http://dx.doi.org/10.1021/ja00329a082
(29) Meshitsuka, S.; Ichikawa, M.; Tamaru, K. "Electrocatalysis by metal phthalocyanines in the reduction of carbon dioxide," *Journal of the Chemical Society, Chemical Communications* **1974**, 158-159. http://dx.doi.org/10.1039/C39740000158
(30) Hashiba, H.; Weng, L.-C.; Chen, Y.; Sato, H. K.; Yotsuhashi, S.; Xiang, C.; Weber, A. Z. "Effects of Electrolyte Buffer Capacity on Surface Reactant Species and the Reaction Rate of CO2 in Electrochemical CO2 Reduction," *The Journal of Physical Chemistry C* **2018**, *122*, 3719-3726. http://dx.doi.org/10.1021/acs.jpcc.7b11316
(31) Zhu, M.; Cao, C.; Chen, J.; Sun, Y.; Ye, R.; Xu, J.; Han, Y.-F. "Electronic Tuning of Cobalt Porphyrins Immobilized on Nitrogen-Doped Graphene for CO2 Reduction," *ACS Applied Energy Materials* **2019**, *2*, 2435-2440. http://dx.doi.org/10.1021/acsaem.9b00368
(32) Zhu, M.; Chen, J.; Huang, L.; Ye, R.; Xu, J.; Han, Y.-F. "Covalently Grafting Cobalt Porphyrin onto Carbon Nanotubes for Efficient CO2 Electroreduction," *Angewandte Chemie International Edition* **2019**, *58*, 6595-6599. http://dx.doi.org/https://doi.org/10.1002/anie.201900499
(33) Birdja, Y. Y.; Vos, R. E.; Wezendonk, T. A.; Jiang, L.; Kapteijn, F.; Koper, M. T. M. "Effects of Substrate and Polymer Encapsulation on CO2 Electroreduction by Immobilized Indium(III) Protoporphyrin," *ACS Catalysis* **2018**, *8*, 4420-4428. http://dx.doi.org/10.1021/acscatal.7b03386
(34) Buttry, D. A.; Anson, F. C. "New strategies for electrocatalysis at polymer-coated electrodes. Reduction of dioxygen by cobalt porphyrins immobilized in Nafion coatings on graphite electrodes," *Journal of the American Chemical Society* **1984**, *106*, 59-64. http://dx.doi.org/10.1021/ja00313a013
(35) Jarzębińska, A.; Rowiński, P.; Zawisza, I.; Bilewicz, R.; Siegfried, L.; Kaden, T. "Modified electrode surfaces for catalytic reduction of carbon dioxide," *Analytica Chimica Acta* **1999**, *396*, 1-12. http://dx.doi.org/https://doi.org/10.1016/S0003-2670(99)00364-5
(36) Marcandalli, G.; Goyal, A.; Koper, M. T. M. "Electrolyte Effects on the Faradaic Efficiency of CO2 Reduction to CO on a Gold Electrode," *ACS Catalysis* **2021**, *11*, 4936-4945. http://dx.doi.org/10.1021/acscatal.1c00272
(37) Schneider, C. R.; Lewis, L. C.; Shafaat, H. S. "The good, the neutral, and the positive: buffer identity impacts CO2 reduction activity by nickel(ii) cyclam," *Dalton Transactions* **2019**, *48*, 15810-15821. http://dx.doi.org/10.1039/C9DT03114F

(38) Banks, C. E.; Compton, R. G. "New electrodes for old: from carbon nanotubes to edge plane pyrolytic graphite," *Analyst* **2006**, *131*, 15-21. http://dx.doi.org/10.1039/B512688F